Solubility and stability of scorodite and adsorbed and coprecipitated arsenical 6-line ferrihydrite in the presence of *Shewanella putrefaciens* CN32 and *Shewanella* sp. ANA-3

Erika Revesz

Thesis submitted to the Faculty of Graduate and Postdoctoral
in partial fulfillment of the requirements for the
Doctorate in Philosophy degree in in Earth Sciences with specialization in Chemical and Environmental Toxicology

University of Ottawa
Ottawa-Carleton Geoscience Centre

Abstract

Mining and mineral processing generate a wide range of As-rich minerals, including scorodite ($FeAsO_4 \bullet 2H_2O$), and arsenical ferrihydrite, which are common secondary minerals found in mine tailings. Scorodite and arsenical ferrihydrite are relatively stable under a wide range of physico-chemical conditions which makes them suitable arsenic sinks in mining environments. However, bacteria can reduce these minerals and release arsenic into the aqueous environment. Two dissimilatory iron and arsenic reducing bacteria, *Shewanella* sp. ANA-3 and *Shewanella putrefaciens* CN32, were used to investigate their effects on the reductive dissolution of scorodite and arsenical 6-line ferrihydrite in a chemically defined medium containing low phosphate concentrations representative of the natural environment. Analysis of the aqueous phase of all biotic reduced samples found mainly As(III), the more toxic form of As, while very little As(V) was reduced in the abiotic samples. Solid state analysis of the scorodite biotic post-reduction minerals identified scorodite, biogenic Fe(II)-As(III) compounds, parasymplesite and tooeleite, while in the biotic reduced arsenical six-line ferrihydrite, biogenic Fe(II)-As(III) compounds, hematite, akaganeite and unconfirmed magnetite were identified as secondary reduction products. Results from this research add to the body of literature on As and Fe biogeochemistry and provide very useful information for future assessments of the long term stability of As-rich minerals.

Résumé

L'activité minière et la transformation du minerai génèrent divers minéraux riches en arsenic, tels la scorodite ($FeAsO_4 \bullet 2H_2O$) et la ferrihydrite riche en arsenic, lesquels sont des minéraux secondaires communs des résidus miniers. Comme la scorodite et la ferrihydrite riche en arsenic sont relativement stables sous une grande gamme de conditions physico-chimiques, ces minéraux peuvent potentiellement être utilisés pour stocker de façon permanente l'arsenic dans les environnements miniers. Cependant, certaines bactéries peuvent réduire ces minéraux, ce qui entraine la solubilisation de l'arsenic. Deux bactéries capables de réduire l'arsenic et le fer, soit *Shewanella* sp. ANA-3 et *Shewanella putrefaciens* CN32, ont été utilisées afin de déterminer leurs effets sur la réduction microbienne de la scorodite et de la ferrihydrite riche en As dans un milieu de culture contenant de faibles concentrations de phosphate. Les analyses de la phase aqueuse ont démontré que dans tous les systèmes biotiques, As(V) a été réduit en As(III), alors que dans les systèmes contrôles abiotiques, peu de As(V) a été réduit. L'analyse des minéraux secondaires présents à la fin réduction dans les systèmes biotiques contenant de la scorodite indique que la scorodite est encore présente, ainsi que des composés organiques riches en Fe(II) et As(III), de la parasymplésite et de la tooéleite, alors que dans les systèmes biotiques contenant de la ferrihydrite riche en As, des composés riches en Fe(II) et en As(III), de l'hématite, de l'akaganéite et de la magnétique ont été identifiés comme minéraux secondaires. Les résultats de cette étude enrichissent la littérature sur le cycle biogéochimique du Fe et de As et

fournissent de l'information importante pour l'évaluation de la stabilité à long terme de minéraux riches en As.

*I dedicate this thesis to my husband **Bob Chlebek** who encouraged and supported me as well as freeing me from household chores by doing all the shopping, laundry, cooking and the dishes during this thesis research. I am hoping that he continue to do so even after I have obtained my degree.*

Acknowledgments

I would like to express my gratitude to my supervisors, Dr. Danielle Fortin and Dr. Dogan Paktunc for encouraging me to work on these projects and directing me with patience during this research.

I would like to thank my thesis examiner committee Dr. Glenn Waychunas, Dr. Brian Cousins, Dr. Keiko Hattori and Dr. Alexandre Poulain for their very valuable comments and suggestions for improving this thesis.

I would also like to express my appreciation to my past and present group members; it was fun to work with them.

Finally, I give my genuine appreciation to my husband, Bob Chlebek, for his unwavering support during this thesis research.

Co-Authorships and Statement of Candidate's Contribution

All the results presented in this thesis are based on measurements performed by the candidate. The experiments include: synthesis and analysis of arsenical adsorbed and coprecipitated ferrihydrite and tooeleite, seven scorodite microbial reduction experiments, three 6-line arsenical ferrihydrite microbial reduction experiments with duplicate and triplicate runs, as well as a series of preliminary reduction experiments for all systems. All calculations including the PHREEQC modeling was done by the candidate.

The crystalline scorodite samples and their analysis were provided by Dr. Paktunc, the bulk XRD measurements were done at CANMET by Derek Smith. TEM/HRTEM imaging of post reduction samples were performed by Dr. Yun Lee at the University of Ottawa. The electron microprobe analysis of hematite was performed by Glenn Poirier. The XAS training and supervision of measurements were done by Dr. Robert Gordon at the Advanced Photon source in Chicago.

All parts of this thesis were written by the candidate with advice and guidance of her supervisors Dr. Fortin and Dr. Paktunc.

Table of Contents

List of Tables

Chapter 2.

List of figures

Chapter 1.

Chapter 2.

List of Tables in the Appendix.

List of Figures in the Appendix.

Chapter 1: Introduction

1. Background information

This thesis research investigated the bacterial reductive dissolution of crystalline scorodite and adsorbed and coprecipitated arsenical 6-line ferrihydrite found in some mine wastes and tailings. The bacteria selected for these experiments were two common and well characterized species of the Genus Shewanella, *Shewanella putrefaciens* CN32, a well-known iron reducer, and *Shewanella* sp. ANA-3, a known arsenate reducer. One of the major incentives for this research was that no previous systematic studies had been performed on the bacterial reduction of scorodite or adsorbed and coprecipitated arsenical 6-line ferrihydrite using *Shewanella putrefaciens* CN32, and *Shewanella* sp. ANA-3. This research is related to the findings of Paktunc et al. (2008c) and a follow up to the solubility of nanocrystalline scorodite (Paktunc and Bruggeman 2010). The scorodite used in the present research is nanocrystalline and pure.

This thesis research was conducted with the purposes to investigate the influence of bacteria on the stabilities of scorodite and arsenical ferrihydrite which are considered to be the most common arsenic carriers in mine wastes stored near the surface, and to determine the kinetics of reductive dissolution of the two compounds.

This thesis is structured as an article thesis, divided into four chapters.

Chapter 1 begins with a survey of the literature on arsenic in the natural environment with a special emphasis on mine wastes, arsenic toxicity, scorodite and

iron oxides and oxyhydroxides, followed by a discussion of dissimilatory iron and arsenic reducing bacteria, and conclude by stating the objectives and hypotheses of this research.

Chapter 2 is written as an article for publication which describes the bacterial reduction of scorodite in the presence of *Shewanella putrefaciens* CN32 and *Shewanella sp*. ANA-3 using 15, 45 and 400 μM phosphate concentrations.

Chapter 3, also in an article format, describes the bacterial reduction of the adsorbed and coprecipitated arsenical 6-line ferrihydrite with the same two bacterial strains at 45 μM phosphate concentration.

Chapter 4 presents the overall findings, conclusions and suggestions for future research.

1.1. Natural occurrence of arsenic

Arsenic is a constituent of the Earth's crust and ranks 20th in natural abundance among the other elements. The average arsenic content of the continental crust is about 1.5 to 3 mg/kg. Arsenic, a chalcophile element has a strong affinity for sulphur, and it tends to be more abundant in ores or minerals containing sulphur. Common arsenic-bearing minerals such as arsenopyrite (FeAsS), arsenian pyrite (FeS_2), realgar (As_4S_4) and orpiment (As_2S_3) can occur in sediments, rocks and soils but they are especially common in hydrothermal ore deposits, coals and felsic igneous rocks (Henke, 2009). As a side note, realgar, a ruby red colored mineral, and orpiment, a yellow to orange colored mineral, were

used as paint pigments through many centuries and poisoned many artists up until synthetic paints appeared in the 19th century.

Naturally occurring inorganic arsenic concentrations in continental material vary greatly. For instance, concentrations range from 0.6 to 120 mg/kg in sandstones, 0.6-120 mg/kg in limestones, 0.1-20 mg/kg in shales and clays, 0.3–490 mg/kg in basalts and 0.06-113 mg/kg in peat coal (Bhattachariya et al., 2007). Usually, arsenic is adsorbed as arsenate oxy-anions on minerals containing iron in oxidized sediments (Henke, 2009).

In large bodies of water, such as the Pacific and the Indian oceans, the distribution of inorganic arsenic varies from 0.35 µg/L to 1.7 µg/L, depending on the water depth (Santosa et al., 1994). These authors suggested that the uptake of arsenic by microorganisms in the surface waters and the co-precipitation of arsenic with hydrated heavy-metal oxides in bottom waters control the concentration of soluble arsenic. There is also evidence of inorganic arsenic being methylated in the oceans, as reported by Santosa et al. (1994). In another study, Bruland (1983) reported an average soluble arsenate value of 1.7 µg/L in deep sea water which agrees with the value reported by Santosa et al.

Natural processes, such as volcanism and weathering of rocks and soil, can contribute to arsenic release into the aquatic environment. Exceptionally high levels of arsenic have been reported in some alkaline closed-basin lakes, such as Mono Lake and Searles Lake in California, as a result of extreme evaporation. In these lakes, the natural arsenic concentrations are as high as 28.4 mg/L and 426 mg/L, respectively (Oremland et al., 2009). For rivers, such as the Columbia River

(Oregon), the average total arsenic reported is 1.6 µg/L, whereas for the Moira River (Ontario), concentrations range from 6 µg/L to 23 µg/L (Bhattachariya et al., 2007).

Anthropogenic sources can however increase the arsenic concentrations of terrestrial and aquatic environments, especially mining, as discussed in the next section.

1.2. Arsenic in mine wastes

Arsenic is commonly found in elevated concentrations in gold and base metal deposits. Mining and metallurgical processing of gold and base metal ores results in solid wastes, effluents and air emissions containing high concentrations of arsenic. Such wastes form an important source of anthropogenic arsenic in the environment (Paktunc, 2009). Pyrite, probably the most abundant sulfide mineral in the lithosphere, can contain significant concentrations of arsenic (Paktunc 2008a). With the exception of certain refractory gold deposits, pyrite is an unwanted gangue mineral; therefore, it is discarded during mineral processing operations. In contrast, pyrite as one of the principal Au-bearing minerals in refractory gold ores is roasted or oxidized under hydrothermal conditions to decompose the pyrite and release the contained gold (Paktunc et al. 2006). During these processes, significant levels of As can be released; therefore, mining and metallurgical wastes are considered to be one of the important sources of anthropogenic As in the environment. The oxidative dissolution of pyrite as shown by equation 1.1 for the overall reaction of pyrite with

water (Nordstrom 1982; Amos et al. 2014), can result in As releases in the form of acid mine drainage if As is present in pyrite.

$$4FeS_2(s) + 14H_2O + 15\ O_2 \rightarrow 4Fe(OH)_3 + 8SO_4^{2-} + 16H^+ \quad (1.1)$$

Arsenopyrite, which contains higher concentrations of arsenic than pyrite, is oxidized under oxic conditions resulting in the formation of an arsenic-bearing secondary mineral such as scorodite (Dove and Rimstidt, 1985).

$$FeAsS(s) + 14Fe^{3+} + 10H_2O \rightarrow 14Fe^{2+} + SO_4^{2-} + FeAsO_4 \cdot 2H_2O(s) + 16H^+ \quad (1.2)$$

In comprehensive characterization studies of mine tailings and ores of a former Yukon gold mine, Paktunc et al. (2003 and 2004) identified complex assemblages of As-bearing minerals, including scorodite, $FeAsO_4 \cdot 2H_2O$, ferric arsenates, arseniosiderite, $Ca_2Fe_3(AsO_4)_3O_2 \cdot 3H_2O$, yukonite ($Ca_2Fe_3(AsO_4)_4(OH) \cdot 12H_2O$), pharmacosiderite ($KFe_4(AsO_4)_3(OH)_4 \cdot 6–7H_2O$), arsenopyrite, (FeAsS), and Fe(III) oxyhydroxides with varying levels of arsenic up to 22 wt%. Walker et al. (2009) found scorodite and amorphous hydrous ferric arsenate as the two most common As-bearing secondary minerals in mine tailings in the Nova Scotia gold mining district. Other major As phases they identified in mine tailings were As-bearing amorphous hydrous ferric oxyhydroxides, kankite $FeAsO_4 \cdot 3.5H_2O$, pharmacosiderite, $KFe_4(AsO_4)_3(OH)_4 \cdot 6\text{-}7H_2O$, yukonite ($Ca_7Fe_{12}(AsO_4)_{10}(OH)_{20} \cdot 15H_2O$), amorphous Ca-Fe arsenates and arsenopyrite. Traces of arsenic were also found in As-bearing ferric oxyhydroxides with up to 10% arsenic, As-bearing sulfate, such as jarosite $(K,Na,H_2O)Fe_3(SO_4)_2(OH)_6$, tooeleite,

$Fe_6(AsO_3)_4(SO_4)(OH)_4 \cdot 4H_2O$ and realgar, As_4S_4 and ~ 0.1 % of arsenic in goethite (Walker et. al. 2009). Other rare iron and arsenic containing minerals related to mining, such as symplesite, parasymplesite, kolfanite, kaatialaite and kankite, have also been identified (Drahota and Filippi, 2009). In addition, sulfate-bearing Fe-As minerals have been identified in mine wastes, including bukovskyite, beudantite, sarmientite and zykaite. These minerals are known to be soluble and can therefore release arsenic into the environment (Drahota and Filippi, 2009).

Arsenic concentration in mine tailings and surrounding waters have been reported by many authors. An international study of arsenic in mine waters from 34 mining localities from Asia, Africa and South America was done by Williams (2001). Another study by Nordstrom et al. (2000) stated that arsenic concentrations in acid mine waters were around 34 to 59 mg/L (0.45 – 0.79 mM) near the Richmond Mine at Iron Mountain, CA. Osborne et al. (2010) reported arsenic concentration in mine waste water in excess of 3745 mg/L (50 mM) in an inactive gold mine south of the Arctic Circle in the Northwest Territories, Canada. Recent work by Andrade et al. (2011) showed that arsenic concentrations in the pore waters of submerged tailings at several sites in Yellowknife Bay, Great Slave Lake, Canada, reached 585 mg/L (7.8 mM), whereas the As content of the tailings was around 1310 mg/kg, (17.5 mM). These authors detected seasonal variations in As concentrations in pore waters with equal proportions of As(III) and As(V) in the range of 16 - 415 mg/L (0.21- 5.5 mM) late summer, and dominated by As(III) in the range of 284-947 mg/L (3.8 – 12.6 mM) in late winter. The seasonal variations were caused by microbially-mediated processes. At the McClean Lake in the Athabasca Basin of northern

Saskatchewan, the untreated acid raffinate solutions associated with uranium mill tailings contained up to 700 mg/L (9.3 mM) of dissolved arsenic (Langmuir et al., 2005). Mine tailings at a former gold mine in northern Ontario were characterized by Paktunc (2013) to assess the impact of a biosolid cover on the stability of As species and to evaluate options for long-term management of the tailings. Arsenic concentrations in the tailings ranged from 0.15 to 0.36 wt%, and were distributed among goethite, pyrite and arsenopyrite. Pyrite and arsenopyrite were found as small particles coated with goethite in the uncovered tailings and the deeper portions of the biosolid-covered tailings. The sulfide particles in the shallower portions of the biosolid-covered tailings were free of goethite rims. As(V) was the predominant oxidation state, with minor amount of As(-I) in the uncovered tailings. Coinciding with the disappearance of goethite rims on sulfide particles, As(III) in the biosolids-covered tailings increased gradually in proportion towards the cover. It was found that the arsenic concentrations in the leachate gradually increased from less than 0.085 to 13 mg/L and iron from 28 to 179 mg/L towards the biosolid cover. These were in contrast to the leachate concentrations of less than 0.085 mg/L arsenic and 24–64 mg/L iron obtained from the uncovered tailings, supporting the role of biosolids-influenced reduction and mobilization of As in the form of As(III) species. Reutilizing barren mine tailings sites while remediating the sites for closure with biosolids can therefore lead to a situation with unintended consequences. The organic material in the biosolids decays and generates organic acids that can form organic iron complexes. The formation of these complexes decreases the availability of iron which normally would sequesters arsenic, thus leading to the

release of arsenic to the surroundings. The biosolid-covering and the decay process produce an anaerobic environment which is ideally suited for dissimilatory iron reducing bacteria (DIRB) and dissimilatory arsenic reducing bacteria (DARB) to thrive. These bacteria can reduce iron and arsenic which results in the mobilization of the more toxic form of arsenic, As(III). Biosolids contain phosphate which forms insoluble complexes with iron and also promotes the release of arsenic. It appears that biosolids-coverage for the closure of abandoned gold mining sites is an example of creating new problems while trying to solve existing ones.

1.3. Arsenic toxicity

Arsenic toxicity on human epidermoid carcinoma A431 cells was studied by Naranmandura et al. (2007). These cells are frequently used in biomedical research in cell cycle progression and cancer-associated cellular signaling pathways. The investigators, using inorganic and organic arsenic compounds, found that the 50 % lethal concentration (LC_{50}) was 571 μM for As(V) and 5.5 μM for As(III), indicating that As(III) was about 100 times more toxic than As(V). The reason for the higher toxicity of As(III) relates to its greater mobility and bioavailability than As(V), and havingmuch higher affinity for sulfhydryl (-SH) groups of proteins than As(V). The -SH groups are part of the catalytic sites of many enzymes, and As(III) blocks these sites more readily than As(V), inactivating up to 200 enzymes such as pyruvate kinase, pyruvate dehydrogenase, thioredoxin, glutathione reductase, S-transferase and peroxidase, thioredoxin reductase and peroxidase and enzymes which repair

DNA, such as poly(ADP-ribose) polymerase-1 (PARP-1), etc. (Shen et al. 2013) have –SH goups. All of these enzymes have crucial functions in the human body and their inactivation by As(III) has severe health consequences.

Arsenic contamination of ground and drinking water is currently a major health issue because arsenic is toxic to living species. Exposure to arsenic can cause a variety of health problems, including cardiovascular diseases (States et al., 2008), diabetes and hypertension (Chen, J., et al., 2007), renal and bladder cancer (Mostafa et al., 2013, Christoforidou et al., 2013), immune system toxicity (Dangleben et al., 2013), health problems related to early life exposure (Farzan et al., 2013) and vision problems (Chen, Y., et al., 2013). In addition, Yang et al., (2013) reported the synergistic effect of arsenic exposure level and cigarette smoking in cases of urothelial carcinoma and lung cancer. New studies are revealing that epigenetic mechanisms, such as DNA methylation, histone modification etc. may also mediate toxicity and carcinogenicity resulting from arsenic exposure (Ren et al., 2011, Chanda et al., 2013).

A provisional guideline value for arsenic in drinking water was set to 10 µg/L or 10 ppb in 1993 by the World Health Organization (WHO, 2003). The WHO guideline value of 10 µg/L is however not currently feasible for a number of countries, including Bangladesh and India, which retain the 50 µg/L or 50 ppb limit (Petrusevski et al., 2007). In Bangladesh and West Bengal in India, roughly 50 % of the drinking water contains arsenic above the WHO guideline and millions of people are at risk (Goswami et al., 2013).

Canada follows the new 10 µg/L arsenic limit. In Ontario, the measured arsenic levels can range from 0.1 to 18 µg/L in treated groundwater and surface water in 726 communities. The data collected by private laboratories indicated that arsenic levels in treated and raw drinking water ranged from less than 2.5 to 68 µg/L for the period 1999–2002, the average value was less than 2.5 µg/L. The higher values came mainly from wells (Health Canada, 2006).

1.4. Scorodite

Scorodite, a ferric arsenate ($FeAsO_4 \cdot 2H_2O$), is one of the most abundant secondary mineral under acidic conditions in mine wastes (Paktunc et al., 2004, Flemming et al., 2005, Walker et al., 2009, Drahota et al., 2009). It is one of the potential compounds to be used to store arsenic in a bound state. It has high arsenic storing capacity, and its solubility and stability, which is dependent on pH and other factors such as redox environment, presence of concentration of other ions such as phosphate, determines its fate in the environment. Scorodite dissolves congruently in the pH range of 0.97 - 2.43 as shown in equation 1.3, (Krause and Ettel, 1988):

$$FeAsO_4 \cdot 2\,H_2O(s) + 3H^+ \rightarrow H_3AsO_4\,(aq) + Fe^{3+} + 2\,H_2O\,(l) \qquad (1.3)$$

At pH above 2.43, scorodite dissolves incongruently, forming Fe(III) hydroxide and arsenate oxyanions as shown in equations 1.4 and 1.5 based on Krause and Ettel, (1988).

$$FeAsO_4 \cdot 2\,H_2O(s) + H_2O\,(l) \rightarrow H_2AsO_4^{-}\,(aq) + Fe(OH)_3(s) + H^+(aq) \qquad (1.4)$$

$$FeAsO_4 \cdot 2\,H_2O(s) + H_2O\,(l) \rightarrow HAsO_4^{2-}(aq) + Fe(OH)_3(s) + 2H^+(aq) \qquad (1.5)$$

The type of arsenate anions formed depends on pH of the solution. The distribution diagrams as a function of pH of the iron and arsenate species for the concentration related to these experiments are shown in Appendix A on Figures A-1 and A-3. Under anoxic conditions, scorodite dissolution can be enhanced by bacteria which use iron and arsenic as terminal electron acceptors in their metabolic processes. Since bacteria are very common in every environment, it is important to study their impact on the solubility and stability of scorodite. There are limited numbers of studies in the literature about microbial reductive dissolution of scorodite and they will be discussed in chapter 2.

1.5. Iron oxides and oxyhydroxides

Iron oxides are common components of soils, sediments and rocks. Iron oxides include hematite (α-Fe_2O_3), maghemite (δ-Fe_2O_3) and magnetite (Fe_3O_4) whereas Fe-oxyhydroxides refer to goethite (α-FeOOH), lepidocrocite (δ-FeOOH), akaganeite (β-FeOOH) and feroxyhyte (δ'-FeOOH) (Cornell and Schwertmann,

2003). Ferrihydrite is another important iron oxide that can be found in mine wastes, acid-mine drainage settings, iron bearing sediments, soils and hydrothermal ore deposits. Ferrihydrite is a poorly crystalline hydrous oxyhydroxide, forming a reddish-brown gelatinous precipitate which is not very soluble at neutral pH. Ferrihydrite is a metastable phase which can transform into a more stable oxide with time (Housecroft and Sharpe, 2001). Structurally, it forms a hexagonally close packed oxygen anions chain structures with edge-sharing FeO_6 octahedra. It has two distinct forms, 2-line and 6-line ferrihydrite after the number of reflections from their atomic planes which appear as peaks on the XRD pattern (Jambor and Dutrizac, 1998). The number of XRD peaks correlate with the crystallinity of the substance. The structure of ferrihydrite has been a subject of controversy with two very different structural models proposed (Drits et al. (1993), Janney et al. (2000, 2001), Michel et al. (2007, 2010), Rancourt and Meunier, (2008), Manceau, (2011), and Manceau et al. 2014). Paktunc et al. (2013) argue that the new structural model proposed by Michel et al. (2007 and 2010) is not satisfactory because the evidence for the presence of Fe in tetrahedral coordination is weak based on Ge and Fe K-edge EXAFS spectra.

The pH condition used in this research to adsorb arsenate on ferrihydrite was based on the studies by Wilkie and Hering (1995), Raven et al (1998) and Dixit and Hering, (2003). Wilkie and Hering (1995) studied the adsorption of arsenic at pH conditions varying from 3 to 9 and found that 100% As(V) adsorption occurred in the pH range of 4 to 6. Their results were in close agreement with an earlier finding by Pierce and Moore (1982). Raven et al. (1998) used Fe/As molar ratios of 1.7 and 4,

and found that As adsorption was almost complete in a few hours, and that As(III) reacted faster than As(V) with ferrihydrite. However, at the lower arsenic concentrations and low pH, they found that As(V) adsorption was faster and the maximum adsorption occurred at pH 4.6. Dixit and Hering (2003) studied the adsorption of arsenic on six-line ferrihydrite and found that more As(V) adsorbed than As(III) below pH 5 to 6, whereas, more As(III) adsorbed above pH 7-8. Fuller et al. (1993) studied the kinetics of arsenate adsorption and coprecipitation on ferrihydrite in a pH range of 7.5 to 9. They found that diffusional processes may be very important in controlling the rates of adsorption and desorption of As(V) from surface coordination sites on ferrihydrite, and suggested that it may be more difficult than expected to apply laboratory results from post synthesis adsorption experiments, including As(V), on ferrihydrites in natural systems because the growth of ferrihydrite crystallites proceeds much further in simpler electrolytes in shorter times, reducing the number of surface sites and increasing the rate of transformation to goethite and hematite. A review of adsorption of arsenic from water and wastewater on a variety of surfaces and compounds, including iron oxides, was presented by Mohan and Pitman (2007). Erbs et al. (2010) studied the dependence of ferrihydrite particles on the kinetics of abiotic reductive dissolution of arsenical 6-line ferrihydrite, ranging in average length from 3.4 to 5.9 nm and found a small dependence on particle size for the freshly prepared ferrihydrite but no dependence on size for the dried ferrihydrite nanoparticles. Dissolved mineral constituents can bind to surfaces of organic matter, such as bacterial surfaces. For example, microbial extracellular exopolymeric substances (EPS), with their many

organic functional groups, can form complexes with iron and arsenic. EPS play a role in the formation of biogenic reduction products and influence the formation of secondary mineral phases (Fortin, 2004, Mikutta et al. 2008, Babechuk et al., 2009, Huang et al. 2011). Hohmann et al. (2011) investigated the interactions of As(V) and As(III) with biogenic Fe(III) oxyhydroxide minerals formed by the nitrate-reducing Fe(II)-oxidizing bacterium Acidovorax and found that in the absence of As and at low As loading (Fe/As molar ratio 125), only goethite was formed. In contrast, at Fe/As a ratio 15–50, a ferrihydrite phase was also formed, and its relative amount systematically increased with increasing Fe/As molar ratios. They concluded that the presence of As influenced the type of biogenic Fe(III) oxyhydroxide minerals, i.e. at 0.008 mol/mol As/Fe goethite formed and 0.067 mol/mol As/Fe ferrihydrite also formed during microbial Fe(II) oxidation, and As(V) preferentially bound to poorly crystalline phases, such as ferrihydrite, while As(III) did not show any preferential association. Langner and Inskeep (2000) investigated the effect of microbial reduction of aqueous and adsorbed As(V) on ferrihydrite with Clostridium sp. strain CN8 and found that 60 % of the aqueous As(V) was reduced to As(III) in less than a day in the absence of ferrihydrite. At Fe/As molar ratio of 10, about 25% of the As was aqueous, while 75% was adsorbed to the ferrihydrite phase and the aqueous As(V) was almost completely reduced to As(III) within 1 day but CN8 did not solubilize As from the Fe oxide phase.

Arsenic adsorption onto ferrihydrite depends on the surface charge which is governed by solution pH and the composition of the surface. The nature of the electrical double layer which forms on the surface of a solid depends on the

interactions between the solid surface and ions present in solution in contact with the surface. The double layer includes the Stern inner and outer spheres as one layer, and the diffuse Gouy layer as the second layer. Arsenic can adsorb indirectly to the ferrihydrite surface through one or more water molecules by forming the Stern outer-sphere complex. Arsenic can form three types of Stern inner-sphere complexes, such as monodentate, bidentate-mononuclear and bidentate-binuclear adsorption complexes (Henke, 2009). The outer or Gouy layer complex can form when arsenic is further outward from the proximity of the solid-liquid interface. The different types of complexes of arsenic on the ferrihydrite surface were investigated by extended X-ray absorption fine structure (EXAFS) spectroscopy and showed that arsenate is adsorbed mainly as a Stern inner-sphere bidentate-binuclear or a bridging complex (Waychunas, et al., 1993 and 1995; Manceau, 1995, Sherman and Randall, 2003, Paktunc et al., 2003 and 2004). The bridging As(V) was attached to adjacent apices of the edge-sharing Fe - OH octahedra. An EXAFS study of As(V) in uranium mine tailings samples by Essilfie-Dughan et al., (2013) also found that As(V) was adsorbed to the surface of ferrihydrite through the inner-sphere bidentate-binuclear linkage. Waychunas et al. (1993) further identified monodentate arsenate linkages on ferrihydrite, but not on the crystalline FeOOH polymorps. Another EXAFS study by Gao et al., (2013) found that As(V) formed an inner sphere, binuclear bidentate complexes, and As(III) formed both, mononuclear bidentate and binuclear bidentate complexes with 6-line ferrihydrite.

Coprecipitation of arsenate with ferrihydrite was investigated by Fuller et al. (1993); who found that the strongly adsorbed arsenate groups disrupted the crystal

structure and prevented the formation of an ordered structure. They revealed that during polymerization of the iron octahedra, chain crosslinking is prevented and dioctahedral chain length was reduced with arsenate occupying chain ends, which, led to a decreased grain size. In contrast, the adsorbed arsenate on ferrihydrite showed more ordered crystallites and had crosslinked dioctahedral chains. Other studies (Riveros et al. 2001; Paktunc et al, 2008c; Refait et al. 2009) published that the formation of a more ordered crystalline structure was prevented by the presence of the As(V) species.

The possibility of As(III) oxidation in the simultaneous presence of goethite and aqueous Fe(II), as commonly observed in environments in the presence of iron-reducing microorganisms, was investigated in a XANES study by Amstaetter et al. (2010). Based on thermodynamic calculations they expected As(V) reduction but instead found As(III) oxidation to As(V) which could explain the presence of As(V) in reduced groundwater aquifers. They concluded that the As(III) oxidation was caused by a reactive Fe(III) species or a secondary iron mineral phase that was formed during electron transfer from Fe(II) to goethite. Under oxic conditions a XANES study by O-Nguema et al. (2010) found that As(III) was oxidized upon adsorption onto ferrihydrite but only after the addition of aqueous Fe(II). They implied that Fe(II) was able to catalyze As(III) oxidation in the presence of dissolved O_2 and suggested that oxidation of As(III) upon adsorption on ferrihydrite under oxic conditions was an Fe^{2+}-mediated Fenton-like reaction.

1.6. Dissimilatory iron and arsenic reducing bacteria

Dissimilatory iron (DIRB) and arsenic (DARB) reduction is important in terms of mobilization of iron and arsenic under anaerobic conditions (Lovley, 1997). *Shewanella* sp. ANA-3 and *Shewanella putrefaciens* CN32 are dissimilatory iron and arsenic reducing bacteria capable of oxidizing organic carbon compounds, e.g., lactate and acetate, and using Fe(III) and As(V) as terminal electron acceptors during anaerobic respiration in order to gain energy and maintain their growth. Under circumneutral pH conditions in the environment where the availability of dissolved iron is limited, these bacteria develop various mechanisms to solubilize iron and consequently mobilize arsenic associated with iron oxides and hydroxides. Fe(III)-respiring bacteria, such as *Shewanella*, can utilize electron shuttles (Van der Zee and Cervantes 2009), Fe(III)-chelating compounds, like flavins (Marsili et al. 2008), direct electron transfers via outer membrane OmcA-MtrCAB protein complexes (Okamoto et al. 2011), protein-based “nanowires” (Gorby et al, 2006), or pili (Roberts et al. 2006, Lovley, 2012). The enzymes identified for Fe(III) respiration include four multiheme c-type cytochrome proteins, CymA, MtrA, MtrC and OmcA, and an outer membrane porin-like protein, MtrB, which are located in the inner (IM) and outer membranes (OM) and in the periplasmic (PS) place as shown in Figure 1 (Shi et al. 2012).

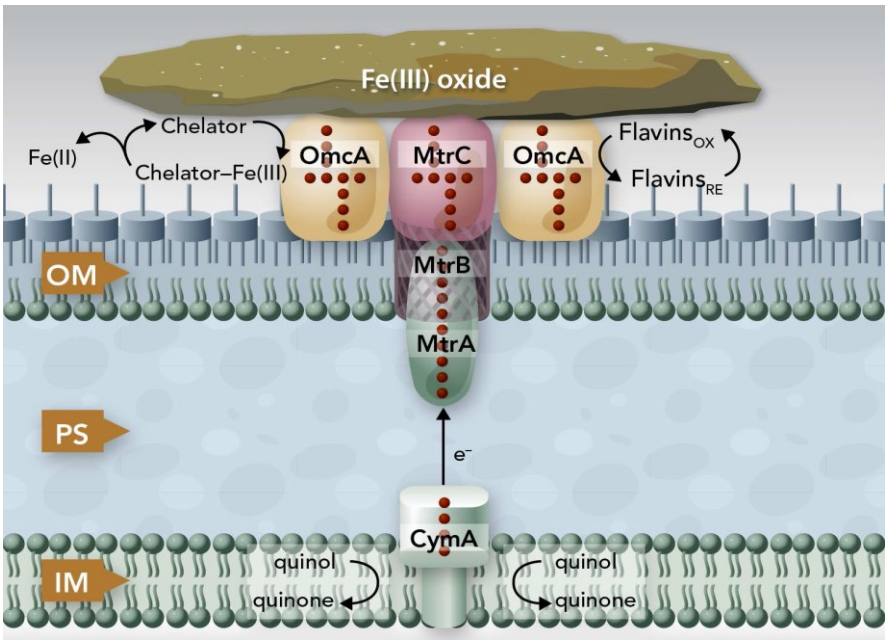

Figure 1.1. The locations of the Fe(III)-reducing proteins in the Mtr pathway for *Shewanella* species transferring electrons from the inner membrane (IM) through the periplasm (PS) and across the outer membrane (OM) to the minerals external to the bacterial cells (Shi et al. 2012).

The enzymes in the Mtr pathway are highly conserved across the metal-reducing *Shewanella* species. This pathway is the best characterized extracellular electron transport pathway as described by Shin et al. (2012) and White et al. (2013). The enzyme CymA in the inner membrane oxidizes the quinol (-OH) to quinone (-C=O) and transfers the released electrons to MtrA either directly or indirectly through other participating periplasmic proteins.

The outer trans-membrane protein, MtrAB, shuttles the electrons to the outer membrane proteins MtrC and OmcA which are on the surface of the outermost bacterial membrane. Terminal reductase enzymes, MtrC and OmcA, can bind to the

surface of Fe(III) oxides and transfer electrons directly to the minerals via their co-factor hemes which are exposed towards the hydrophilic solvent surface. MtrC and OmcA enzymes can also catalyze the reduction of dissolved Fe(III) in solution.

In dissimilatory arsenic reduction there are two known As(V) reducing bacterial systems, a respiratory system expressed by the *arr* operon and a detoxification system expressed by the *ars* operon. In *Shewanella* sp. strain ANA-3, the *ars* operon is expressed under both aerobic and anaerobic conditions, and the *arr* systems only under anaerobic conditions. As(III) can induce both the *arr* and *ars*, but As(V) can only induce the *arr* genes. The two As(V) reductase systems in ANA-3 respond to different concentrations and types of inorganic arsenic (Saltikov et al. 2005). The As(V) detoxification is the best studied system which allows the reduction of As(V) to As(III) in the cytoplasm by the arsenate reductase ArsC. The reduced arsenic is then pumped out of the cell via an As(III)-specific transporter, ArsB. In *Shewanella* sp. ANA-3, ArrA and ArrB are expressed by a two-gene operon, ArrAB (Saltikov and Newman, 2003). Another enzyme, a membrane associated tetraheme c-type cytochrome, expressed by the *cym-A* gene, is also required as a terminal electron acceptor for arsenate respiration (Murphy and Saltikov, 2006, Murphy et al. 2008). The brief overview of the mechanism includes the oxidation of lactate to pyruvate with the removal of 2H's (hydride generation) by lactate dehydrogenase. The H's with the electrons are shuttled through NAD, FAD, menaquinone to CymA to the ArrAB enzyme and finally to As(V) as described in detail by van Lis et al., (2013) and by Silver and Phung, (2005).

2. Objectives and hypotheses:

The objectives of this thesis are: (1) to determine the changes in the speciation of As and Fe under the influence of bacteria, (2) to assess the stability of various arsenical compounds in mine wastes and (3) to assess the long-term environmental stability of common arsenical minerals and compounds for predicting As releases from mining and metallurgical wastes.

The information generated by the study can be used to assess integrity of various disposal scenarios, such as water covers and soil covers in terms of preventing arsenic releases from mining wastes.

The specific goals of this research were to investigate the solubility and stability of scorodite ($FeAsO_4 \cdot 2H_2O$), and adsorbed and coprecipitated arsenical 6-line ferrihydrite, common secondary arsenic minerals in mine tailings, in the presence of dissimilatory iron and arsenic reducing bacteria, *Shewanella* sp. ANA-3 and *Shewanella putrefaciens* CN32. Among the common As minerals, scorodite has the lowest known solubility (Paktunc et al. 2010) and dissolution rate, and 6-line ferrihydrite also has a low solubility and has been shown to adsorb arsenic. They both represent suitable arsenic sinks in mining environments. However, dissimilatory iron and arsenic reducing bacteria, such as *Shewanella*, can reduce the constituents of scorodite and arsenical ferrihydrite, and cause the release of arsenic into the environment. The effect of phosphate on the microbial reduction of these minerals was investigated because phosphate competes with arsenic for dissolved iron to form insoluble iron compounds. Phosphate also binds to sites on

iron oxides, such as ferrihydrite surfaces, which prevents access to the sites by arsenic.

The composition of the arsenical 6-line ferrihydrites, Fe/As molar ratios 10/1, was chosen to avoid the presence of ferric arsenate in the synthesized product as described by Paktunc et al. (2008c).

3. References:

Amos, R.T., Blowes, D.W., Bailey, B. L., Sego, D. C., Smith, L., Ritchie, A. I. M., 2014. Waste-rock hydrogeology and geochemistry. Appl. Geochem. http://dx.doi.org/10.1016/j.apgeochem.2014.06.020

Amstaetter, K., Borch, T., Casanova, P.L., Kappler, A., 2010. Redox Transformation of Arsenic by Fe(II)-Activated Goethite (α-FeOOH). Environ. Sci. Technol. 44, 102–108.

Andrade, C.F., Jamieson, H.E., Kyser, T.K., Praharaj, T., Fortin, D., 2010. Biogeochemical redox cycling of arsenic in mine-impacted lake sediments and co-existing pore waters near Giant Mine, Yellowknife Bay, Canada. Appl. Geochem. 25,199-211.

Battacharya, P., Mukherjee, A.B., Bundschuh, J., Zevenhoven, R., Loeppert, R.H., Arsenic in soil and groundwater environment: Biogeochemical Interactions, Health Effects and Remediation, Amsterdam, Oxford: Elsevier, 2007.

Bruland, K.W., Trace elements in sea water, in: Riley, J.P., Chester, R., Chemical Oceanography, 2nd ed, vol.8, Academic Press, 1983, London, pp-157-220

Chanda, S., Dasgupta, U.B., Mazumder, D.J., Saha, J., Gupta, B., 2013. Human GMDS gene fragment hypermethylation in chronic high level of arsenic exposure with and without arsenic induced cancer. SpringerPlus, 2, 557-567.

Chen, C.J., Wang, S.L., Chiou, J.M., 2007. Arsenic and diabetes and hypertension in human populations: A review. Toxicol. Appl. Pharmacol., 222, 298-304.

Chen, Y., Wu, F., Graziano, J.H., Parvez, F., Liu, M., Paul, R.R., Shaheen, I., Ahsan, H., 2013. Arsenic exposure from drinking water, arsenic methylation capacity, and carotid intima-media thickness in Bangladesh. Am. J. Epidemiology 178, 372-381.

Christoforidou, E.P., Riza, E., Kales, S.N., Hadjistavrou, K., Stoltidi, M., Kastania, A.N., Linos, A., 2013. Bladder cancer and arsenic through drinking water: A systematic review of epidemiologic evidence. J. Environ. Sci. Health - Part A Toxic/Hazardous Substances and Environmental Engineering 48, 1764-1775.

Cornell, R. M., Schwertmann, U., 2003. The iron oxides, properties, reactions, occurrences, and uses. Wiley-VCH Verlag: Weinheim.

Dangleben, N.L., Skibola, C.F., Smith, M.T., 2013. Arsenic immunotoxicity: A review. Environmental Health: A Global Access Science Source 12 , art. no. 73.

Dixit, S., Hering, J.G., 2003. Comparison of As(V) and As(III) sorption onto iron oxide minerals: Implications for arsenic mobility. Environ. Sci. Technol. 37, 4182-4189.

Drits, V. A., Sakharov, B. A., Salyn, A. L., and Manceau, A., 1993. Structural model for ferrihydrite. Clay Miner. 28, 185–207.

Dove, P.M., Rimstidt, J.D., 1985, The solubility and stability of scorodite, $FeAsO_4 \cdot 2H_2O$. Am. Mineral., 70, 838–44.

Drahota, P., Filippi, M., 2009. Secondary arsenic minerals in the environment: A review. Environ. International, 35, 1243–1255.

Erbs, J.J, Gilbert, B., Penn, R.L., 2008. Influence of Size on Reductive Dissolution of Six-Line Ferrihydrite, J. Phys. Chem. C., 112, 12127–12133.

Erbs, J. J., Berquo, T. S., Reinsch, B. C., Lowry, G. V., Banerjee, S. K., Penn, R. L., 2010. Reductive dissolution of arsenic-bearing ferrihydrite. Geochim. Cosmochim. Acta., 74, 3382–3395.

Essilfie-Dughan, J., Hendry, M.J., Warner, J., Kotzer, T., 2013. Arsenic and iron speciation in uranium mine tailings using X-ray absorption spectroscopy, Appl. Geochem., 28, 11-18.

Farzan, S.F., Karagas, M.R., Chen, Y. 2013. In utero and early life arsenic exposure in relation to long-term health and disease (Review) Toxicol. Appl. Pharmacol. 272 (2), 384-390

Flemming, R.L., Salzsauer, K.A., Sheriff, B.L., Sidenko, N.V., 2005. Identification of scorodite in fine-grained, high sulfide, arsenopyrite mine-waste using micro X-ray diffraction (XRD), Can. Mineral. 43, 1243-1254

Fortin, D., 2004. What Biogenic Minerals Tell Us, Science, 12, Vol. 303. 1618.

Fuller, C. C., Davis, J. A., Waychunas, G. A., 1993, Surface chemistry of ferrihydrite: Part 2. Kinetics of arsenate adsorption and coprecipitation. Geochim. Cosmochim. Acta 57, 2271-2282.

Gao, X., Root, R.A., Farrell, J., El, W., Chorover, J. 2013. Effect of silicic acid on arsenate and arsenite retention mechanisms on 6-L ferrihydrite: A spectroscopic and batch adsorption approach, Appl. Geochem. 38, 2013, 110 -120

Gorby, Y.A., Yanina,S., McLean, J.S., Rosso, K.M., Moyles, D., Dohnalkova, A., Beveridge, T.J., Chang, I.S., Kim, B.H., Kim, K.S., Culley, D.E., Reed, B.S., Romine, F.M., Saffarini, A.D., Hill, A.E., Shi, L., Elias, D.A., Kennedy, D. W., Pinchuk, G., Watanabe, K., Ishii, S., Logan, B., Nealson, K.H., Fredrickson, J. K. 2006. Electrically conductive bacterial nanowires produced by Shewanella oneidensis strain MR-1 and other microorganisms. Proc. Natl. Acad. Sci. USA, 103(30):11358-63.

Goswami, R., Rahman, M.M., Murrill, M., Sarma, K.P., Thakur, R., Chakraborti, D., 2013, Arsenic in the groundwater of Majuli - The largest river island of the Brahmaputra: Magnitude of occurrence and human exposure. J. Hydrol. (in press)

Health Canada 2006. Guidelines for Canadian Drinking Water Quality: Guideline Technical Document - Arsenic. Water Quality and Health Bureau, Healthy Environments and Consumer Safety Branch, Health Canada, Ottawa, Ontario.

Henke, K., Arsenic: Environmental Chemistry, Health Threats and Waste Treatment, John Wiley & sons Ltd. Chichester, UK, 2009.

Hohmann, C., Morin, G., Ona-Nguema, G., Guigner, J-M., Brown, G. E. Jr., Kappler, A., 2011. Molecular-level modes of As binding to Fe(III) (oxyhydr)oxides

precipitated by the anaerobic nitrate-reducing Fe(II)-oxidizing Acidovorax sp. strain BoFeN1, Geochim. Cosmochim. Acta 75, 4699–4712

Housecroft, C.E., Sharpe, A.G., Inorganic chemistry. Prentice Hall, 2001.

Huang, J-H., Elzinga, E.J., Brechbuehl, Y., Voegelin, A., Kretzschmar, R., 2011. Impacts of *Shewanella putrefaciens* strain CN-32 cells and extracellular polymeric substances on the sorption of As(V) and As(III) on Fe(III)-(hydr)oxides. Environ. Sci. Technol. 45, 2804–2810

Jambor, J.L., Dutrizac, J.E., 1998. Occurrence and constitution of natural and synthetic ferrihydrite, a widespread iron oxyhydroxide. Chem. Rev. 98, 2549-2585.

Janney, D.E., Cowley, J.M., Buseck, P.R., 2000. Structure of synthetic 2-line ferrihydrite by electron nanodiffraction. Am. Mineral. 85, 1180–1187.

Janney, D.E., Cowley, J.M., Buseck, P.R., 2001. Structure of synthetic 6-line ferrihydrite by electron nanodiffraction. Am. Mineral. 85, 327–335.

Krause, E., Ettel, V.A., 1988. Solubility and stability of scorodite, New data and further discussion. Am.Mineral. 73, 850-854.

Langley, S., Gault, A., Ibrahim, A., Renaud, R., Fortin, D., Clark, I.D., Ferris, F.G., 2009. A Comparison of the rates of Fe(III) reduction in synthetic and bacteriogenic iron oxides by *Shewanella putrefaciens* CN32, Geomicrobiol. J. 26, 57–70

Langmuir, D., Aqueous Environ. Geochem. Prentice Hall, 1997.

Langner, H.W., Inskeep, W.P., 2000, Microbial reduction of arsenate in the presence of ferrihydrite. Environ. Sci. Technol. 34, 3131-3136.

Lovley, D.R., 1997. Microbial Fe(III) reduction in subsurface environments. FEMS Microbiol. Rev. 20, 305-315.

Lovley, D.R., 2012. Long-range electron transport to Fe(III) oxide via pili with metallic-like conductivity. Biochem. Soc. Trans. 40, 1186–1190.

Mahoney, J., Langmuir, D., Gosselin, N., Rowson, J., 2005. Arsenic readily released to pore waters from buried mill tailings, Appl. Geochem. 20, 947–959

Manceau A., 1995. The mechanism of anion adsorption on iron oxides: evidence for the bonding of arsenate tetrahedra on free $Fe(O,OH)_6$ edges. Geochim. Cosmochim. Acta 59, 3647–3653.

Manceau, A., 2011, Critical evaluation of the revised akdalaite model for ferrihydrite Am. Mineral. 96, 521–533,

Manceau, A., Skanthakuma, S., Soderholm, L., 2014. PDF analysis of ferrihydrite: Critical assessment of the under-constrained akdalaite model. Am. Mineral. 99, 102–108.

Marsili, M., Baron, D. B., Shikhare, I.D., Coursolle, D., Gralnick, J.A., Bond, D.R., 2008. Shewanella secretes flavins that mediate extracellular electron transfer. PNAS, 105(10) 3968–3973

Michel, F.M., Ehm, L., Antao, S.M., Lee, P.L., Chupas, P.J., Liu, G., Strongin, D.R., Schoonen, M.A.A., Phillips, B.L., Parise, J.B., 2007. The structure of ferrihydrite, a nanocrystalline material. Science 316, 1726–1729.

Michel, F.M., Barrónc, V., Torrent, J., Morales, M.P., Serna, .J., Boily, J.F., Liu, Q., Ambrosini, A., Cismasu, A.C., and Brown, G.E.Jr., 2010. Ordered

ferrimagnetic form of ferrihydrite reveals links among structure, composition, and magnetism.

PNAS, 107, 2787–2792.

Mikutta, C., Mikutta, R., Bonneville, S., Wagner, F.,Voegelin. A., Christl, I., Kretzschmar, R., 2008. Synthetic coprecipitates of exopolysaccharides and ferrihydrite. Part I: Characterization, Geochim. Cosmochim. Acta., 72, 1111–1127.

Mohan, D., Pitman, U.C., 2007. Arsenic removal from water/wastewater using adsorbents-A critical review, J. Hazard. Mat. 142, 1–53

Mostafa, M.G., Cherry, N., 2013. Arsenic in drinking water and renal cancers in rural Bangladesh. Occup. Environ. Med. 70 (11), 768-773.

Murphy, J.N., Durbin, K.J., Saltikov, C.W., 2008. Functional roles of arcA, etrA, cyclic AMP (cAMP)-cAMP receptor protein, and cya in the arsenate respiration pathway in *Shewanella* sp. Strain ANA-3. J. Microbiol. 1035–1043.

Murphy, J.N., and C.W., Saltikov. 2007. The *cymA* gene encoding a tetrahemec-type cytochrome is required for arsenate respiration in Shewanella species. J. Bacteriol. 189, 2283–2290.

Naranmandura, H., Ibata, K., Suzuki, K.T., 2008. Toxicity of dimethylmonothio-arsinic acid toward human epidermoid carcinoma A431 Cells. Chem. Res. Toxicol. 20, 1120–1125.

Nordstrom, D.K., 1982. Aqueous pyrite oxidation and the consequent formation of

secondary iron minerals. In: Hossner, L.R., Kittrick, J.A., and Fanning DF (eds.) Acid Sulfate Weathering. Madison, Wisconsin: Soil Science Society of American Press.

Nordstrom, D.K., Alpers, C.N., Ptacek, C.J., Blowes, D.W., 2000. Negative pH and extremely acidic mine waters from Iron Mountain, California, Environ. Sci. Technol. 34, 254-258

Okamoto, A., Nakamura, R., Hashimoto, K., 2011. In-vivo identification of direct electron transfer from Shewanella oneidensis MR-1 to electrodes via outer-membrane OmcA–MtrCAB protein complexes. Electrochim. Acta, 56 (16) 5526–5531

O-Nguema, G., Morin, G., Wang, Y., Foster, A. L., Juillot, F., Calas, G., Brown, G. E., 2010. XANES Evidence for rapid arsenic(III) oxidation at magnetite and ferrihydrite surfaces by dissolved O_2 via Fe^{2+}-mediated reactions. Environ. Sci. Technol. 44, 5416–5422

Oremland, R.S., Saltikov, C.W., Wolfe-Simon, F., Stolz, J.F., 2009, Arsenic in the evolution of earth and extraterrestrial ecosystems, Geomicrobiol. J. 26, 522–536.

Osborne, T.H., Jamieson, H.E., Hudson-Edwards, K.A., Nordstrom, K.D., Walker, S. W.R., Ward, S.A., Santini, J.M., 2010. Microbial oxidation of arsenite in a subarctic environment: diversity of arsenite oxidase genes and identification of a psychrotolerant arsenite oxidizer, BMC Microbiol. 10, 205-212.

Paktunc, D., Foster, A., Laflamme, G., 2003. Speciation and characterization of

arsenic in Ketza River mine mailings using X-ray absorption spectroscopy, Environ. Sci. Technol. 37, 2067-2074

Paktunc, D., Foster, A., Heald, S., Laflamme, G., 2004. Speciation and characterization of arsenic in gold ores and cyanidation tailings using X-ray absorption spectroscopy. Geochim. Cosmochim. Acta. 68, No. 5, pp. 969–983,

Paktunc, D., Kingston, D., Pratt, A., McMullen, J., 2006. Distribution of gold in pyrite and in products of its transformation resulting from roasting of refractory gold ores. Can. Mineral. 44, 213-227.

Paktunc, D., 2008a. Speciation of arsenic in pyrite by micro-X-ray absorption fine-structure spectroscopy (XAFS). Ninth International Congress for Applied Mineralogy, Brisbane. QLD, 8 - 10 September.

Paktunc, D., 2008b. Speciation of arsenic in an anaerobic treatment system at a Pb-Zn smelter site, gold roaster products, Cu smelter stack dust and impacted soil. Ninth International Congress for Applied Mineralogy Brisbane, QLD, 8 - 10 September.

Paktunc, D., Dutrizac, J., Gertsman, V., 2008c. Synthesis and phase transformations involving scorodite, ferric arsenate and arsenical ferrihydrite: Implications for arsenic mobility. Geochim. Cosmochim. Acta., 72, 2649–2672.

Paktunc, D., 2009. Arsenic speciation in wastes resulting from pressure oxidation, roasting and smelting. Proceedings of the 24th IAGS, Fredericton.

Paktunc, D., Bruggeman, K., 2010. Solubility of nanocrystalline scorodite and amorphous ferric arsenate: Implications for stabilization of arsenic in mine wastes, Applied Geochemistry 25, 674–683

Paktunc, D., 2013. Mobilization of arsenic from mine tailings through reductive dissolution of goethite influenced by organic cover, Appl. Geochem. 36, 49–56.

Petrusevski, B.J., Sharma, S., Schippers, J.C., Shordt, K., 2007. Arsenic in Drinking Water Thematic Overview Paper 17, March 2007, IRC International Water and Sanitation Centre

Pierce, M.L., Moore, C.B., 1982. Adsorption of Arsenite and Arsenate on amorphous iron hydroxide. Water Res. 16, 1247

Rancourt, D.G., and Meunier, J.-F., 2008. Constraints on structural models of ferrihydrite as a nanocrystalline material. Am. Mineral. 93, 1412–1417.

Raven, K.P., Jain, A., Loeppert, R.H., 1998. Arsenite and arsenate adsorption on ferrihydrite: kinetics, equilibrium, and adsorption envelopes, Environ. Sci. Technol. 32, 344–349.

Refait, P., Girault, P., Jeannin, M., Rose, J., 2009. Influence of arsenate species on the formation of Fe(III) oxyhydroxides and Fe(II–III) hydroxychloride, Colloids Surf. A-Physicochem. Eng. Aspects. 332, 26–35

Ren, X., McHale, C.M., Skibola, C.F., Smith, A.H., Smith, M.T., Zhang, L., 2011. An Emerging Role for Epigenetic Dysregulation in Arsenic Toxicity and Carcinogenesis, Environ. Health Persp. 119(1) 11-19

Riveros, P.A., Dutrizac, J.E., Spencer, P., 2001. Arsenic disposal practices in the metallurgical industry. Can Metall. Q. 40, 395–420.

Roberts, J., Fowle, D.A., Hughes, B.T., Kulczycki, E., 2006. Attachment behavior of *Shewanella putrefaciens* onto magnetite under aerobic and anaerobic conditions. Geomicrobiol. J. 23, 631–640.

Saltikov, C.W., Newman, D.K., 2003. Genetic identification of a respiratory arsenate reductase. Proc. Natl. Acad. Sci. USA 100, 10983–10988.

Saltikov, C.W., Wildman, R.A.Jr., Newman, D.K., 2005. Expression dynamics of arsenic respiration and detoxification in Shewanella sp. strain. ANA-3. J. Bacteriol. 187, 7390–7396.

Santosa, S.J., Wada, S., Tanaka, S., 1994. Distribution and cycle of arsenic compounds in the ocean, Appl. Organomet. Chem. 8(3), 273–283.

Shen, S., Li, X-F., Cullen, W.R., Weinfeld, M., Le, C.X., 2013. Arsenic Binding to Proteins. Chem. Rev. 113, 7769−7792

Sherman D.M., Randall S.R., 2003. Surface complexation of arsenic(V) to iron(III) (hydro)oxides: structural mechanism from ab initio molecular geometries and EXAFS spectroscopy. Geochim. Cosmochim. Acta 67(22), 4223–4230.

Shi, L., Rosso, K.M., Clarke, T.A., Richardson, D.J., Zachara, J.M., Fredrickson, J. K., 2012. Molecular underpinnings of Fe(III) oxide reduction by *Shewanella oneidensis* MR-1, Frontiers in Microbiology, Microbiol. Chem. Vol.3, Article 50.

Silver, S., Phung, L,T., 2005. Genes and enzymes involved in bacterial oxidation and reduction of inorganic arsenic. Appl. Environ. Microbiol. 71, 599–608

States, J.C., Srivastava, S., Chen, Y., Barchowsky, A., 2009. Arsenic in cardiovascular disease, Review, Toxicol. Sci. 107(2), 312-323

Van der Zee, F.P., Cervantes, F.J., 2009. Impact and application of electron shuttles on the redox (bio)transformation of contaminants: A review, Biotechnol. Adv. 27, 256–277.

Van Lis, R., Nitschke, W., Duval, S., Schoepp-Cothenet, B., 2013. Arsenics as bioenergetic substrates, BBA-Bioenergetics, 1827, 176–188.

Walker, S.R., Parsons, M.B., Jamieson, H.E., Lanzirotti, A., 2009, Arsenic mineralogy of near-surface tailings and soils: influences on arsenic mobility and bioaccessibility in the Nova Scotia gold mining districts, Can. Mineral. 47 (3). 533-556.

Waychunas, G.A., Rea, B.A., Fuller, C.C., Davis, J.A., 1993. Surface chemistry of ferrihydrite: Part 1. EXAFS studies of the geometry of coprecipitated and adsorbed arsenate. Geochim. Cosmochim. Acta 57, 2251–2269.

Waychunas, G.A., Davis, J.A., Fuller, C.C., 1995. Geometry of sorbed arsenate on ferrihydrite and crystalline FeOOH: Re-evaluation of EXAFS results and topological factors in predicting sorbate geometry, and evidence for monodentate complexes. Geochim. Cosmochim. Acta., 59, 3655–3661.

White, G.F., Shi, Z., Shi, L., Wang, Z., Dohnalkova, A.C., Marshall, M.J., Fredrickson, J.K., Zachara, J.M., Butt, J.N., Richardson, D.J., Clarke, T.A., 2013. Rapid electron exchange between surface-exposed bacterial cytochromes and Fe(III) minerals, PNAS, 110, 16, 6346–6351.

WHO, World Health Organization 2003. Arsenic in Drinking-water, Background document for development of WHO Guidelines for Drinking-water Quality, WHO/SDE/WSH/03.04/75

Wilkie, J.A., Hering, J.G. 1996. Adsorption of arsenic onto hydrous ferric oxide:effects of adsorbate/adsorbent ratios and co-occurring solutes, Colloid Surf. A: Physicochem. Eng. Aspects 107, 97–110.

Williams, M., 2001. Arsenic in mine waters: An international study. Environmental Geology,40(3), 267-278.

Yang, T.Y., Hsu, L.I., Chen, H-C., Chiou, H.Y., Hsueh, Y-M., Wu, M-M., Chen, C.L., Chen, C-J. 2013. Lifetime risk of urothelial carcinoma and lung cancer in the arseniasis-endemic area of Northeastern Taiwan, Journal of Asian Earth Sciences 77, 332-337.

CHAPTER 2

Solubility and stability of scorodite in the presence of *Shewanella* sp. CN32 and *Shewanella* sp. ANA-3 under variable phosphate concentrations

Erika Revesz[a], Danielle Fortin[a*], Dogan Paktunc[a,b,*]

Manuscript to be submitted to a journal

Abstract

Mining and mineral processing operations may generate a wide range of As-rich compounds including scorodite ($FeAsO_4 \cdot 2H_2O$), a common secondary arsenate found in some gold mine tailings. Scorodite has a low solubility in a limited pH range and is relatively stable under near-surface conditions, but our understanding of its reductive dissolution under the influence of bacteria is less well known. Considering that reducing conditions may develop in mine tailings with depth under prolonged disposal conditions, the present study was undertaken to determine the influence of bacteria on the reductive dissolution of scorodite. Two well characterized dissimilatory iron and arsenic reducing bacteria, i.e., *Shewanella* sp. ANA-3 and *Shewanella putrefaciens* CN32, were used in a chemically defined medium, at circumneutral pH, containing various phosphate concentrations (i.e., 15, 40 and 400 μM). Both types of bacteria caused the reductive dissolution of scorodite, but *Shewanella* sp. ANA-3 was more efficient, under the conditions of the experiment than *Shewanella putrefaciens* CN32 at reducing Fe(III) and As(V), based on both, the initial rates of reduction, and the plateau concentration of reduced species formed in the aqueous phase. The initial rate of reduction was found to increase with increasing phosphate concentration, however, plateau concentrations of the dissolved reduced species, Fe(II) and As(III), formed in the aqueous phase were highest at the lowest phosphate concentration.

Analysis of the solid phase of the post-reduction biotic samples by synchrotron X-ray absorption spectroscopy (XAS) and powder X-ray diffraction (XRD), scanning,

transmission and high resolution electron microscopy (SEM/TEM/HRTEM) and energy dispersive spectrometry (EDS) indicates that the reduced samples contain mainly scorodite, a biogenic Fe(II)-As(III) compound, parasymplesite ($Fe_3(AsO_4)_2 \cdot 8H_2O$) and tooeleite ($Fe_6(AsO_3)_4(SO_4)(OH)_4 \cdot 4H_2O$). In the aqueous phase, the concentration of the dissolved As(III) was close to 3 mM and the dissolved Fe(II) about 1.5 mM for ANA-3, and for CN32 the dissolved As(III) was about 2.3 mM and Fe(II) about 1.2 mM depending on the phosphate concentration in the medium. Phosphate concentration has an effect on the concentration of the dissolved species and on the formation of secondary mineral phases. Thus, these factors must be taken into account when scorodite is considered for use as a compound to sequester arsenic.

1. Introduction

Anthropogenic activities such as mining of gold and base metal ores, and related metallurgical processing including gold roasters and base metal smelters can result in the generation of significant arsenic concentrations in the waste products (Vaughan, 2004; Paktunc, 2008a, 2009). For instance, roasting operations at the Giant Mine alone produced 237,000 tons of arsenic trioxide dust, currently stored in sealed underground chambers at the mine site. Mine tailings produced from the gold mining and processing operations at the Ketza River Mine contain significant As concentrations reaching to ~7 wt % (Paktunc et al. 2003), which amounts to ~ 17,000 tons of arsenic in the tailings.

Pyrite (FeS_2) one of the principal Au-bearing minerals in some refractory gold ores is enriched in arsenic. Residual pyrite and its oxidation products formed during pressure-leaching, roasting and bacterial oxidation to liberate the gold constitutes one of the primary sources of arsenic in mining and metallurgical wastes (Paktunc, 2008b; Paktunc et al. 2013). Under atmospheric conditions, arsenic can be released into the environment as a result of the oxidative dissolution of pyrite which may be present in mine tailings, sludge and waste rock.

Scorodite ($FeAsO_4 \cdot 2H_2O$), an important arsenic carrier occurring in near surface environments, can form as a result of As-pyrite and arsenopyrite oxidation and as a precipitate from mine drainage and effluents (Paktunc et al. 2004; 2008a, Walker et al. 2009 ; Corriveau et al., 2011). Under acidic conditions, scorodite forms as a result of the oxidation of arsenopyrite (FeAsS) or As-bearing pyrite (FeS_2) (Drahota and Filippi, 2009). Other As-bearing minerals include arsenical ferrihydrite originating from waters from mine sites and tailings and weathering of gangue minerals from processing gold ores.

Scorodite has the potential for stabilize arsenic in mine effluents because of its high arsenic removal capacity, relatively low iron demand (Riveros et al. 2001), and its formation from ferric arsenate solutions at atmospheric conditions (Paktunc et al. 2008c). Consequently, the stability and solubility of scorodite has been the subject of many investigations. Scorodite has a relatively low solubility, Ksp = 10^{-24} to 10^{-26} (Langmuir, 2006; Paktunc and Bruggeman, 2010; Majzlan et al. 2011) therefore, it can control arsenic concentrations in tailings pore waters within a very narrow pH range. Recently, Paktunc and Bruggeman, (2010) investigated the

solubility of nanocrystalline scorodite and found that particle size did not influence its solubility, as is the case for crystalline scorodite. The solubility of scorodite is pH dependent (ibid), and it dissolves incongruently above pH ~3 (Krause and Ettel, 1989; Harvey et al. 2006. Dissolution of scorodite leads to the formation of iron oxyhydroxides (such as ferrihydrite) above pH ~2.5 and to the release of arsenate into solution (Langmuir, 2006 and references therein; Paktunc and Bruggeman, 2010; Majzlan 2011).

Although scorodite has a relatively low solubility in a narrow pH range and in the absence of bacteria, it can undergo microbial reductive dissolution resulting in the release of As(V) when dissimilatory iron reducing bacteria (DIRB) are used (Cummings et al. 1999; Papassiopi et al., 2003), resulting in the release of As(III) when dissimilatory arsenic reducing bacteria (DARB) are used (Newman et al., 1997). Drewniak et al., (2009, 2010) at the Zloty Stok gold mining site found scorodite and a variety of bacteria including dissimilatory arsenate reducers which reduced As(V) in scorodite to As(III) and released it to the groundwater. As(III) is more mobile and more bioavailable than As(V), and As(III) has a much higher affinity for sulfhydryl (-SH) groups of proteins than As(V). The -SH groups are part of the catalytic sites of many enzymes, and As(III) blocks these sites more readily than As(V), inactivating up to 200 enzymes such as pyruvate kinase, pyruvate dehydrogenase, thioredoxin, glutathione reductase, S-transferase and peroxidase, thioredoxin reductase and peroxidase and enzymes which repair DNA, such as poly(ADP-ribose) polymerase-1 (PARP-1), etc. (Shen et al. 2013). All of these

enzymes have crucial functions in the human body and their inactivation by As(III) has severe health consequences.

No previous systematic studies were found in the literature on the microbial reduction of scorodite that used bacteria which can function both as dissimilatory iron and arsenic reducers. In our studies we used bacteria, *Shewanella* sp.ANA-3 and *Shewanella putrefaciens* CN32, that can reduce both Fe(III) and As(V) resulting in the simultaneous formation Fe(II) and As(III).

Arsenic respiring microorganisms are fairly common in nature, and belong to several genera in the domain of Bacteria and also Archaea (Macur et al., 2004; Oremland and Stolz, 2005; Stolz et al. 2006). A phylogenetic tree based on 16S rRNA sequences of bacteria and archaea that are capable of transforming arsenic in a variety of habitats and range of environmental conditions was recently published by Cavalca et al. (2013). The dissimilatory arsenic reducing bacteria (DARB) are metabolically diverse and capable of using different organic compounds as electron donors including lactate, acetate, butyrate, pyruvate, malate etc. (Newman et al., 1998) and electron acceptors, such as Fe^{3+} in iron oxides, sulphate and nitrate (Lovely, 2001). The genus *Psychrobacter* was recently reported to have As(V) reducing ability (Liao et al., 2011), whereas *Sulfurospirillum barnesii* has been found to be able to respire a broad spectrum of potential electron acceptors including As(V) and Fe(III) (Zobrist et al. 2000).

Phosphate, especially at high concentrations, can enhance the desorption of As because of competition for adsorption sites (Smedley, D.G. Kinniburgh, 2002). Phosphate also can influence bacterial activity by adsorbing on the solid surface of

the scorodite which alters surface reactivity (Borch et al. (2007), and can influence the formation of post-reduction secondary mineral phases. Although Newman et al., (1997) used 1 mM phosphate, and Papassiopi et al., (2003) used 0.72 mM phosphate, which are within the range of typical 0.1-1.5 mM phosphate concentrations in tailings pore waters (Langmuir et al. 1999; Praharaj and Fortin, 2008), the bacteria they used only reduced either As(V) or Fe(III), but not both. Microbial reduction studies involving ferrihydrite have been performed at different phosphate concentrations (Frederickson et al., 1998; Kukkadapu et al. 2004; Borch et al. 2007; Amstaetter et al., 2012). Kukkadapu et al. (2004) found that the phosphate concentration has a significant effect on the extent of reduction and biotransformation of ferrihydrite, with the formation of vivianite at 20 mM phosphate concentration. Other examples of microbial reduction of ferrihydrite at 4mM phosphate concentrations resulted in the formation of secondary phases of siderite and vivianite (Fredrickson et al. 1998), and magnetite, vivianite and green rust (Borch et al. 2007). Amstaetter et al. (2012) reported that phosphate decreased the reduction rates by adsorption onto ferrihydrite and blocked the surface sites. Comparable microbial reduction studies using different phosphate concentrations have not been done for scorodite previous to our study.

In this paper, we examine the relative scorodite reducing abilities of two different bacterial strains, *Shewanella putrefaciens* CN32 and *Shewanella* sp. ANA-3 at three different phosphate concentrations (15, 45, 400 μM) representative of the natural environments, and provide the characterization of the secondary solid phases by X-ray diffraction, X-ray absorption fine structure spectroscopy and

scanning and transmission electron microscopy. In a sister paper, we provide our results on the microbial reduction of arsenical 6-line ferrihydrite. The goals of these two reduction studies are to report experimental evidence that can be used to help predict the potential fate of arsenic in mine wastes and tailings subjected to bacterial action, and consequently to better assess the solubility and stability of scorodite and arsenical 6-line ferrihydrite in the environment.

2. Materials and methods

2.1. Scorodite synthesis

Scorodite samples were prepared at the CANMET laboratories in Ottawa, Canada, using 0.2 M $Fe(SO_4)_{1.5}$ and 0.2 M Na_2HAsO_4 solutions heated at 70 °C and adjusted to pH 2 in a batch mode as described by Paktunc et al., (2008). Gamma-radiation was used to sterilize the samples prior to their use in the microcosms. The total exposure was 48 kGray. According to McNamara et al. (2003) and Langley et al. (2009), gamma radiation causes little physical and mineralogical changes. The synthetic scorodite was characterized by X-ray diffraction (XRD) using a Rigaku rotating anode X-ray powder diffractometer with a Cu Kα radiation at 55 kV, 180 mA, a step-scan of 0.04° and a scan rate of 1 and 2° /min in 2θ.

2.2. Maintenance and growth of the bacterial strains

Shewanella sp. strain ANA-3 was provided by Dr. Chad Saltikov (University of California, Santa Cruz). *Shewanella putrefaciens* CN32 and *Shewanella sp.* ANA-3 were maintained on tryptic soy agar (TSA) at room temperature (~23 °C).

A chemically defined growth medium (CDM) was used for the anaerobic growth of both strains during the microcosm experiments. The medium contained 20 mM sodium lactate, 4.5 mM 1,4-piperazine-diethanesulfonic acid (PIPES) buffer, 0.01 mM nitriloacetic acid and trace element salts, including 0.1 mM $MgSO_4 \cdot 7H_2O$, 2.6 μM $MnSO_4 \cdot H_2O$, 0.15 mM NaCl, 3.2 μM $FeSO_4 \cdot 7H_2O$, 3.8 μM $CoCl_2 \cdot 6H_2O$, 6.1 μM $CaCl_2 \cdot 2H_2O$, 0.93 μM $NaMoO_4 \cdot 2H_2O$, 0.36 μM $CuSO_4 \cdot 5H_2O$, 0.19 μM $AlK(SO_4)_2 \cdot 12H_2O$, 1.5 μM H_3BO_3, 0.68 μM $Na_2WO_4 \cdot 2H_2O$, 0.91 μM $NiCl_2 \cdot 6H_2O$ (Langley et al., 2009). In order to test the effect of phosphate concentration on the reduction rates, the concentration of PO_4^{3-} (Na_2HPO_4) was progressively lowered from ~ 4 mM to 400 μM, 45 μM and 15 μM, which is far less than the usually recommended phosphate concentration of 3.9 mM (Glasauer et al., 2003).

Prior to the reduction experiment, a single colony of each strain was transferred aseptically from the TSA plates to 50 mL of autoclaved tryptic soy broth (TSB) at 23 °C and grown aerobically on a rotary shaker set at 160 rpm. After 24 hours, 0.5 mL of each culture was transferred into 50 mL of 50:50 TSB:CDM mixtures containing 30 μM phosphate. After another 24 hours, the sub-culturing procedure was repeated with 5:95 TSB:CDM mixtures containing 50 μM phosphate in order to acclimate the cells to the nutrient conditions of the CDM. The final step involved growing the bacteria in 100% CDM and 50 μM phosphate concentration for

36 h at 23 °C, prior to their use in the microcosms (containing either 400 μM, 45 μM or 15 μM of phosphate). Each final culture contained 0.5 μg/mL of total protein, based on the protocol used by Glasauer et al. (2003), which corresponded roughly to 10^8 cells/mL.

2.3. Microcosms setup and sampling

The biotic systems consisted of 150 mL of sterile CDM (containing 15 μM, 45 μM or 400 μM PO_4^{3-}) in 500 mL acid-washed, sterilized Kimax bottles. Synthetic scorodite (0.40 ± 0.02 g) was added to each bottle, which amounted to 11.5 mM of Fe(III) and As(V) in the form of $FeAsO_4 \cdot 2H_2O$. The pH was adjusted to 7.00 ± 0.03 by the addition of 3 drops of 6 M NaOH prior to placing the microcosm bottles into the anaerobic chamber. The Kimax bottles were wrapped with aluminum foil in order to avoid possible photochemical effects. The microcosm bottles were inoculated inside the anaerobic chamber. Abiotic control samples were identical to the biotic ones, but did not contain *Shewanella putrefaciens* CN32 or *Shewanella* sp. strain *ANA-3*. Sampling was performed at room temperature inside the anaerobic chamber (atmosphere of 5% H_2:95% N_2). Some of the experiments were conducted in triplicate (*Shewanella* sp. *ANA-3)* or duplicate (Control and *Shewanella putrefaciens* CN32). The reason for the duplicate runs for the control and *Shewanella putrefaciens* CN32 samples is that these experiments had been previously performed by the same authors with consistent results. However, in order to get a direct comparison of the 2 strains, they were run in duplicate at the same time as the experiments with *Shewanella* sp. *ANA-3.* Sub-sampling of each system

was performed right after the systems were inoculated (time 0) and then periodically at 24-hour intervals over a period of 7 days. For each sub-sampling, the bottles were first shaken vigorously and 10 mL aliquots were immediately removed into sterile 10 mL centrifuge tubes while the solid phase material remained suspended in the bottle. An aliquot of 7 mL of sample was passed through a 0.22 μm nylon syringe filter into another 10 mL centrifuge tube for the determination of dissolved Fe. The rest of the aliquots were used for total Fe, culturing, Eh and pH measurements. To prevent possible bacterial cross contamination during sampling, only one microcosm bottle was open at a time and after sampling, the bottle cap was rinsed with 70 % ethanol.

2.4. Cell counts

The Most Probable Number (MPN) method was used for cell counting and was performed as follows. A 0.5 mL sub-sample was aseptically removed from each bottle. From this sub-sample, 0.1 mL was used to prepare a 10 fold dilution series (five times) for cell count as described by Langley et al. (2009). The cells were placed onto sterile TSA plates and incubated at 23 °C for 24 to 48 hours prior to counting the colonies for both strains.

2.5. Chemical analyses

Redox potential measurements were performed inside the anaerobic chamber on a ~2 mL sub-sample from each microcosm bottle using a portable Eh meter and probe (Corning redox Platinum and Ag/AgCl combination electrode, Corning Inc.). The same sub-sample was then removed from the anaerobic chamber for the measurement of pH using a standard laboratory pH meter and probe (VWR). Dissolved iron and arsenic concentrations were determined immediately following each sampling after removing the samples from the anaerobic chamber.

The ferrozine method (Stookey, 1970) modified to allow for the analysis of small sample volumes (Pepper et al., 2010), was used for the determination of Fe(II) and Fe(III) concentrations. Iron(II) ethylenediammonium sulfate tetrahydrate 98% (Sigma-Aldrich) was used to prepare the Fe(II) standard, and the molar absorptivity of the Fe(II)-ferrozine complex was found to be 27884, which is in a good agreement with the literature value of 27900 (Stookey, 1970). A 0.5 mL aliquot of the filtrate was transferred into 4.5 mL of 0.5 M HCl, and used for the determination of dissolved Fe(II), arsenate, arsenite and phosphate. The dissolved Fe(II) concentration was determined by adding 100 μL of acidified filtrate to 900 μL of 4.06×10^{-4} M ferrozine (0.2 g L^{-1} in 0.25 M HEPES, N-2-hydroxyethylpiperazine-N'-2-ethanesulfonic acid buffer, Sigma-Aldrich). The absorbance of this solution was measured within 15 minutes at 562 nm using an Ultrospec 1100 Pro UV/VIS spectrophotometer (GE Healthcare). A 0.5 mL aliquot of unfiltered suspension was mixed with 0.5 mL of 12 M trace metal grade HCl, to dissolve the solids, and this

solution was used for the determination of bulk Fe(II) in solution and suspended solids combined. A 1.00 mL aliquot of this solution was diluted to 5.00 mL of Millipore deionized water, and 100 μL of this diluted solution was mixed with 900 μL of reducing agent, 0.28 M hydroxylamine hydrochloride in a 0.28 M HCl solution. After allowing 40 minutes for the reduction of Fe(III), 100 μL of this solution was added to 900 μL of the ferrozine solution, and the absorbance was measured after 20 minutes.

The dissolved Fe(III) concentration in the filtered samples was determined as the difference between the Fe(II) concentration after hydroxylamine reduction and the Fe(II) concentration prior to reduction (Viollier et.al. 2000; Pepper et. al. 2010).

The dissolved As(III) (arsenite), As(V) (arsenate) and phosphate concentrations were determined with the spectrophotometric molybdenum blue method developed by Johnson and Pilson (1972) and modified by Dhar (2004). Arsenate and phosphate form a blue colored complex with reduced molybdate which absorbs at 880 nm, while arsenite does not. Three portions of a given sample were used to determine the concentration of these three species. One portion was treated with a reducing agent, sodium metabisulfite $Na_2S_2O_5$ with sodium thiosulfate $Na_2S_2O_3 \cdot 5\ H_2O$, which reduces arsenate to arsenite. This reduced portion mixed with the molybdate color agent had an absorbance A_{Red}, related to phosphate concentration. A second portion mixed with a color agent gave an absorbance A_{Untr}, which was the sum of the absorbances due to arsenate and phosphate.

$A_{Untr} - A_{Red}$, the difference between the absorbance for the untreated sample (Untr) and the reduced sample (Red), provided the absorbance due to arsenate. A third

portion of the sample was treated with an oxidizing agent KIO_3, which oxidizes arsenite to arsenate. A_{Ox}, the absorbance for the oxidized sample mixed with the color agent was the sum of the absorbance values of phosphate and total arsenic. Therefore, $A_{Ox} – A_{Untr}$ equals the absorbance of arsenic proportional to the arsenite, As(III) concentration.

Standard mixtures of known concentrations of arsenite, arsenate and phosphate were used to validate the molybdenum blue method. As a further check on this method, total arsenic, total phosphorus, arsenite and arsenic where determined by inductively coupled plasma – optical emission spectroscopy (ICP-OES) using a Varian Vista–PRO CCD. The arsenite was isolated as the eluent obtained by passing a sample of filtrate through a solid phase extraction cartridge (Waters, Sep-Pak Plus) which retains the anionic species arsenate and phosphate, but does not retain $As(OH)_3$ at the pH condition used for separation.

2.6. Solid phase characterization

XRD analyses of the bacterial post-reduction samples were carried out after washing and centrifuging the solids five times, and drying under N_2. A small amount of the powdered sample was placed in a 0.5 or 0.7 mm diameter glass capillary tube and sealed with carnauba wax in the anaerobic chamber. The samples were kept in sealed containers, mounted on zero background plates and analyzed at CANMET with a Rigaku rotating anode X-ray powder diffractometer with Cu K_α radiation at 50 kV, 260 mA, a step-scan of 0.04° and a scan rate of 1 and 2° /min in 2θ.

2.7. Electron microscopy analysis

The sample preparation for field emission electron microscopy (FE-SEM) was done by suspending a few mg of the solid sample in 99% ethanol, sonicating for 5 minutes and then placing one drop of the suspension onto a 300 mesh copper grid. After 10 minutes of drying, the sample was placed in the sample holder of the JEOL JSM-7500F Field Emission SEM equipped with an Oxford Instruments Silicon detector (University of Ottawa's Centre for Catalysis Research and Innovation (CCRI)). The sample was analyzed at 1 kV accelerating voltage in a lower secondary electron imaging mode.

For environmental SEM analysis, a thin layer of the dry powdered sample was placed on a sticky carbon tape and analyzed using a JEOL JSM-6510LV SEM in low vacuum mode at 30 Pa in the Department of Earth Sciences at the University of Ottawa. For energy dispersive X-ray spectrometry (EDS) analysis, the X-Max Large Area Silicon Drift Detector (SDD) with a 20 mm^2 active area was used. The applied accelerating voltage was 20kV. The instrument was calibrated with a Cu tape, and the EDS spectrum was collected in the *Analyzer Mode* of the INCA Energy 350 spectrum analyzer software.

For transmission (TEM) and high resolution transmission electron microscopy (HRTEM) examination, the method of sample preparation was the same as for the FE-SEM. The Cu grid with the sample was placed into a JEOL JEM -2100F Field Emission Electron Microscope equipped with Oxford Instruments Silicon detector at the CCRI, University of Ottawa. The applied voltage was 200 kV and the current density 0.6 nA/cm^2.

2.8. X-ray absorption spectroscopy of arsenic and iron

X-ray Absorption Spectroscopy (XAS) measurements were carried out at the undulator and at the bending magnet beamlines of the PNC-CAT facility at the Advanced Photon Source, Argonne National Laboratory.

The undulator beamline, 20-ID, was equipped with a Si(111) monochromator with 10^{-4} eV resolution and a Vortex-ME4™ Silicon Drift Detector.

The sample was prepared as a thin layer powder distributed evenly on ~3 x 2 cm Kapton tape. The X-ray beam diameter used was 4 μm, and nine 12 dB low pass, low noise filters were used to prevent beam damage. The fluorescence measurements included two-dimensional mapping of the As K_α X-ray fluorescence intensity by using two slightly different As K-edge excitation energies. One was optimized to excite As(III) and the other to excite As(V). The two data sets were then superimposed in order to investigate the 2-D spatial distribution of As(III) and As(V) in the sample. Following fluorescence mapping, XANES spectra were collected from selected regions.

The second set of measurements were performed on bulk samples at the bending magnet beamline, 20-BM. This setup included a Si(111) monochromator, cryogenic apparatus, ionization chambers, Vortex-Si Drift detector, and a 13 element Ge detector. Sample preparation for these measurements, done in the anaerobic chamber, involved mixing the powdered sample with boron nitride to dilute the arsenic concentration to about 1 wt %. The samples were mounted in 15 x 4 mm Al sample holders, and sealed with Kapton tape, and were shipped to the measurement site in a sealed anaerobic container, and then stored in an anaerobic

chamber. The samples were positioned into the cryogenic apparatus at an angle of 45 degrees to the incident focused beam and to the Ge fluorescence detector. The K-edge transmission and fluorescence spectra were collected simultaneously at -91 ± 0.5 K, using a beam size of 3500 x 800 μm. Gold foil was used as a reference to monitor the shift in the K-edge energy. Data analysis was done with ATHENA (0.8.856 2001-2008 Bruce Ravel) analysis software (Ravel and Newville, 2005).

3. Results

3.1. Reduction experiments

3.1.1. *Redox conditions and cell counts*

There was an initial small drop in pH after the bacteria were added to the microcosm, but the pH returned to the initial value of 7.00 +/- 0.03 at the end of the reduction experiments in all systems (Table S2.1, Supplementary information). The pH decreased from pH 7.00 +/- 0.03 to pH 6.83 in the abiotic control systems at all different phosphate concentrations. The initial redox values (Eh) were in the range of 350 mV to 400 mV for all systems at all phosphate concentrations (Figure 2.1). During the first 72 hours, Eh values decreased significantly in both biotic systems reaching values of 0 mV to -100 mV, whereas over the same time interval, Eh values of the abiotic controls decreased to 230 to 280 mV (Figure 2.1).

No viable bacterial cells were detected in the abiotic controls over the entire duration of the experiment. Initial cell counts in the biotic systems, were in the order of (1.2 to 1.4) x 10^8 CFU/mL for CN32 and (1.0 to 1.2) x 10^8 CFU/mL for ANA-3, which declined steadily over the course of the experiment to reach final values in the

orders of 7.9 x 10^4 to 3.2 x 10^5 CFU/mL for *Shewanella putrefaciens* CN32 and 2.5 x 10^5 to 3.2 x 10^5 for *Shewanella* sp. ANA-3, respectively (Figure 2.1 and Table S2.2, Supplementary information).

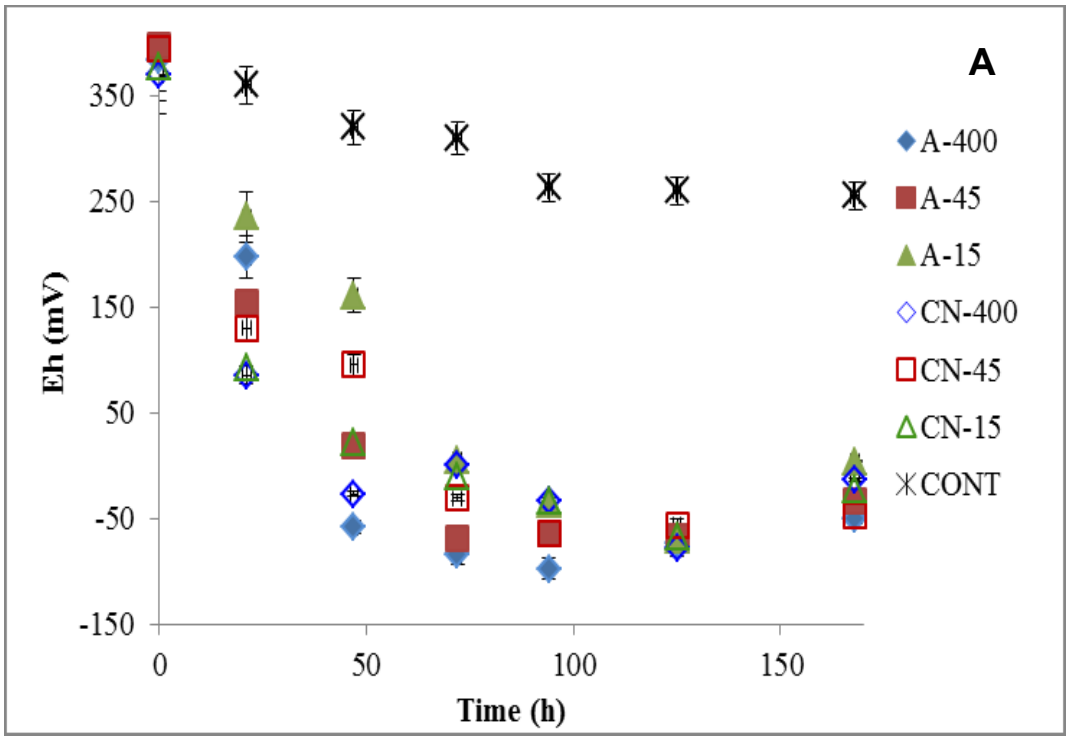

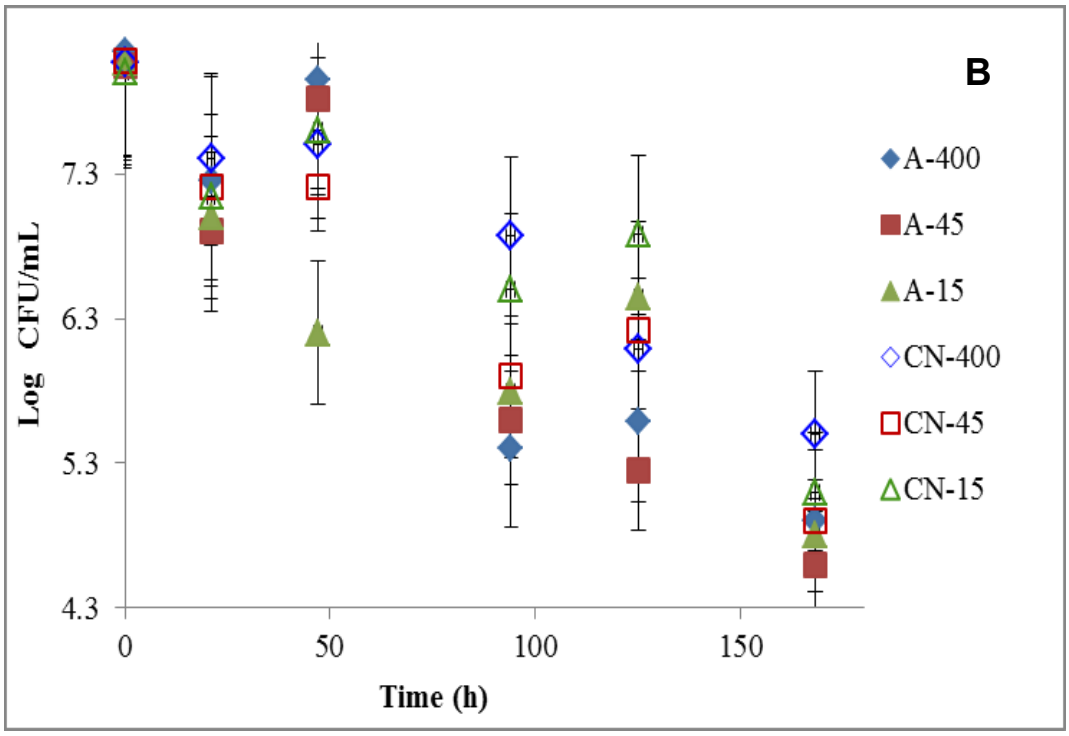

Figure 2.1. Redox conditions (A) and bacterial cell counts (B) during the reduction of scorodite in the control (CONT) and two biotic systems (labels on the charts represent A for ANA and CN for CN32) in the presence of 400, 45 and 15 μM of phosphate.

3.1.2. Fe and As speciation during microbial reduction

Both Fe and As were reduced and released into solution in all biotic systems (Figure 2.2 and 2.3), whereas only negligible amounts of dissolved Fe (II) and As (III) were present in the abiotic control systems. The plateau concentrations of dissolved Fe(II) and As(III) in all biotic systems at all phosphate concentrations were always greater in the systems containing the ANA-3 strain than those containing CN32 and also appeared greatest at the 15 μM phosphate concentrations (Figure 2.2 and 2.3).

Decreasing the concentration of phosphate in the growth medium appeared to delay the release of both dissolved Fe(II) and As (III). In other words, for ANA-3, the 15 μM and for CN32, the 45 μM phosphate concentration took longer to release iron and arsenic than those containing 400 μM (Figure 2.2 and 2.3).

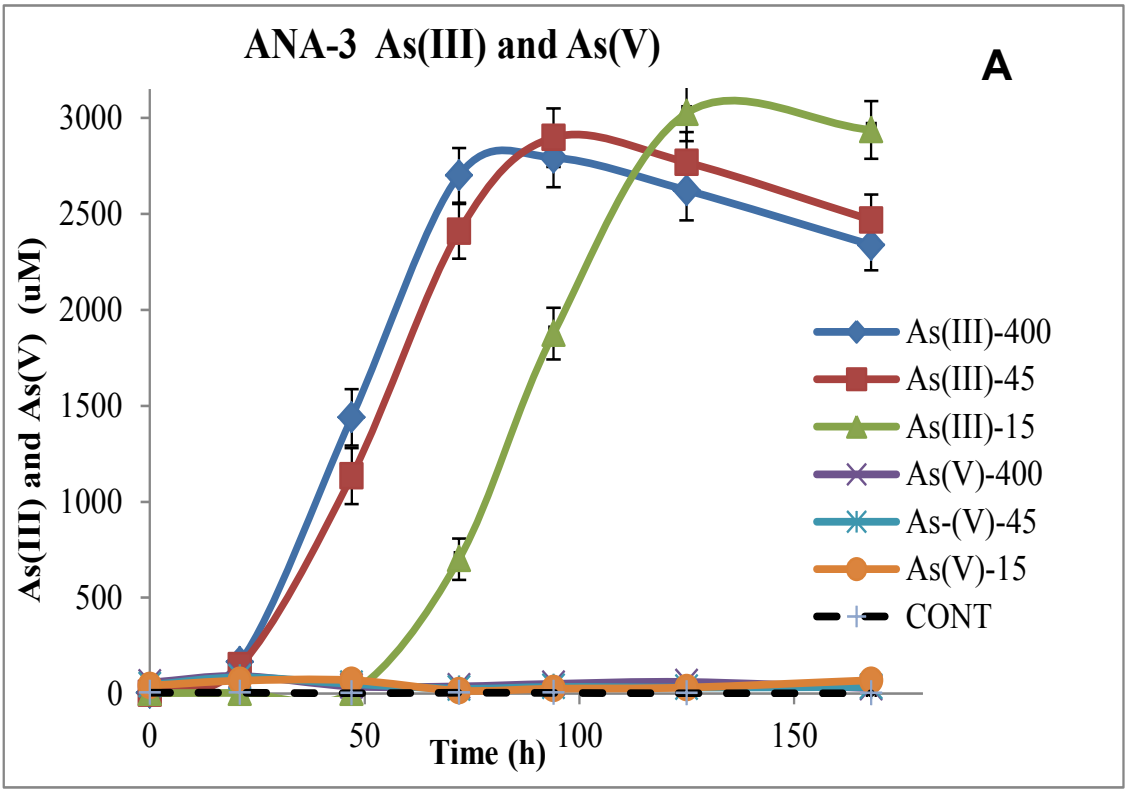

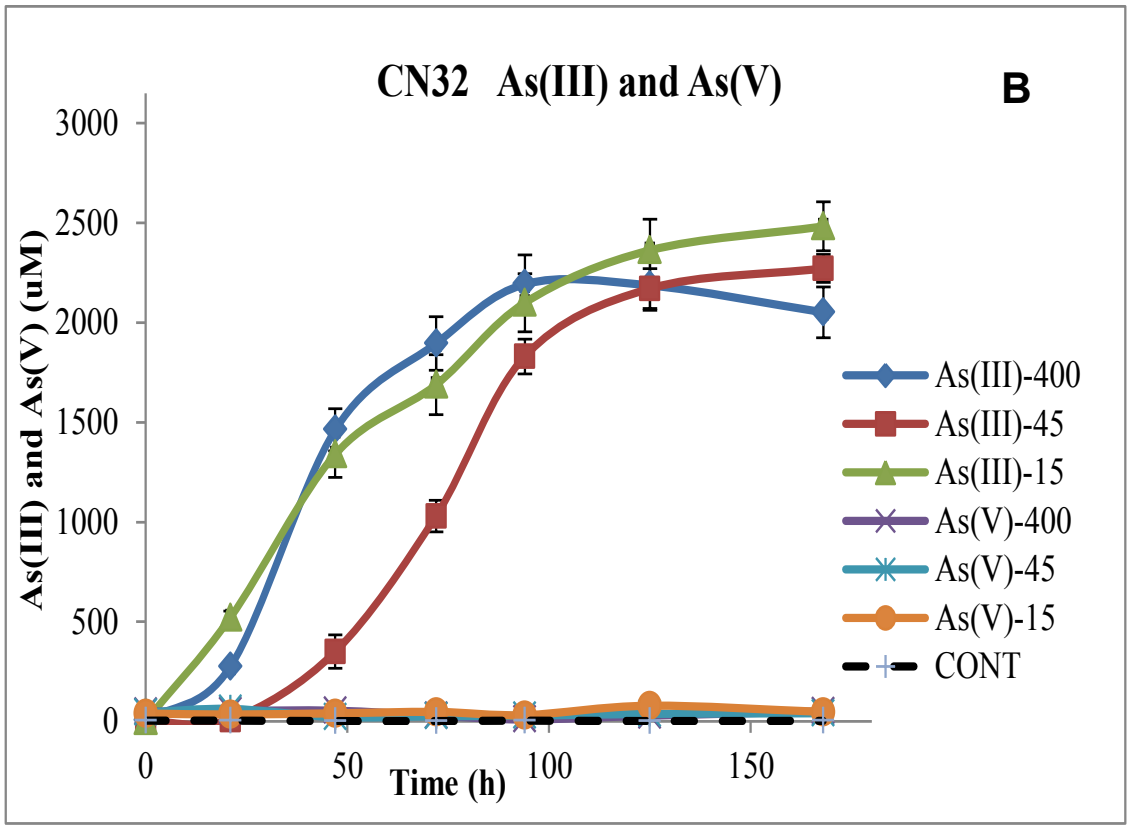

Figure 2.2. Release of dissolved As(III) and As(V) in the control and biotic systems (A) ANA-3 (B) CN32 in the presence of 400, 45 and 15 μM phosphate.

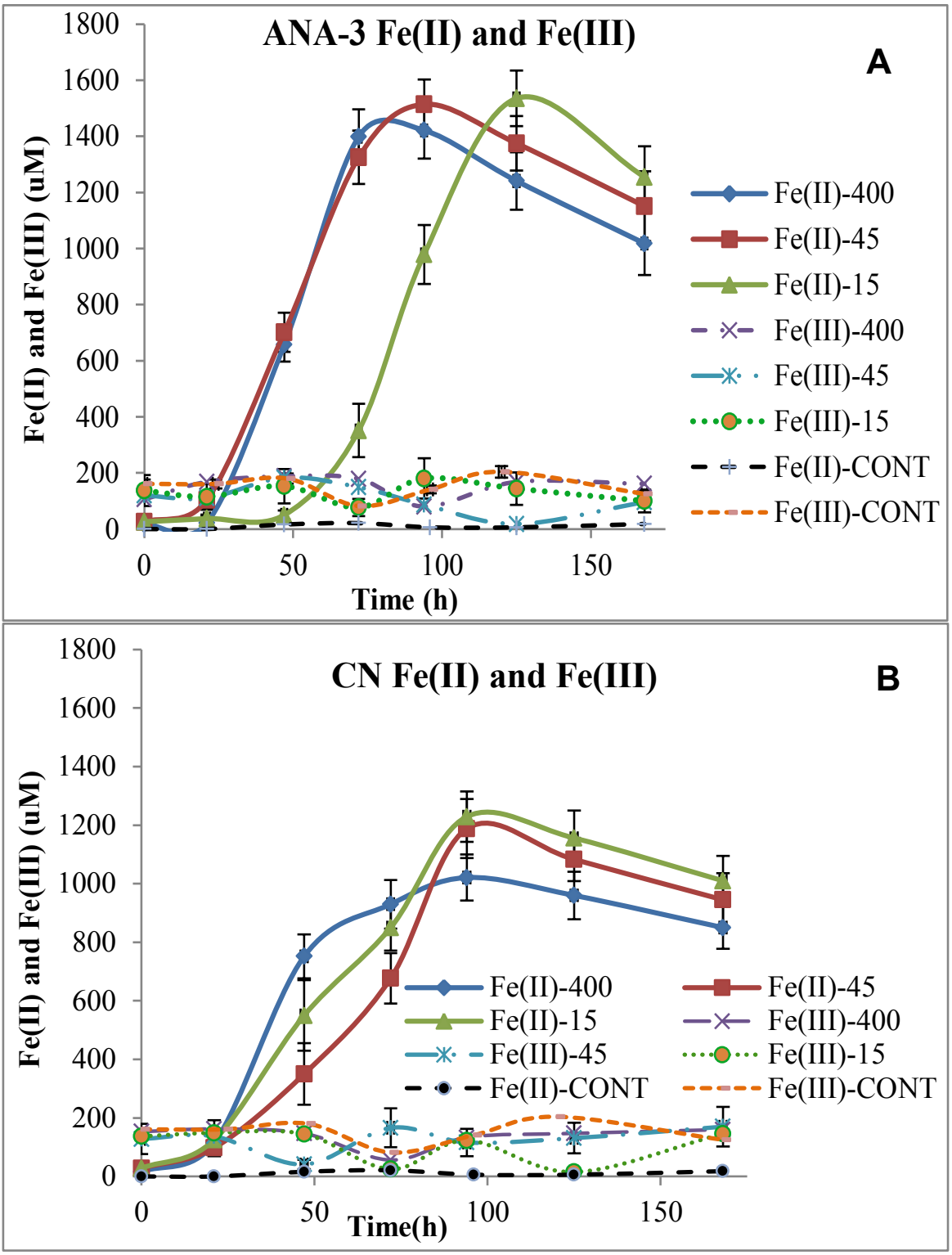

Figure 2.3. Release of dissolved Fe(II) and Fe(III) in the control and biotic systems (A) ANA-3 (B) CN32 in the presence of 400, 45 and 15 μM phosphate.

3.1.3. The effect of phosphate concentration on the initial reduction rates

Initial rates of reduction were determined from the initial linear section of the concentration-time plots for all kinetic runs. The results in Table 2.1 indicate that the initial reduction rates increased with increased phosphate concentrations.

Student's t-test calculations were done to determine if the differences in the calculated initial rates were in fact significant for the different phosphate concentrations for a given bacterial species. The results of the t-tests are summarized in Table S2.4 for As(III) and in Table S2.5 for Fe(II) (Supplementary information).

Table 2.1. Initial reduction rates with *Shewanella* sp. CN32 and *Shewanella* sp. ANA-3 at 15, 45 and 400 μM phosphate concentrations.

Phosphate Concentration (μM)	CN32 As(III) (μM/h)	CN32 Fe(II) (μM/h)	ANA-3 As(III) (μM/h)	ANA-3 Fe(II) (μM/h)
15	28.5 ± 1.8	14.7 ± 0.7	40.0 ± 3.0	23.3 ± 2.3
45	31.7 ± 2.4	14.6 ± 2.1	44.3 ± 3.0	23.9 ± 0.5
400	45.7 ± 1.0	24.2 ± 0.5	49.7 ± 0.4	27.0 ± 1.5

In the case of As (III) and Fe(II), the initial rates were significantly different between the 45 μM phosphate and 400 μM phosphate concentrations but the differences between the 15 and 45 μM phosphate concentrations for both strains of *Shewanella* were insignificant. The initial rates of reduction for the two bacterial strains at the same phosphate concentrations were significantly different (Tables S2.6 and S2.7) (Supplementary information).

3.1.4. The effect of phosphate concentration on the plateau concentrations of dissolved As(III) and Fe(II)

Table 2.2 summarizes the plateau concentrations of the dissolved As(III) and Fe(II) species, where both bacteria and all phosphate concentration were run at the same time for 170 hours. In the experiments with ANA-3, the concentration of As(III) was about 2800 μM for the 400 μM phosphate, and about 3030 μM for the 15 μM phosphate. The Fe(II) concentration was about 1420 μM for the 400 μM phosphate and about 1550 μM for the 15 μM phosphate concentration with ANA-3. A similar trend was found in the experiments performed with CN32. These results show that the reduced dissolved species, As(III) and Fe(II) concentrations were lower at the higher phosphate concentrations.

Table 2.2. Summary of the 170 h experiment with *Shewanella* sp. ANA-3 and CN32 strains based on the plateau of dissolved As(III) and Fe(II) concentrations at 15, 45 and 400 μM phosphate concentrations.

PO_4^{3-} (μM)	As (III) *(μM) ± 30 CN32	As(III) (μM) ± 30 ANA-3	Fe(II) (μM) ± 30 CN32	Fe(II) (μM) ± 30 ANA-3
15	2483	3025	1229	1545
45	2272	2897	1188	1514
400	2193	2793	1019	1415

***** The values shown with ± are the standard deviations.

3.2. Characterization of the pre and post reduction minerals

3.2.1. Bulk XRD analysis

The method of synthesis of crystalline scorodite, sample (10B1:1-9), used in all microcosm experiments and its detailed characterization can be found elsewhere (Paktunc et. al., 2008c.) The background subtracted powder XRD spectra of the post-reduction samples, reduced with *Shewanella* sp. CN 32 (middle), and with *Shewanella* sp. ANA-3 (top) at 45 μM phosphate concentrations, is shown in Figure 2.4.

The XRD patterns indicate the presence of residual scorodite in the post reduction biotic samples. In addition, there are lower intensity peaks marked by arrows labelled Ps centered at 2θ values of 10.77°, 13.06° and 29.67° corresponding to parasymplesite. Furthermore, the low intensity peak centered at 2θ 8.3° suggests the presence of tooeleite in the reduced samples.

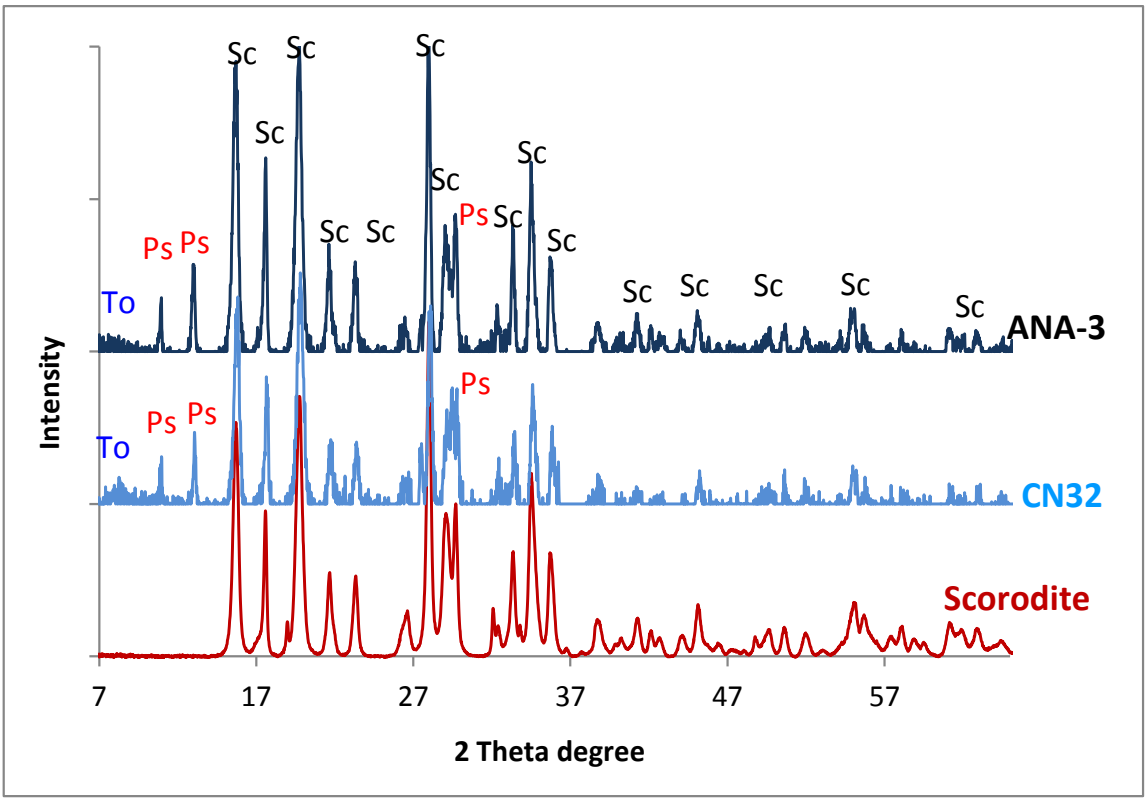

Figure 2.4. Background subtracted bulk XRD patterns of the scorodite control (CTN) and biotic ANA-3 and CN 32 reduced samples at 45 µM phosphate concentration after 170 hours of reduction. Labels are (Ps) parasymplesite, (To) tooeleite and (Sc) scorodite.

3.2.2. Electron microscopy analyses

Field-emission SEM (FE-SEM) imaging of the post-reduction samples in the presence of both bacterial strains at the various phosphate concentrations showed that scorodite with a platy morphology remained after 120 hours (Figures 2.5 A and B), and after 170 hours of reduction (Figures 2.5 C), along with fine reduced particles.

The biotic sample (FE-SEM Figure 2.5 A) for *Shewanella* sp. ANA-3 had a less flaky appearance than the *Shewanella* sp. CN32 sample (Figure 2.5 B), which suggests that the *Shewanella* sp. ANA-3 sample may be more reduced. A distinctly larger particle without a crystalline, platy morphology is characteristic of the scorodite post-reduction product (Figure 2.5 C, dotted-arrow). The platy structures of the remaining unreduced scorodite is visible in all of the post-reduction images, along with reduced amorphous particles (Figures 2.5 A, B, C and D).

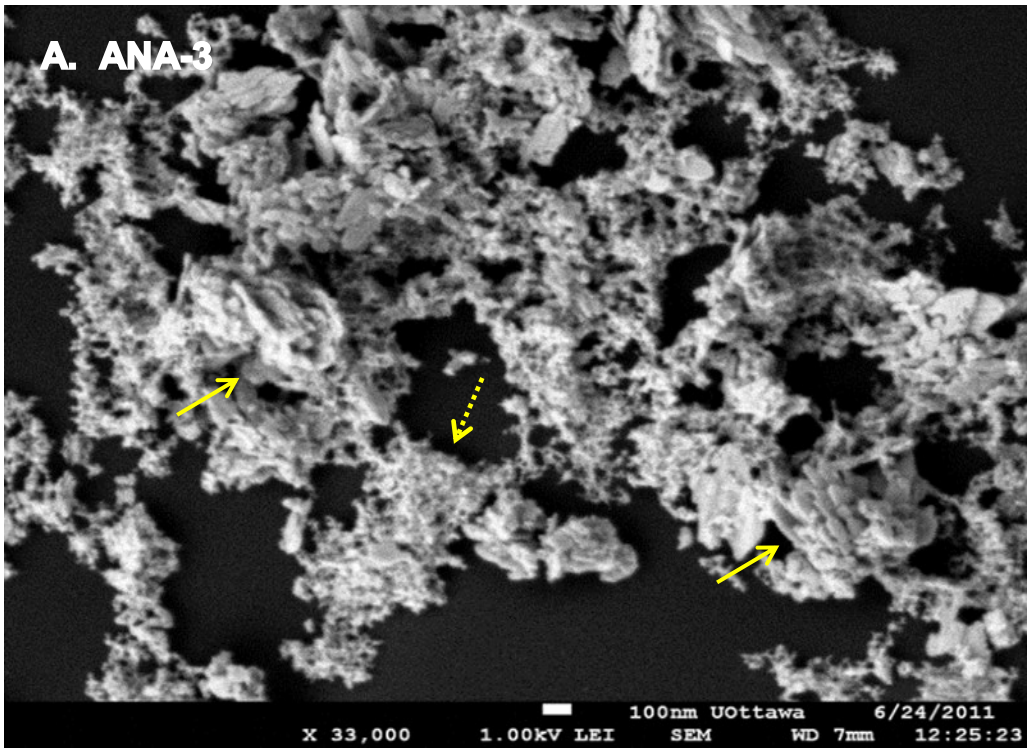

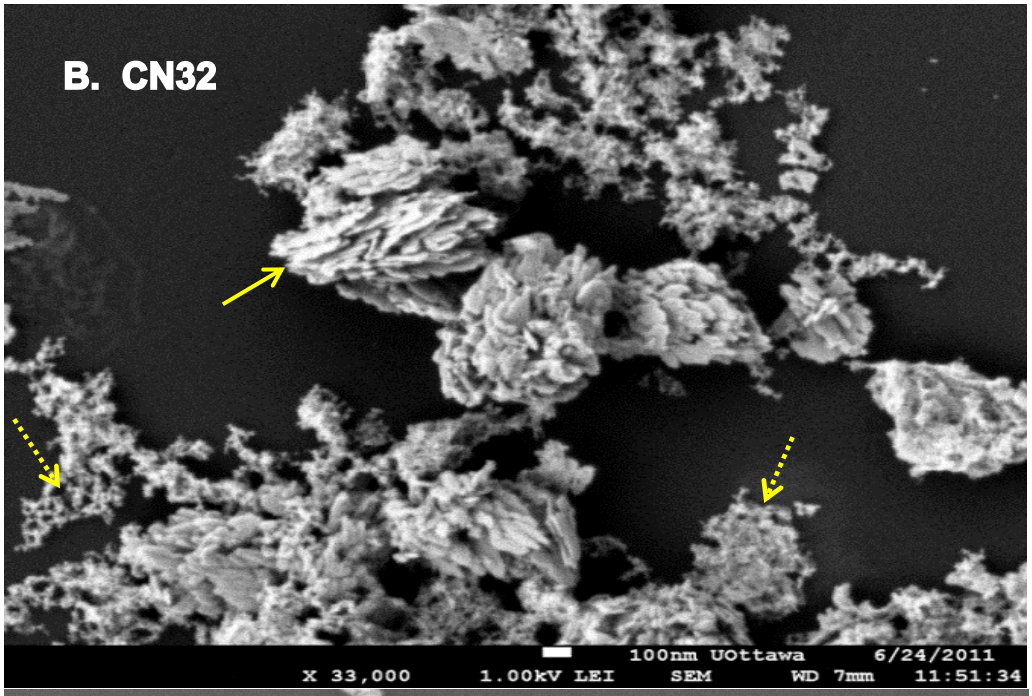
B. CN32
100nm UOttawa 6/24/2011
X 33,000 1.00kV LEI SEM WD 7mm 11:51:34

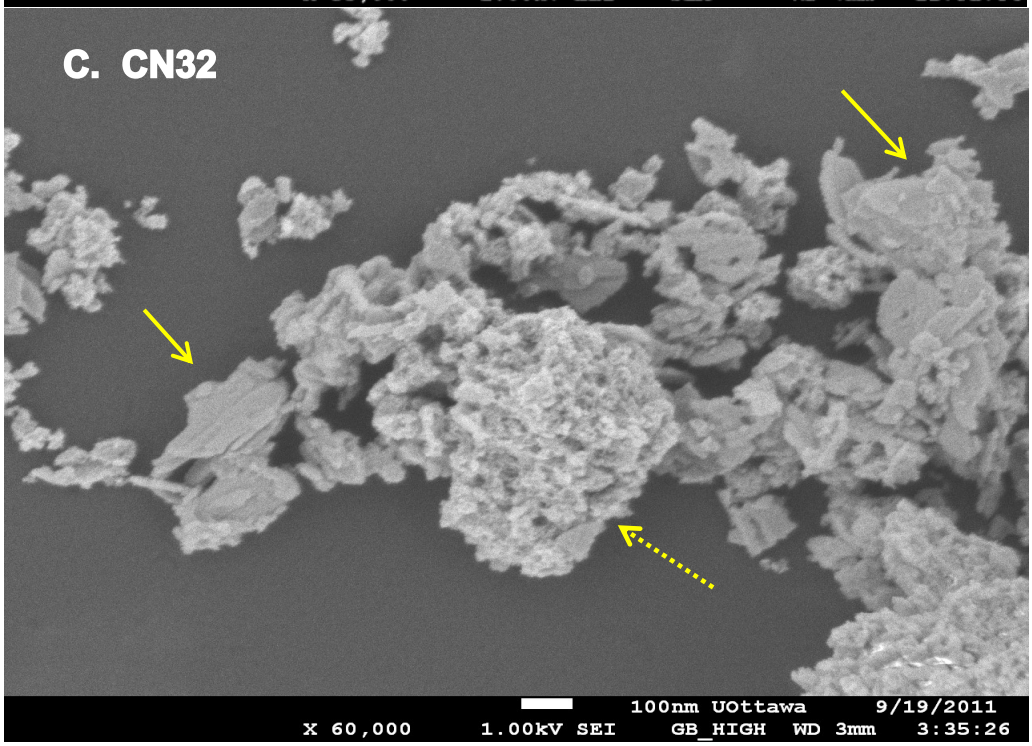
C. CN32
100nm UOttawa 9/19/2011
X 60,000 1.00kV SEI GB_HIGH WD 3mm 3:35:26

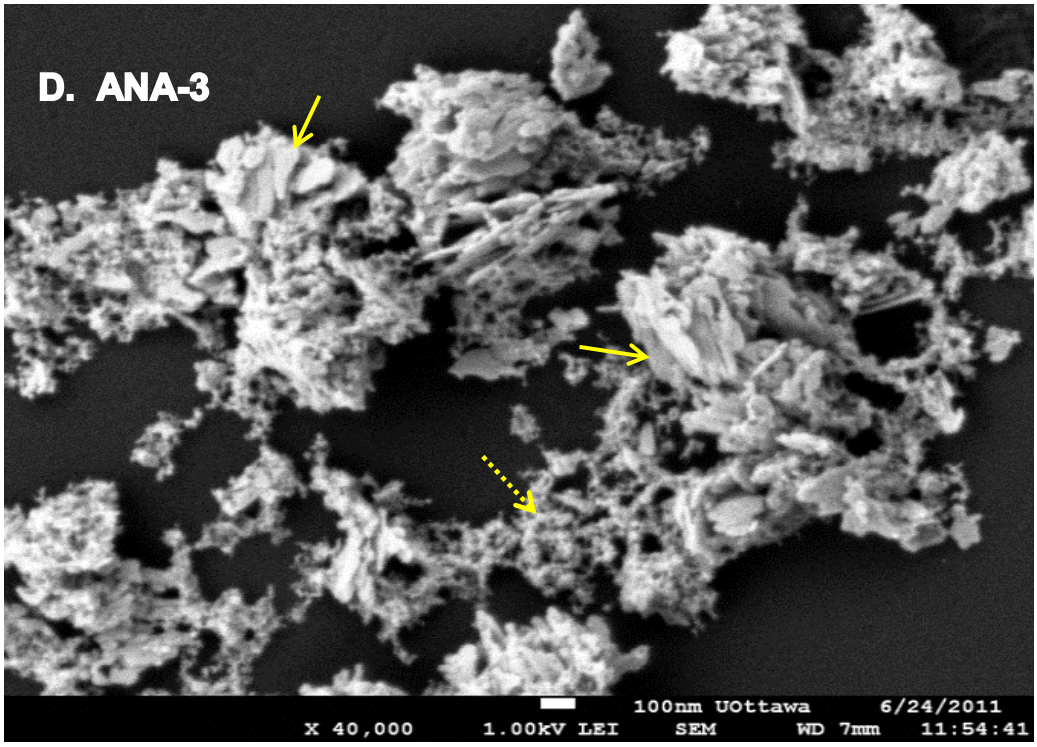

Figure 2.5. Field emission-SEM images of the biotic samples with (A) ANA-3 and (B) CN32. (A, B) 400 µM phosphate medium, 120 hours, (C, D) 45 µM phosphate medium after 170 hours. Unreduced scorodite, platy structures (arrows), biotic reduced structures (dotted arrows). Scale: 100 nm for all images.

The post-reduction product is also shown in Figure 2.6 with *Shewanella* sp. CN32 distributed on the surface after 120 hours of reduction in the 400 µM phosphate medium. In comparison to the control samples which have platy appearance, the reduced samples seem to have blobby irregular structures.

The results of the EDS analysis done on about 30 randomly selected solid particles for each phosphate concentration indicate that the reduced biotic samples have an overall Fe/As molar ratio greater than 1.

Since the sizes of the particles were not identical and the magnifications were not always the same, averaging of the Fe/As molar ratio is not given. In addition, when the averages of Fe/As molar ratios were calculated, the uncertainties were larger than the calculated averages, e.g. for the 15 μM phosphate with CN32 the average is 2.78 ± 3.4. The range of Fe/As molar ratios that were found for the randomly selected particles is shown in Table 2.3. For example, for CN32, the range of 1 to 7 means that various Fe/As molar ratios were found within that range.

Table 2.3. The range of Fe/As ratio as atomic % found on the surface of representative grains of reduced samples by semi-quantitative EDS analysis after 170 hours. The abiotic control Fe/As = 1/1.

Phosphate Concentration (μM)	***Shewanella* CN32 Fe/As Ratio by EDS**	***Shewanella* ANA-3 Fe/As Ratio by EDS**
15	(1 to 7) /1	(1 to 18) /1
45	(1 to 6) /1	(1 to 5) /1
400	(1 to 14) /1	(1 to 14) /1

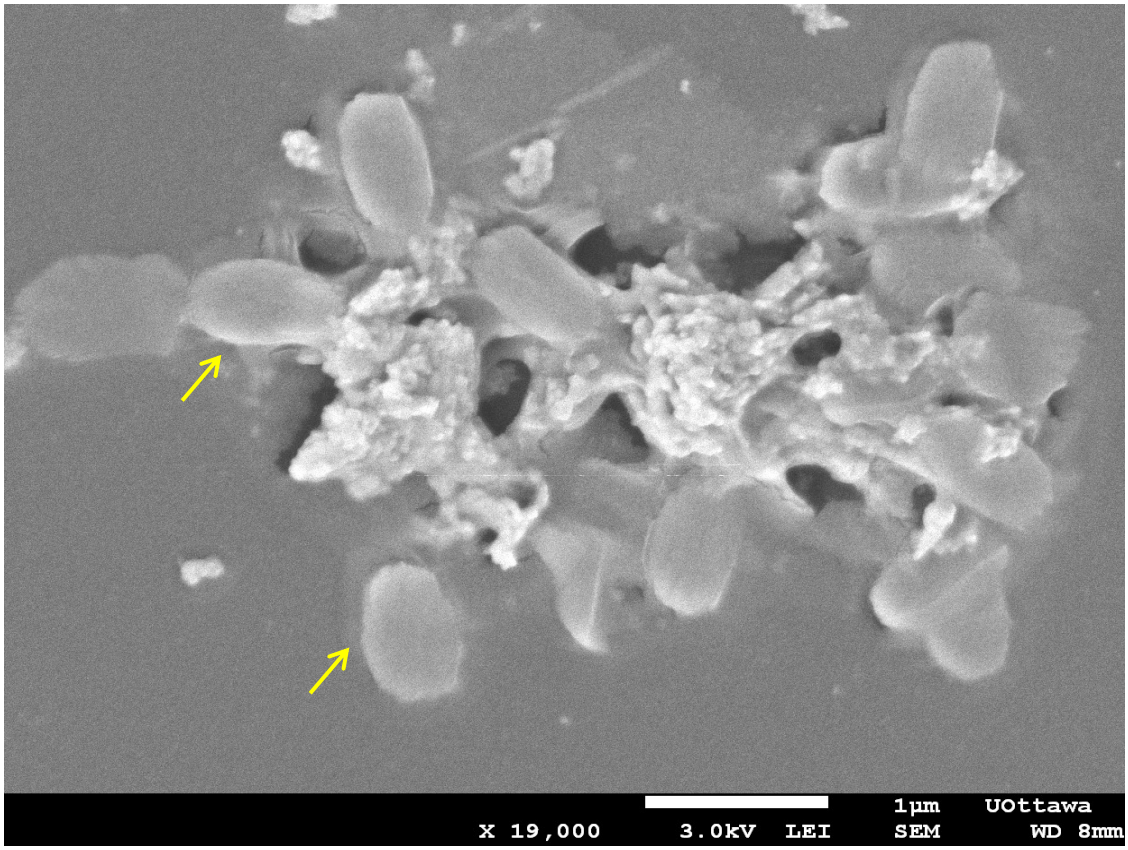

Figure 2.6. SEM image of *Shewanella putrefaciens* CN32, (arrows) with 400 µM phosphate medium at 120 hours of reduction. Scale 1 µm.

The TEM image on Figure 2.7 A depicts a post-reduction particle, with about 20 % more arsenic than iron, which resembles a material of biogenic origin.

The HRTEM image (Figure 2.7 B) of the area labelled by the arrow shown on Figure 2.7 A, revealed no periodic atomic rows as shown on the HRTEM images of the original samples by Paktunc et al. (2008c). The selected area electron diffraction (SAED) pattern on inset Figure 2.7 B has no diffraction rings, which suggests an amorphous structure resulting from bacterial reduction.

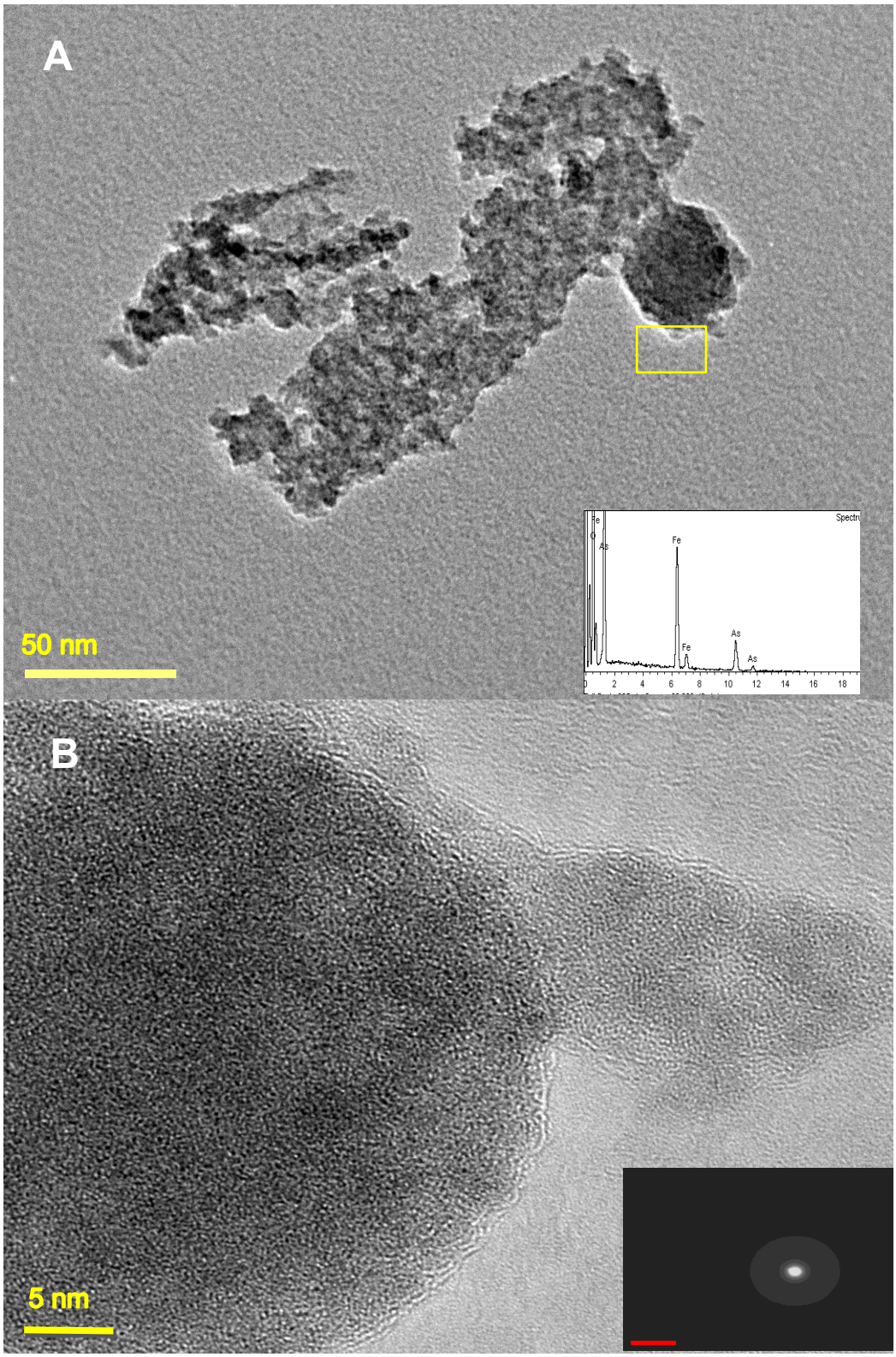

Figure 2.7. (A) TEM and (B) HRTEM images of post reduction particle in the presence of CN32 at 45 μM phosphate medium after 170 hours. Inset (A): EDS of

Fe and As peaks. (B) From the region labelled in (A). Inset on (B) is selected area electron diffraction (SAED).

3.2.3. X-ray absorption (XAS) spectroscopy:

The fluorescence maps of As(III) and As (V) (Figure 2.8), of the post reduction samples using *Shewanella* sp. ANA-3 (A) and *Shewanella* sp. CN32 (B) in a 45 μM phosphate medium, show distinct areas of high As(III) concentration (yellow), and areas of mixed As(III) and As(V) (red) and only As(V) (blue). The fluorescence maps illustrate a non-uniform or spatially heterogeneous distributions of regions rich in As(III) for both bacteria at all phosphate concentrations. The corresponding As K-edge XANES spectra (Figure 2.8 E) were collected to identify the As(III) and As(V) species in the distinct areas of the spatial distribution maps. The spectrum of scorodite (#4), not subjected to the biotic reduction experiments, is used as a reference for the location of the As(V) peak on the energy axis.

The bright yellow region on the fluorescence map indicates the highest As(III) concentration as shown by the prominent As(III) peak which is located at a lower energy than As(V) on spectrum #1. Spectra #2 and #3, having less prominent As(III) peaks, represent the less reduced regions (green and red regions of the map).

Normalized As K-edge XANES spectra of the post reduction solid samples of *Shewanella* ANA-3 and CN32 at all phosphate concentrations are shown in Figure 2.9 A. The As(III) peaks are, in general, more prominent for the ANA-3 than for CN32, and this observation is more apparent in the direct comparison between the two strains at the same phosphate concentrations shown in Figure 2.10.

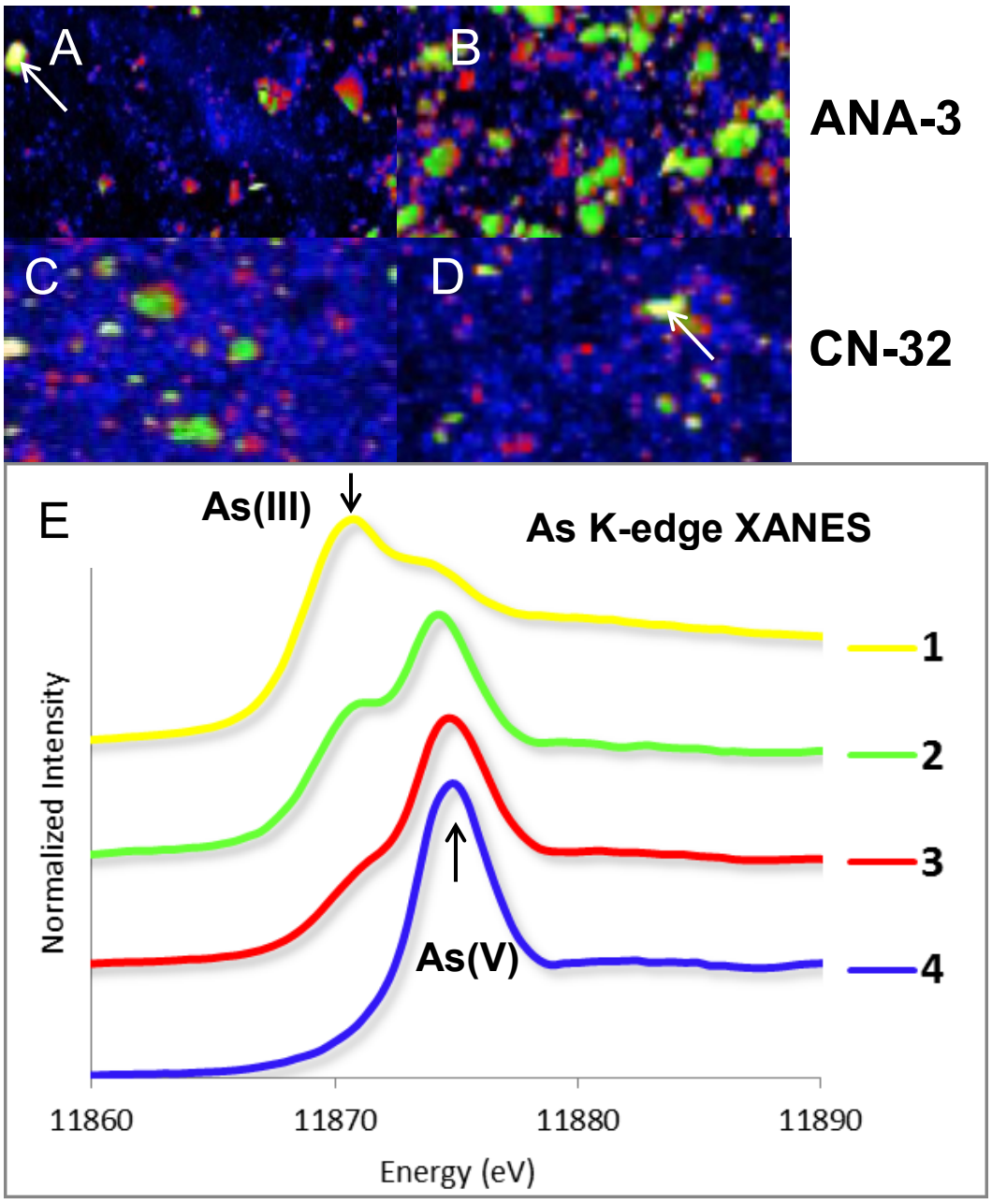

Figure 2.8. As X-ray fluorescence maps showing the spatial distribution of As(III) and As(V) in the biotic solid samples. (A, B) ANA-3 and (C, D) CN32, at 45 μM phosphate medium. The highest As(III) regions are labelled by the arrows, and #1 on the XANES spectra (E). As(V) is #4 on (E).

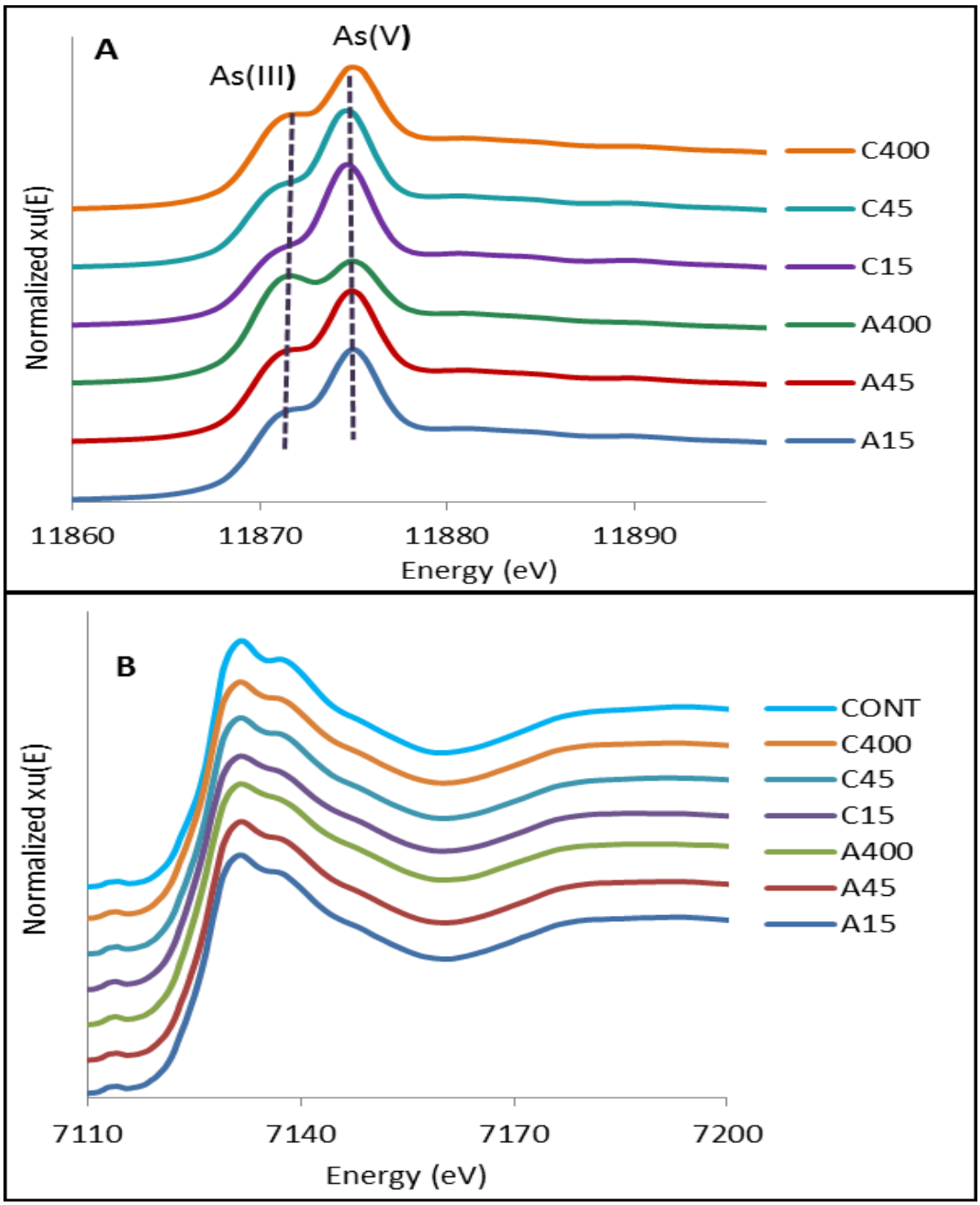

Figure 2.9. (A) The normalized As K-edge XANES spectra for As(III) and As(V) in the biotic solid samples at 15, 45 and 400 μM phosphate concentrations, labelled as A15, A45, A400 for ANA-3 and C15, C45 and C400 for CN32. (B) The normalized Fe K-edge XANES spectra.

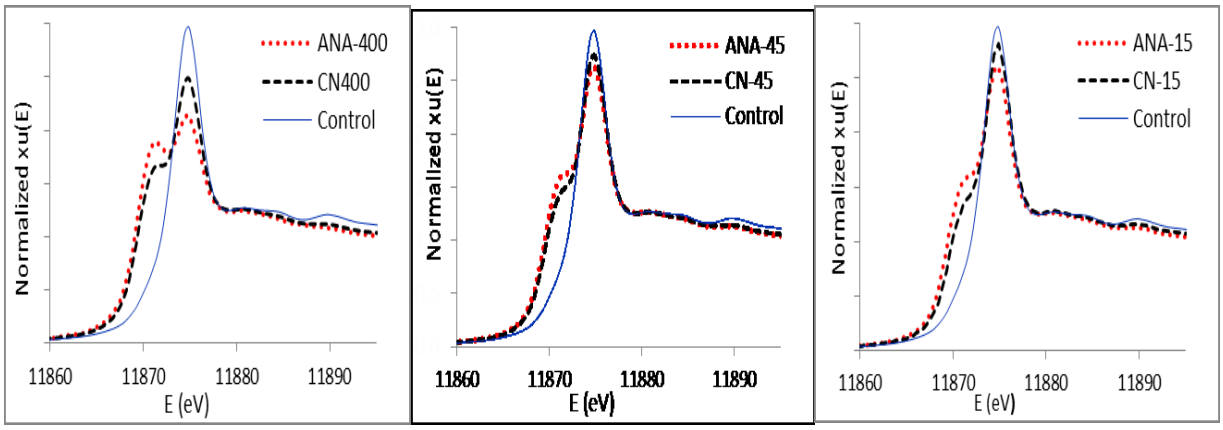

Figure 2.10. The normalized As K-edge XANES spectra of the biotic reduction products of ANA-3 and CN32 paired at 400, 45 and 15 μM and phosphate concentrations with the abiotic scorodite control.

The Fe K-Edge XANES spectra of the reduced samples at all phosphate concentrations are similar and resemble the spectrum of the abiotic control (Figure 2.9 B).

The fractional compositions of arsenic in the reduced samples were determined by least-squares fitting (Paktunc, 2003 and 2004) using over 27 inorganic and organic arsenic reference compounds, and the best fits were found with biogenic Fe(II)-As(III) mineral, tooeleite and the abiotic scorodite control. Representatives of the normalized XANES and the k^3-weighted EXAFS spectra of the end members that gave the best fit are shown in Figure 2.12.

The normalized As K-edge XANES fitting results of the As(III) listed in Table 2.4, indicate that the reduced sample is composed of 30 to 60 % scorodite, 35 to 60 % biogenic Fe(II)-As(III) and 3-6 % tooeleite, depending on the bacterial strain and phosphate concentrations used for the reduction.

The normalized As K-edge XANES fitting for both strains showed a good fit with biogenic Fe(II)-As(III) mineral, tooeleite and goethite for all phosphate concentrations (Figure 2.11 and 2.12 A).

Table 2.4. Fractional compositions of arsenic of the solid residues in the biotic samples obtained by the normalized As K-edge XANES least-squares fitting.

Compound	CN15	CN45	CN400	ANA15	ANA45	ANA400
Scorodite	0.604	0.551	0.438	0.543	0.526	0.354
Fe(II)As(III)*	0.366	0.411	0.505	0.406	0.427	0.565
Tooeleite	0.029	0.038	0.057	0.051	0.047	0.080
R-Factor	0.0016	0.0025	0.0018	0.00088	0.0023	0.00068

*Biogenic ferrous arsenite compound

The k^3-weighted As K-edge EXAFS fittings, (Table 2.5 and Figure 2.11 B), were performed in the range of 3-14 $Å^{-1}$. The results for the fractional composition of the reduced samples obtained by EXAFS fittings agreed with the result of the XANES fitting (Table 2.4, Figure 2.11 and 2.12 B).

Table 2.5. Fractional compositions of arsenic in the reduced biotic samples obtained from k^3-weighted EXAFS least-squares fitting results.

Compound	CN15	CN45	CN400	ANA15	ANA45	ANA400
Scorodite	0.649	0.607	0.394	0.517	0.504	0.286
Fe(II)As(III)*	0.319	0.371	0.520	0.437	0.459	0.621
Tooeleite	0.032	0.022	0.087	0.046	0.037	0.093
R-Factor	0.0099	0.0053	0.047	0.0069	0.010	0.016

*Biogenic ferrous arsenite compound

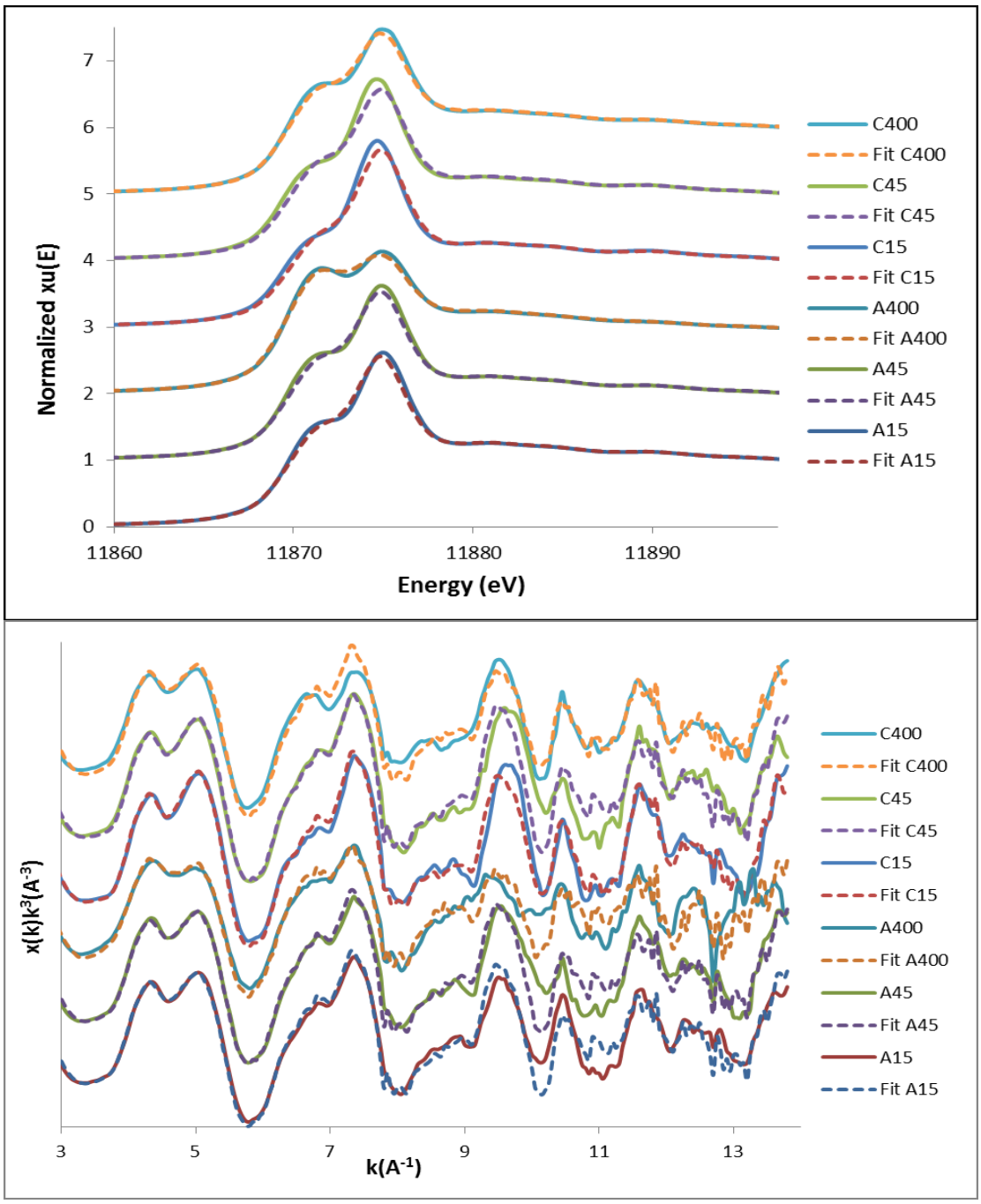

Figure 2.11. (A) The normalized As K-edge XANES spectra (solid lines) and fits (dotted lines) for ANA-3 and CN32 at 400, 45 and 15 μM and phosphate concentrations, where in the labels, A stands for ANA-3 and C for CN32, followed by the phosphate concentration, (B) k^3-weighted As XAFS K-edge spectra and fitting of the post-reduction samples.

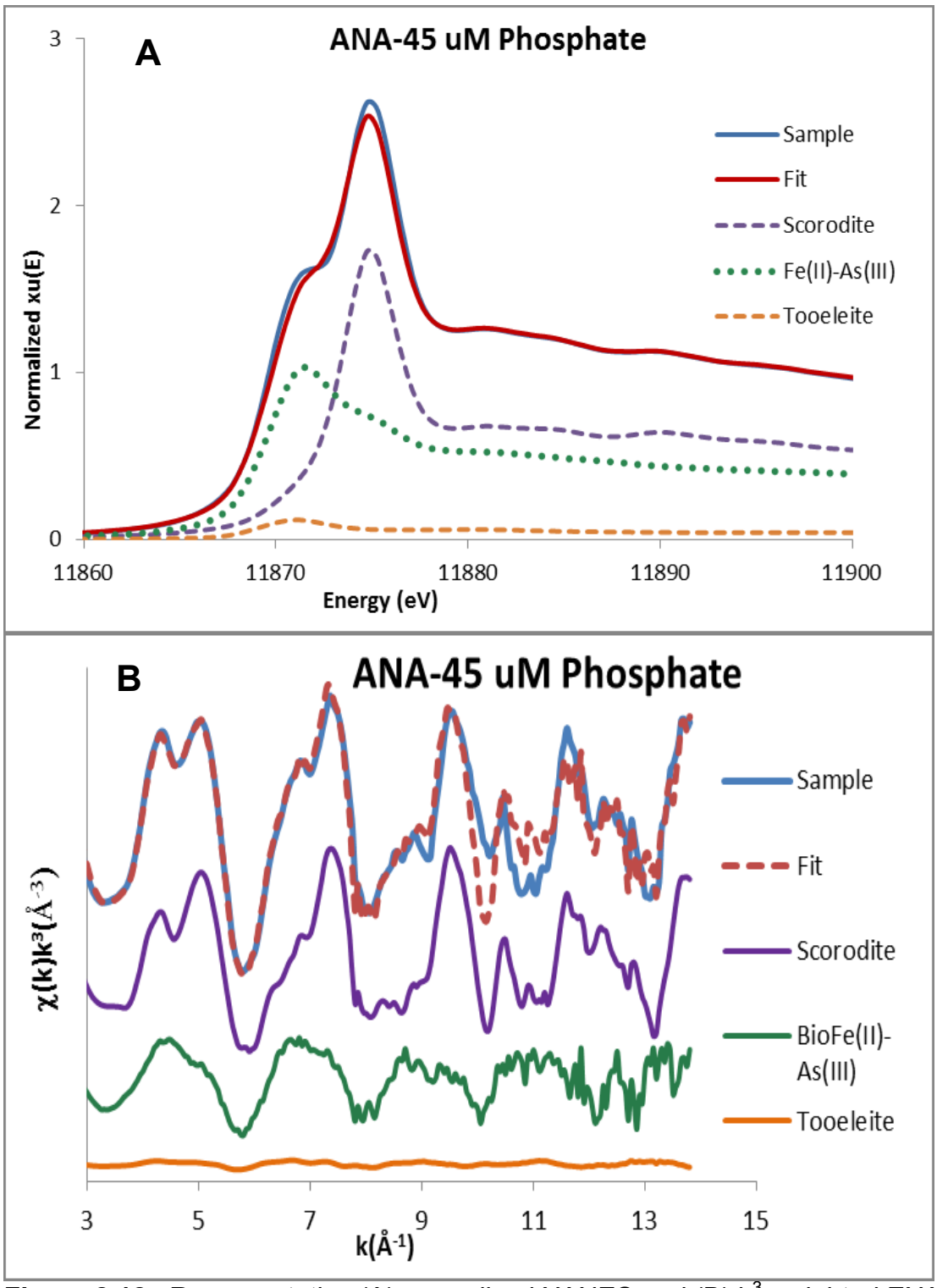

Figure 2.12. Representative (A) normalized XANES and (B) k^3-weighted EXAFS spectra of the microbial reduction product of scorodite and their linear combination fitting (dashed lines), as well as the end members that gave the best fitting.

4. Discussion

In comparing the two bacterial strains, it was found that the initial rates of reduction and the plateau concentrations of the dissolved reduced species, Fe(II) and As(III), were greater for the *Shewanella* sp. ANA-3 than for *Shewanella putrefaciens* CN32. These results suggest that *Shewanella* sp. ANA-3 is more efficient at reducing iron and arsenic than the CN32 is under the conditions used in these experiments. The question arises as to why the two strains of bacteria have different reducing efficiencies. The epigenetics, including experimental growth conditions, are known to control the expression of the cell membrane proteins. More specifically phosphorylation of the membrane and other proteins are crucial for cellular signaling which is part of the sensory system for detecting the environmental conditions which also regulates cell adhesion, quorum sensing (Miller-Bassler, 2001), and motility (Mijakovic, 2010). Both strains were grown in the same low phosphate medium during the growth phase. Murray and Saltikov (2007), who analyzed the genome sequence of *Shewanella putrefaciens* strain CN-32, demonstrated that the *arrAB* gene cluster, which is responsible for arsenate reduction, is identical to the *arrAB* of *Shewanella* sp. strain ANA-3. Both strains are believed to respire arsenate via very similar mechanisms. A possible explanation for the differences of reduction efficiencies could be that CN32 is more sensitive than ANA-3 to the experimental growth conditions i.e. low phosphate, used in this research.

With respect to the effect of the phosphate concentration on the reduction rates, it was found that the initial rates of reaction were greatest at the highest phosphate concentration for both bacteria, but the plateau concentrations of reduced species, Fe(II) and As(III), were found to be the lowest at the highest phosphate concentration.

The highest initial rates were observed with the 400 μM phosphate concentrations, which may be due to the greater bioavailability of phosphate at this concentration. The bioavailability of phosphate is decreased by the amount that is adsorbed on the surfaces of the solids. This decrease in bioavailable phosphate is most significant at the 45 and 15 μM phosphate concentrations. Phosphate diffuses into the interior of the bacterial cell membranes of Gram negative bacteria, such as *Shewanella,* through transmembrane β-barrel protein channels or porins (Luckey, 2008a). The bacteria require soluble inorganic phosphate, but the adsorbed inorganic phosphate is relatively inaccessible. Low phosphate concentrations can limit bacterial growth, which may only allow survival of the cells but not their growth as shown by the decrease in log CFU counts with time (Figures 2.1 and S2.2). High arsenic concentration, compared to phosphate, may have induced toxic effects on the bacteria and further retarded their growth. Saltikov et al. (2005) reported that during the early growth phases, ANA-3 preferentially uses the respiratory pathway instead of the detoxification pathway because transcription of the ars operon is blocked. As time progresses, the need to secrete As(III) increases as As(III) accumulates to toxic concentrations, and ANA-3 turns on the ars operon. Detoxification likely happened during scorodite reduction since the As(III) concentration did reach a toxic

level. The log of colony forming units (CFU) on Figure 2.1 (B) shows no bacterial growth, and it is only maintaining itself.

Saltikov et al. (2005) studied the effect of phosphate on *Shewanella* sp. ANA-3 using 100 μM, 600 μM, and 5 mM inorganic phosphate and found that high concentrations of phosphate promoted more robust growth of ANA-3 on As(V), which can promote As(V) reduction by bacteria in environments where aqueous As(V) and P concentrations are both high.

The observed effect of phosphate on the plateau concentrations of reduced species is consistent with Fredrickson et al. (1998), Kukkadapu et al., (2004) and Borch et al. (2007) who reported that increasing phosphate concentrations correlated with decreased Fe(II) in solution as a result of vivianite formation. The results of our calculations using PHREEQC (Table S2.3) indicate that the solutions were indeed saturated with respect to vivianite, with the greatest saturation indices at the 400 μM phosphate concentrations. The presence of vivianite was not confirmed with the characterization techniques employed. The plateau concentration of dissolved As(III) was appreciably greater than the dissolved Fe(II) concentration in all experiments for both strains (Table 2.2), because under the experimental conditions used, some of the Fe(II) precipitated as a biogenic Fe(II)-As(III) compound, parasymplesite and tooeleite. The presence of tooeleite ($Fe_6(AsO_3)_4(SO_4)(OH)_4 \cdot 4H_2O$) is based on the evidence provided by XRD and XAFS fittings. The XRD peak at 2θ 8.3°, attributed to tooeleite (Figure 2.4), is very weak, as is to be expected based on the low concentration of sulfate (i.e., 106 μM) in the chemically defined medium which limits the maximum amount of tooeleite that could

possibly form. The best fit of the reference compounds used for XANES and EXAFS fitting was obtained using tooeleite (Table 2.4 and 2.5, Figure 2.11 A and B). The endmembers used in fitting with ANA-3 at 45 μm phosphate concentration are shown in Figure 2.12.

The normalized relative peak intensities of As(III) to As(V) in the As XANES spectra (Figures 2.9 and 2.10) of the solid samples are greater for the *Shewanella* sp. ANA-3 than for CN32, and similarly for the arsenic fitting results (Figure 2.11). These findings are consistent with the greater reduction efficiency of *Shewanella* sp. ANA-3 over CN32. SEM imaging (Figure 2.5) revealed the presence of unreduced scorodite (with a platy structure) mixed with reduced amorphous minerals in the systems containing *Shewanella putrefaciens* CN32 whereas imaging of the post reduction material in the ANA-3 systems appeared to show more reduced material. XRD analysis (Figure 2.4) confirmed that the post reduction samples were composed of scorodite, parasymplesite and tooeleite. PHEEQC modeling also predicted the formation of other mineral phases, such as $Fe(OH)_2$, $Fe(OH)_3$, goethite, hematite, magnetite, maghemite and strengite which were not detected by XRD and XANES (Table S2.3). Finally, EDS analyses of individual post-reduction material revealed a wide range of Fe/As ratios in particles, ranging from 1:1 (in scorodite) to 18:1 (Table 2.3), indicating the presence of different Fe and As-rich particles in the presence of both strains.

The bacteria must be directly attached to the surface of scorodite for reductive dissolution of Fe(III) and As(V) to occur. This conclusion is supported by

the SEM images showing the bacterial colonies on the surfaces of the solid particles (Figures 2.6) while no bacteria were found in the subcultured clear solution.

The enzymes required for the reduction of Fe(III) are the terminal reductases, MtrC and OmcA, which are hydrophilic, and found on the outermost bacterial membrane exposed to the scorodite surface. MtrC and OmcA can supply the electrons via their co-factor hemes which are attached directly to the Fe(III) on the scorodite surface (Shi et al, 2012). The mechanistic aspects of electron transfer reactions in biological systems, including rates of the self-exchange reactions, with the cytochrome heme proteins and iron complexes were described by Marcus and Sutin (1985). The rate of electron transfer of the outer membrane heme proteins of the enzymes was investigated by Smith et al. (2006), and they found that the rate of electron-transfer was controlled by the distance between the heme and Fe(III) redox centers, and their orientation which was controlled by the protein and solvent dynamics at the surface of the enzyme. Kerisit et al. (2007) used computational quantum mechanical modelling study of the interface between the cytochrome heme and the hematite (α-Fe_2O_3) surface and found that the cytochrome heme remained attached to the hematite surface via direct contact with electron-transfer distances as small as 9 Å. The electron-transfer rate was sensitive to the fluctuations of the heme configuration at the interface, orientation of the porphyrin ring, electron-transfer distance, and to the mineral surface termination. The heme group of the enzymes transferred the electrons to Fe(III), which after reduction to Fe(II), was eventually detached from the surface of the scorodite. Since the density of the iron active sites on the surface of scorodite is lower than it is on the surface of iron

oxides such as hematite, the bacteria can use shuttle compounds such as siderophores to abstract Fe(III) further away from their colony.

Drewniak et al. (2008) isolated 22 arsenic hypertolerant bacterial strains in an ancient gold mine and found that 16 bacterial strains showed the presence of siderophores which was correlated with the highest arsenate reductase activity and mobilization of arsenic into the environment. Siderophores can transport Fe(III) through the β-barrel protein channels embedded in the cell membrane as found by Shi et al, (2012) for *Shewanella onedensis*.

The reduction of species in solution depends only on the rate of electron transfer from reducing agent to the oxidizing agent, whereas reduction in the solid requires both electron transfer and the breaking of bonds resulting in the detachments of iron and arsenic from the scorodite surface. Langner and Inskeep (2001) studied the bacterial reduction of As(V) in solution, and the bacterial reduction of As(V) adsorbed on ferrihydrite by measuring the rate of formation of dissolved As(III). They found that the rate of formation of As(III) from the bacterial reduction of As(V) in solution was much faster than the rate of formation of dissolved As(III) from the bacterial reduction of As(V) adsorbed on the solid. These result are consistent with the fact that reduction in solution involves only electron transfer, a fast step, whereas reduction in solids includes both electron transfer, and detachment of the reduced As(III) from the solid, the slow and therefore rate determining step.

Fe(III) can be reduced directly on the scorodite surface or indirectly by being transported into the cell by shuttle compounds such as siderophores. However, the

precise location, (on the surface or in the solution), of As(V) reduction is not known. To find the answer we have to look at the locations of the As(V) reducing enzymes in the bacterial cell membrane. Are they enclosed within the cell membranes or are outside like the Fe(III) reducing enzymes? The anaerobic respiratory arsenate reductase enzymes, the ArrA and ArrB, are periplasmic or membrane bound proteins (Silver and Phung, 2005; Murphy and Saltikov, 2007). The ArrA is in the periplasm and ArrB is embedded in the membrane interior because their quinone substrate is very hydrophobic and the semiquinone intermediate needs to be shielded from the aqueous environment to avoid the damaging ROS species (Luckey, 2008b). For this reason the As(V) has to cross the cell membrane for As(V) reduction to occur. ArrA is the subunit that binds As(V) and reduces it to As(III). ArrB serves as a passage for electrons coming from the c-type cytochromes in the respiratory chain (Macy et al. 2000). The As(V) reduction must be happening either in the periplasm or close to the membrane inside the cell. Therefore, As(V) has to be detached from the scorodite to be reduced to As(III). Shewanella also has an arsenic detoxification system within the cytoplasm which is induced at high arsenate concentration (Saltikov et al. 2003 and 2005).

It was found in this research that significant amount of the more mobile and toxic dissolved As(III) was released into the aqueous phase. How are the findings of this research applicable to real world arsenic problem? As discussed earlier, Drewniak at al. (2008) found that there are many strains of bacteria in the mining environment that can reduce As(V). Chatain et al., (2005) found that under anaerobic conditions (at pH ~ 7) indigenous bacterial activity can release arsenic

from a contaminated mining soil. Kocar et al., (2010) reported that in the presence of sulfate reducing bacteria, the sulfide which is formed can reduce ferrihydrite and arsenate.

Scorodite sequester arsenic effectively under anaerobic conditions at circumneutral pH in the absence of bacteria. Under these conditions the presence of bacteria, which are both dissimilatory iron and arsenic reducers, results in the reductive dissolution of scorodite with the formation of significantly higher concentrations (by at least a factor of 10) of dissolved arsenic than in the abiotic systems, mainly as the more bioavailable and more soluble As(III).

The severe negative consequence of the effect of such bacterial activity brings into question the effectiveness of scorodite in sequestering arsenic unless practical measures can be taken to retain the arsenic released by bacterial action such as significantly increasing the Fe/As ratio as observed in our other publication.

Concerning the real world implications of arsenic in mine waste, it was found in our research that the effect of bacterial reductive dissolution of scorodite resulted in extensive concentrations of dissolved As(III), about 3 mM As(III) was released into solution. These findings should be taken into consideration for mine wastes with scorodite in that there is the potential for As mobilization from the wastes under the influence of bacteria. The practical measures that are used to prevent arsenic contamination of ground and surface waters in the mining environment need to be effective and economical. The options available to deal with this problem include various cover materials which have been used to try to control or stop the spread of contamination in mining sites. Covers are designed for various reasons including the

most common ones which are to prevent oxygen ingress and minimize water infiltration for sulfidic mine wastes. Otherwise, sulphide oxidation would result in the generation of acid mine drainage. The use of a cover could be an option for tailings with arsenopyrite and As-pyrite, but not for scorodite or As-ferryhydrite containing tailings.

Organic or biosolid cover: Biosolid cover can protect against gullying and scouring by wind and surface water, and can minimize erosion. A recent publication by Paktunc (2013) characterized mine tailings at a former gold mine in northern Ontario to assess the impact of a biosolid cover, meant to form substrate for +energy crops, on the stability of As species and to evaluate options for long-term management of the tailings. He found that the arsenic concentrations in the leachate gradually increased from less than 0.085 to 13 mg/L and iron from 28 to 179 mg/L towards the biosolid cover. These were in contrast to the leachate concentrations of less than 0.085 mg/L arsenic and 24–64 mg/L iron obtained from the uncovered tailings, supporting the role of biosolids-influenced reduction and mobilization of As in the form of As(III) species. It seems that reutilizing barren mine tailings sites while remediating the sites for closure with biosolids can therefore lead to a situation with unintended consequences. The biosolid-covering and the decay process produce an anaerobic environment which is ideally suited for dissimilatory iron reducing bacteria (DIRB) and dissimilatory arsenic reducing bacteria (DARB) to thrive. These bacteria can reduce iron and arsenic which results in the mobilization of the more toxic and bioavailable form of arsenic, As(III). It appears that biosolid-coverage for

the closure of abandoned gold mining sites is an example of creating new problems while trying to solve existing ones.

Soil covers can minimize erosion by deflecting runoff and can promote evapotranspiration through the growth of vegetation and also provide a physical barrier between potential receptors and waste material. However it creates an anaerobic environment in which bacteria can thrive and promote further release of arsenic. The consequences of a water cover are similar to those of a soil cover, since the deeper the water cover, the more anaerobic and reducing the environment would be, which would further promote the release of dissolved As(III).

The no cover option could result in increased oxidation of pyrite and arsenopyrite creating acidic conditions and enhancing the formation of scorodite and arsenical ferrihydrites, which do sequester arsenic. These oxidizing and acidic conditions suppress the activity of DIRB/DARB bacteria that function near circumneutral pH. An apparent additional benefit of these conditions is the potential bacterial oxidation of As(III) to the less toxic As(V) by bacteria which can survive under acidic and oxidizing conditions. The decision of the type of covering or even no covering is not a simple one since acidic leaching of materials as well as the mobility of polluted sites must also be taken into account.

5. Summary and Conclusion

In this research we found that both Shewanella putrefaciens CN32 and ANA-3 reduced scorodite, and that ANA-3 was more efficient. Increasing the phosphate

concentration increased the initial rate of reduction for both strains. Whereas the plateau concentration of the dissolved As(III) and Fe(II) was highest at the lowest phosphate concentration. The concentration of the dissolved As(III), the more bioavailable and toxic form of arsenic, was about twice the concentration of the dissolved Fe(II). The post-reduction secondary solid state products were biogenic Fe(II)-As(III) mineral, parasymplesite and tooeleite.

It is postulated that the Fe(II) reduction occurs through direct contact of the heme groups of the reducing enzymes with Fe(III) on the surface of the scorodite, with the possible simultaneous reduction through siderophores.

Arsenic must be detached from the scorodite surface for reduction to occur due to the reduction enzymes being in the periplasmic place within the inner and outer membranes of the bacteria. The detachment of Fe(II) and the As(V) from the surface of scorodite are the rate determining steps in the bacterial reductive dissolution of scorodite.

The implications of our findings for the real world arsenic problem in mine wastes need to be taken into account. The various cover materials used may not be the best option because they may promote the formation of an anaerobic environment that can enhance reductive dissolution of scorodite through bacterial reduction of Fe(III) and As(V).

6. Supplementary Information for Chapter 2.

Molybdenum Blue Method for the analysis of aqueous arsenic:

Solution Preparation:

Diluent: 3 μmol/L sodium phosphate, Na_3PO_4, in 1% v/v (0.12 mol/L HCl). PO_4^{3-} was added to the diluent to promote colour development of arsenate, AsO_4^{3-}, with the molybdate colour reagent. 2% v/v (0.24 mol/L) HCl used for samples that were not treated with oxidizing or reducing agent.

Oxidizing Agent: Potassium iodate, KIO_3 (214.0 g/mol) 0.0425 % m/v (2 mmol/L) in 2 % v/v (0.24 mol/L) HCl. This solution stored at room temperature was stable for a number of months.

Reducing Agent:

Sodium metabisulfite, $Na_2S_2O_5$ (190.1 g/mol)

Sodium thiosulfate, $Na_2S_2O_3$ (158.1 g/mol) 1.4 % m/v (89 mmol/L) solution stored refrigerated in the absence of light in a glass container.

H_2SO_4, 10 % v/v (1.8 mol/L)

The reducing agent solution was prepared just prior to use as follows: ~0.56 g of $Na_2S_2O_5$ was weighed in a glass 15 mL vial. 4.00 mL of H_2O added, and the solid was allowed to dissolve. In a fume hood, 4.00 mL of 89 mmol $Na_2S_2O_3$ solution was added to the vial and mixed, 2.00 mL 1.8 mol/L H_2SO_4 was added immediately and mixed.

Colour Reagent:

Ammonium molybdate, $(NH_4)_6Mo_7O_{24}\cdot 4H_2O$ (1236 g/mol), 3 % m/v (24 mmol/L) in H_2O stored at room temperature was found stable for a number of months.

Potassium antimonyl tartrate, $K_2Sb_2(C_4H_2O_6)_2$ (613.8 g/mol), 0.5 % m/v (8 mmol/L) in H_2O stock solution was stored at room temperature.

L-ascorbic acid $C_6H_8O_6$ (176 g/mol) powder.

The colour reagent solution was freshly prepared on the day used as follows:

~ 0.22 g of ascorbic acid was dissolved in 2.00 mL of water. 2.00 mL of 24 mmol/L ammonium molybdate was added and mixed, 1.00 mL 8 mmol/L potassium antimonyl tartrate was added and mixed, and 5.00 mL of 2.5 mol/L H_2SO_4 was added and mixed.

B. Procedure:

The determination of phosphate, arsenate and arsenite for a typical sampling involved two abiotic controls, five biotic samples and blanks containing distilled water in place of control or biotic samples to provide a means of checking on the absorbance measurements.

Three sets of samples were prepared. A set of untreated samples, to which neither oxidizing nor reducing agent was added, a set of oxidized samples, to which potassium iodate, KIO_3 oxidizing agent was added, and a set of reduced samples, to which the reducing agent was added. Three sets of seven samples plus a blank for each set resulted in twenty four tubes. Tubes in the first set were labelled U for

untreated, next X for oxidized and the last R for reduced. 5.00 mL of diluent 3 μmol/L PO_4^{3-} in 1 % (0.12 mol/L) HCl was added to all tubes,

0.500 mL of abiotic control, biotic sample or distilled water blank was added to the appropriately labelled tube.

0.500 mL of KIO_3 oxidizing agent was added to each tube labelled X.

0.500 mL of reducing agent was added to each tube labelled R.

0.500 mL of 2% (0.24 mol/L) HCl was added each tube labelled with U.

Each set of tubes included a blank containing 0.500 mL of H_2O in place of control or biotic sample.

Samples were allowed to stand at room temperature for about 20 minutes to allow for the oxidation/reduction reactions to proceed.

0.500 mL of colour reagent was added to all tubes. The untreated and oxidized samples were heated at ~65 °C for ~ 25 minutes. The reduced samples were not heated to minimize the risk of decomposition of thiosulfate which could result in turbidity due to formation of colloidal sulphur particles.

The heated samples were cooled to room temperature, and the absorbance was measured at 880 nm after setting the absorbance to 0.000 with MilliQ distilled water reference.

Molar absorptivities of $(2.22 \pm 0.02) \times 10^4$ L/(mol cm) and $(2.04 \pm 0.03) \times 10^4$ L/(mol cm) for PO_4^{3-} and AsO_4^{3-} complexes of molybdate respectively obtained from measurements done on standard phosphate and arsenate solutions were used to calculate the concentrations of the PO_4^{3-}, AsO_4^{3-} and AsO_3^{3-}.

The volume of sample, 0.500 mL, used in the initial part of a run was adjusted as the sampling time increased to ensure that the measured absorbance was in a favourable range.

Calculation of concentrations

Beer's Law: $A = \varepsilon bC$; $C = A / \varepsilon b$

A – absorbance

ε – molar absorptivity; $\varepsilon(PO_4^{3-}) = 2.22 \times 10^4$ L/(mol·cm),

$\varepsilon(AsO_4^{3-}) = 2.04 \times 10^4$ L/(mol·cm) at 800 nm.

b – cell path length = 1.00 cm

C – concentration

A_U, A_X, A_R absorbance readings of the untreated, oxidized and reduced samples

$C(PO_4^{3-}) = [A_R / \varepsilon(PO_4^{3-})b] \cdot DF$

$C(PO_4^{3-})$ – concentration of phosphate

DF – dilution factor = VT/VS

VT – volume of diluted sample = 6.50 mL

VS – volume of filtrate = 0.500 mL

Similarly for the concentration of arsenate and arsenite.

$C(AsO_4^{3-}) = [(A_U - A_R) / \varepsilon(AsO_4^{3-})b] \cdot DF$

$C(AsO_3^{3-}) = [(A_X - A_U) / \varepsilon (AsO_4^{3-})b] \cdot DF$

Table S2.1. pH measurements during the reduction experiments in the biotic and abiotic systems at various phosphate concentrations (μM) with *Shewanella* sp. ANA-3 (abbreviated as ANA), *Shewanella putrefaciens* CN32 (abbreviated as CN) and the control systems (CONT). The numbers under the abbreviations represent the phosphate concentrations.

Time (h)	CN 15	CN 45	CN 400	ANA 15	ANA 45	ANA 400	CONT
0	6.99	7.00	6.99	6.99	7.02	7.01	7.00
21	6.80	6.83	6.71	6.77	6.76	6.92	6.92
44	6.85	6.91	6.74	6.84	6.88	6.91	6.87
72	6.97	7.03	6.95	6.94	6.87	7.01	6.80
94	6.93	6.94	6.93	6.95	6.94	6.94	6.84
116	7.02	7.02	7.01	6.94	6.95	6.92	6.91
168	7.03	6.99	6.97	6.89	7.02	6.99	6.83

Table S2.2. Initial and final bacterial counts (CFU/mL)

Time (h)	CN 15	CN45	CN400	ANA 15	ANA 45	ANA 400
0	1.41×10^8	1.10×10^8	1.17×10^8	1.16×10^8	1.19×10^8	1.00×10^8
170	1.27×10^5	7.94×10^4	3.17×10^5	3.15×10^5	2.20×10^5	2.51×10^5

Table S2.3. Saturation Indices calculated with PHREEQC* at equilibrium As and Fe concentrations.

Sample	PO_4^{3-} (μM)	$Fe(OH)_2$	$Fe(OH)_3$	$Fe_3(OH)_8$	Goethite	Hematite	Maghemite	Magnetite	Scorodite	Strengite	Vivianite
ANA	**15**	6.15	1.47	3.28	7.29	16.6	6.33	19.4	3.47	0.75	4.37
ANA	**45**	6.16	1.47	3.23	7.29	16.6	6.34	19.5	3.12	1.26	5.21
ANA	**400**	6.02	1.33	2.96	7.15	16.3	6.06	19.2	2.97	2.07	7.11
CN3	**15**	6.31	1.62	3.39	7.44	16.9	6.64	19.6	3.43	0.99	3.95
CN3	**45**	6.36	1.68	3.66	7.50	17.0	6.75	19.9	3.40	1.46	5.25
CN3	**400**	6.14	1.45	3.03	7.27	16.5	6.30	19.3	3.32	2.25	6.75

***** Parkhurst, D.L., Appelo, C.A.J., 1999.

Table S2.4. Statistical t-test calculations for the dissolved As(III) species for CN32 and ANA-3.

Phosphate Conc. (μM)	**CN 15**	**CN 45**	**CN 400**	**ANA 15**	**ANA 45**	**ANA 400**
Initial rates (μM/h)	28.5	31.7	45.7	40.0	44.3	49.7
STDEV	1.8	2.4	1.0	3.0	3.0	0.4
t-experimental*	1.8	9.3		1.8	3.1	

The statistical t-cut off values are 2.13 for 90% and 2.78 for the 95 % confidence level.

*The t-values relate to two consecutive phosphate concentrations, e.g. 15 - 45 and 45 - 400 μM.

Table S2.5. Statistical t-test calculations for the dissolved Fe(II) species for CN32 and ANA-3.

Phosphate conc.(μM)	**CN 15**	**CN 45**	**CN 400**	**ANA 15**	**ANA 45**	**ANA 400**
Initial rates (μM/h)	14.7	14.6	24.2	23.3	23.9	27.0
STDEV	0.7	2.1	0.5	2.3	0.5	1.5
t-experimental*	0.08	7.7		0.4	3.4	

The statistical t-cut off values are 2.13 for 90% and 2.78 for the 95 % confidence level.

*The t-values relate to two consecutive phosphate concentrations, e.g. 15 - 45 and 45 - 400 μM.

Table S2.6. Comparison of the initial dissolved As(III) rates between CN32 and ANA-3 at the same phosphate concentrations.

Phosphate conc.(µM)	**CN 15**	**ANA 15**	**CN 45**	**ANA 45**	**CN 400**	**ANA 400**
Initial rates (µM/h)	28.5	39.9	31.7	44.3	45.7	49.7
STDEV	1.8	3.0	2.4	3.0	1.0	0.4
t-experimental*	5.6		5.7		6.4	

The statistical t-cut off values are 2.13 for 90% and 2.78 for the 95 % confidence level.

* The t-values relates to the same phosphate concentrations for each bacterial strain.

Table S2.7. Comparison of the initial dissolved Fe(II) rates between CN32 and ANA-3 at the same phosphate concentrations.

Phosphate conc.(µM)	**CN 15**	**ANA 15**	**CN 45**	**ANA 45**	**CN 400**	**ANA 400**
Initial rates (µM/h)	14.7	23.3	14.6	23.9	24.2	27.0
STDEV	0.7	2.5	2.1	0.5	0.5	1.5
t-experimental*	5.7		7.5		3.1	

The statistical t-cut off values are 2.13 for 90% and 2.78 for the 95 % confidence level.

* The t-values relates to the same phosphate concentrations for each bacterial strain.

Table S2.8 Equilibrium As and Fe concentrations used for PREEQC* calculations.

Sample	PO_4^{3-} (μM)	As(III) (μM)	As(V) (μM)	Fe(II) (μM)	Fe(III) (μM)
ANA-3	15	2938	70	960	226
ANA-3	45	2381	35	850	221
ANA-3	400	2338	29	1018	161
CN32	15	2383	48	604	317
CN32	45	2381	35	889	357
CN32	400	2016	51	714	215

***** Parkhurst, D.L., Appelo, C.A.J., 1999.

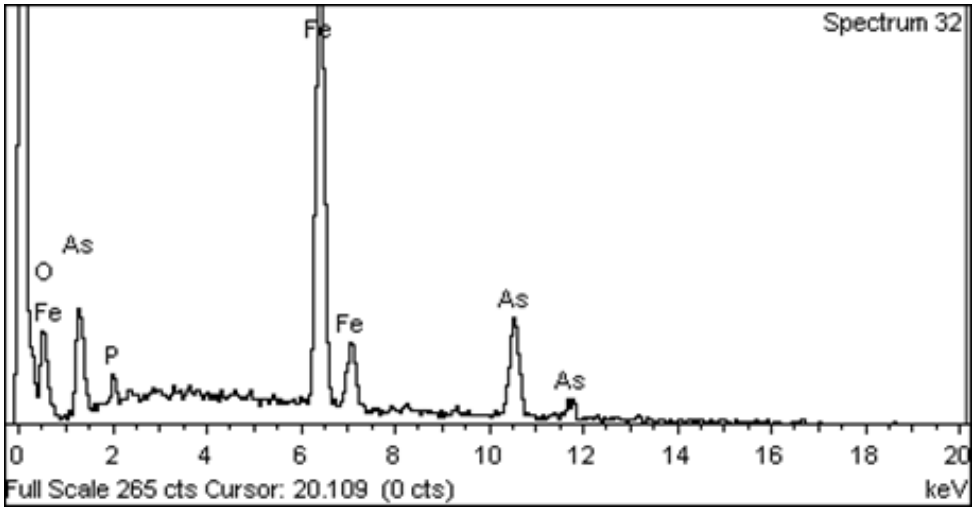

Figure S2.1. A small phosphate peak is visible at 2 keV on the energy dispersive spectrum of the post-reduction scorodite at the 400 μM phosphate concentration in the presence of Shewanella sp. ANA-3 after 120 hours of reduction.

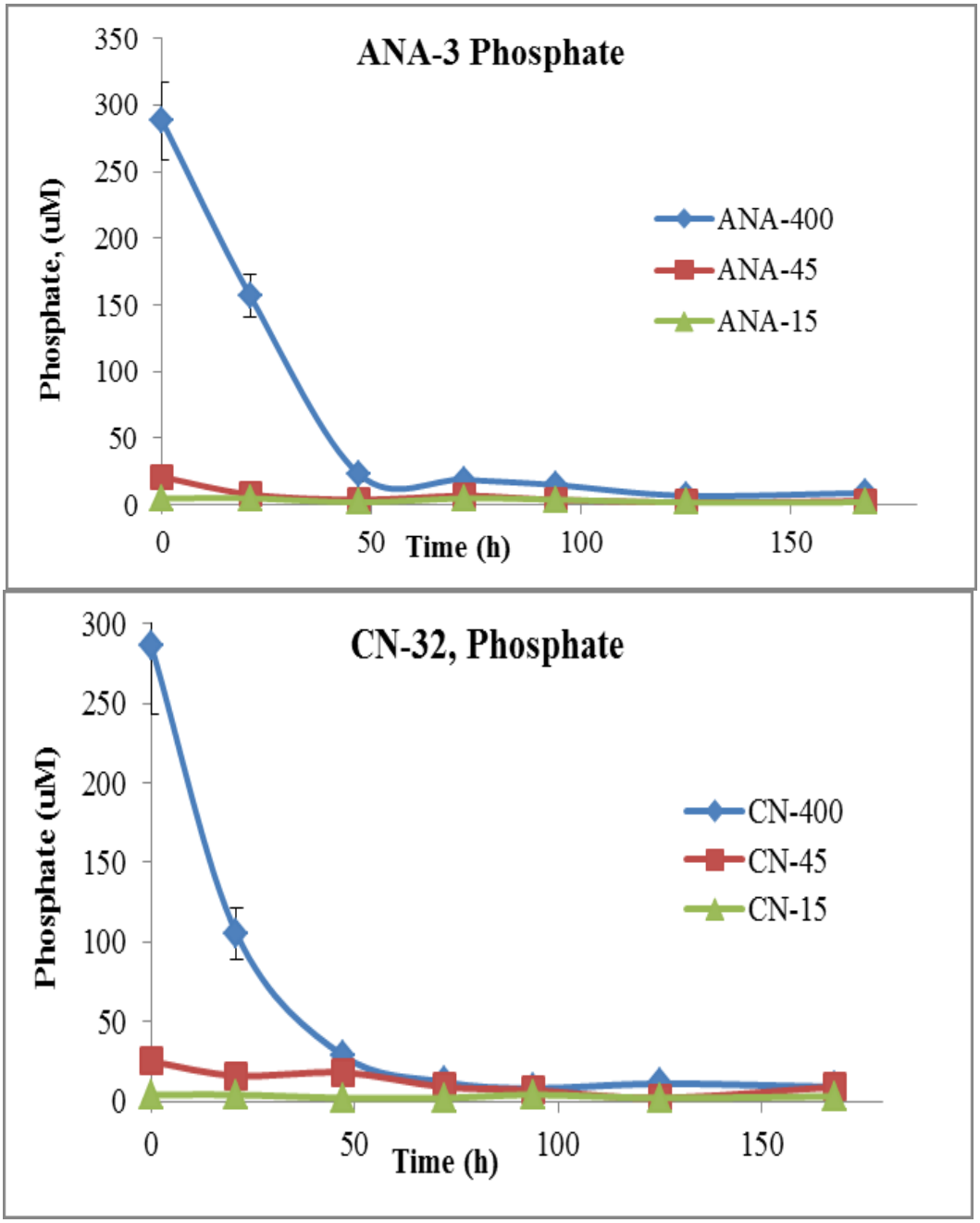

Figure S2.2. Decrease of the phosphate concentrations with time for experiments starting at 400, 45 and 15 μM.

Note the significant decrease of the phosphate at the 400 μM phosphate (blue) concentration possibly due to adsorption on the scorodite surface.

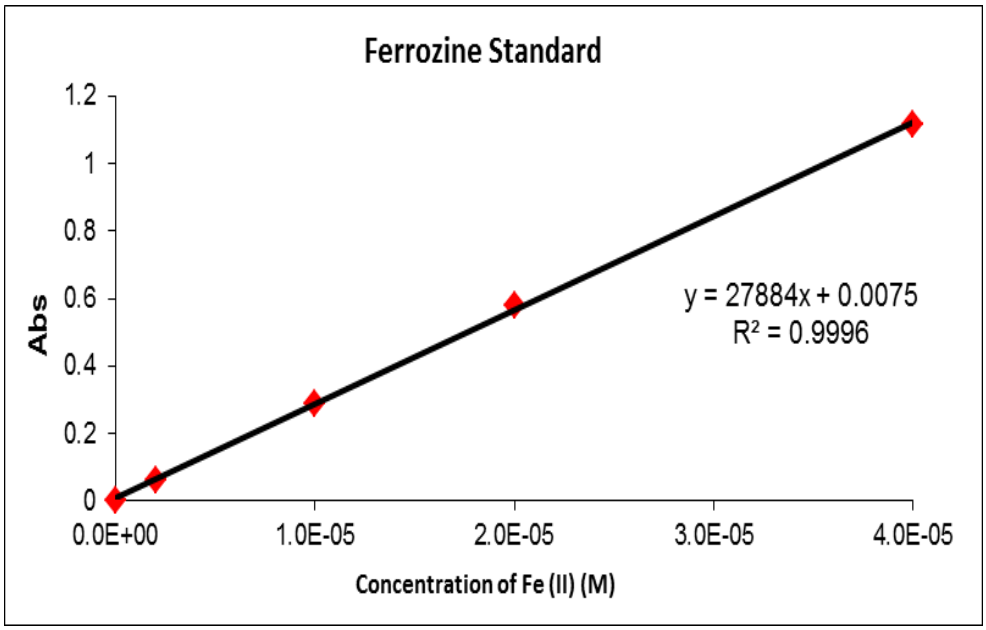

Figure S2.3. The slope of this graphs equals the molar absorptivity of the Fe(II)-ferrozine complex and was used to calculate the dissolved Fe(II) concentrations.

Calculation of the maximum amount of Vivianite in the scorodite sample

MW vivianite: 501.61 g/mol of $Fe_3(PO_4)_2 \cdot 8H_2O$

Sample Volume: 150 mL

1. $[PO_4^{3-}]$ = 400 µM

Initial: {[(400 x 10^{-6} mol/L x 0.150 L]/2} x 501.61 g/mol = 0.015048 g = 15.04 mg

Equilibrium: {[(15 x 10^{-6} mol/L x 0.150 L]/2} x 501.61 g/mol = 0.000564 g = 0.564 mg

2. $[PO_4^{3-}]$ = 45 µM

Initial: {[(45 x 10^{-6} mol/L x 0.150 L]/2} x 501.61 g/mol = 0.00169 g = 1.69 mg

Equilibrium: {[(8 x 10^{-6} mol/L x 0.150 L]/2} x 501.61 g/mol = 0.000301 g = 0.301 mg

1. $[PO_4^{3-}]$ = 15 µM

Initial: {[(15 x 10^{-6} mol/L x 0.150 L]/2} x 501.61 g/mol = 0.000564 g = 0.564 mg

Equilibrium: {[(4 x 10^{-6} mol/L x 0.150 L]/2} x 501.61 g/mol = 0.000150 g = 0.150 mg

Table S2.9. Calculated theoretical maximum of vivianite, ($Fe_3(PO_4)_2 \cdot 8H_2O$) at time zero and at the equilibrium.

[PO4] (µM)	400	45	15
Initial theoretical maximum vivianate (mg)	15.0	1.69	0.564
Equilibrium theoretical vivianate (mg)	0.564	0.301	0.150

Note: These are the theoretically maximum possible vivianite masses that could be formed if the phosphate used for the formation of possible phosphate complexes and used by the bacteria is not taken into account. The actual masses of vivianite formed would be expected to be less than the calculated maximums.

Acknowledgements

This project was partially funded by NSERC Discovery grants to D.F. and D.P. and by CANMET. We kindly thank C. Saltikov for providing the *Shewanella* sp. ANA-3 strain. E. Revesz thanks D. Smith at CANMET for XRD and Y. Liu at the University of Ottawa's Centre for Catalysis Research and Innovation (CCRI) for the FE-SEM/TEM and HRTEM imaging, R. Gordon for the XAFS experiments at the Pacific Northwest Consortium—Collaborative Access Team's (PNC/XOR) beamline at the Advanced Photon Source (APS) at the Argonne facility under the user agreement to the senior author. Argonne National Laboratory is supported by the US Department of Energy under Contracts W-31-109-Eng-38 (APS) and DE-FG03-97ER45628 (PNC-CAT). Robert Gordon helped with the experiments at the beamline.

7. References:

Amstaetter, K., Borch, T., Kappler, A., 2012. Influence of humic acid imposed changes of ferrihydrite aggregation on microbial Fe(III) reduction, Geochim. Cosmochim. Acta. 85, 326–341.

Babechuk, M.G., Weisener, C.G., Fryer, B. J., Paktunc, D., Maunders, C., 2009. Microbial reduction of ferrous arsenate: Biogeochemical implications for arsenic mobilization. Appl. Geochem. 24, 2332-2341.

Borch, T., Masue, Y., Kukkadapu, R.K., Fendorf, S., 2007. Phosphate imposed limitations on biological reduction and alteration of ferrihydrite. Environ. Sci. & Technol. 41, 166–172.

Brunsting, J.H., McBean, A.E., 2014. Phosphate interference during in situ treatment for arsenic in groundwater. J. Environ. Sci. Health A Tox. Hazard Subst. Environ. Eng. 49, 671–678.

Cavalca, L., Corsini, A., Zacheo, P., Andreoni, V., Muyzer, G., 2013. Microbial transformation of arsenic: prespectives for biological removal of As from water. Future Microbiol. 8, 753-768.

Chatain,V.,Bayard, R., Sanchez, F., Moszkowicz, P., Gourdon, R., 2005. Effect of indigenous bacteria activity on arsenic mobilization under anaerobic conditions. Environ. Int. 31:221–226.

Châtellier, X., Grybos, M., Abdelmoula, M., Kemner, K.M., Leppard, G.G., Mustin, C., West, M.M., Paktunc, D., 2013. Immobilization of P by oxidation of Fe(II)

ions leading to nanoparticle formation and aggregation, Appl. Geochem. 35, 325–339.

Cummings, D.E., Caccavo, F., Fendorf, S., Rosenzweig, R.F., 1999. Arsenic mobilization by the dissimilatory Fe(III)-reducing bacterium *Shewanella alga* BrY. Environ. Sci. Technol. 33, 723–729.

Corriveau, M.C., Jamieson, H.E., Parsons, M.B., Hall, G.E.M., 2011. Mineralogical characterization of arsenic in gold mine tailings from three sites in Nova Scotia. Geochem. Explor. Environ. Anal. 11, 179

Cornell, R.M., Schwertmann, U., The Iron Oxides, Structure, Properties, Reactions, Occurrence and Uses, VCH, NY, 2nd Ed, 2003. 663 p.

Dhar, R.K., Zhenga, Y., Rubenstonec, J., van Geenc, A., 2004. A rapid colorimetric method for measuring arsenic concentrations in groundwater, Anal. Chim. Acta. 526, 203–209.

Drahota, P., Filippi, M., 2009. Secondary arsenic minerals in the environment: A review, Environ. Int. 35. 1243–1255.

Fortin, D., 2004. What biogenic minerals tell us, Science, 12, 303. 1618.

Drewniak, L., Matlakowska, R., Sklodowska, A., 2009. Microbial impact on arsenic mobilization in Zloty Stok gold mine, Adv. Mat. Res. 71-73, 121-124.

Drewniak, L., Matlakowska, R., Rewerski, B., Sklodowska, A., 2010. Arsenic release from gold mine rocks mediated by the activity of indigenous bacteria, Hydrometallurgy 104, 437–442

Fredrickson, J.K., Zachara, J.M., Kennedy, D.W., Dong, H., Onstott, T.C., Hinman, N.W., Li S-M. 1998. Biogenic iron mineralization accompanying the

dissimilatory reduction of hydrous ferric oxide by a groundwater bacterium. Geochim. Cosmochim. Acta., 62, 3239–3257.

Glasauer, S., Weidler, P. G., Langley, S., Beveridge, T.J., 2003. Controls on Fe reduction and mineral formation by a subsurface bacterium. Geochim. Cosmochim. Acta. 67, 1277–1288.

Hao, L., Zheng, T., Jiang,J., Hu, Q., Li, X., Wang, P., 2015. Removal of As(III) from water using modified jute fibres as a hybrid adsorbent. RSC Adv., 5, 10723-10732

Harvey, M.C., Schreiber, M.E., Rimstidt, D.J., Griffith, M.M., 2006, Scorodite dissolution kinetics: Implications for arsenic release. Environ. Sci. Technol. 40, 6709-6714.

Johnson, D.L., Pilson, M.E.Q., 1972. Spectrophotometric determination of arsenite, arsenate and phosphate in natural waters. Anal. Chim. Acta 58, 289–299.

Kerisit, S., Rosso, K.M., Dupuis, M., Valiev, M., Molecular computational investigation of electron-transfer kinetics across cytochrome-iron oxide interfaces, J. Phys. Chem. C, 111, 11363-11375

Kocar, B.D., Borch, T., Fendorf, S. 2010. Arsenic mobilization and repartitioning during biogenic sulfidization and transformation of ferrihydrite. Geochim. Cosmochim. Acta. 74, 980-994.

Krause, E. Ettel, V.A. 1989. Solubilities and stabilities of ferric arsenates. Hydrometallurgy 22, 311–337.

Kukkadapu, R.K., Zachara. J.M., Fredrickson. J.K., Kennedy, D.W., 2004. Biotransformation of two-line silicaferrihydrite by a dissimilatory Fe(III)-

reducing bacterium: Formation of carbonate green rust in the presence of phosphate. Geochim. Cosmochim. Acta. 68, 2799–2814.

Langley, S., Gault, A.G., Ibrahim, A., Renaud, R**.,** Fortin, D., Clark, I.D. and Ferris, F.G., 2009. A comparison of the rates of Fe(III) reduction in synthetic and bacteriogenic iron oxides by *Shewanella putrefaciens* CN32. Geomicrobiol. J. 26, 57-70.

Langmuir, D., Mahoney, J., Rowson, J., 2006. Solubility products of amorphous ferric arsenate and crystalline scorodite ($FeAsO_4 \cdot 2H_2O$) and their application to arsenic behaviour in buried mine tailings, Geochim. Cosmochim. Acta. 70, 2942–2956.

Langmuir, D. Mahoney, J. MacDonald, A. Rowson, J., 1999, Predicting arsenic concentrations in the porewaters of buried uranium mill tailings. Geochim. Cosmochim. Acta. 63, 3379–3394.

Langner, H.W., Inskeep, W.P., 2000, Microbial reduction of arsenate in the presence of ferrihydrite. Environ. Sci. Technol. 34, 3131-3136.

Liao, V.H.-C., et al., 2011. Arsenite-oxidizing and arsenate-reducing bacteria associated with arsenic-rich groundwater in Taiwan, J. Contam. Hydrol. 123(1-2): 20-29.

Lovely, D.R., 2001. Anaerobes to the rescue. Science. 293, 1444-1446.

Luckey, M., Membrane structural biology. 2008, (a) p:120. (b) p:281. Cambridge University Press.

32 Avenue of the Americas, New York, NY 10013-2473, USA.

Macur, R.E., Jackson, C.R., Botero, L.M., McDermott, T.R., Inskeep, W.P., 2004. Bacteria populations associated with the oxidation and reduction of arsenic in an unsaturated soil. Environ. Sci. Technol. 38, 104-111.

Macy, J.M., Santini, J.M., Pauling, B.V., O'Neill, A.H., Sly, L.I., 2000. Two new arsenate/sulfate-reducing bacteria: mechanisms of arsenate reduction. Arch. Microbiol. 173:49–57

Marcus, R.A.; Sutin, N. 1985. Electron transfers in chemistry and biology. Biochim. Biophys. Acta. 35, 437.

Majzlan, J., 2011, Thermodynamic Stabilization of Hydrous Ferric Oxide by Adsorption of Phosphate and Arsenate. Environ. Sci. Technol. 45(11), 4726-4732

Miller, M.B., Bassler, B.L., 2001, Quorum sensing in bacteria. Annu. Rev. Microbiol. 55: 165–99.

Mijakovic, I., 2010, Protein Phosphorylation in Bacteria, Microbe, Vol5, 1. 21-25.

Mohan, D., Pittman, C.U. Jr., 2007. Arsenic removal from water/wastewater using adsorbents-A critical review. J. Hazard. Mater. 142. 1–53,

Murphy, J.N., Saltikov, C.W., 2007. The *cymA* gene, encoding a tetraheme *c*-type cytochrome, is required for arsenate respiration in *Shewanella* species, J. Bacteriol. 2283–2290.

Newman, D.K., Kennedy, K., Coates, J.D., Ahmann, D., Ellis, D.J., Lovley, D.R., Morel, F. M. M., 1997, Dissimilatory arsenate and sulfate reduction in *Desulfotomaculum auripigmentum* sp. nov. Arch Microbiol, 168, 380–388

Newman, D.K., Ahmann, D., Morel, F.M.M., 1998, A brief review of microbial arsenate respiration, Geomicrobiol J. 15,255–268

Oremland, R.S., Stolz, J.F, 2005, Arsenic, microbes and contaminated aquifers. Trends in Microbiology.13, 45-49.

Paktunc, D., Foster, A., Laflamme, G., 2003. Speciation and Characterization of Arsenic in Ketza River Mine Tailings Using X-ray Absorption Spectroscopy. Env. Sci. Tech. 37, 2067-2074.

Paktunc, D., 2004. Analysing complex bulk XAFS spectra. J. Synchrotron Rad. 11, 295 - 298

Paktunc, D., Foster, A., Heald, S., Laflamme, G., 2004, Speciation and characterization of arsenic in gold ores and cyanidation tailings using X-ray absorption spectroscopy. Geochim. Cosmochim. Acta. 68, 969–83.

Paktunc, D., 2008a. Speciation of Arsenic in Pyrite by Micro-X-Ray Absorption Fine-Structure Spectroscopy (XAFS) Ninth International Congress for Applied Mineralogy Brisbane, QLD, 8 - 10 September.

Paktunc, D., 2008b. Speciation of arsenic in an anaerobic treatment system at a Pb-Zn smelter site, gold roaster products, Cu smelter stack dust and impacted soil. The AusIMM. 8, 343-348.

Paktunc, D., Dutrizac, J., Gertsman, V., 2008c. Synthesis and phase transformations involving scorodite, ferric arsenate and arsenical ferrihydrite: Implications for arsenic mobility. Geochim. Cosmochim. Acta., 72, 2649–2672

Paktunc, D., Bruggeman, K., 2010. Solubility of nanocrystalline scorodite and amorphous ferric arsenate: Implications for stabilization of arsenic in mine wastes, Appl. Geochem., 25, 674–683

Papassiopi, N., Vaxevanidou, K., Paspaliaris, I., 2003. Investigating the use of iron reducing bacteria for the removal of arsenic from contaminated soils. Water, Air, & Soil Poll.: Focus, 81–90.

Parkhurst, D.L., Appelo, C.A.J., 1999. User's guide to PHREEQC (Version 2), A computer program for speciation, batch reaction, one-dimensional transport, and inverse geochemical calculation. U.S. Geol. Surv. Water-Resour. Invest. Rep., 99–4259.

Pepper, S.E., Borkowski, M., Richmann, M.K., Reed, D.T., 2010. Determination of ferrous and ferric iron in aqueous biological solutions. Anal. Chim. Acta., 663, 172-177.

Praharaj, T., Fortin, D., 2008. Seasonal variations of microbial sulfate and iron reduction in alkaline Pb–Zn mine tailings (Ontario, Canada). Appl. Geochem., 23, 3728–3740.

Ravel, B. Newville, M., 2005. ATHENA, ARTEMIS, HEPHAESTUS: data analysis for X-ray absorption spectroscopy using IFEFFIT. J. Synchrotron Rad. 12, 537–541.

Riveros, P.A., Dutrizac, J.E., Spencer, P., 2001. Arsenic disposal practices in the metallurgical industry. Can. Metall. Q., 40, 395–420.

Saltikov, C.W., Wildman, R.A. Jr., Newman, D.K., 2005. Expression Dynamics of Arsenic Respiration and Detoxification in Shewanella sp. Strain ANA-3. J. Bacteriol. 7390–7396.

Saltikov, C.W., Newman, D.K., 2003. Genetic identification of a respiratory arsenate reductase. Proc. Natl. Acad. Sci. USA 100:10983–10988.

Silver, S., Phung, L.T., 2005. Genes and enzymes involved in bacterial oxidation and reduction of inorganic arsenic. Appl. Environ. Microbiol. 599–608

Shi, L., Rosso, K.M., Clarke, T.A., Richardson, D.J., Zachara, J.M., Fredrickson, J. K. 2012. Molecular underpinnings of Fe(III) oxide reduction by *Shewanella oneidensis* MR-1, Frontiers in Microbiology, Microbiol. Chem. Vol.3, Article 50.

Slaughter, D.C., Macur, R.E., Inskeep, W.P., 2012. Inhibition of microbial arsenate reduction by phosphate. Microbiol. Research, 167,151–156.

Smith, M.A.D., Rosso, M.K., Dupuis, M., Valiev, M., Straatsma, T.P., 2006. Electronic Coupling between Heme Electron-Transfer Centers and Its Decay with Distance Depends Strongly on Relative Orientation. J. Phys. Chem. B 110, 15582-15588.

Smedley, P.L., Kinniburgh, D.G., 2002. A review of the source, behavior and distribution

of arsenic in natural waters, Appl. Geochem. 17, 517–568.

Stolz, J.F., Basu, P., Santini, J.M., Oremland, R.S. 2006. Arsenic and Selenium in Microbial Metabolism. Annu. Rev. Microbiol., 60, 107-130.

Stookey, L.L., 1970. Ferrozine, a new spectrophotometric reagent for iron: Anal. Chem., 42, 779-781.

Straatsma, T.P., 2005. Scalable molecular dynamics. Journal of Physics: Conference Series 16, 287–299.

Twidwell, L.G., McCloskey, J.W., 2011. Removing Arsenic from Aqueous Solution and Long-term Product Storage, JOM, 63, 94-100.

Van Lis, R., Nitschke, W., Duval, S., Schoepp-Cothenet, B., 2013. Arsenics as bioenergetic substrates, BBA-Bioenergetics, 1827, 176–188.

Viollier, E., Inglett, P.W., Hunter, K., Roychoudhury, A.N., Van Cappellen, P., 2000. The ferrozine method revisited: Fe(II)/Fe(III) determination in natural waters. App. Geochem., 15, 785-790.

Walker, S.R., Parsons, M.B., Jamieson, H.E., Lanzirotti, A., 2009. Arsenic mineralogy of near-surface tailings and soils: influences on arsenic mobility and bioaccessibility in the Nova Scotia gold mining districts, Can. Mineral., 47(3), 533-556.

Weisener, C.G., Guthrie, J.W., Smeaton, C.M., Paktunc, D., Fryer, B. J., 2011. The effect of Ca–Fe–As coatings on microbial leaching of metals in arsenic bearing mine waste. J. Geochem. Explor., 110, 23–30.

White, G.F., Shi, Z., Shi, L., Wang, Z., Dohnalkova, A., Marshall, M.J., Fredrickson, J.K., Zachara, J.M., Butt, J.N., Richardson, D.J., Clarke, T.A., 2013. Rapid electron exchange between surface-exposed bacterial cytochromes and Fe(III) minerals, PNAS, 110, 6346-6351.

Zobrist. J., Dowdle, P.R., Davis, J.A, Oremland, R.S., 2000, Mobilization of arsenite by dissimilatory reduction of adsorbed arsenate. Environ. Sci. Technol., 2000, 34:4747-4753.

CHAPTER 3

Solubility and stability of adsorbed and coprecipitated arsenical 6-line ferrihydrite in the presence of *Shewanella putrefaciens* CN32 and *Shewanella* sp. ANA-3 at 0.045 mM phosphate concentrations.

Erika Revesz[a], Danielle Fortin[a*], Dogan Paktunc[a,b]

To be submitted by: E. Revesz, D. Fortin, D. Paktunc to a journal.

Abstract

Base metal and gold processing can lead to the release of arsenic into the aqueous environment as a result of the weathering of As-bearing sulphide minerals (such as arsenopyrite) discarded during processing. Ferrihydrite, a common secondary mineral in mine wastes, can effectively immobilize arsenic in processing solutions and mine drainage, but ferrihydrite is susceptible to microbial reduction under anaerobic conditions imposed by burial and various waste cover systems. This research, stimulated by the paucity of information on, and consequential limited understanding of the microbial reduction of arsenical ferrihydrite, was conducted on synthetic adsorbed and coprecipitated arsenical 6-line ferrihydrite (Fe/As molar ratio of 10/1) using *Shewanella* sp. ANA-3 and *Shewanella putrefaciens* CN32 in a chemically defined medium at 0.045 mM phosphate concentration. The two bacteria were equally effective in their reducing abilities around pH 7, and Eh from 350 mV to -60 mV with cell counts of 3 x 10^8, resulting in initial rates of formation of dissolved As(III) of 0.10 μM/h for the adsorbed, and 0.08 μM/h for the coprecipitated arsenical 6-line ferrihydrite samples. Measurable concentrations of dissolved Fe(II) and As(III) were found as early as the initial sampling, time 0 hours, for Fe(II) and about 100 hours for As(III) for the adsorbed samples, and about 100 hours for Fe(II) and about 200 hours for As(III) for the coprecipitated samples. The solid phases present in the post-reduction samples were examined by powder X-ray diffraction (XRD), micro-XRD, scanning and transmission electron microscopy (SEM/TEM), electron microprobe and X-ray absorption near edge spectroscopy (XANES) techniques. The results of these solid state analytical methods indicate that, in addition to original

adsorbed or co-precipitated 6-line ferrihydrite, the presence of new secondary mineral phases, such as a biogenic Fe(II)-As(III) compound, akaganeite, goethite, hematite and possibly magnetite. Holes and imprints of about 1-2 micron in size, resembling bacterial shapes, were observed on the surfaces of the secondary mineral phases formed in the adsorbed and co-precipitated samples after 1200 hours of reduction. This study demonstrates that the presence of Fe and As reducing bacteria would result in the formation and release into the environment of significant concentrations of mobile and toxic As(III) species from arsenical 6-line ferrihydrite, more readily from the adsorbed than from the coprecipitated ferrihydrite with implications on the mobilization of arsenic from mine wastes where As is hosted by ferrihydrite.

1. Introduction

Arsenic can be released to the environment from the weathering of arsenopyrite (FeAsS) and As-bearing pyrite (FeS_2). Mining and metallurgical processing of gold and base metal ores results in solid wastes, effluents and air emissions containing high concentrations of arsenic. Such wastes form an important source of anthropogenic arsenic in the environment (Paktunc, 2009). Pyrite is one of the principal Au-bearing minerals in refractory gold ores which is also enriched in arsenic as exemplified by a study reported by Paktunc (2008a) on the speciation of As in pyrite by XAFS. Wastes produced as a result of pressure oxidation, roasting and smelting of gold and base metal ores are a significant source of high concentrations of arsenic (Paktunc, 2008a and 2008b). In order to remove arsenic

from hydrometallurgical solutions, acid mine drainage and wastewaters, coprecipitation processes with iron are being used, which has been designated as the best-demonstrated available technology by the USEPA (Twidwell et al. 2005). In the Canadian metallurgical industry, coprecipitation is the preferred method for the removal of arsenic from solutions (Riveros et al. 2001). These are practical and cost effective strategies because ferric iron is widely available in metallurgical processing solutions.

In a detailed study, using various Fe/As molar ratios, Paktunc et al. (2008c) reported that below Fe/As molar ratios of 4, ferric arsenate, which is more soluble than scorodite and ferrihydrite, was present in the precipitates. Above Fe/As ratios of 5, two-line ferrihydrite was transformed to the more crystalline 6-line ferrihydrite, and the presence of arsenic in the 2-line ferrihydrite retarded this phase transformation. The high Fe/As molar ratio (greater than ~5) was more effective at lowering dissolved As concentration because ferrihydrite was the only phase present in the precipitates providing surface sites for arsenate adsorption (Paktunc et al. 2008c). An additional consideration of the Fe/As ratio is the cost effectiveness of using iron as a means of sequestering As; the goal being to use the smallest Fe/As ratio to effectively bind the greatest amount of As. A clear answer to the ideal Fe/As ratio question would be of great economic importance.

Under anaerobic conditions, dissimilatory iron (DIRB) and arsenic respiring bacteria (DARB) use iron and arsenic as terminal electron acceptors as part of their metabolic processes (Lovely, 1997). Many studies have shown that the reduction of both Fe(III) and As(V) in scorodite and arsenical iron-oxyhydroxide minerals is

microbially mediated (Cummings et al., 1999; Papassiopi et al, 2003, Hansel et al., 2003, Slowey et al., 2011). Bacterial reduction of arsenic containing minerals results in the formation of more toxic and mobile As(III). A number of studies on the bacterial reduction of arsenical ferrihydrites have shown that dissolved As(III) is produced and that a wide range of secondary minerals can form during the reduction. For instance, the reduction of 6-line ferrihydrite using *Shewanella oneidensis* MR-1 can produce vivianite (Peretyazhko et al., 2010), while the reduction of adsorbed, arsenical 2-line ferrihydrite with *Shewanella putrefaciens* CN32 generates magnetite, goethite and minor amounts of green rust (Hansel et al., 2003). The reduction of adsorbed, arsenical 2-line ferrihydrite in the presence of *Shewanella* sp. ANA-3 also showed that dissolved As(III) was produced and that magnetite and vivianite formed as secondary mineral phases (Slowey et al., 2011).

A study by Burnol et al. (2007), on the microbial reduction of co-precipitated and adsorbed arsenical 2-line ferrihydrite using *Clostridium* strain FRB1 revealed the presence of vivianite and bobierrite in the solid phases. These microbial reduction studies of ferrihydrites, that found vivianite as a secondary mineral phase, were done using phosphate concentrations ranging from 1 to 2.5 mM which are significantly higher than the concentrations generally encountered in the environment. To date, no microbial reduction studies have been performed on coprecipitated or adsorbed arsenical ferrihydrites at low phosphate concentrations such as the one used in the present study (i.e., 0.045 mM). The presence of high phosphate concentration could lead to phosphate adsorption on the ferrihydrite surface which blocks active sites from the bacteria, and in turn affects the rates of

reduction, as found by Amstaetter et al. (2012), making the results obtained at high phosphate concentration non-applicable to mining environments. Saltikov et al (2005) found that phosphate and arsenate have an effect on the transcription of the *arr/ars* genes in *Shewanella* because phosphate is a structural analog of arsenate, and both can compete for uptake through the phosphate transporters, and both adsorb similarly to Fe(III) oxyhydroxides.

The present study was designed to investigate the microbial reduction of arsenical adsorbed and co-precipitated 6-line ferrihydrite, at a Fe/As molar ratio of 10 using *Shewanella* sp. ANA-3 and *Shewanella putrefaciens* CN32 in a chemically defined growth medium containing 0.045 mM phosphate. The concentrations of the dissolved aqueous species were measured, and the post-reduction solid products were characterized by X-ray diffraction, electron microscopy, electron microprobe and X-ray absorption spectroscopy techniques.

2. Materials and Methods

2.1. Synthesis of adsorbed and co-precipitated arsenical 6-line ferrihydrite

Similar methods were used to synthesize the adsorbed and co-precipitated arsenical 6-line ferrihydrites except for the order of addition of the ferric nitrate ($Fe(NO_3)_3 \cdot 9H_2O$) and the sodium arsenate ($Na_2HAsO_4 \cdot 7\ H_2O$), and the removal of counter ions present from the synthesis.

The synthesis of adsorbed arsenical 6-line ferrihydrite was based on Schwertmann's method (Schwertmann and Cornell, 2000) with some modification in

concentrations of the reactants in order to obtain the optimal yield. Two liters of MilliQ water were heated to 75 ± 1°C in a thermostated Pyrex reaction vessel mounted in a heating mantle, and solid $Fe(NO_3)_3 \cdot 9H_2O$ (40.4 g), was added with continuous stirring at 1600 rpm. The temperature of the solution was maintained at 75 °C for 12 minutes, and then the Pyrex vessel containing the solution was plunged into ice cold water to cool the solution to room temperature. The measured pH of the solution at this stage was 1.7, and the color was dark brown and free of precipitates. The solution was left to stand for a few hours at room temperature, then 3M NaOH was added dropwise to increase the pH to ~2.7, which resulted in the formation of a brown precipitate. After about 5-6 hours, the precipitate settled to the bottom of the beaker, and the clear liquid was removed by decantation. The precipitate was washed and centrifuged until no nitrate was detected in the supernatant solution. The suspension was then re-suspended in about 2 L MilliQ water, and 100 mL of solution containing 3.16 g of sodium arsenate, $Na_2HAsO_4 \cdot 7\ H_2O$ was added with a syringe. The resulting slurry was stirred with a magnetic stirrer for 24 hours at 500 rpm. After the addition of sodium arsenate, the pH rose to 4.6, which is considered to be the optimal pH for the adsorption of As (Loppert et al. 1998). The suspension was left to settle for about a day, and the clear supernatant liquid was removed by decantation. The suspension was centrifuged, transferred to plastic dishes and left to dry in a fume hood. The resulting dry solid was pulverized using a mortar and pestle, and a sample was subjected to XRD to verify its structure.

The co-precipitated arsenical 6-line ferrihydrite was prepared by dissolving 3.16 g of $Na_2HAsO_4 \cdot 7\ H_2O$ to 2 L of MilliQ water and heated to 75 °C in a Pyrex

reaction vessel. The pH of the sodium arsenate solution was decreased from ~ 8 to ~3 by the dropwise addition of trace metal grade concentrated nitric acid. Ferric nitrate, 40.5 g as $Fe(NO_3)_3 \cdot 9H_2O$, was added to the vigorously stirred (~1800 rpm) sodium arsenate solution. The temperature of the stirred solution was maintained at 75 °C for 25 minutes, and the vessel was then plunged into ice water to cool the solution quickly to room temperature. The solution was then transferred into dialysis tubing (Fisherbrand; Type: T2 Membranes: 6000 to 8000 Dalton MWCO; Dia. x Length: 20.4 mm x 30 m), and left immersed in MilliQ water to dialyze for 6 days to remove the counter ions. The MilliQ water was changed at least 3 times a day during the dialysis period. After 6 days, the sample was transferred to large flat plastic dishes and left to evaporate to dryness in the fume hood. The solid sample was pulverized using an agate mortar and pestle. The dark reddish-brown powder was stored in glass vials. A sample of the product was subjected to XRD analysis to verify its structure.

The Fe/As ratios in the adsorbed and coprecipitated 6-line ferrihydrite samples were determined by dissolving weighed masses of the solid, dry samples in 0.50 mL of HCl and diluting to 50.00 mL in a volumetric flask. Triplicate samples of each compound were analyzed by ICP-OES using yttrium as an internal standard for arsenic, and external iron standards for iron. The Fe/As ratios determined by ICP analysis were in good agreement with those determined by visible spectrophotometry (i.e. ferrozine method for iron and molybdenum blue method for arsenic).

2.2. Growth of the bacterial strains

The chemically defined growth medium included 20 mM sodium lactate, 4.5 mM 1,4-piperazine-diethanesulfonic acid (PIPES) buffer, 0.01 mM nitriloacetic acid, and trace element salts, including 0.1 mM $MgSO_4 \cdot 7H_2O$, 2.6 μM $MnSO_4 \cdot H_2O$, 0.15 mM NaCl, 3.2 μM $FeSO_4 \cdot 7H_2O$, 3.8 μM $CoCl_2 \cdot 6H_2O$, 6.1 μM $CaCl_2 \cdot 2H_2O$, 0.93 μM $NaMoO_4 \cdot 2H_2O$, 0.36 μM $CuSO_4 \cdot 5H_2O$, 0.19 μM $AlK(SO_4)_2 \cdot 12H_2O$, 1.5 μM H_3BO_3, 0.68 μM $Na_2WO_4 \cdot 2H_2O$, 0.91 μM $NiCl_2 \cdot 6H_2O$ (Langley et al., 2009). The phosphate (Na_2HPO_4) concentration in the chemically defined growth medium was much lower than the recommended 3.9 mM (Glasauer et. al., 2003).

For the microbial reduction experiments, a single colony of ANA-3 or CN32 was transferred aseptically from the TSA plates to 50 mL of autoclaved tryptic soy broth (TSB) at 23 °C and grown aerobically for 24 hours on a rotary shaker set at 160 rpm. From each culture, 0.5 mL was transferred into 50 mL of 50:50 TSB:CDM mixtures containing 100 μM phosphate. After one day, the sub-culturing was repeated with 5:95 TSB:CDM mixtures with 100 μM phosphate. The final step of growing included the use of 100% CDM with 500 μM phosphate concentration for 36 h at 23 °C. The final cultures contained 0.5 μg/mL of total protein, based on the protocol used by Glasauer et al. (2003), which corresponded to 10^8 cells/mL.

2.3. Microcosms setup and sampling

The microcosm setup was composed of 400 mL of sterile CDM in a 500 mL acid-washed, sterilized Kimax bottles. Adsorbed and coprecipitated arsenical 6-line ferrihydrite precipitates (0.85 g) were added to the bottles, and the pH was adjusted

to 7. The microcosm bottles were wrapped with aluminum foil to prevent possible photochemical reactions. The bottles were inoculated with bacterial culture at time zero, inside the anaerobic chamber, using volumes of inoculum based on the protein assay absorbance measurements. Abiotic controls for the ADS and COP samples were identical to the biotic ones, but did not contain bacteria. The experiments were conducted in duplicate at room temperature inside the anaerobic chamber (atmosphere of 5% H_2:95% N_2). Sampling of each system was performed immediately after they were inoculated at time 0, and subsequently at 93, 190, 383, 600, 838 and 1200 hours or 50 days, where the choices of times for sampling were based on a preliminary ADS and COP experiments that were run for 650 hours. The biotic systems were re-inoculated with bacteria at about 620 hours to ensure the continuation of biotic reduction, because in the previous experiment the bacteria died after 650 hours. For each sub-sampling, the bottles were first shaken vigorously, and 50 mL aliquots were immediately withdrawn while the solid phase material remained suspended. The aliquots were placed into sterile 50 mL centrifuge tubes. A sample of about 7 mL was filtered through a 0.22 μm cellulose acetate syringe filter into a 10 mL centrifuge tube for the determination of dissolved Fe. The cellulose acetate filters were recommended by Heimann and Jakobsen, (2007) for low concentrations of arsenic, because they found that filtering arsenic or phosphate-containing solutions (1.5–47.6 μM) with nylon syringe filters significantly reduced the absorbance readings with the molybdenum blue method. Aliquots of about 3 mL were used for the determination of total Fe, culturing of bacteria and the measurement of Eh and pH. The solid in the remaining 40 mL was isolated by

centrifugation, decantation of supernatant and washing of the sample 5 times after which it was dried in the anaerobic chamber and subsequently subjected to characterization studies.

2.4. Chemical analyses of the aqueous phase

Redox potential measurements, using a portable Eh meter and probe (Corning redox Platinum and Ag/AgCl combination electrode, Corning Inc.), were performed inside the anaerobic chamber on a 2 mL sub-sample from each microcosm bottle. The same sub-sample was then removed from the anaerobic chamber for the measurement of pH using a standard laboratory pH meter and probe (VWR).

The dissolved Fe(II), Fe(III), As(III) and As(V) concentrations were determined immediately following each sampling using the ferrozine method for iron and the molybdenum blue method for arsenic as described in our previous publication (in press).

2.5. Calculations of the initial reduction rates

The initial rates of reduction, in μM/h, were calculated using the slopes of the linear sections of the graphs of the dissolved Fe(II) and As(III) concentrations versus time.

2.6. X-ray diffraction

X-ray diffraction (XRD) analysis of the pre- and post-reduction samples were performed at CANMET with a Rigaku rotating anode X-ray powder diffractometer using a Cu Kα radiation at 55 kV, 180 mA, a step-scan of 0.02° and a scan rate of 1 and 2°/min in 2θ from 5° to 70°.

Sample preparation for the pre-reduction samples was done by grinding the solids with a mortar and pestle, and passing the powder through a 0.45 μm sieve onto a zero background plate.

Post-reduction solid samples were prepared in the anaerobic chamber by placing a few mg of sample, finely ground with an agate mortar and pestle, in a 0.5 or 0.7 mm diameter quartz capillary tube, and sealing the tube with carnauba wax. The capillary tubes were mounted on a zero background plate for analysis.

Micro-XRD analyses were carried out at CANMET with a Rigaku MicroMax-007HF diffractometer, using Cr Kα radiation at 35 kV, 25 mA with a resolution of 100 x 100 pixels. In the goniometer setup, the position of the omega axis was 8°-20° with speed 2 °/sec, the phi axis was from 20°-80° with a speed of 2 °/sec. Collimators used were 50 and 100 μm with exposure times from 5 to 15 minutes. JADE9 MDI software was used for the powder diffraction and micro-XRD data analysis.

2.7. Scanning electron microscopy and electron microprobe analysis

Scanning electron microscopy (SEM) analysis included placing the dried, biotic solid sample, without altering it, directly on a sticky carbon tape and imaging

with a JEOL JSM-6510LV SEM in low vacuum mode. Energy dispersive X-ray spectrometry (EDS), X-Max Large Area Silicon Drift Detector (SDD) size 20 mm^2 with an applied voltage 20 kV, was used for elemental analysis. The EDS spectra were collected with the INCA Energy 350 spectrum analyzer software.

The sample particles were prepared for electron microprobe analysis (EPMA) by embedding them in epoxy, mounting them on a glass slide then polishing and carbon coating before analysis. The analysis was done with a JEOL 8230 SuperProbe electron microprobe fitted with five wavelength dispersive spectrometers and with a high count-rate silicon drift detector EDS spectrometer. The standards used were marcasite for S (Kα), hematite for Fe (Kα), tugtupite for Cl (Kα) and GaAs for As (Lα).

2.8. *X-ray absorption spectroscopy*

X-ray Absorption Spectroscopy (XAS) measurements were carried out at the bending magnet beamline, 20-BM, of the PNC-CAT facility at the Advanced Photon Source, Argonne National Laboratory. This setup included a Si(111) monochromator, cryogenic apparatus, ionization chambers, Vortex-Si Drift detector, and a Canberra 13 element Ge detector (Figures A-8 and A-9 in Appendix). Sample preparation, done in an anaerobic chamber, involved mixing the pulverized sample with boron nitride to dilute the arsenic concentration to about 1 wt %. The samples were mounted in 15 x 4 mm Al sample holders, sealed with Kapton tape on both sides, sent to the measurement site in a sealed anaerobic container, and then stored in an anaerobic chamber. The samples were positioned into the cryogenic

apparatus at an angle of 45 degrees to the incident focused beam and to the Ge fluorescence detector. The K-edge transmission and fluorescence spectra were collected simultaneously at 91 ± 0.5 °K using a beam size of 3500 x 800 μm. Gold foil was used as a reference to monitor energy calibration. Data analysis was done with IFFEFIT (1.2.11. 2008 Matt Newville) and ATHENA (0.8.856 2001-2008 Bruce Ravel) analysis software (Ravel and Newville, 2005).

3. Results

3.1. Aqueous phase analysis

3.1.1. Redox conditions and cell counts

The pH of all biotic samples increased from 7.0 to 7.4 after 600 hours, and then decreased slightly to 7.3 at 1200 hours for all systems. The abiotic control sample displayed no change in pH. The redox values, Eh, for all biotic and abiotic systems were initially 275 ± 3 mV (Figure 3.1 A and C). During the first 93 hours, the Eh values of the biotic systems decreased significantly to 10-60 mV. Over the same time interval, Eh of the abiotic controls only decreased to 245 mV.

Initial cell counts in the biotic systems were in the order of ~3 x 10^8 CFU/mL for both strains, and decreased over the course of the experiment reaching a final value of 1-2 x 10^4 CFU/mL for ANA-3 and CN32 by 1200 hours (Figure 3.1 B and D). No viable bacterial cells were detected in the abiotic controls over the entire duration of the experiment.

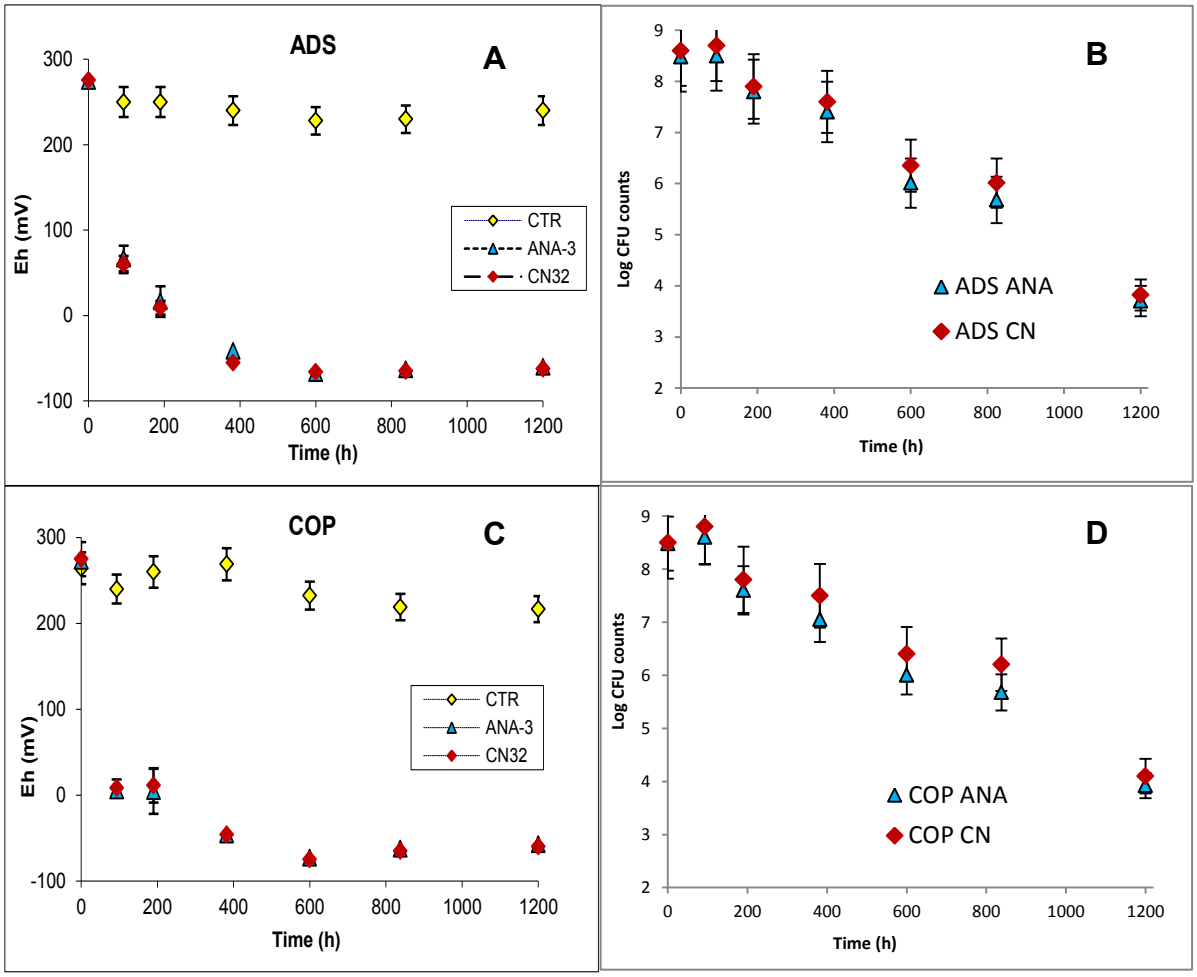

Figure 3.1. (A, C) Redox conditions and (B, D) bacterial cell counts of the ADS and COP arsenical 6-line FH and controls reduced with *Shewanella* sp. ANA-3 and *Shewanella* sp. CN32. CTR is the abiotic control on (A) and (C).

3.1.2. *Arsenic speciation during microbial reduction*

As(V): In the abiotic control, the concentration of dissolved As(V) was ~ 6 µM for the ADS samples and ~ 2 µM for the COP samples at the 93 hour sampling.

In both ADS and COP biotic samples, the dissolved As(V) concentrations were below ~2 μM at the 93 hour sampling and increased slightly to ~ 5 μM at 1200 hours.

As(III): There was no measurable dissolved As (III) present in the abiotic controls over the duration of the experiment as shown on Figure 3.2. In the biotic ADS samples, the release of significant concentrations of dissolved As(III) started after 93 hours and increased to the plateau concentrations of about 41 μM by 600 hours (Figure 3.2). After ~ 620 hours, labelled by an arrow on Figure 3.2, some fresh bacteria were added to keep the colony alive, which resulted in the release of additional dissolved As(III) up to about 60 μM by 1200 hours. In the biotic COP samples, the release of dissolved As(III) started at around 190 hours, ~100 hours later than in the ADS samples.

The addition of fresh bacteria to the COP samples at ~620 hours also resulted in further release of dissolved As(III) to a plateau concentration of 57 μM at 1200 hours for CN32 and ANA-3 (Figure 3.2).

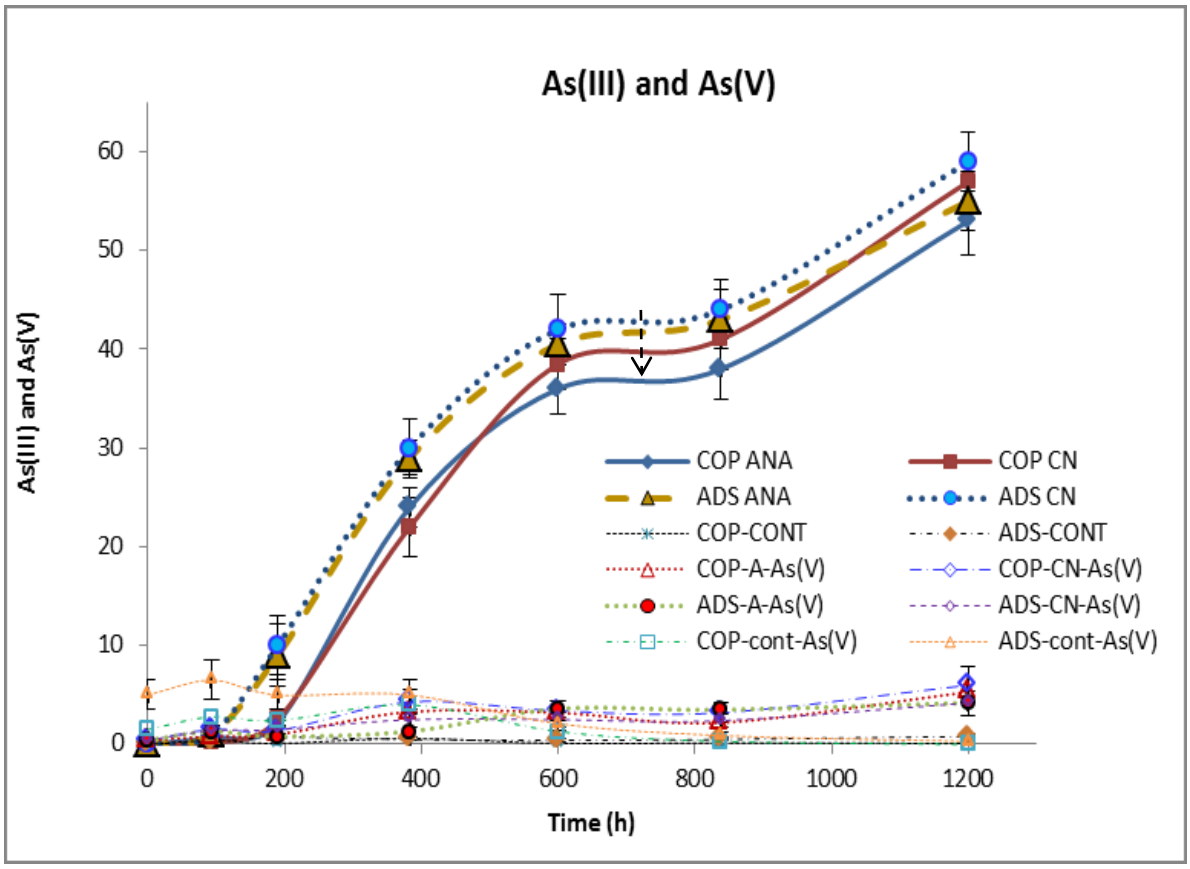

Figure 3.2. Dissolved As(III) and As(V) in the biotic coprecipitated and adsorbed arsenical 6-line FH samples with ANA-3 and CN32 and controls. At the arrow fresh bacteria was added.

3.1.3. *Fe speciation during microbial reduction*

In the abiotic control samples, the concentration of dissolved Fe(III) reached a plateau at the beginning of the experiment of ~120 μM for the ADS and ~100 μM for the COP control samples, and then remained in this range for the rest of the experiment. In the biotic samples, the concentrations of the dissolved Fe(III) reached values of ~ 400 μM for the ADS and ~ 350 μM for the COP samples at 93 h, and then decreased to ~150 μM for both. After the addition of some fresh bacteria

at ~ 620 hours, the Fe(III) concentration increased again to about 300 μM for the ADS and 260 μM for the COP samples (Figure 3.3).

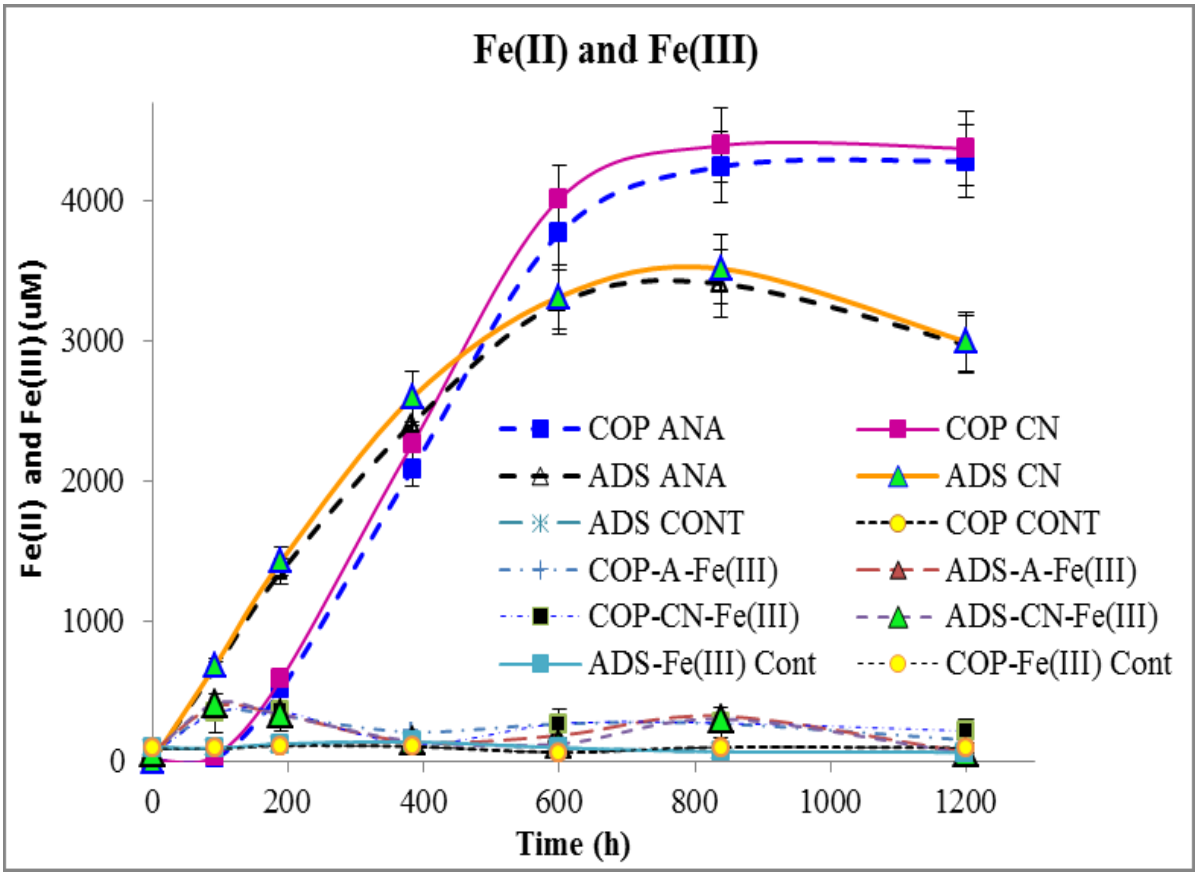

Figure 3.3. Dissolved Fe(III) and Fe(II) in the reduced coprecipitated and adsorbed arsenical 6-line FH samples with ANA-3 and CN32 and controls.

The release of dissolved Fe(II) in the biotic ADS samples started at time 0, reached a plateau of ~ 3500 μM at ~ 700 hours and then decreased steadily to ~ 3000 μM by the end of the run for both bacteria. In the biotic COP samples the release of dissolved Fe(II) did not start until 93 hours, reached a plateau of ~ 4300 μM at ~ 700 hours and stayed around that level until the end of the experiment for both strains.

3.1.4. The initial reduction rates of As and Fe

The initial reduction rates based on the concentration of the dissolved As(III) were ~0.10 μM/h for the ADS samples, and 0.082 μM/h for the COP samples (Table 3.1). The rates were not significantly different for the two bacteria for the corresponding samples.

The initial reduction rates based on the concentration of the dissolved Fe(II) are higher than those based on dissolved As(III) for the corresponding samples. The results indicate that there is no significant difference in the rates determined either for the ADS and COP samples or for the two bacteria (Table 3.1).

Table 3.1. Calculated initial As(V) and Fe(III) reduction rates for adsorbed and co-precipitated arsenical 6-line ferrihydrite, and scorodite for both bacterial strains, *Shewanella* sp. CN32 and *Shewanella* sp. ANA-3 at 0.045 mM phosphate concentration in (μM/h)

Species	**ADS* CN32 Fe/As=10*****	**ADS ANA-3 Fe/As=10**	**COP** CN32 Fe/As=10**	**COP ANA-3 Fe/As=10**	**Scorodite**** CN32 Fe/As=1**	**ANA-3**
As(III)	0.100	0.098	0.086	0.082	23.0	33.7
s.d.	0.0027	0.0043	0.0060	0.0016	2.1	1.6
Fe(II)	7.5	7.1	7.8	7.3	11.9	20.6
s.d.	0.082	0.023	0.74	0.76	1.9	1.3

*adsorbed samples, ** co-precipitated samples, *** Molar ratio

****Results from the average of 6 scorodite biotic reduction experiments each with duplicate runs.

3.2. Solid phase analysis

3.2.1. X-ray diffraction

Powder XRD pattern of the post-reduction ADS and COP 6-line ferrihydrite samples, reduced with *Shewanella* sp. ANA-3, are shown in Figures 3.4 (A) and (B), with times of bacterial reduction in hours listed on the right. In the case of the ADS samples (Figure 3.4 A), the major component in the post-reduction end products remained as 6-line ferrihydrite, but new secondary mineral phases appeared as time progressed, and their proportions increased with time. Analysis of the reduced ADS solids at the 190 hours sampling showed no new secondary mineral phases.

Analysis of the ADS solids after 383 hours of bacterial reduction found a small peak at 2θ of 11.9°, a doublet, suggesting the presence of akaganeite, and another small peak centered at 21.2° suggesting the presence of goethite. As time progressed, these peaks became more prominent.

After 1200 hours, another akaganeite peak appeared at 26.6°. Other peaks, suggesting the presence of goethite, were observed at 17.8° and 36.7°. At 1200 hours, peaks suggesting the presence of hematite appeared at 24.2° and 33.2°.

In the case of the reduced COP samples, the 6-line ferrihydrite was again the major component as for the ADS sample and the new secondary mineral phases appeared as the bacterial reduction progressed. XRD pattern of the sample representing 190 h is identical to the original starting material. After 383 hours, a weak akaganeite doublet appeared at ~11.5° and a weak goethite peak centered at 21.2°. After 600 hours, the akaganeite and goethite peak intensities further increased until 1200 hours. At 1200 hours a weak hematite peak appeared.

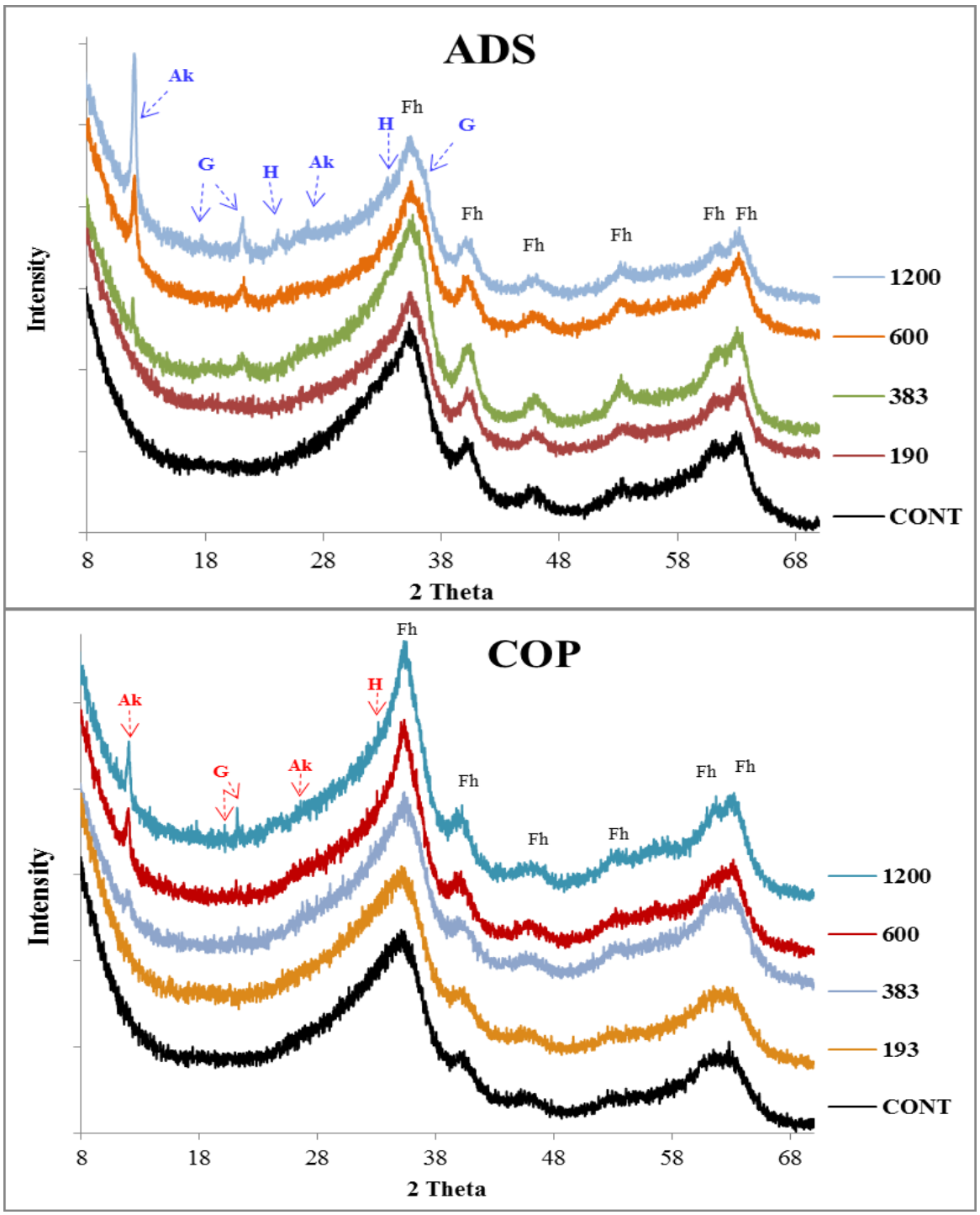

Figure 3.4. Powder XRD patterns of the ADS and COP biotic samples from 90 to 1200 hours with controls. The labels are, akaganeite (Ak), goethite (G), hematite (H) and the original 6-line ferrihydrites (Fh). Numbers on the right are the times in hours.

The micro-XRD analysis of particles in the post-reduction ADS sample, (Figure 3.5 ADS) shows the original 6-line ferrihydrite peaks (Fh), and peaks indicating the presence of new secondary mineral phases, akaganeite (Ak), goethite (G) and a peak, labelled as M? at 90.4° (d spacing of 1.62 Å), believed to represent magnetite, but whose identity could not be confirmed. Goethite (G) and hematite (H) were identified in the post-reduction COP samples by their peaks G and H, shown in Figure 3.5 COP.

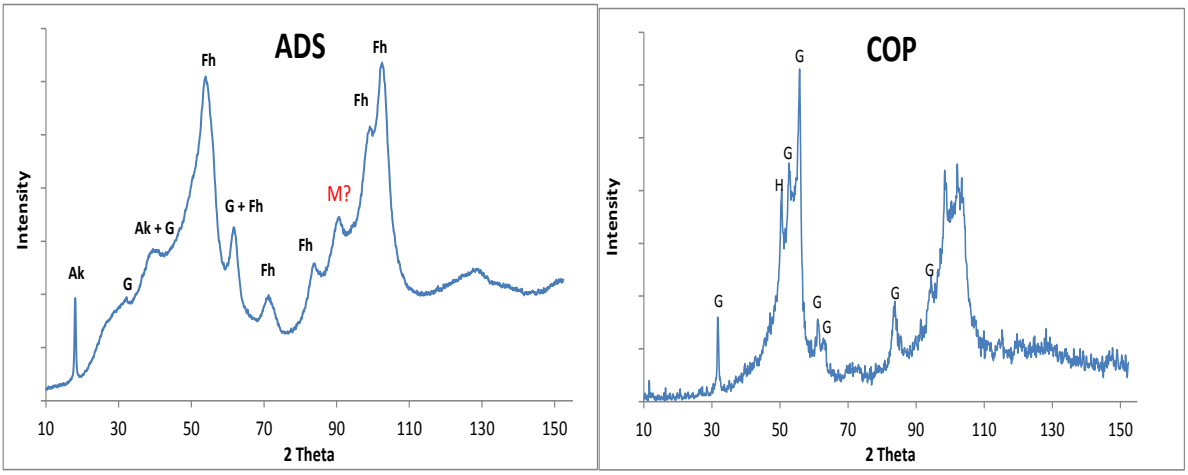

Figure 3.5. Micro-XRD analysis of the post-reduction solid samples. On the ADS figure the reflections labelled identified as akaganeite (Ak), goethite (G), a peak marked M? at 90.4° degree 2θ is unconfirmed magnetite. On the COP figure the reflections are goethite (G) and hematite (H).

3.2.2. Scanning electron microscopy and electron microprobe

The new secondary compounds identified in the post reduction samples by SEM (Figure 3.6) are (A) akaganeite, (B) hematite, (C) goethite and (E and F) possibly magnetite An unidentified multifaceted microcrystalline mineral observed

after 600 hours of bacterial reduction in the COP-CN sample (Figure 3.6 D). The energy dispersive analyses (EDS) (Figure 3.6 G) show iron as the only main component for all new secondary minerals found in the reduced samples. No arsenic emission peaks were present on the EDS spectra of these new secondary compounds.

Further morphological features observed during SEM examinations are bacterial imprints or “footprints” with sizes of about 1 to 2 μm on the surfaces of the washed ADS and COP samples (Figures 3.7A-B). The bacterial “footprints” were either singular or occurred in colonies which appear to be randomly distributed on the surfaces of the particles, and were not visibly associated with specific surface features. Energy dispersive analysis of these particles revealed the concentrations of ~1% As and ~35 % Fe.

The most striking features are rod like patterns etched onto the surface, about 2 to 3 μm in length which resemble the shape of *Shewanella* bacteria (Figure 3.7). Other notable features are circular imprints ranging from about 0.2 μm to about 1.5 μm in diameter etched on the surfaces of the post reduction mineral phases. These etched patterns were abundant on the surfaces of the crystalline secondary compounds formed after 1200 hours of bacterial reduction. In some particles with hexagonal outlines (Figures 3.6 B and 3.7 D), the etched circular holes appear to accumulate towards the center of the particle, indicating new growth at the edges. There are visible irregular cracks and crevasses on some of the SEM images (Figures 3.6 B and 3.7 C) and many of the etched patterns seem to be associated with them.

Based on the hexagonal morphology and chemical composition, such particles shown on Figures 3.7 C, D, E and F were interpreted to be hydrohematite.

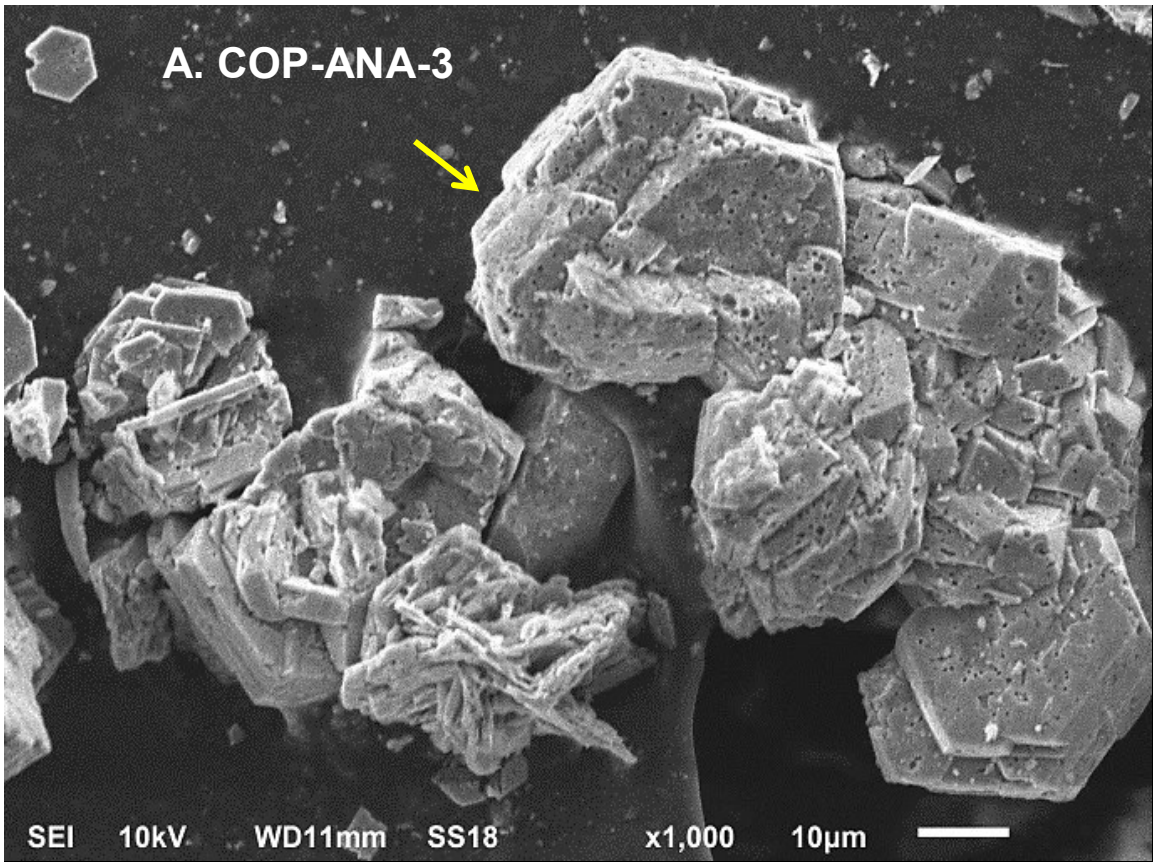

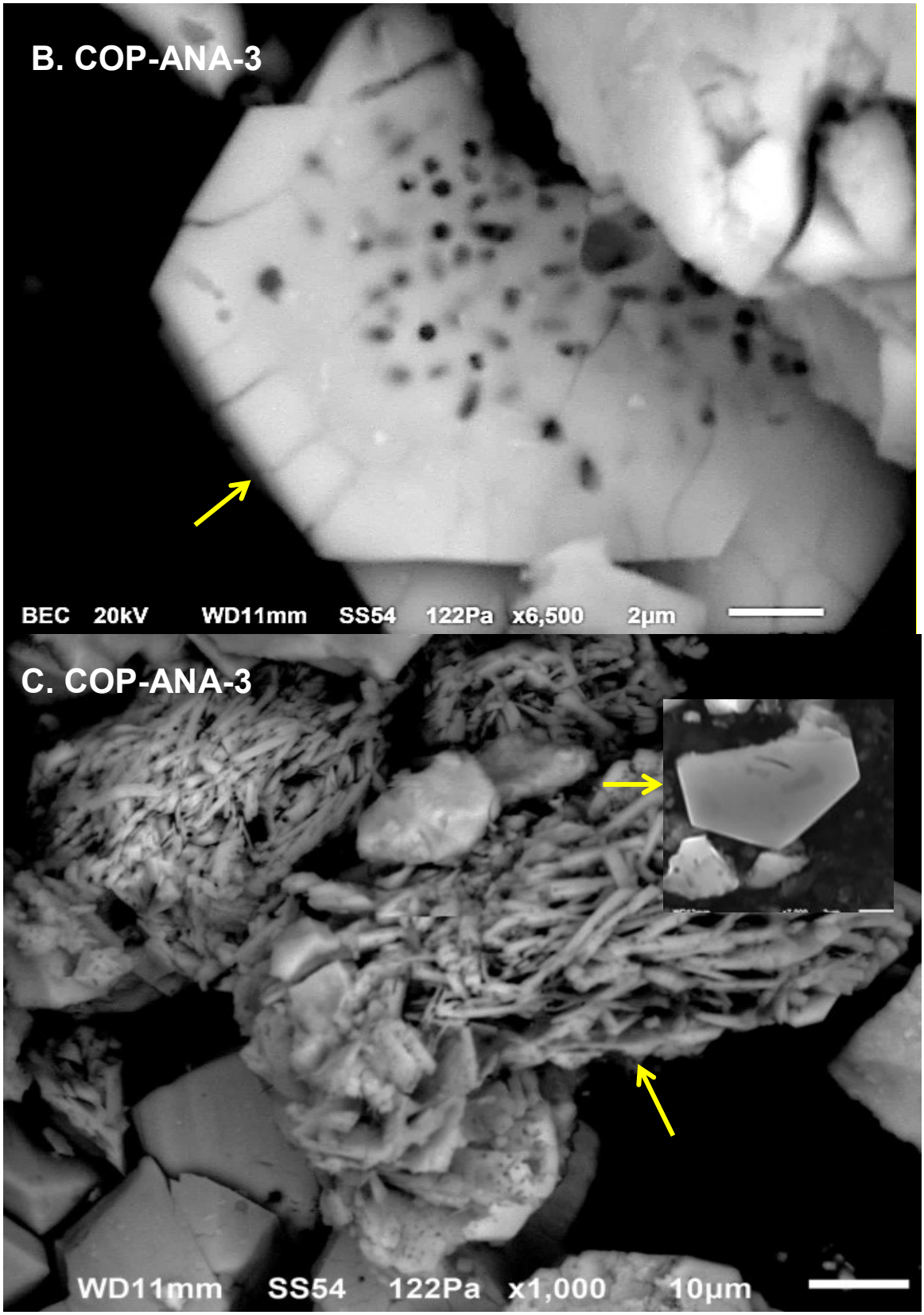
B. COP-ANA-3
BEC 20kV WD11mm SS54 122Pa x6,500 2µm
C. COP-ANA-3
WD11mm SS54 122Pa x1,000 10µm

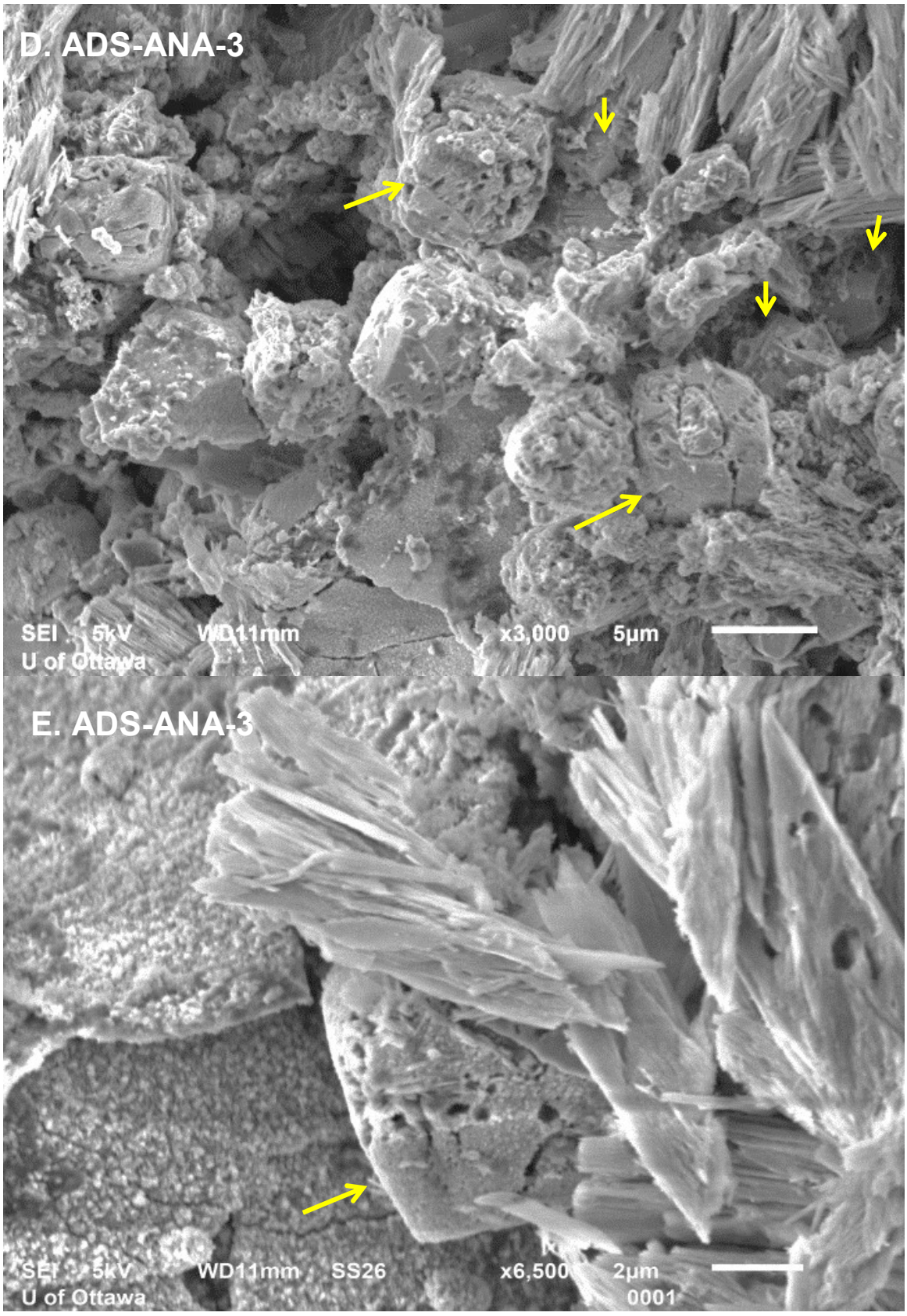
D. ADS-ANA-3
SEI 5kV WD11mm x3,000 5µm
U of Ottawa
E. ADS-ANA-3
SEI 5kV WD11mm SS26 x6,500 2µm
U of Ottawa 0001

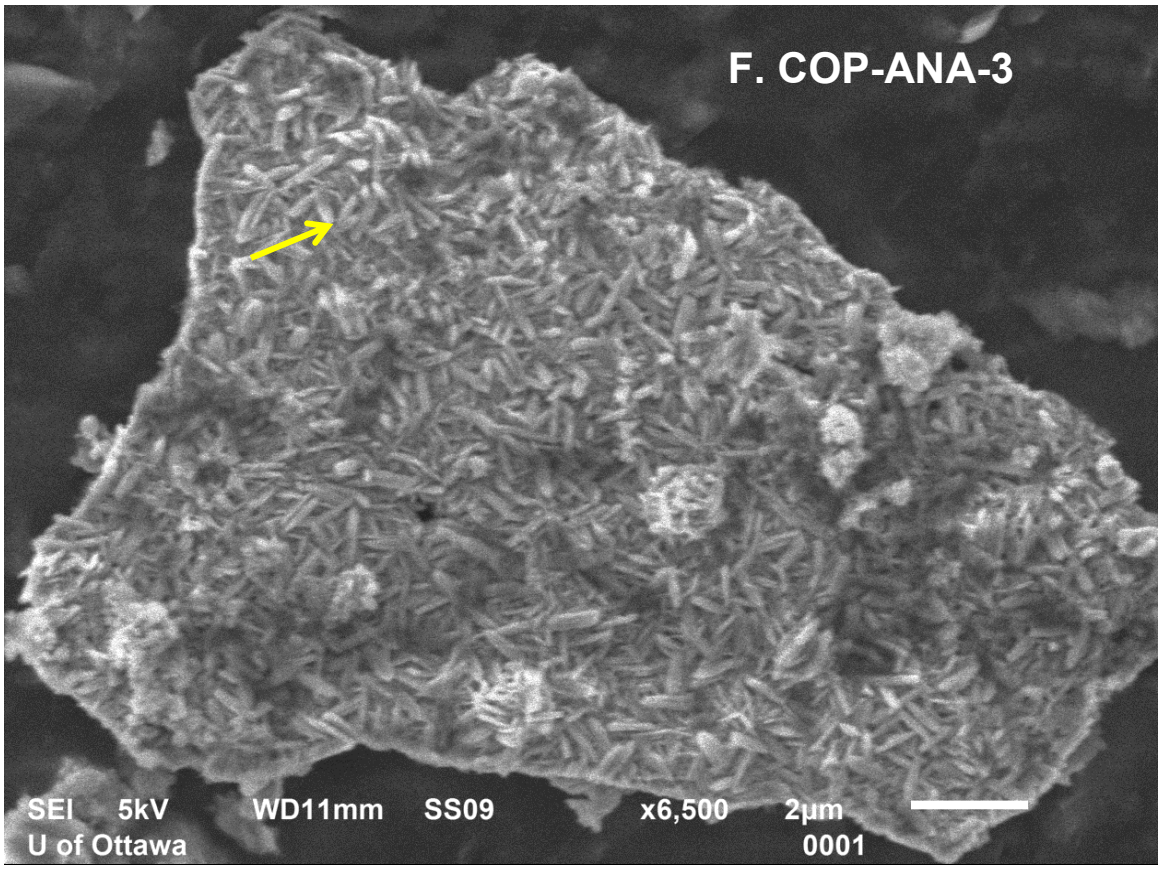
F. COP-ANA-3
SEI 5kV WD11mm SS09 x6,500 2µm
U of Ottawa 0001

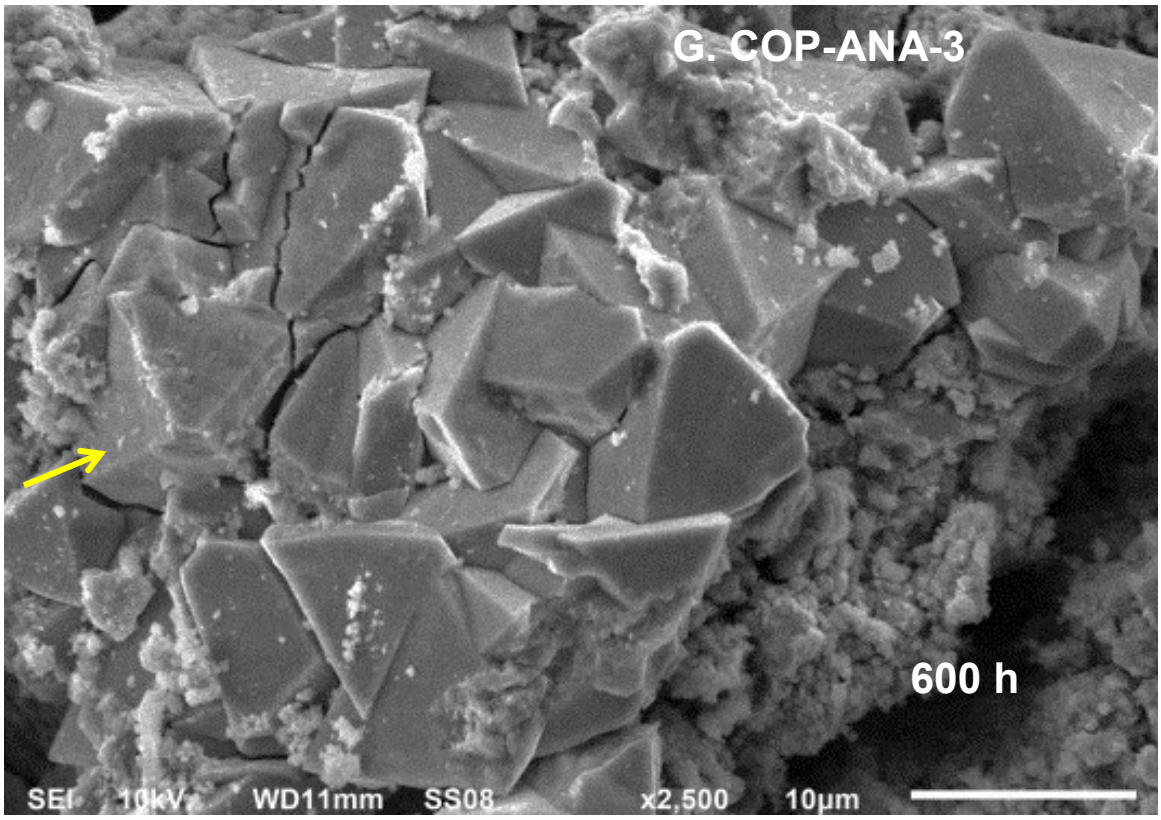
G. COP-ANA-3
600 h
SEI 10kV WD11mm SS08 x2,500 10µm

Figure 3.6. SEM images of the secondary minerals (arrows) at 1200 hours in the biotic coprecipitated (COP) and adsorbed (ADS) samples. Inset on (B) is 600 hours in the COP-CN sample. (F) Goethite crystals on the COP-ANA-3 sample. (G) A multifaceted mineral in the COP-CN sample at 600 h.

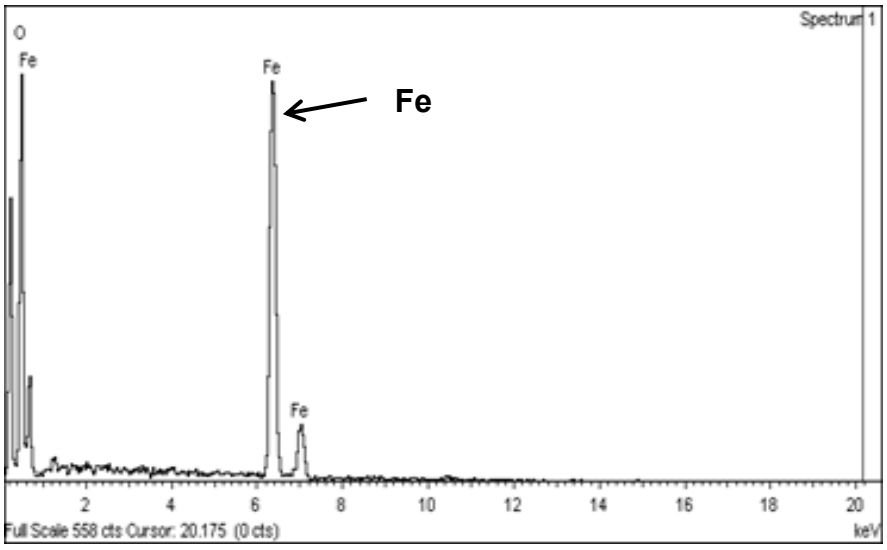

Figure 3.6 H. Representative energy dispersive spectrum (EDS) analysis detected only Fe in the newly formed secondary minerals.

Figure 3.8 shows the hexagonal particles which were analyzed by electron microprobe (EPMA) to determine if they were hematite or green rust. The different zones are visible on Figure 3.8 of an EPMA image of a hexagonal particle. The crosses mark the areas analyzed. The cracks in the particles are due to dehydration during storage.

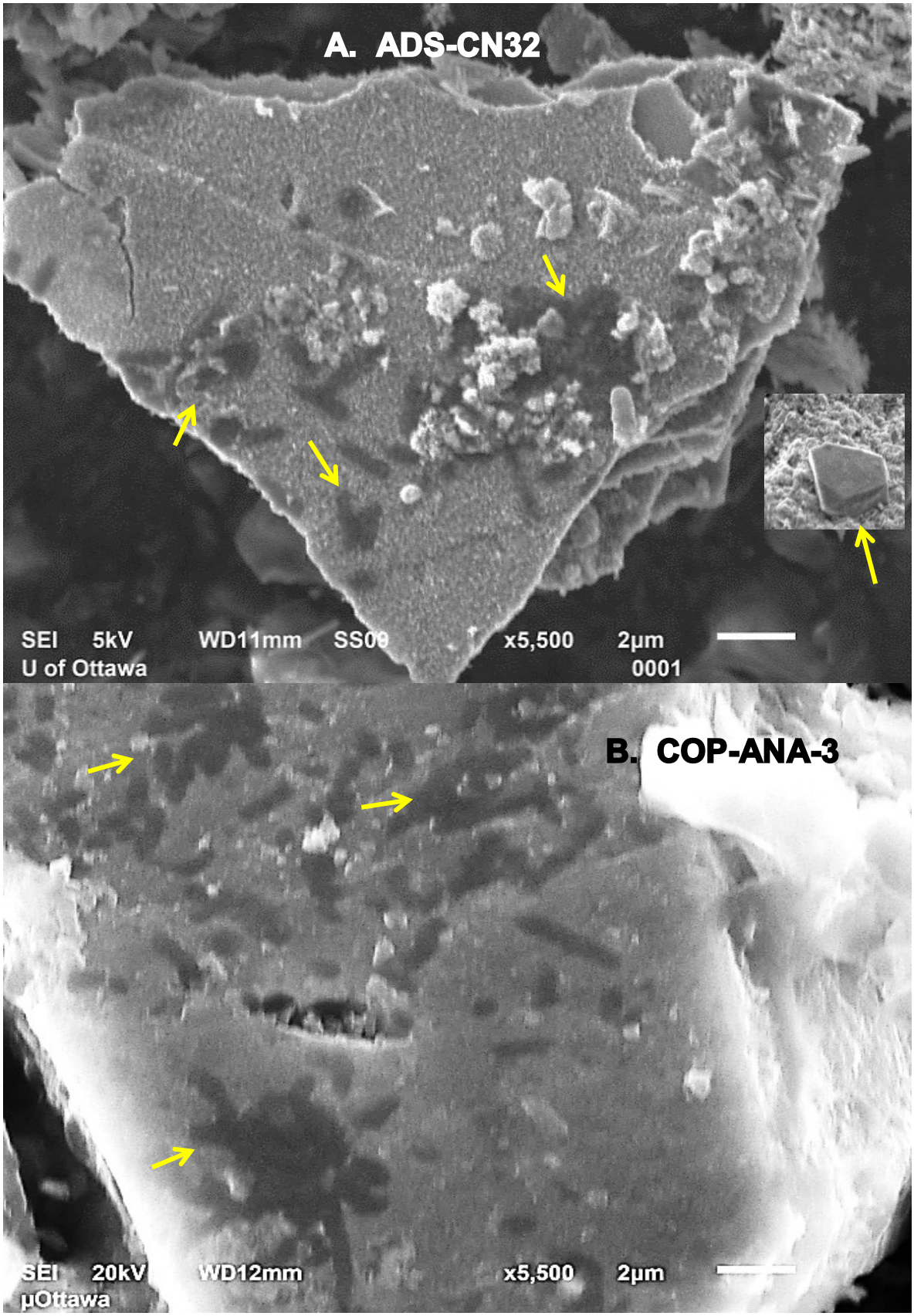
A. ADS-CN32
SEI 5kV WD11mm SS09 x5,500 2µm
U of Ottawa 0001
B. COP-ANA-3
SEI 20kV WD12mm x5,500 2µm
µOttawa

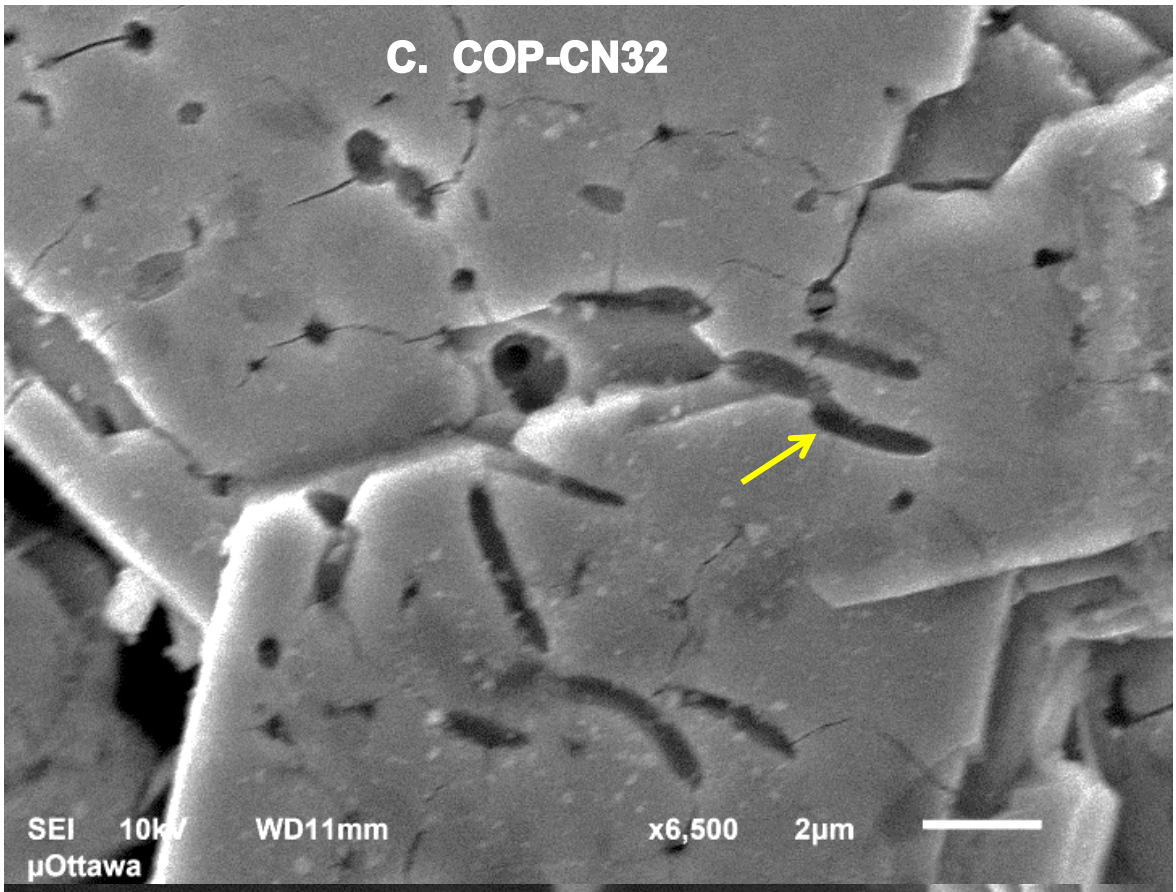
C. COP-CN32
SEI 10kV WD11mm x6,500 2µm
µOttawa

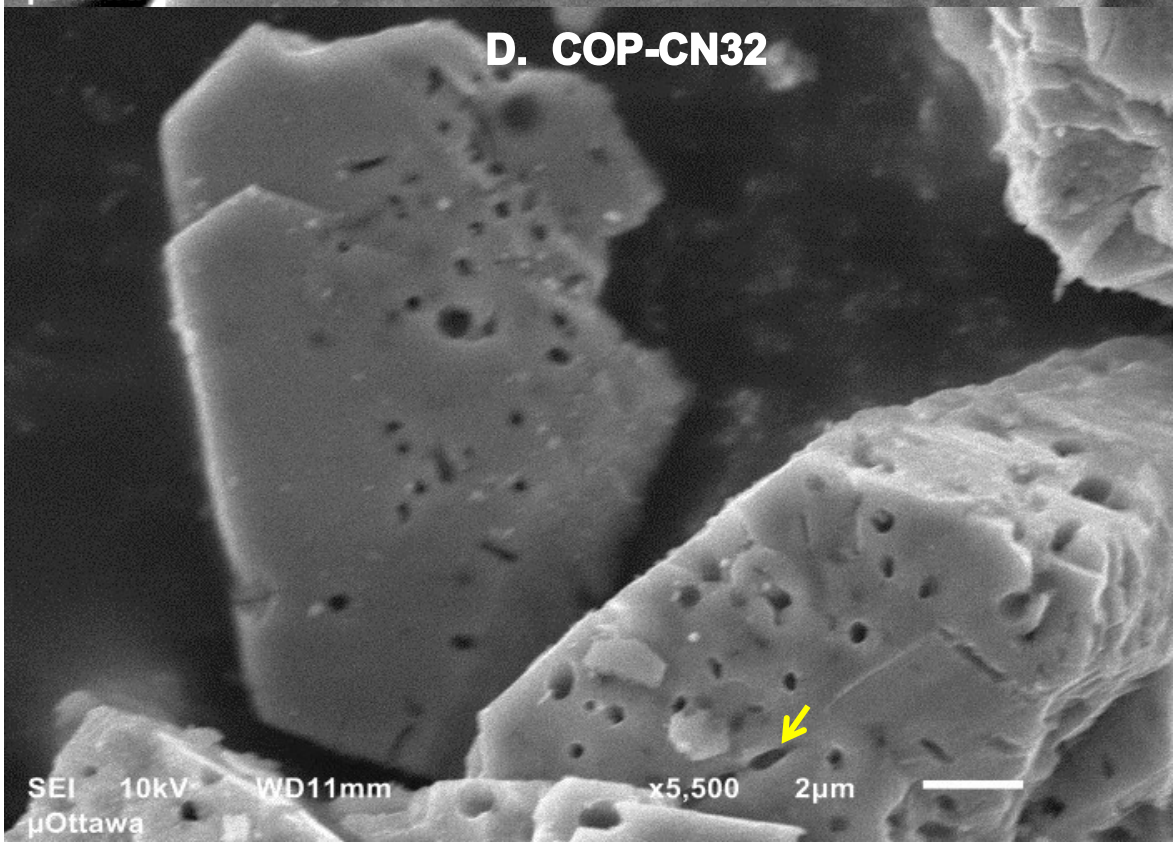
D. COP-CN32
SEI 10kV WD11mm x5,500 2µm
µOttawa

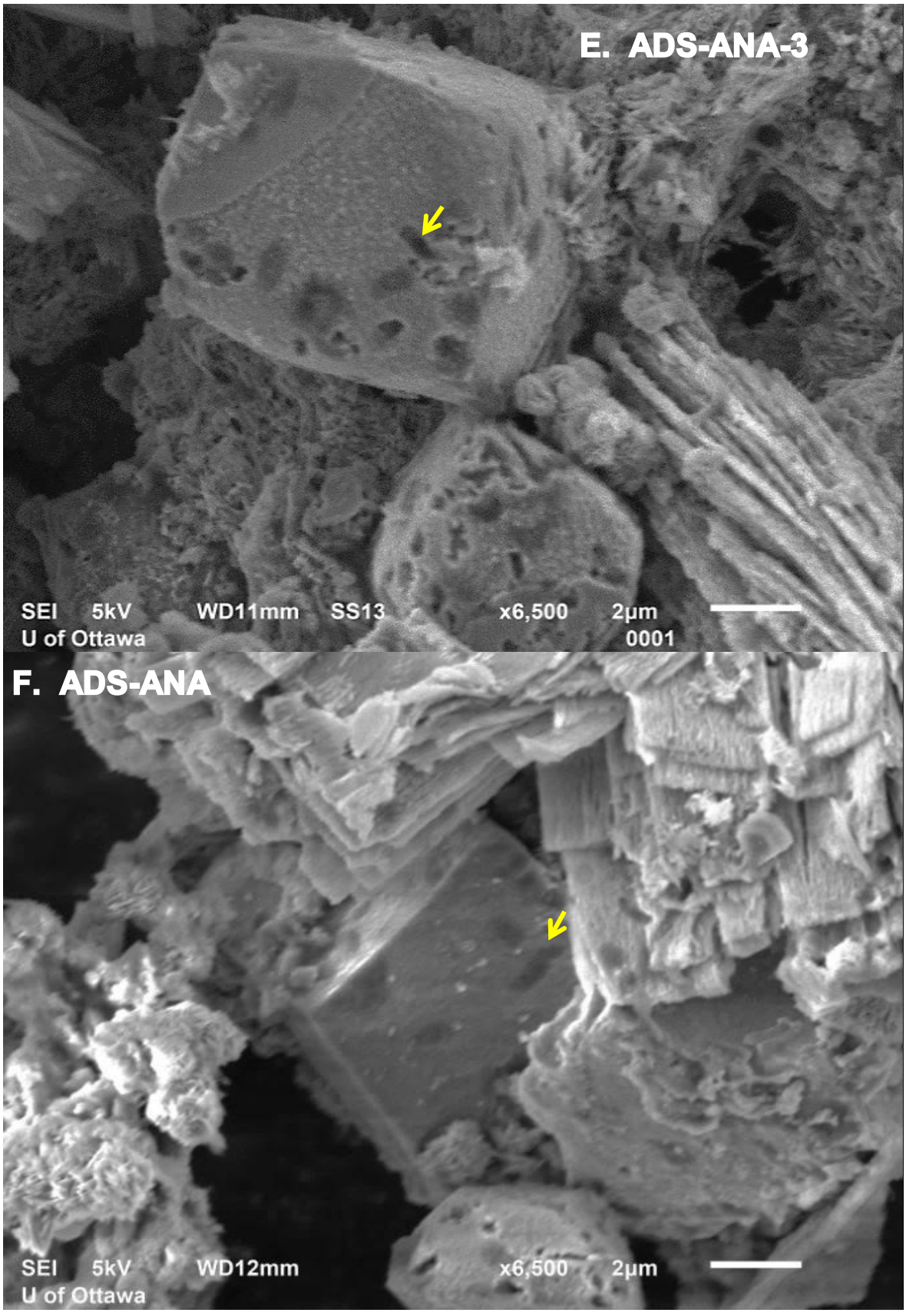
E. ADS-ANA-3
SEI 5kV WD11mm SS13 x6,500 2µm
U of Ottawa 0001
F. ADS-ANA
SEI 5kV WD12mm x6,500 2µm
U of Ottawa

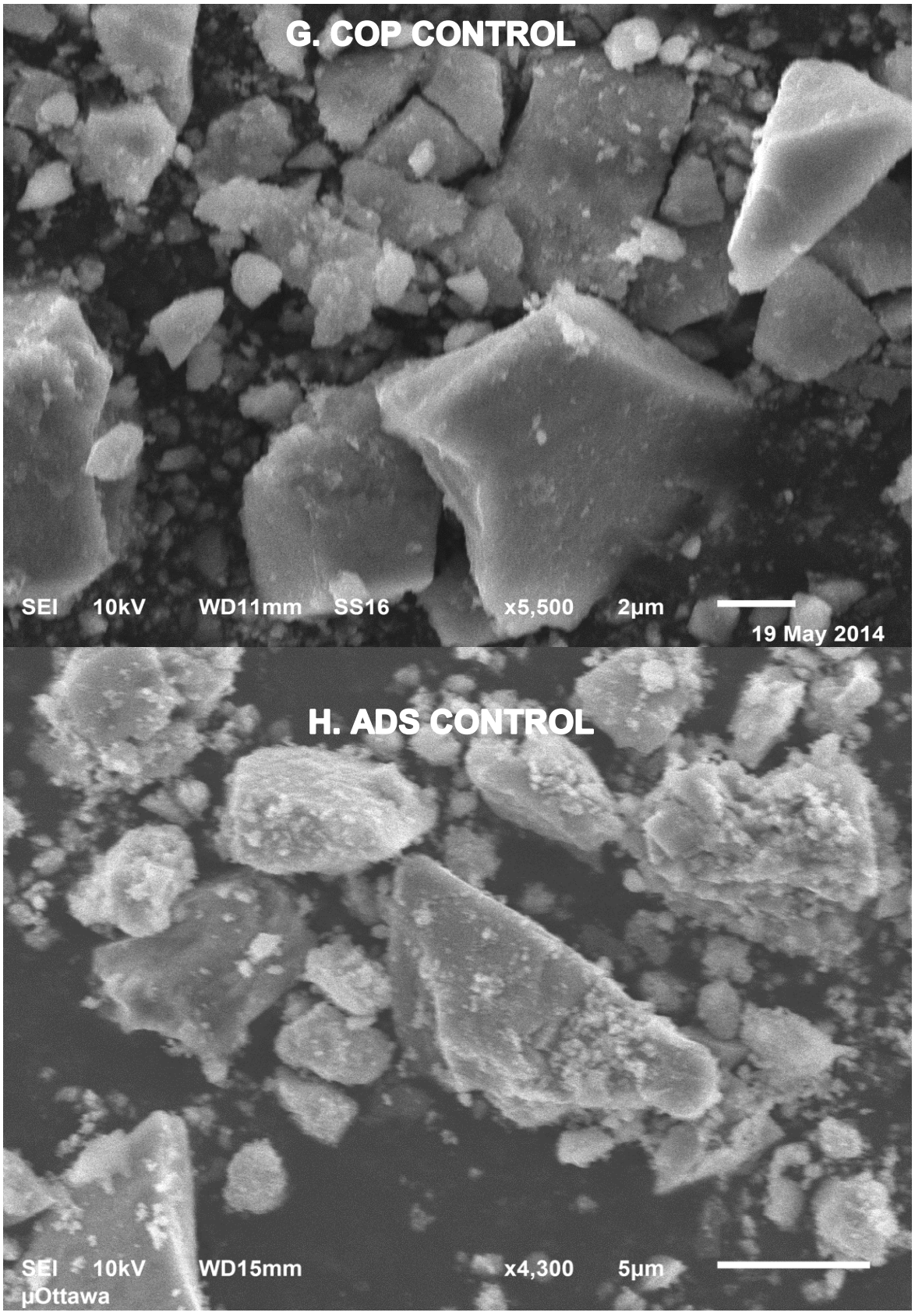
G. COP CONTROL
SEI 10kV WD11mm SS16 x5,500 2µm
19 May 2014
H. ADS CONTROL
SEI 10kV WD15mm x4,300 5µm
µOttawa

Figures 3.7. SEM images at 1200 hours showing bacterial “footprints” (A and B) and deeper imprints (C, D, E, F) on the surfaces of adsorbed (ADS) and coprecipitated (COP) solids using ANA-3 and CN32 (arrows). The inset shows a particle (A) at 600 hours with no holes on the top of a rugged surface. (G) COP Control, (H) ADS Control.

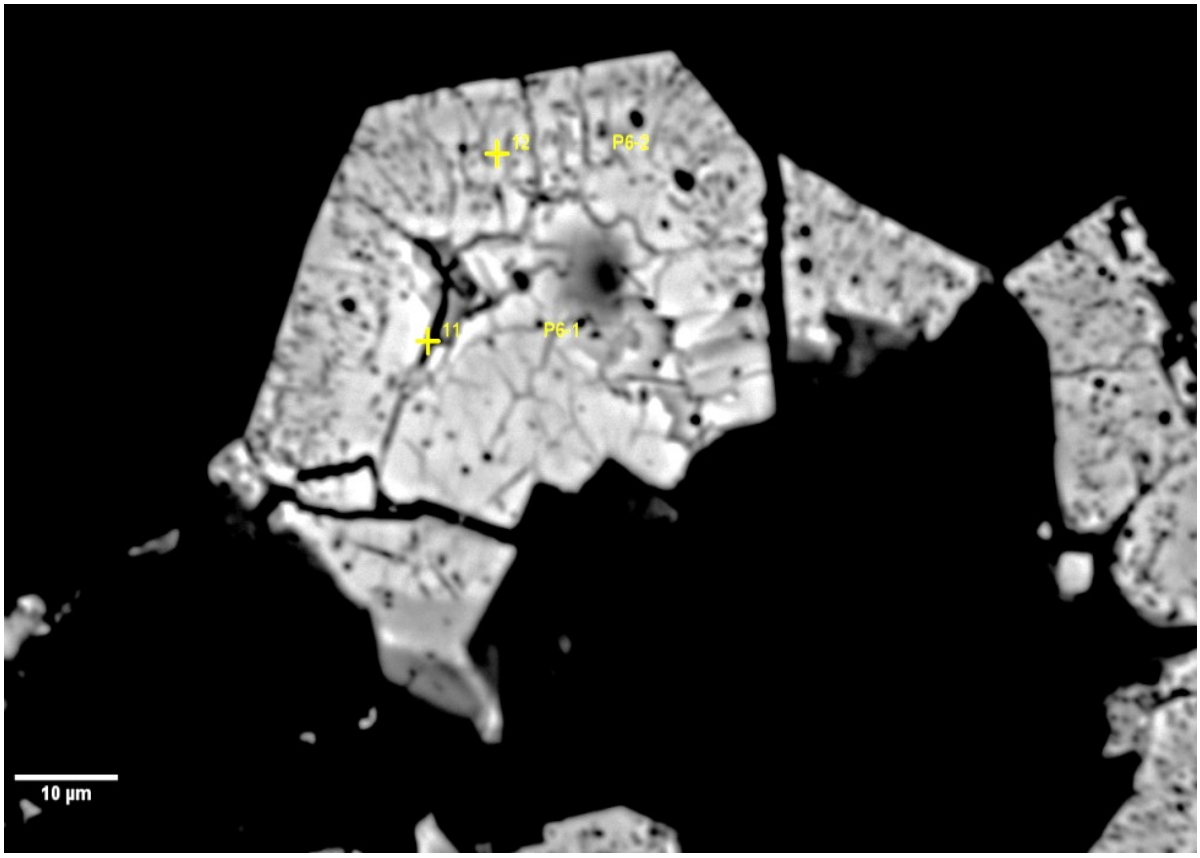

Figure 3.8. Backscattered electron image of a hexagonal particle identified as hydrous hematite by electron microprobe analysis. Areas analyzed marked by the crosses.

3.2.3 X-ray absorption spectroscopy (XAS)

Normalized As K-edge XANES spectra in Figure 3.9 show the time development of the As(III) peaks of the ADS and COP arsenical 6-line ferrihydrite (6LFH) samples. The top 4 curves on Figure 3.9, labelled on the right as CN-383 to CN-1200, are the CN32 reduced samples at different sampling times, and the bottom 4 curves are the ANA-3 samples. As the bacterial reduction progressed, the As(III) peak at ~11871 eV became more prominent whereas the As(V) peak, at ~11875 eV gradually diminished.

The normalized As K-edge XANES linear combination fitting of the ADS and COP samples (Figures 3.10 and 3.11) were done using over 27 inorganic and organic arsenic reference compounds, and the best fit values were found with the original adsorbed arsenical 6LFH and a biogenic Fe(II)-As(III) mineral (Tables S1-S4, Supplementary material). The normalized XANES and the k^3-weighted As K-edge EXAFS spectra representative of the reduced As-6LFH samples and their linear combination fitting along with the two end members are shown in Figures 3.14. The two bottom curves represent the two end members, the original COP arsenical 6LFH and the biogenic Fe(II)-As(III) compound (Figure 3.14). The fractional composition of the endmembers changed as a function of time, that is the fraction of the original COP arsenical 6LFH is decreased whereas the biogenic Fe(II)-As(III) compound increased from 383 to 1200 hours (Figure 3.14).

Figure 3.15 shows the component fractions of (A) XANES and (B) EXAFS fitting results. The data used for Figure 3.14 are listed in Tables S1-S4 for the ADS and COP samples with ANA-3 and CN32. The bottom curves on Figure 3.14 show the

change of the As(V) fractions with time, and the top curves show the As(III) accumulation as a result of the bacterial reductive dissolution for the ADS and COP samples.

In the biogenic Fe(II)-As(III) mineral Fe(II) and As(III) are associated with the exopolymeric substance (EPS) of the bacterial surface which was characterized with EXAFS fitting by Babechuk et al. (2009). As time progressed the proportion of the biogenic Fe(II)-As(III) mineral increased in both ADS and COP samples.

The fractions of As(III) in the post-reduction ADS solid samples using As K-edge XANES linear combination fitting are listed in Table S1. The composition of the solid sample at 383 hours was about 50 % biogenic Fe(II)-As(III) compound and about 50 % the original ADS 6LFH. The composition of the post-reduction end products, after 1200 hours of bacterial reduction, was ~70 % biogenic Fe(II)-As(III) compound and ~30 % ADS arsenical 6LFH for both bacterial strains. Linear combination fittings of the k^3-weighted As K-edge EXAFS spectra for the ADS arsenical 6LFH are shown in Figure 3.12 and Table S2. The composition of the post-reduction products at the 383 hour, were about 50 % biogenic Fe(II)-As(III) compound and about 50 % ADS arsenical 6LFH for both strains. The composition of the final products were 70 % biogenic Fe(II)-As(III) compounds and about 30 % of the ADS arsenical 6LFH, in agreement with the XANES fitting results.

The linear combination fitting of the As K-edge XANES spectra for the COP arsenical 6LFH post-reduction samples are shown in Figure 3.11 and Table S3. The composition at 383 hour, were close to 50 %, within experimental error for the biogenic Fe(II)-As(III) compound and the COP arsenical 6LFH for both strains. The

final compositions of the post reduction solids were about 65 % biogenic Fe(II)-As(III) compound and about 35% COP arsenical 6LFH for both strains. The EXAFS linear combination fitting results of the k^3-weighted As K-edge spectra for the post reduction COP samples are shown in Figure 3.13 and Table S4. The approximate compositions of the reduced solids were 40 % biogenic Fe(II)-As(III) compound and 60 % COP arsenical 6LFH for CN32 and ANA-3 at 383 hours, and 65 % biogenic Fe(II)-As(III) compound and 35 % for CN32 and ANA-3 after 1200 hours.

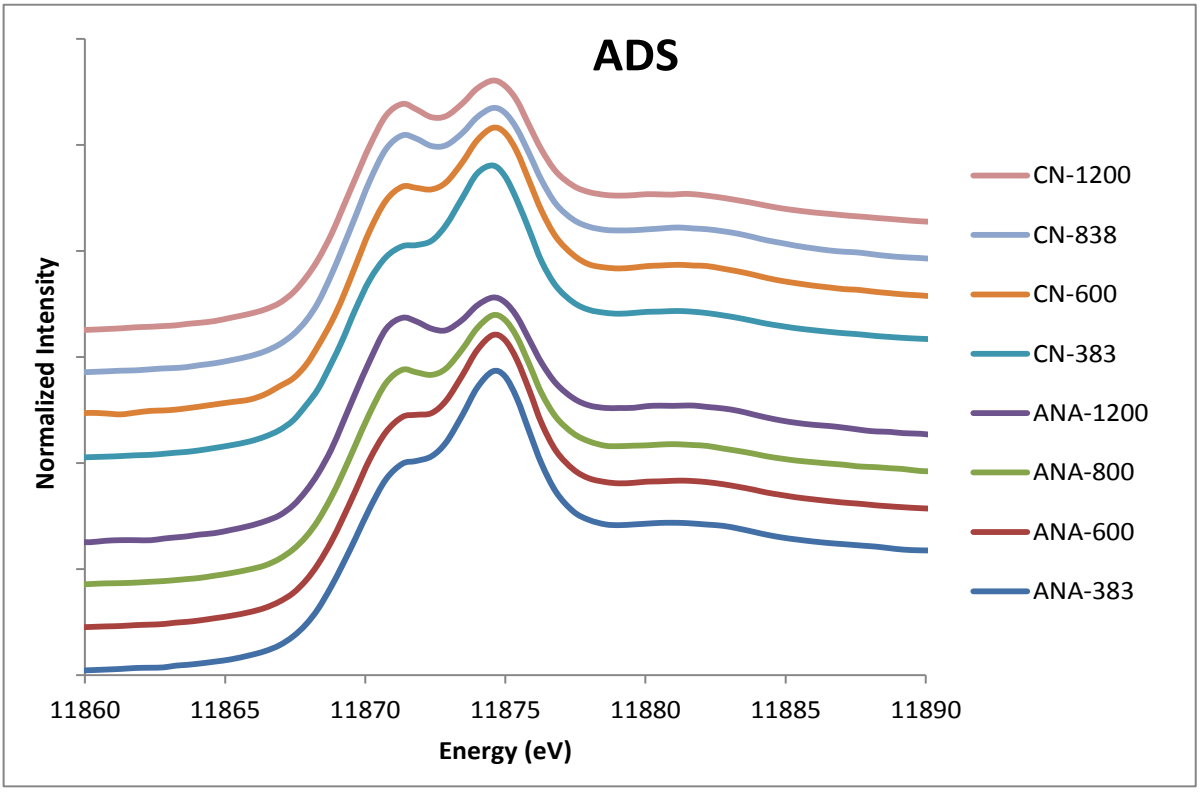

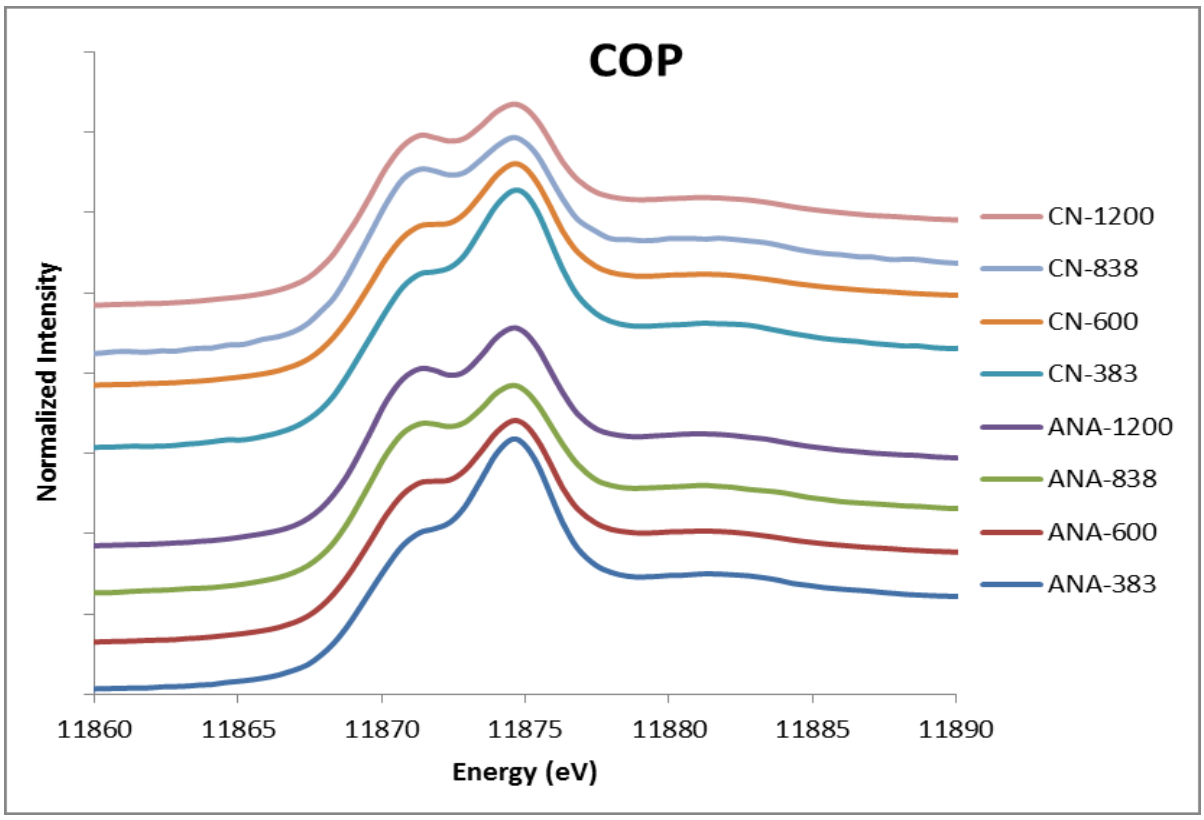

Figure 3.9. Arsenic K-edge XANES spectra show the biotic adsorbed (ADS) and coprecipitated (COP) arsenical 6-line ferrihydrite samples after 1200 hours. On the top CN32 and on the bottom ANA-3.

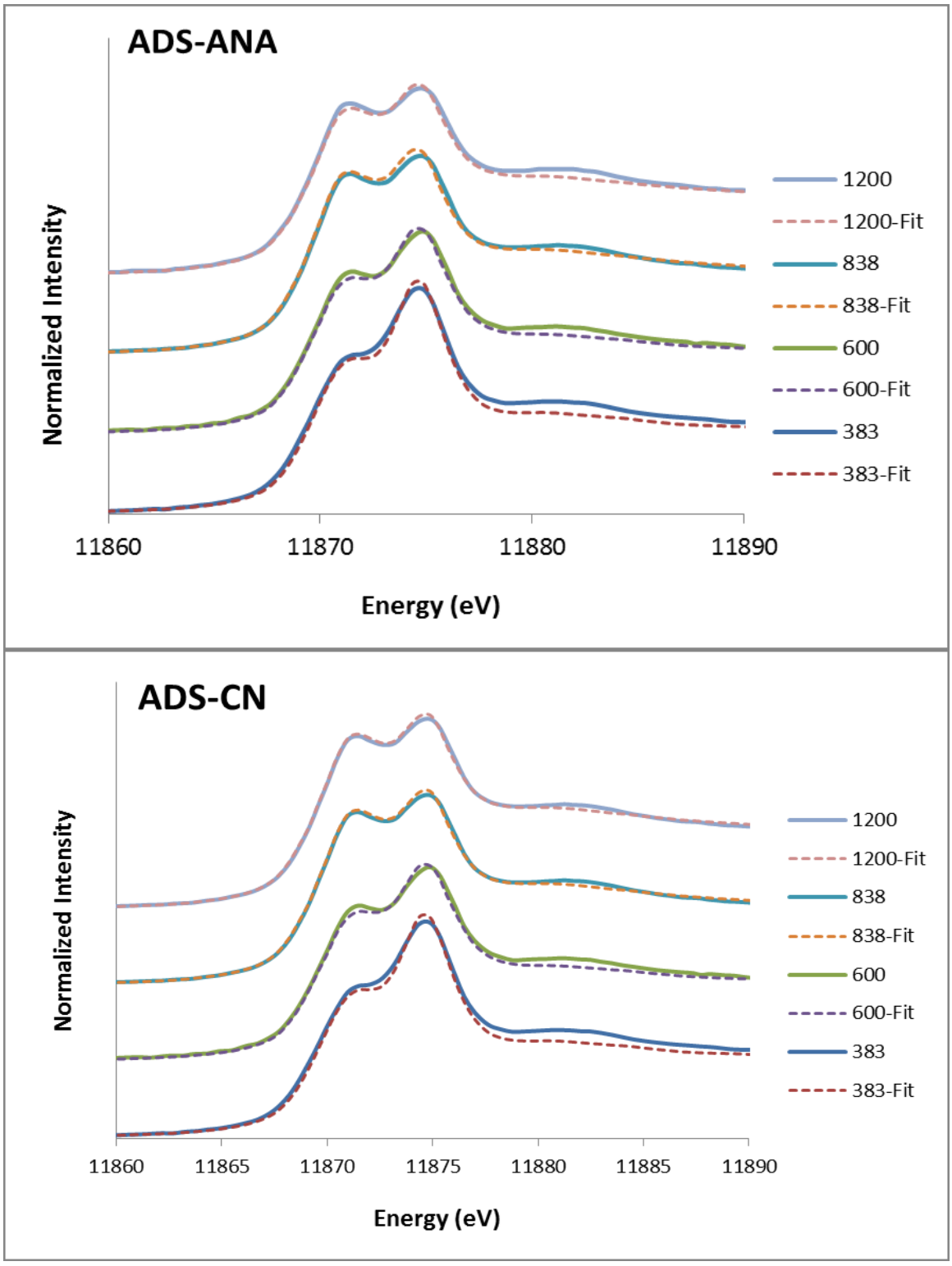

Figure 3.10. As K-edge XANES spectra (solid lines) and linear combination fitting (dotted lines) of biotic ADS arsenical 6-line ferrihydrite with CN32 and ANA-3.

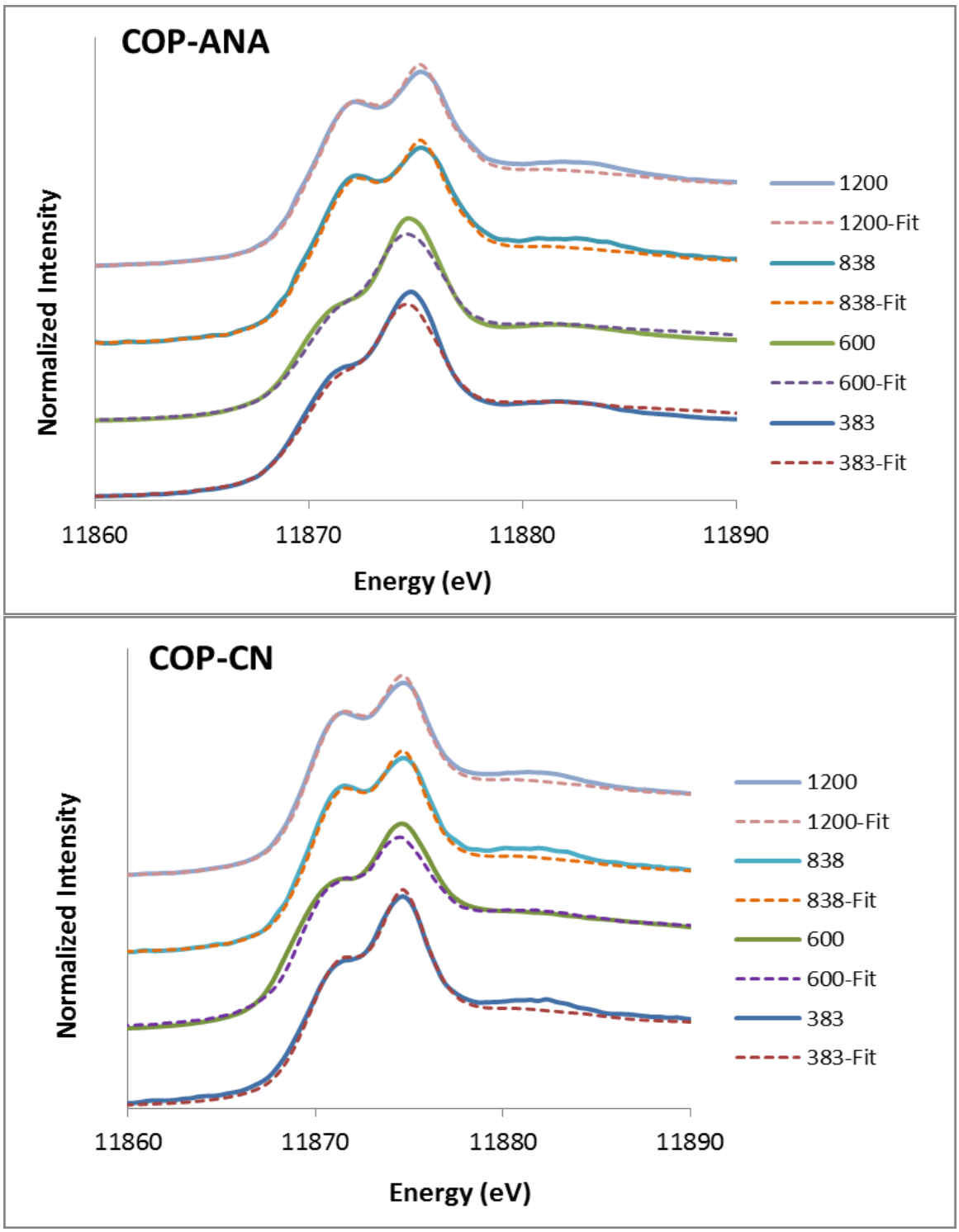

Figure 3.11. As K-edge XANES spectra (solid lines) and linear combination fitting (dotted lines) of biotic COP arsenical 6-line ferrihydrite with CN32 and ANA-3.

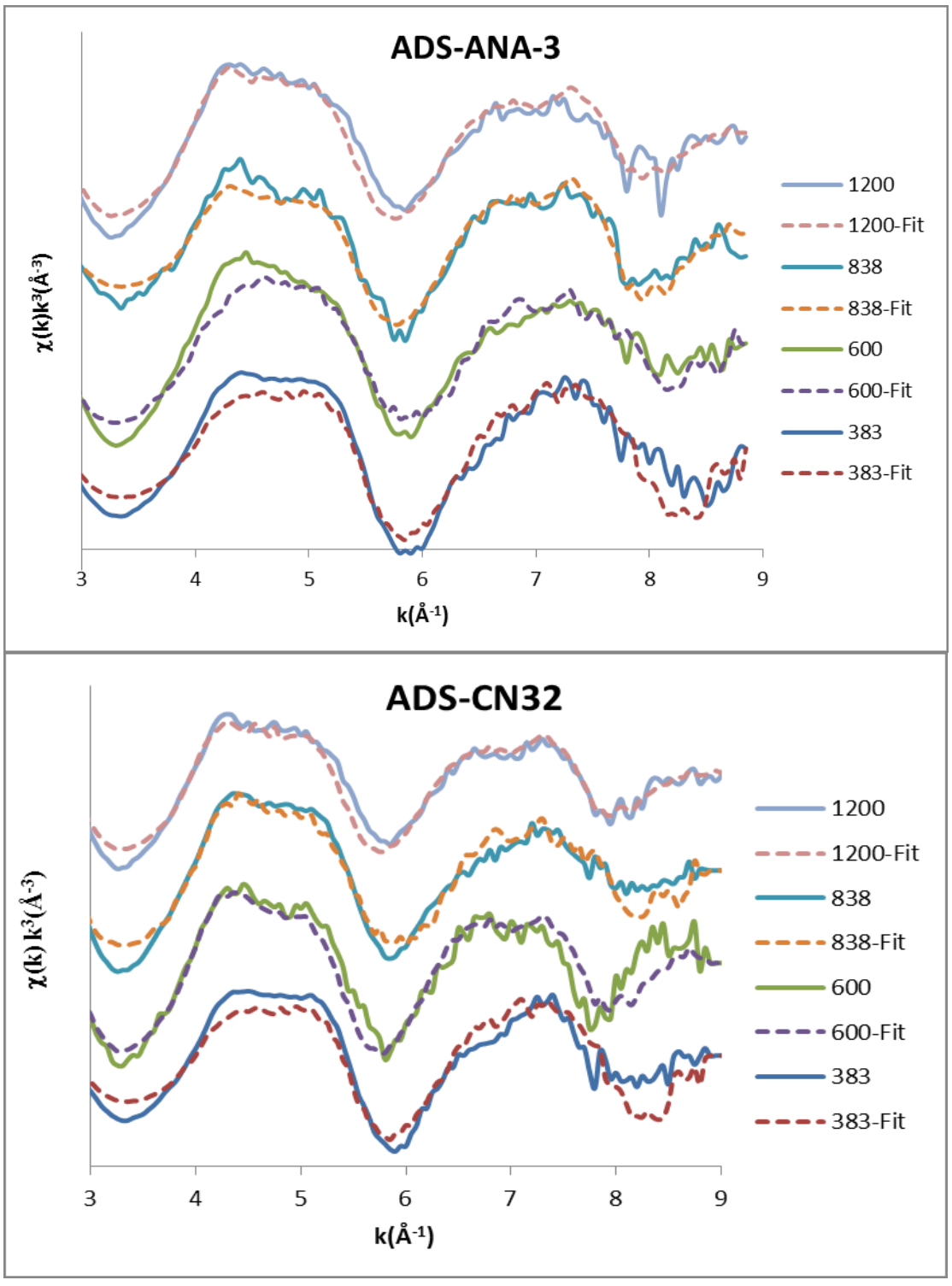

Figure 3.12. As K-edge EXAFS spectra (solid lines) and linear combination fitting (dotted lines) of biotic ADS arsenical 6-line ferrihydrite with CN32 and ANA-3.

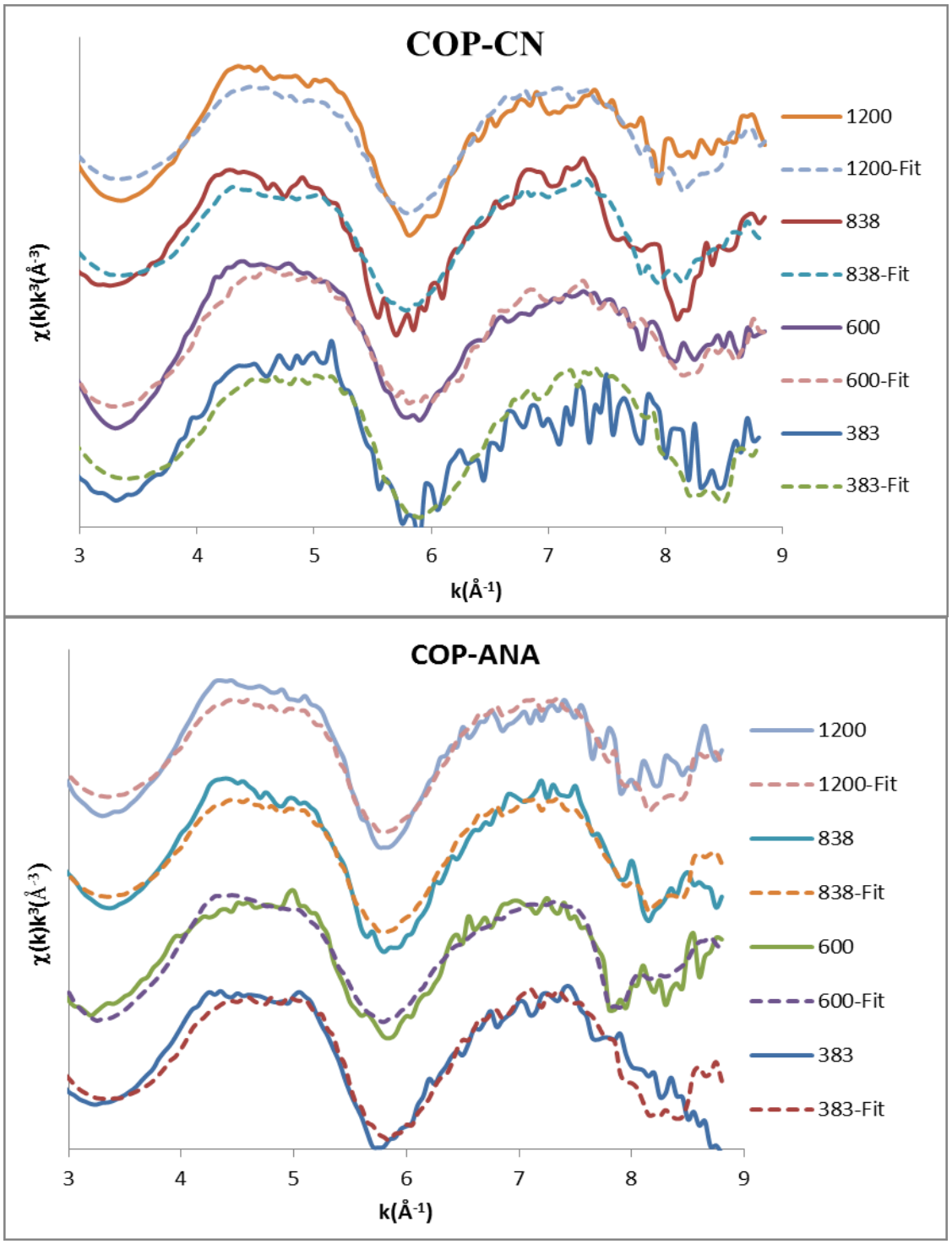

Figure 3.13. As K-edge EXAFS spectra (solid lines) and linear combination fitting (dotted lines) of biotic COP arsenical 6-line ferrihydrite with CN32 and ANA-3.

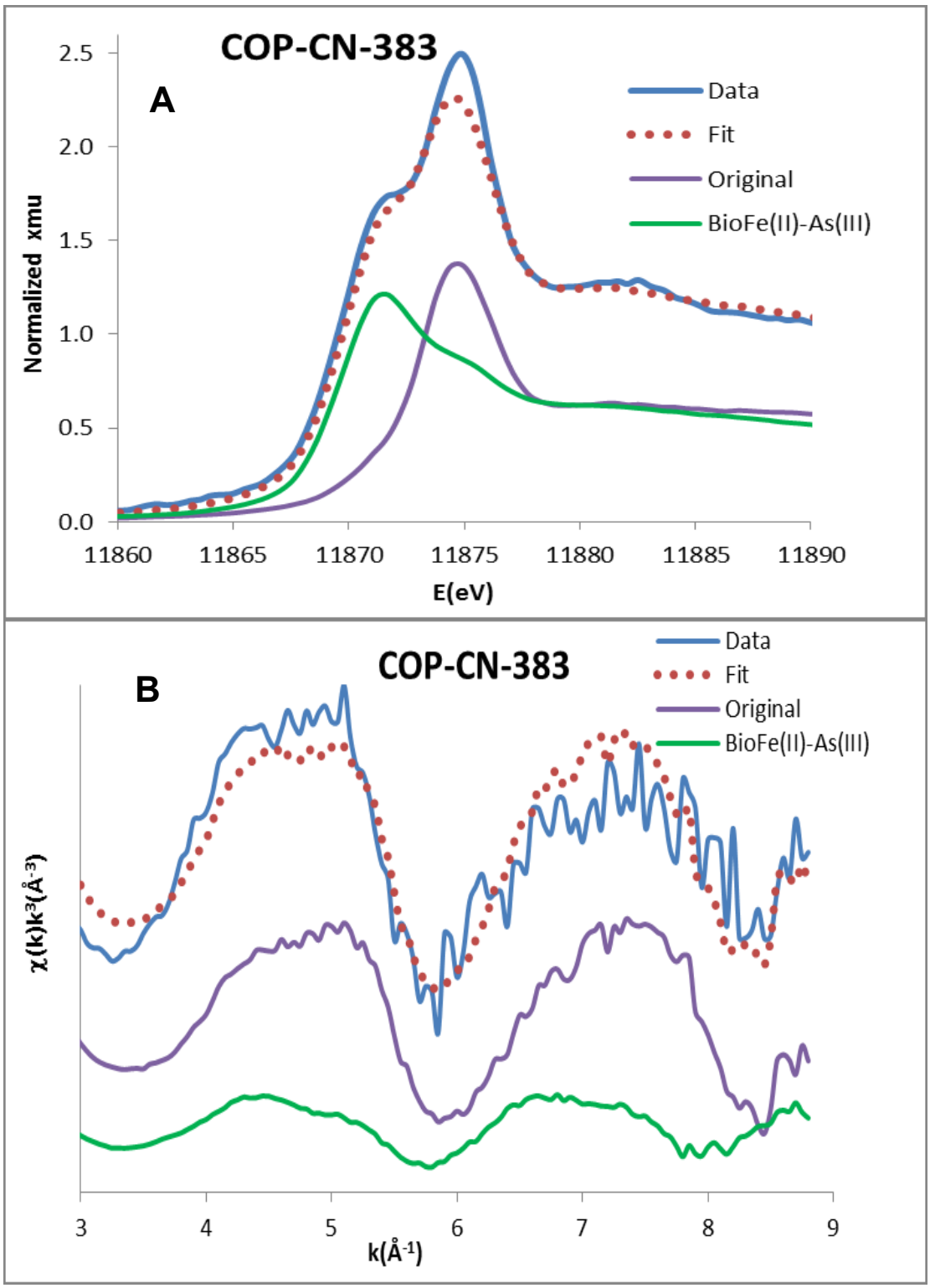
COP-CN-383
A
Data
Fit
Original
BioFe(II)-As(III)
Normalized xmu
2.5
2.0
1.5
1.0
0.5
0.0
11860
11865
11870
11875
11880
11885
11890
E(eV)
COP-CN-383
B
Data
Fit
Original
BioFe(II)-As(III)
χ(k)k³(Å⁻³)
3
4
5
6
7
8
9
k(Å⁻¹)

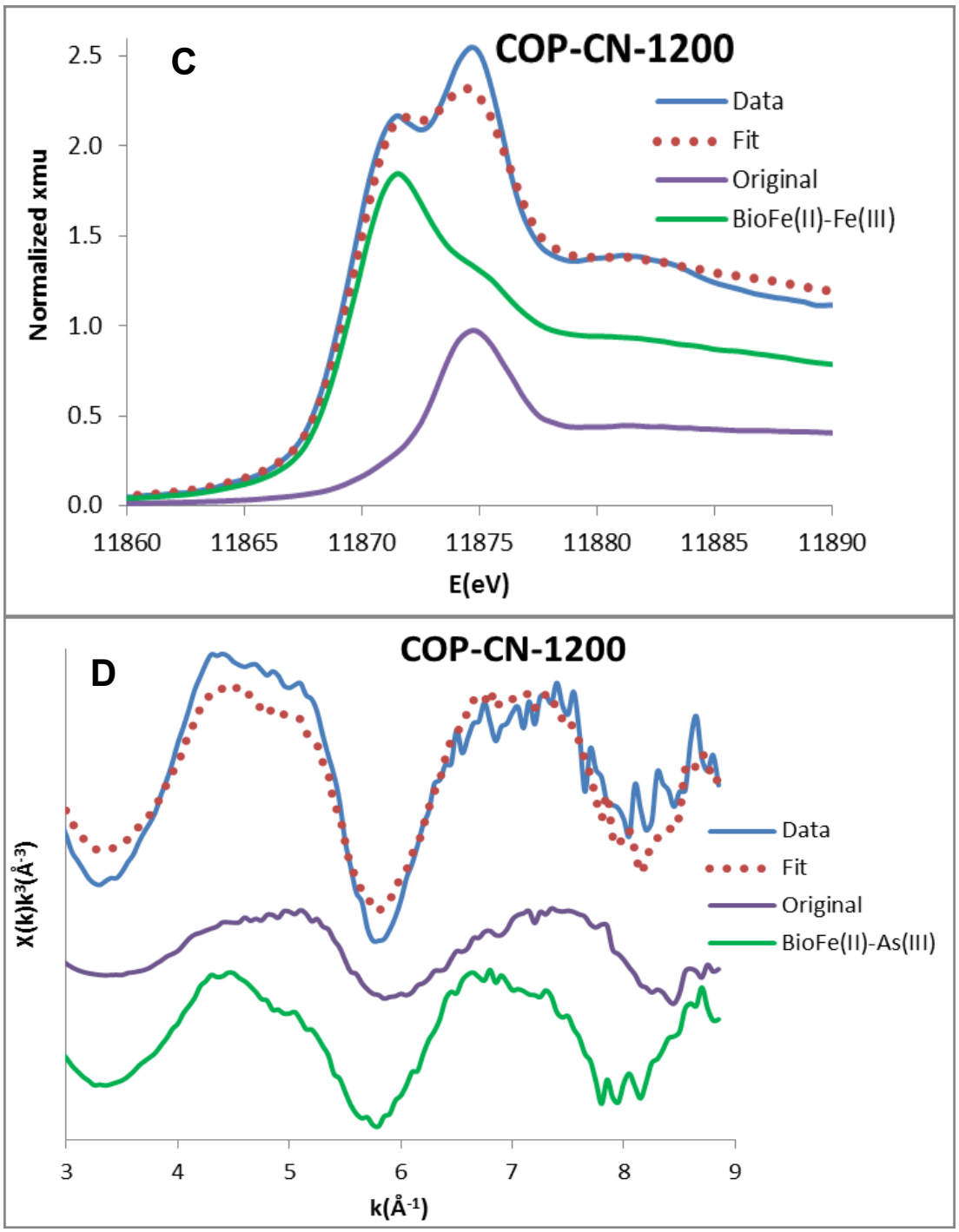

Figures 3.14. (A, C) Normalized XANES and (B, D) k^3-weighted As K-edge EXAFS spectra representative of the reduced COP samples and their linear combination fitting (dashed lines) along with the two end members (bottom) that gave the best fit, (A, B) after 383 and (C, D) after 1200 hours.

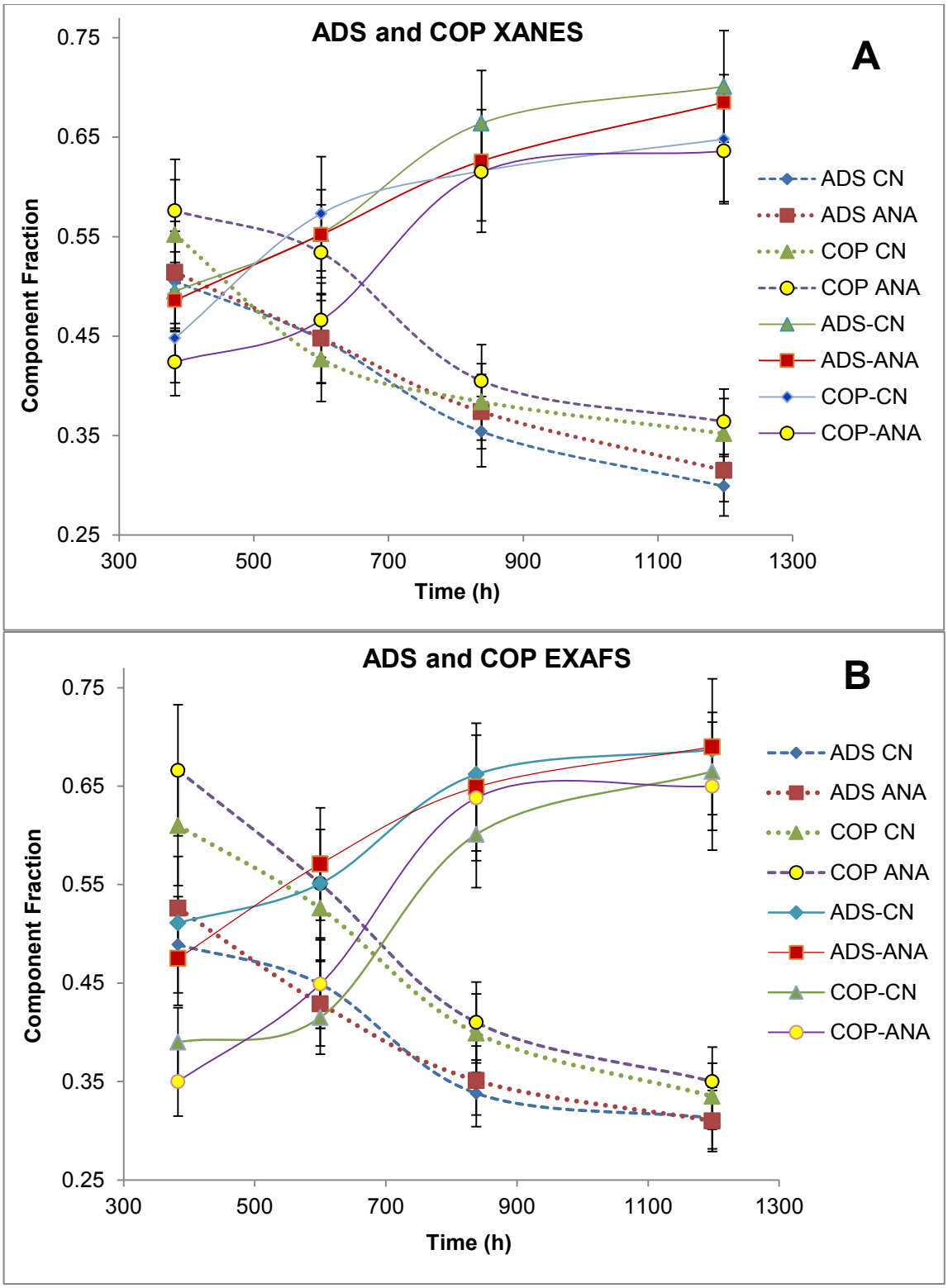

Figure 3.15. Rate of conversion of As(V) to As(III) in the biotic solids. (A) XANES (B) EXAFS. The data used for these figures are listed in Tables S1-S4.

4. DISCUSSION

4.1. Aqueous phase

4.1.1. *Arsenic speciation during microbial reduction*

No dissolved As(III) was detected in the abiotic controls, which indicates that no reduction of arsenic occurred in the absence of bacteria under the circumneutral pH and anaerobic conditions during the 50 days of experimental period. The concentration of dissolved As(V) was 6.5μM in the ADS control and about 2 μM in the COP control, which may indicate that As(V) is more readily released into solution from the ADS arsenical ferrihydrite than from the COP samples. The difference in the ease of release of As(V) may reflect a difference in the greater accessibility of solvent to the As(V) in the two samples.

The plateau concentrations of dissolved arsenic, mainly As(III) in the biotic samples, was about 10 times higher than the total dissolved arsenic concentrations in the abiotic controls. These results indicate that the bacteria used in the biotic samples were very effective in promoting the release of As(III) from the arsenical ferrihydrites.

A time of 93 hours, in the case of the biotic ADS samples, and 193 hours for the biotic COP samples, elapsed before significant concentrations of dissolved As(III) were detected as shown in Figure 3.2. The shorter time before the detection of As(III) in the ADS sample is consistent with the ease of release of As(V) from ADS compared to COP samples. The concentration of dissolved As(V) in the

controls early in the run, before 100 hours, was higher than As(V) in the biotic samples.

The lag phase, or the adaptation phase of the bacteria which is the period of time before appreciable concentrations of the dissolved As(III) were detected in the biotic samples, suggests that the rate of formation of As(III) may be dependent on the rate of release of As(V) from the solids. Zobrist et al. (2000) reported that the rate of biotic reduction of dissolved As(V) to As(III) was faster than the rate of desorption of As(V) from 2-line ferrihydrite. However, our evidence of the presence of bacteria on the surface of the solid (Fig. 3.7 A and B) suggests that bacterial reduction of As(V) may also be occurring on the surface of the solid followed by the release of the As(III) formed into solution. Therefore, both pathways to the formation of dissolved As(III) may be followed simultaneously.

4.1.2. *Iron speciation during microbial reduction*

Concentrations of the dissolved Fe(III) in the abiotic controls remained relatively constant during the experiment, and no dissolved Fe(II) was detected, indicating that no iron reduction occurred in the absence of bacteria. Concentrations of the dissolved Fe(III) in the biotic samples reached a maximum value at about 93 hours, and then gradually decreased while the concentration of the reduced iron increased. At about 620 hours when fresh bacteria were added to ensure that the microbial reduction continued, the concentration of dissolved Fe(III) increased slightly, and then decreased with time. Since the addition of fresh bacteria resulted in an increase in the concentrations of the reduced species, it appears that as long

as the bacteria are viable, As(III) continues to be released from the arsenical ferrihydrites.

The plateau concentrations of dissolved Fe(II) in the biotic ADS samples were lower than those of the biotic COP samples due to the formation of new solid phases which is addressed later in this discussion. The plateau concentrations of the dissolved Fe(II) in the biotic ADS and COP samples were significantly higher than the concentrations of the dissolved As(III). The dissolved Fe(II)/As(III) ratios were about 60/1 for the ADS biotic sample, and about 80/1 for the COP biotic original arsenical ferrihydrites. The relatively high molar ratio of dissolved Fe(II)/As(III) in the biotic arsenical ferrihydrite samples may have resulted from the re-adsorption of the dissolved As(III) onto the particle surfaces, and in the formation of new solid phases, such as biogenic Fe(II)-As(III) compound. The Fe/As ratio for the biogenic particle was 1/2 based on EDS analysis. It has been reported that As(III) is preferentially adsorbed over As(V) on ferrihydrite at pH 7 (Qi and Pichler, 2014) which suggests that the arsenic re-adsorbed on these particles could be in the form of As(III).

4.1.3. *The initial reduction rates of As and Fe*

The initial rates of reduction, based on the concentrations of dissolved As(III), are higher for the ADS samples than for the corresponding COP samples, which is consistent with the greater ease of release of As(V) by the ADS samples (Table 3.1). The initial rates of reduction based on the concentration of the dissolved Fe(II), are significantly greater than the rates based on As(III).

As a comparison (Table 3.1), the rates in the case of scorodite (Fe/As molar ratio 1/1) were higher for the reduction based on As(III) than on Fe(II). No significant difference in rates, based on Fe(II), were found between ADS and COP samples, nor did the two bacteria exhibit any significant difference in their influence on rates.

Initial reduction rates of Fe(III) in arsenic-free 2-line ferrihydrite reduced with *Shewanella putrefaciens* CN32 were reported as 26 μM/h by Roden et al., (2003) and 55 μM/h, under advective flow conditions, by Hansel et al., (2004). Our initial reduction rates of Fe(III) in arsenical 6-line ferrihydrite are 7.5 μM/h for the ADS samples with CN32 and 7.1 μM/h with ANA-3, and 7.8 μM/h with CN32 and 7.3 μM/h with ANA-3 for the COP samples. The lower Fe(III) reduction rates measured in our experiments for the arsenical ADS and COP samples, compared to the arsenic-free ferrihydrite reduction rates reported in the literature, may be explained by the blockage of the reactive Fe(III) sites on the ferrihydrite surface by arsenic (Waychunas et al. 1993; Erbs et al. 2010). Similarly, Chow and Taillefert (2009) found that the microbial reductive dissolution of iron oxides was inhibited when the dissolved As(V) concentration was greater than about 1 μM. The lower reduction rate of As(V) in the COP samples suggests that the COP arsenical 6-line ferrihydrite is more effective than the ADS in terms of arsenic sequestration and stabilization.

4.2. Solid phase analysis

Dissolved Fe(II) concentrations in the biotic ADS samples are lower than those in the COP samples (Figure 3.3 B). The fate of this apparent Fe(II) deficit in the ADS samples is revealed in evidence obtained from investigations of the solid

phases by XRD, XANES, and SEM. A comparison of the powder XRD results for the ADS and COP samples (Figure 3.4) shows that the intensity of peaks characteristic of secondary mineral phases are higher for ADS than for COP samples, indicating the presence of more reduced solid phases and formation of the secondary akaganeite, goethite, hematite and possibly magnetite. This difference between the ADS and COP samples may be attributed to the differences in particle size and crystallinity. The average size of the particles of the ADS samples was smaller than those of the COP samples. HRTEM images showed an average of 4-5 nm for ADS particles vs 6-8 nm for COP particles as time progressed, and as more arsenate was lost, the COP samples became more crystalline, indicated by the sharper peaks on the XRD (Figure 3.4). The XRD patterns over time shown in Figure 3.4 indicate that the formation of the secondary compounds was a gradual process with the akaganeite and goethite peaks appearing around 400 hours for the ADS and around 600 hours for the COP samples, while the magnetite and hematite appeared later in time.

The proportion of biogenic Fe(II)-As(III) increased with time at a greater rate in the ADS samples than in the COP post-reduction solid samples. In the XANES spectra, the intensity of the As(III) peak increased with time, while the As(V) peak of the original starting materials decreased with time at the expense of the formation of the new biogenic Fe(II)-As(III) compound, less so in the COP samples (Tables 3S1-S4, Figure 3.9 and 3.14 A). The association of iron and arsenic with microbial exopolymeric substances (EPS) was reported by Babechuk et al. (2009), Peretyazhko et al. (2010), Hohmann et al. (2011) and Huang et al. (2011).

One of the main reason for the As(III) binding to exopolymeric substances is that, the proteins contain amino acids with sulfhydryl (-SH) functional groups which have a high affinity for As(III) (Shen et al. 2013). The high affinity of As(III) for -SH groups in proteins is one of the main reasons why As(III) is much more toxic than As(V). The active sites of many enzymes in the human body have -SH functional groups, and As(III), which is more mobile and bioavailable than As(V), can inactivate these enzymes and cause serious diseases. Other studies suggested that As(III) produced during bacterial reduction could be incorporated in the structure during the formation of the secondary mineral phases (Kocar et al., 2006; Tufano and Fendorf, 2008). Hansel et al. (2003) observed precipitation of Fe(II) on the extracellular surface of *Shewanella putrefaciens* CN32 after 9 days of reduction. The surface of the dead bacterial extracellular matrix could have provided available binding sites for the dissolved Fe(II) and As(III) which could form a "seed" for nucleation. In 50 days, the duration of our experiment, it could have built up to a biogenic Fe(II)-As(III) (Figure S3.2). The formation of the biogenic Fe(II)-As(III) compounds probably controlled the plateau concentration of the dissolved Fe(II) and As(III), explaining the low As(III) concentration in solution. Neil et al. (2014) found that arsenate and phosphate can significantly impact the nucleation and growth of Fe(III) (hydr)oxides and the extent of water molecules in their structure. Exopolymeric substances have other surface functional groups such as carboxyl and phosphoryl groups, which are deprotonated at pH 7 and can bind the Fe(II) from the close proximity of the ferrihydrite surface. Therefore the structure of the bacterial exopolymeric

substances may have played a role in the formation of biogenic Fe(II)-As(III) compounds.

SEM imaging (Figure 3.6) confirmed the presence of akaganeite, hematite and goethite, identified by the powder and micro-XRD analyses (Figures 3.4 and 3.5). Semi-quantitative energy dispersive (EDS) analyses confirmed iron and oxygen as the main components of the secondary phases as shown by a representative spectrum on Figure 3.6 G. A secondary compound, shown on Figures 3.6 D, 3.6 E, 3.7 E and 3.7 F, is suspected to be magnetite, but its identity could not be definitively confirmed since only one peak in the μ-XRD pattern matched that of magnetite on Figure 3.5 A. Formation of magnetite during bacterial reduction of ferrihydrite with *Shewanella putrefaciens* CN32 was reported by Hansel et al. (2003), Kukkadapu et al. (2003) and Pallud et al. (2010), and with *Shewanella* sp. ANA-3 by Slowey et al. (2011). A study of an abiotic system by Baumgartner et al. (2013) found magnetite after the addition of Fe(II) to 6-line ferrihydrite in solution. In our study, identification of magnetite is based on the isometric morphology of the particles as shown on Figures 3.6 (D, E, F) and 3.7 (E, F), resembling magnetite. The magnetite particles were not easy to find during SEM examinations, and when they occurred, they were usually clustered together as shown in Figure 3.6 D.

The ferrihydrite peaks on the XRD of Figure 3.4, the biotic COP samples became progressively sharper with time, suggesting the formation of the more crystalline 6-line ferrihydrite at the expense of the less crystalline COP arsenical ferrihydrite because of the release of the entrapped arsenic from the solid structure from bacterial action. This is not apparent in the case of the biotic ADS samples

because the arsenic was adsorbed on the surface and not entrapped in the structure of ferrihydrite.

The peak intensities of the powder XRD of the post-reduction samples (Figure 3.4) suggest that there was more akaganeite, hematite, goethite and magnetite in the post-reduction ADS than in the COP samples. Other studies (Kukkadapu et al. 2004; Pedersen at al. 2005; Rosso et al. 2010) revealed that, the dissolved Fe(II) catalyze the formation of new secondary minerals. Hansel et al. (2003) found that the addition of as little as 0.04 mM Fe(II) lead to the transformation of half of the ferrihydrite to more stable secondary iron hydroxide phases in a period just over a week. In our experiments, accumulation of the dissolved Fe(II) started 100 hours earlier for the ADS samples than for the COP samples, which may have contributed to the formation of more new phases for the ADS than for the COP post-reduction samples.

Particles with hexagonal morphology were found as one of the secondary phases resulting from bacterial reduction (Figures 4, 5, 6 B and 6 D inset). Both hematite and green rust have hexagonal morphology. Green rust is a mixed-valent iron phase, which can form by microbial reductive processes under anaerobic conditions (Glasauer et al, 2003; Hansel et al. 2003). Green rust is likely to form since it is an Fe(II) compound, and the biotic samples contained high concentrations of dissolved Fe(II). Green rusts can have variable compositions as shown by the formula $\{Fe(II)_{(1-x)}Fe(III)\ x(OH)_2\}^{x+}$ $\{(x \diagup n)A^{n-})(m)H_2O\}^{x-}$), and they are double hydroxyl salt minerals that have a structure consisting of positively charged hydroxide layers, with two edge-sharing and a single-corner sharing octahedra,

separated by an interlayer, containing the A^{n-} anions and m water molecules (Zegeye et al. 2010). It can incorporate anions such as Cl^-, OH^-, CO_3^{2-}, $C_2O_4^{2-}$, or SO_4^{2-} in its structure (Wander et al. 2007). In their biotic experiments Zegeye et al. (2010) found hexagonal green rust particles containing CO_3^{2-} anions. In the biotic reduction of lepidocrocite, Ona-Nguema et al. (2009) found hydroxycarbonate green rust ($Fe(II)_4Fe(III)_2(OH)_{12}CO_3$. In addition to XRD analysis, the hexagonal particles in our samples were subjected to further analysis by electron microprobe, which confirmed that the hexagonal particles were hydrohematite (α-$Fe_2O_3 \cdot nH_2O$).

Even though there were no reflections identified on the XRD pattern for green rust, we cannot exclude its presence because it may have been formed at an earlier stage during the biotic reduction experiment, as was found by Hansel et al. (2003) in their study. Green rust is known to be reactive, and it may have transformed into other phases during the 50 days of the experiment. Other microbial reduction studies have shown that a variety of factors may influence the relative tendencies to form hematite, green rust or other secondary minerals. Zegeye et al. (2010) showed that the formation of green rust as opposed to magnetite depended on bacterial cell density, and Jorand et al (2013) found that, in addition to phosphate concentrations, properties of polymers that can include bacterial exopolymers are critical parameters that control the formation of secondary phases in the presence of bacteria.

The akaganeite peaks appeared at around 400 hours on the XRD (Figures 3.4) of the biotic ADS and COP samples, and the peak for the ADS sample was more intense than the peak for the COP sample. The akaganeite

($FeO_{0.833}OH_{1.167}Cl_{0.167}$) structure has edge and corner-sharing $Fe(O,OH)_6$ octahedra forming channels containing chloride ions. The Cl^- ions are important to the stabilize the structure, attract positively charged $Fe(OH)_2^+$ species at circumneutral pH, and act as a template for the channel formation. Akaganeite will not release chloride or transform to other phases at temperatures below 200 °C (Stahl et al. 2003). In our ADS and COP experiments, the amount of akaganeite increased as the experiment progressed, and reached the highest value after 1200 hours.

As in the case of akaganeite, goethite, which was identified by XRD, μXRD and SEM, appeared around 400 hours. Goethite has two geometric configurations in which Fe atoms are arranged in an O network with edge-sharing and corner-sharing octahedra. The corner-sharing octahedra connect two Fe atoms through a single O atom. Morphologically, two different types of goethite were identified on the SEM images. (1). Longer striped structures (Figure 3.6 C) and (2.) shorter, crystallized needles on the surface of the COP sample (Figure 3.6 F).

The hematite in our experiments was identified as hydrohematite (α-$Fe_2O_3 \cdot nH_2O$) because its structure contained H_2O. Peterson et al. (2015) refined the new structure of hydrohematite which precipitated in the monoclinic space group *Ic/a*, They observed peak splitting in the hydrohematite diffraction pattern which violated the 3-fold rotational symmetry. Hematite was among the most thermodynamically stable secondary minerals formed.

Magnetite (Fe_3O_4), which was identified by morphology during SEM examinations (Figures 3.6 D, E and 3.7 E, F) but its presence could not be confirmed by XRD. Magnetite is thermodynamically more stable than green rust,

formed preferably and incorporated some Fe(II). Hansel et al. (2005) and Yang et al. (2010) found in biotic experiments that magnetite was the main secondary phase when the concentration of Fe(II) reached and exceeded 1.8 mM.

The bacterium shaped “footprints” found on the SEM images on the irregular shaped original solids, (Figures 3.7 A and B), appear to be the same as those observed by Brookshaw et al. (2014) on biotite solids reduced by *Shewanella.* The etched rod shaped and circular bacterial imprints observed on hematite particles (Figures 3.6 B, 3.7 C and D), resemble those found in other studies performed with different minerals and bacteria showing that, etched imprints with defined shapes on mineral surfaces can be made by bacteria (Edwards and Rutenberg, 2001; Mustin et al., 2003; Rojas-Chapana and Tribusch, 2004; Ndlovu and Monhemius, 2005 and Baranska and Sadowski, 2013).

After 600 hours of reduction, we found very few imprints on the surfaces of some of the newly formed secondary precipitates (Figures 3.6 B inset, 3.6 D and 3. 7D inset). However, after re-inoculation, around 620 hours, it seems that the freshly added bacteria found fewer available binding sites on the surfaces of the original arsenical 6-line ferrihydrites, and instead started to colonize on the surfaces of the newly formed secondary precipitates. Rosso et al. (2003) also found less dissolved Fe(II) with each successive re-inoculation during hematite reduction in the presence of *Shewanella* sp. CN32, because bioavailability of the mineral surface to the bacteria decreased with time. We found more etched imprints towards the middle of the hematite surface (Figure 3.6 B and Figure 3.7 C) suggesting that more bacterial activity was occurring on the flat platy surface compared to crystalline faces of other

secondary minerals, like magnetite on Figure 3.7 E and F. Neal et al. (2003) also found significantly more *Shewanella* bacteria on the hematite basal face compared to the magnetite (100) and (111) faces, and their modeling predicted electron transfer rates about two orders of magnitude higher for the hematite basal face than for the two faces of magnetite. Yanina and Rosso (2008) and Chatman et al. (2013) found surface electric potential gradients across structurally distinct crystal faces of hematite exposed to solution, which makes it more favourable for the bacteria to associate with crystal faces where they can get the highest electron supply possible for maintenance. It has been shown that the strength of attachments of surface hydroxyls is different in the different crystal faces (Eggleston et al. 2003; Trainor et al. 2004). The carboxyl group ($-COO^-$) of lactate (pKa 3.86) is negatively charged at pH 7, and it adsorbs on the positively charged surfaces of secondary iron oxide minerals. More lactate can adsorb on the newly formed secondary iron oxide mineral surfaces than on the aged ADS and COP arsenical ferrihydrite surfaces, therefore more food sources are available for bacterial maintenance. The lactate concentration is another factor that can influence the selection of a surface by the bacteria. More lactate could have adsorbed on the newly formed surfaces which have higher iron density than the original surfaces, and this may explain why more deeply etched imprints occur on the surfaces of the secondary minerals. The bacteria can maintain their electron transfer through the outer membrane enzymes at one fixed location, in direct contact with lactate and Fe(III), eventually etching the surface. In addition to lactate that is adsorbed on the surface, the main forces that govern bacterial attachment to surfaces include the electrostatic interaction between

the ferrihydrite and the bacteria. The surface of *Shewanella putrefaciens* CN32 is hydrophobic and the Fe (hydr)oxides are hydrophilic resulting in an overall attractive interaction between negatively charged CN32 cells and positively charged Fe(hydr)oxides (Glasauer et al. 2001). This is supported by atomic force microscopy (AFM) imaging studies, where the outer membrane enzymes of one *Shewanella* cell is in contact with the hematite surface during Fe(III) reduction (Lower et al. 2009). In another AFM study, two *Shewanella* cells were entrenched in a biotically formed, 130 nm deep pit in a calcite cleavage face (Lüttge et al. 2005). This does not exclude the possibility that the bacteria used shuttle compounds, such as siderophores, to reduce and dissolve iron at the surfaces of iron oxides, which are not in close proximity to the attachment site.

Bacterial imprint patterns accumulated towards the middle of the hematite particle (Figure 3.6B) suggests that the middle section of the particle was older and the outer perimeter was still growing. It has been shown by theoretical calculations that the low index faces of hematite have different surface energies (Cornell and Schwertmann, 2003). Yanina and Rosso (2008) measured the potential gradients between basal and edge surfaces of hematite which can dissolve one surface and grow on the other through conduction of the bulk oxide. They found that when both surfaces were exposed to the solution, the basal surface did not reductively dissolve but instead oxidized the aqueous Fe(II). Aqueous Fe(II) can make the Fe(III) oxide more reactive (Williams and Scherer, 2004), and nearly complete Fe atom exchange between the aqueous and solid phase can occur (Handler et al., 2009). It is unlikely that the bacteria would burrow channels, like wormholes, deeply into the

body of the mineral, because their metabolic processes would be limited by diffusion. However, etching through a thin plate with apical attachment would not limit their metabolic activities, especially if it is part of an already present current flow driven by the potential gradient between the different crystal faces. Grantham et al. (1997) used *Shewanella putrefaciens* CN32 under anaerobic conditions and found circular pits with surprisingly uniform and homogeneous size distribution equaling the apical diameters of the bacterium, although they found no bacterium shaped imprints. The experimental evidence in this study along with the reasons provided above indicates that the bacterium shaped imprints on the secondary precipitates were of bacterial origin. The etched circular imprints found on the secondary precipitates may also be of bacterial origin, but some of them could be dissolution etch pits as reported by Rosso et al. (2003) who found random, 100 nm diameter or less, mostly circular erosion pits across the basal plane of hematite. Lasaga and Lüttge (2001, 2003), developed a mechanism for the etch pit formation by finding that the highly reactive parts of the surface, resulting from defects and dislocations, can lead to the formation of etch pits. These etch pits were the source of the dissolution stepwaves which propagated across the surface and were the main cause of surface-normal retreat and thus the overall dissolution rate. Surface defects and dislocations play an important role in crystal growth and dissolution kinetics.

Defect structures can also play a role in reactivity as in the case of hydrohematite that were found in our biotic ADS and COP arsenical 6-line ferrihydrite samples. Burgina et al. (2000) found higher catalytic activity of the more

hydrous form of hematite compared to the stoichiometric hematite, and they explained this higher activity by the lower symmetry of the oxygen sublattice and by the effective tetrahedral environment of some iron cations in the structure.

Crystallization of goethite on the COP-ANA-3 surface (Figure 3.6 F) was found during the course of the bacterial reductive dissolution, which likely occurred because the concentration of Fe(III) near the mineral surface was higher than in the bulk of the solution. Bacterial reductive dissolution mainly occurs at the mineral surface due to the proximity of the heme cofactors of the enzymes participating in Fe(III) reduction.

A possible mechanism of As(V) reduction in scorodite ($FeAsO_4 \cdot 2H_2O$) was discussed already in our sister paper, where it was proposed that As(V) has to be detached from the structure prior to reduction because the As(V) reducing enzyme is located in the periplasm. *Shewanella* sp. ANA-3 and *Shewanella putrefaciens* CN32 employ the MtrC and OmcA terminal reductase pathways which contain the heme cofactors necessary for the final steps in Fe(III) reduction (Saltikov et al, 2003, 2005). The hydrophilic heme cofactors can bind directly to the Fe(III) on the surface of As-6LFH and transfer electrons directly to these minerals via their solvent-exposed hemes (Shi et al. 2012). The mechanism of electron transfer reactions in biological systems such as the cytochrome heme proteins and iron complexes were described by Marcus and Sutin (1985). Smith et al. (2006) found that the rate of electron transfer was controlled by the distance between the heme group and Fe(III), and their orientation. Kerisit et al. (2007) used molecular dynamics simulation to investigate the electron-transfer kinetics across the cytochrome

heme and the iron oxide interface and found that direct contact between hemes and the oxide surface is possible and thermodynamically favorable. They demonstrated that the rate of electron-transfer were sensitive to the fluctuations of the heme configuration at the interface, orientation of the porphyrin ring, electron-transfer distance, and to the mineral surface termination. The direct contact of the Shewanella heme cofactor and the surface of the As-6LFH resulted in the release of dissolved Fe(II). The Fe(II) subsequently re-adsorbed onto the As-6LFH surface and transferred an electron to the surface Fe(III) by the self-exchange reactions mechanism (Marcus 1956, 1992 and references therein). As a result of the self-exchange electron transfer reactions between Fe(II) and surface Fe(III), the concentration of Fe(III) in solution reached saturation, and resulted in the precipitation of secondary minerals, such as akaganeite (β-FeOOH), goethite (α-FeOOH), hematite (α-Fe_2O_3) and possibly magnetite (Fe_3O_4). This suggested mechanism is in agreement with one by Boland et al. (2014) who proposed that the adsorbed Fe(II) on the ferrihydrite surface is oxidized to Fe(III) and the electron is transferred to the Fe(III) atom within the ferrihyrite which was then released into solution as Fe(II). They concluded that the freshly precipitated Fe(III) formed the nuclei for the formation of secondary minerals which elicited further uptake of Fe(II) from solution. Hansel et al. (2005) found that the reaction of aqueous Fe(II) with ferrihydrite resulted in the precipitation of goethite (α-FeOOH), lepidocrocite (γ-FeOOH), and magnetite (Fe_3O_4), depending on the Fe(II) concentration. Yang et al. (2008) found that aqueous Fe(II) adsorption on 6-line ferrihydrite formed different secondary minerals depending on the aqueous Fe(II) concentration, goethite formed

at lower Fe(II) concentration and magnetite formed at higher Fe(II) concentration. In our experiments it is possible that at the early stages of the reduction, goethite (α-FeOOH) and akaganeite (β-FeOOH) formed as shown on the XRD (Figure 3.4), and later in the experiment at higher dissolved Fe(II) concentration, magnetite and hematite also formed. The formation of the secondary minerals occurred over an extended period of time.

In the ADS samples, after the As(V) desorbed, more Fe(III) active sites may have been available than was the case for the COP samples. A comparison of the secondary compounds formed from the biotic reduction As-6LFH to those formed from scorodite is summarized in Table 3.7 biogenic Fe(II)-As(III) was found in both cases. The secondary compounds found for the biotic reduction of scorodite all contained arsenic, whereas the other secondary compounds found for arsenical 6LFH were all As free iron (hydr)oxides. This difference in the types of secondary compounds formed may be due to:

(1) the Fe/As molar ratio of the starting materials, 1/1 for scorodite compared to 10/1 for As-6LFH, i.e. ten times more iron than arsenic in the arsenical ferrihydrites, which is reflected both in the solution composition as well as the secondary minerals.

(2) the plateau concentrations of dissolved arsenic, as As(III), ~ 3000 µm for the biotic reduced scorodite samples compared to ~ 60 µM for As-6LFH, i.e. 50 times more dissolved arsenic for the scorodite samples than for the As-6LFH.

(3) the greater adsorption potential of As-6LFH for the dissolved arsenic which is supported by Paktunc et al. (2008c). Since there was such a low

concentration of arsenic, only trace amounts of secondary arsenic containing minerals may have formed as a result of arsenic adsorption on ferrihydrite which were too low to detect.

Table 3.7. Summary of the secondary compounds found as a result of bacterial reduction of scorodite and adsorbed and coprecipitated arsenical 6-line ferrihydrites.

Scorodite	**ADS and COP arsenical 6LFH**
Biogenic Fe(II)-As(III) compound	Biogenic Fe(II)-As(III) compound
Parasymplesite ($(Fe_3(AsO_4)_2 \cdot 8H_2O$)	Akaganeite (β-FeOOH)
Tooeleite ($Fe_6(AsO_3)_4(SO_4)(OH)_4 \cdot 4H_2O$).	Goethite (α-FeOOH)
	Hydrohematite (α-$Fe_2O_3 \cdot nH_2O$)
	Magnetite* (Fe_3O_4)

*Unconfirmed by XRD

Various cover options are discussed in detail in our sister paper. Covers are designed for various reasons. The most common one is to prevent oxygen ingress and minimize water infiltration for sulfidic mine wastes. Otherwise, sulphide oxidation would result in the generation of acid mine drainage. This could be an option for tailings with arsenopyrite and As-pyrite but not for scorodite or As-ferrihydrite containing tailings. The no cover options appear to apply in the case of arsenic sequestered by scorodite and arsenical ferrihydrite, and in addition would inhibit the activity of anaerobic bacteria. However the decision on the choice of

cover is complex because of the large number of factors which must be considered in coming to the final decision.

5. Overall Summary and Conclusion

The biotic reduction experiments of arsenical ferrihydrites described in this paper have a number of features in common with the biotic reduction experiments of scorodite, reported in our previous publication. The common features include the use of the same bacteria, use of low phosphate concentrations, and the same methods of speciation of dissolved and solid phase substances. These commonalities, and the fact that ferrihydrites and scorodite are both key participants in the control of dissolved arsenic, invite comparison of the findings in the two studies.

The new secondary minerals found in the post-reduction products of the ADS and COP arsenical 6-line ferrihydrite solid samples were biogenic Fe(II)-As(III) compound, akaganeite, goethite, hematite and possibly magnetite for both bacteria. In comparison, the post-reduction products for scorodite were biogenic Fe(II)-As(III) compound, parasymplesite and minor amounts of tooeleite (Table 3.7).

The dissimilatory iron and arsenic reducing (DIRB/DARB) bacteria, *Shewanella* sp. ANA-3 and *Shewanella putrefaciens* CN32, used in this experiment at circumneutral pH and under anaerobic conditions caused the reductive dissolution of scorodite, ($FeAsO_4 \cdot 2H_2O$), and adsorbed and coprecipitated arsenical 6-line arsenical ferrihydrite, (Fe/As molar ratio 10/1), resulting in the release into solution of Fe(II) and of As(III), a more toxic form of arsenic than As(V).

The concentrations in solution of the products of bacterial reduction of scorodite were about 1.5 mM Fe(II) and about 3 mM As(III), a Fe/As molar ratio of 1/2 compared to a molar ratio of 1/1 in the parent compound.

The concentrations of the products of bacterial reduction of the adsorbed and coprecipitated arsenical 6-line ferrihydrites were about 3.5 mM Fe(II) and about 0.057 mM As(III) for the ADS, and about 4.3 mM Fe(II) and about 0.055 mM As(III) for the coprecipitated samples. The molar ratio of dissolved Fe/As in the adsorbed arsenical 6-line ferrihydrite samples was 60/1 compared to the Fe/As ratio of 80/1 for the coprecipitated samples. These results indicate that the adsorbed ferrihydrite samples released more arsenic than the coprecipitated samples.

These findings indicate that under anaerobic conditions and circumneutral pH scorodite and arsenical ferrihydrites are unstable with respect to microbial reduction, and this finding should be taken into account when evaluating the environmental impact.

Based on the log CFU plots, the bacterial counts decreased throughout the experiments for both scorodite and arsenical 6LFH, indicating that the bacteria are only surviving.

Based on the available literature on the reduction mechanism of arsenate, As(V) must be detached from scorodite or the arsenical ferrihydrite, and released into solution before being taken up by the bacteria.

Ferrous iron formed by the bacterial reduction of scorodite and arsenical 6-line ferrihydrite is re-adsorbed on the surfaces of the remaining solid, underwent a series of mineral transformations, particularly in the case of 6LFH (Fe/As = 10), to

form akaganeite, goethite, hydrohematite and possibly magnetite. It is therefore proposed, based on a mechanism originally developed by Marcus (1956), that the biotically reduced aqueous Fe(II) is re-adsorbed on the solid surfaces and the Fe(III) reduction occurred by a self-exchange reaction between Fe(II) and Fe(III) leading to the formation of the secondary compounds.

Cover materials, such as biosoil, soil and water covers may not be completely effective because of the potential for bacterial activity under the anaerobic conditions created by these covers.

The results of the bacterial reduction of arsenical 6-line ferrihydrite and scorodite which indicate that the higher the Fe/As molar ratio, the less As(III) is released to the environment, correlates with the findings in a publication by Paktunc et al. (2008c). It was found that high Fe/As molar ratios were more effective at controlling dissolved As concentrations because ferrihydrite is the only phase in the precipitates.

6. Supplementary information for Chapter 3.

Table S3.1. Fractional compositions of arsenic in the reduced ADS arsenical 6-line ferrihydrite determined by normalized As K-edge XANES least-squares fitting.

Mineral phase	ADS CN 383h	ADS CN 600h	ADS CN 838h	ADS CN 1200h	ADS ANA 383h	ADS ANA 600h	ADS ANA 838h	ADS ANA 1200h
Original ADS	0.505	0.447	0.354	0.299	0.514	0.448	0.374	0.315
Fe(II)As(III)*	0.495	0.553	0.664	0.701	0.486	0.552	0.626	0.685
R-Factor	0.0054	0.0073	0.0059	0.0039	0.0087	0.0043	0.0026	0.0031

*Biogenic ferrous arsenite

Table S3.2. Fractional compositions of arsenic in the reduced ADS arsenical 6-line ferrihydrite determined by the k^3-weighted As K-edge EXAFS linear combination fitting.

Mineral phase	ADS CN 383h	ADS CN 600h	ADS CN 838h	ADS CN 1200h	ADS ANA 383h	ADS ANA 600h	ADS ANA 838h	ADS ANA 1200h
Original ADS	0.489	0.449	0.338	0.313	0.526	0.429	0.351	0.310
Fe(II)As(III)*	0.511	0.551	0.662	0.687	0.475	0.571	0.649	0.690
R-Factor	0.129	0.289	0.430	0.0751	0.405	0.307	0.421	0.0831

*Biogenic ferrous arsenite

Table S3.3. Fractional compositions of arsenic in the reduced COP arsenical 6-line ferrihydrite determined by normalized As K-edge XANES least-squares fitting.

Mineral phase	COP CN 383h	COP CN 600h	COP CN 838h	COP CN 1200h	COP ANA 383h	COP ANA 600h	COP ANA 838h	COP ANA 1200h
Original COP	0.552	0.427	0.384	0.352	0.576	0.534	0.385	0.364
Fe(II)-As(III)*	0.448	0.573	0.616	0.648	0.424	0.466	0.615	0.636
R-Factor	0.010	0.0089	0.0035	0.0077	0.0027	0.0046	0.0099	0.0083

*Biogenic ferrous arsenite

Table S3.4. Fractional compositions of arsenic in the reduced COP arsenical 6-line ferrihydrite determined by the k^3-weighted As K-edge EXAFS linear combination fitting.

Mineral phase	COP CN 383h	COP CN 600h	COP CN 838h	COP CN 1200h	COP ANA 383h	COP ANA 600h	COP ANA 838h	COP ANA 1200h
Original COP	0.610	0.585	0.399	0.335	0.666	0.551	0.362	0.350
Fe(II)As(III)*	0.390	0.415	0.601	0.665	0.334	0.449	0.638	0.650
R-Factor	0.683	0.187	0.271	0.153	0.119	0.0819	0.0786	0.075

*Biogenic ferrous arsenite

Table S3.5. Comparison of initial Fe(III) reduction rates* in arsenical 6-line ferrihydrites, this research, with literature values for arsenic free 2-line ferrihydrites.

Substance	Authors	Bacteria	Initial Rates (μM/h)	Initial Counts (CFU/mL)
Synthetic As ADS 6LFH	Our result	*Shewanella* sp. CN32	7.5	2.9×10^8
Synthetic As ADS 6LFH	Our result	*Shewanella* sp. ANA-3	7.1	2.7×10^8
Synthetic As COP 6LFH	Our result	*Shewanella* sp. CN32	7.8	2.6×10^8
Synthetic As COP 6LFH	Our result	*Shewanella* sp. ANA-3	7.3	3.0×10^8
Synthetic 2LFH No Arsenic	Hansel et al. 2004	*Shewanella* sp. CN32	55	5.0×10^8
Synthetic 2LFH No arsenic	Roden et al. 2003	*Shewanella* sp. CN32	26	2.5×10^8

* values calculated using the linear portions of the concentration-time graphs.

Table S3.6. Results of the electron microprobe analysis of selected biotic COP As-6LFH particles.

No.	SO_3	FeO	Cl	As_2O_5	Total	Comment
1	0	89.89	0.001	0.0908	89.9818	hematite
2	0.0608	100.01	0	0.0692	100.1399	hematite
3	0	70.57	0.0487	12.39	83.0088	P1 not reduced
4	0.162	73.46	0.0171	12.95	86.5891	P2 not reduced
5	0.089	67.11	0	12.79	79.9891	P3 not reduced
6	0.0051	81.83	0.014	0.1246	81.9738	P4-1 secondary
7	0	84.25	0.0212	0.1412	84.4125	P4-2 secondary
8	0	80.96	0.0097	0.1523	81.122	P5-1 secondary
9	0.0811	80.35	0.0182	0.2021	80.6515	P5-2 secondary
10	0	89.18	0.0162	0.1468	89.343	P5-3 secondary
11	0.0406	86.13	0.0125	0.0471	86.2302	P6-1 secondary
12	0.1114	81.55	0.0129	0.1494	81.8238	P6-2 secondary
13	0	6.57	0.0019	0	6.572	P7-1 secondary
15	0	82.23	0.0143	0.2408	82.4852	P7-1 secondary
16	0.0355	89.38	0.0103	0.1025	89.5284	P7-2 secondary
17	0.0658	83.24	0.0156	0.2021	83.5236	P7-3 secondary
18	0.12	69.07	0.0059	11.94	81.136	P8-1 primary

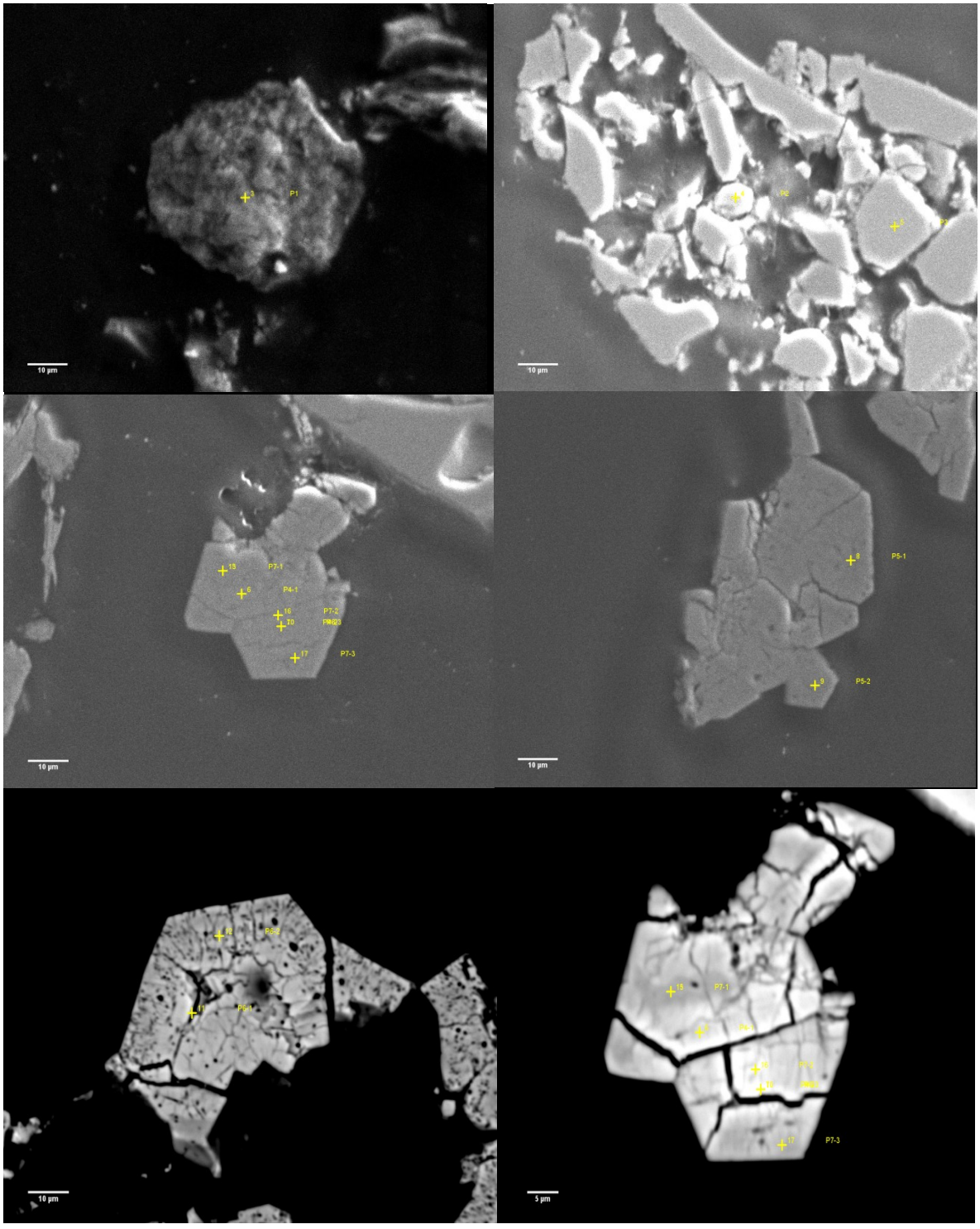
3
P1
10 µm
P2
10 µm
15
P7-1
6
P4-1
16
P7-2
10
P7-3
17
10 µm
8
P5-1
9
P5-2
10 µm
12
P5-2
11
P5-1
10 µm
15
P7-1
17
P7-3
5 µm

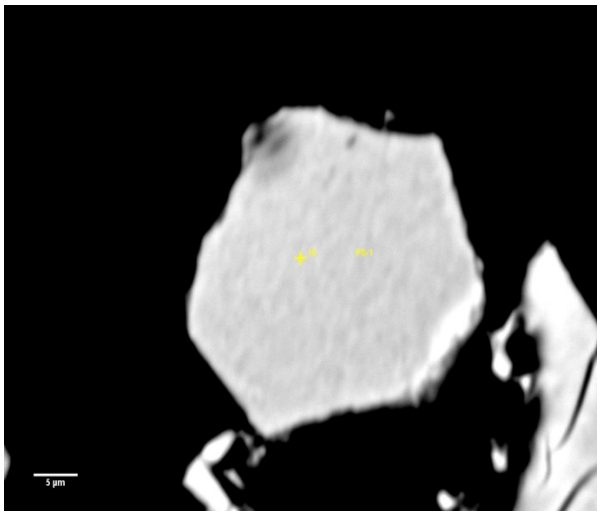

Figure S3.1. Particles analyzed by electron microprobe (areas labelled by crosses) from the As-6 LFH microcosm bottles. The results are shown in Table S3.6.

Additional SEM images of imprints on the secondary minerals are shown in Figures S3.2 below.

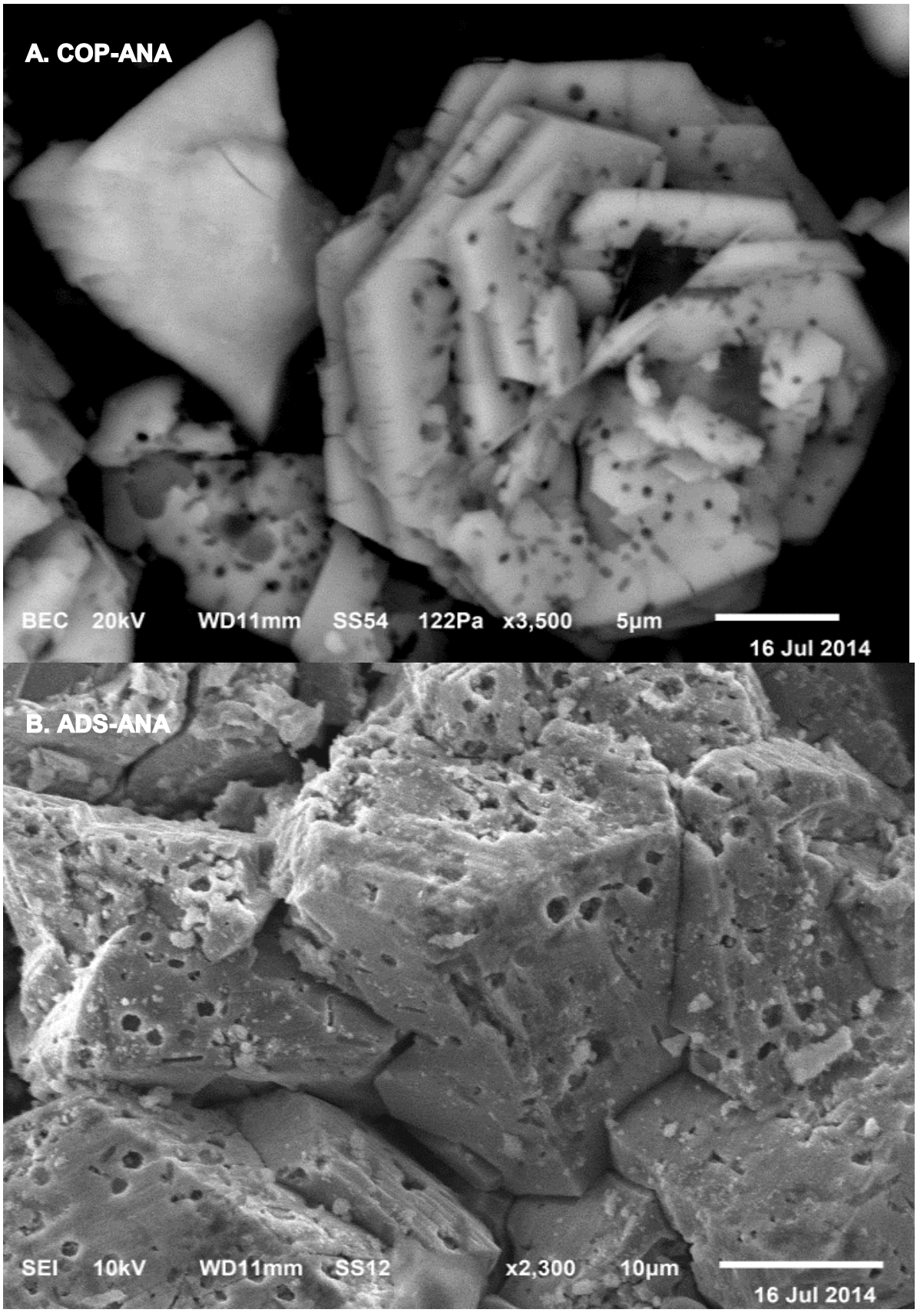
A. COP-ANA
BEC 20kV WD11mm SS54 122Pa x3,500 5µm
16 Jul 2014
B. ADS-ANA
SEI 10kV WD11mm SS12 x2,300 10µm
16 Jul 2014

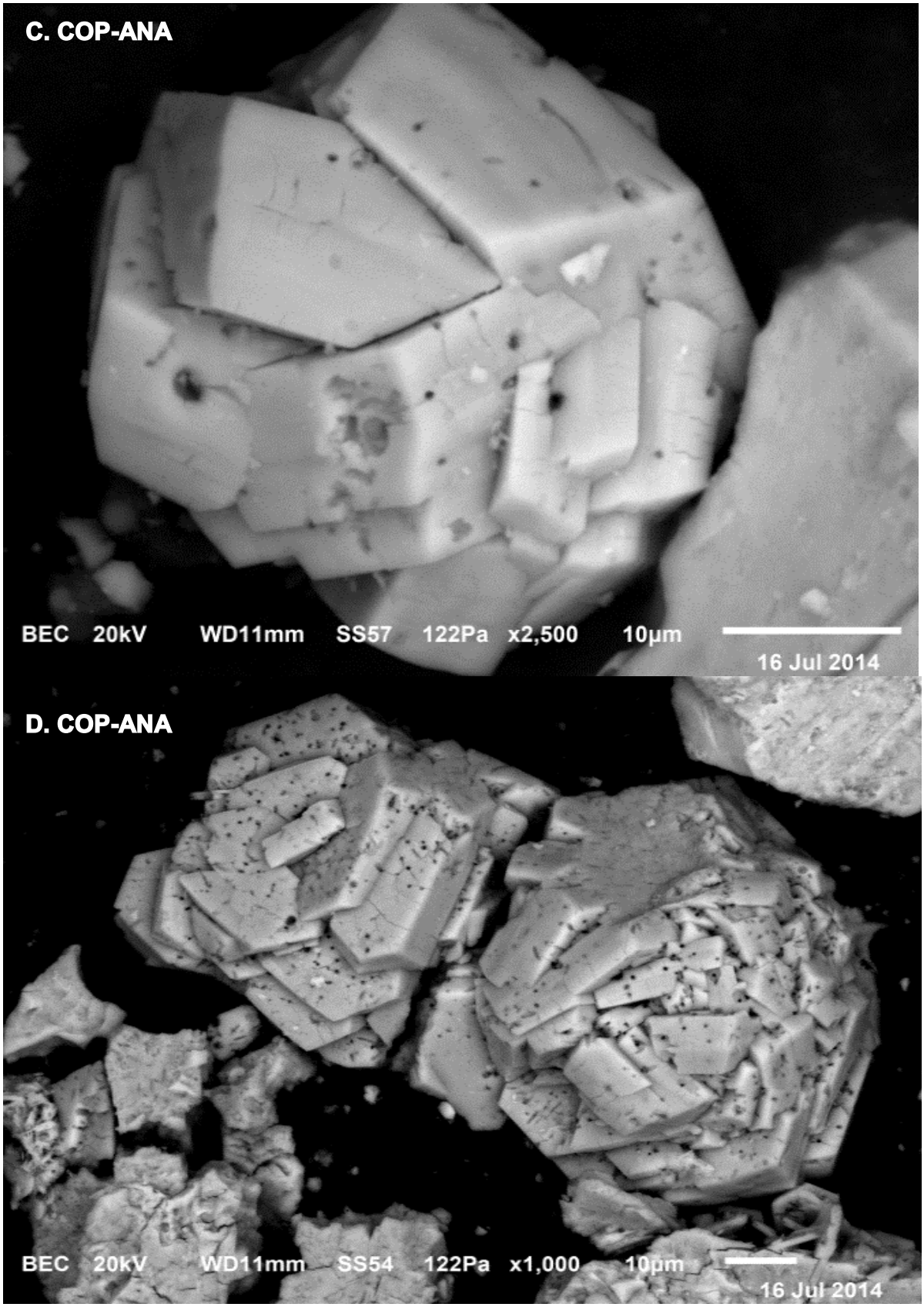
C. COP-ANA
BEC 20kV WD11mm SS57 122Pa x2,500 10µm
16 Jul 2014
D. COP-ANA
BEC 20kV WD11mm SS54 122Pa x1,000 10µm
16 Jul 2014

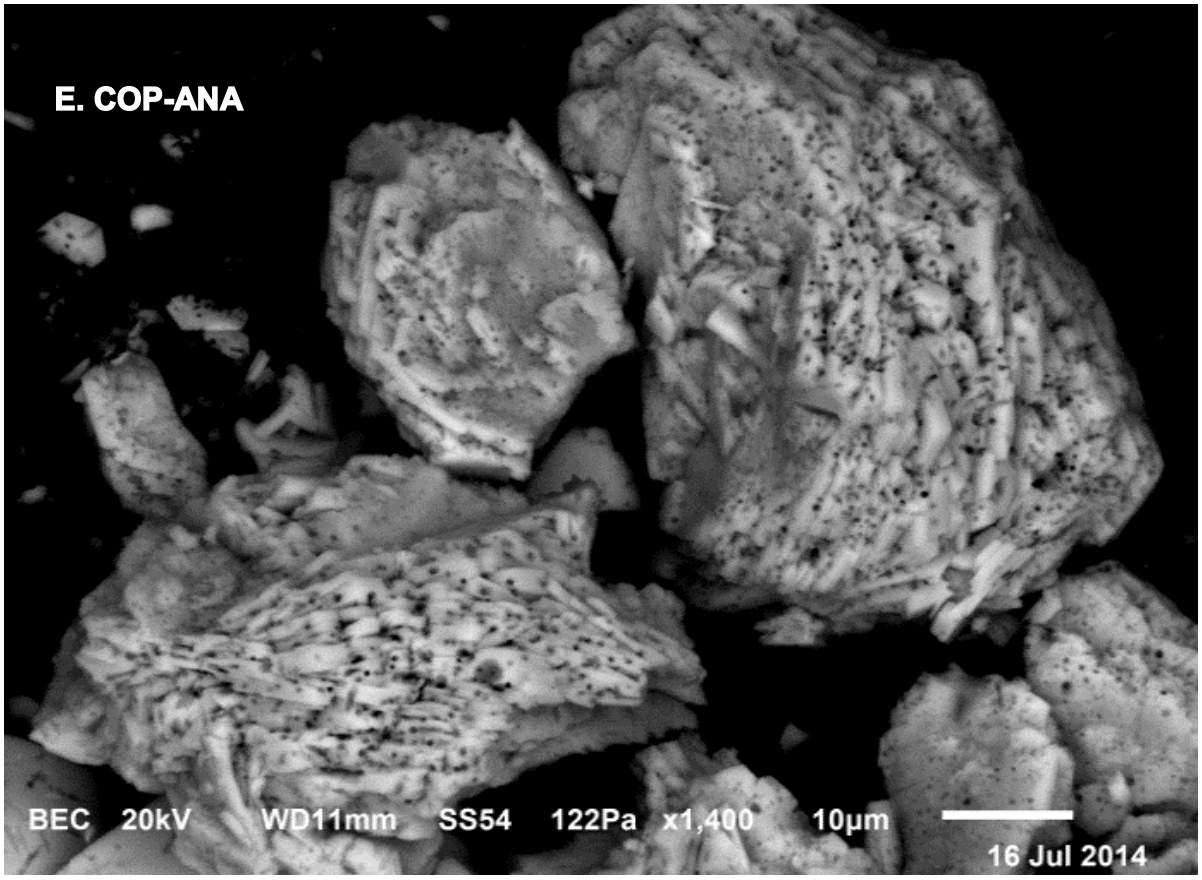

Figures S3.2. SEM images of imprints on unidentified secondary minerals.

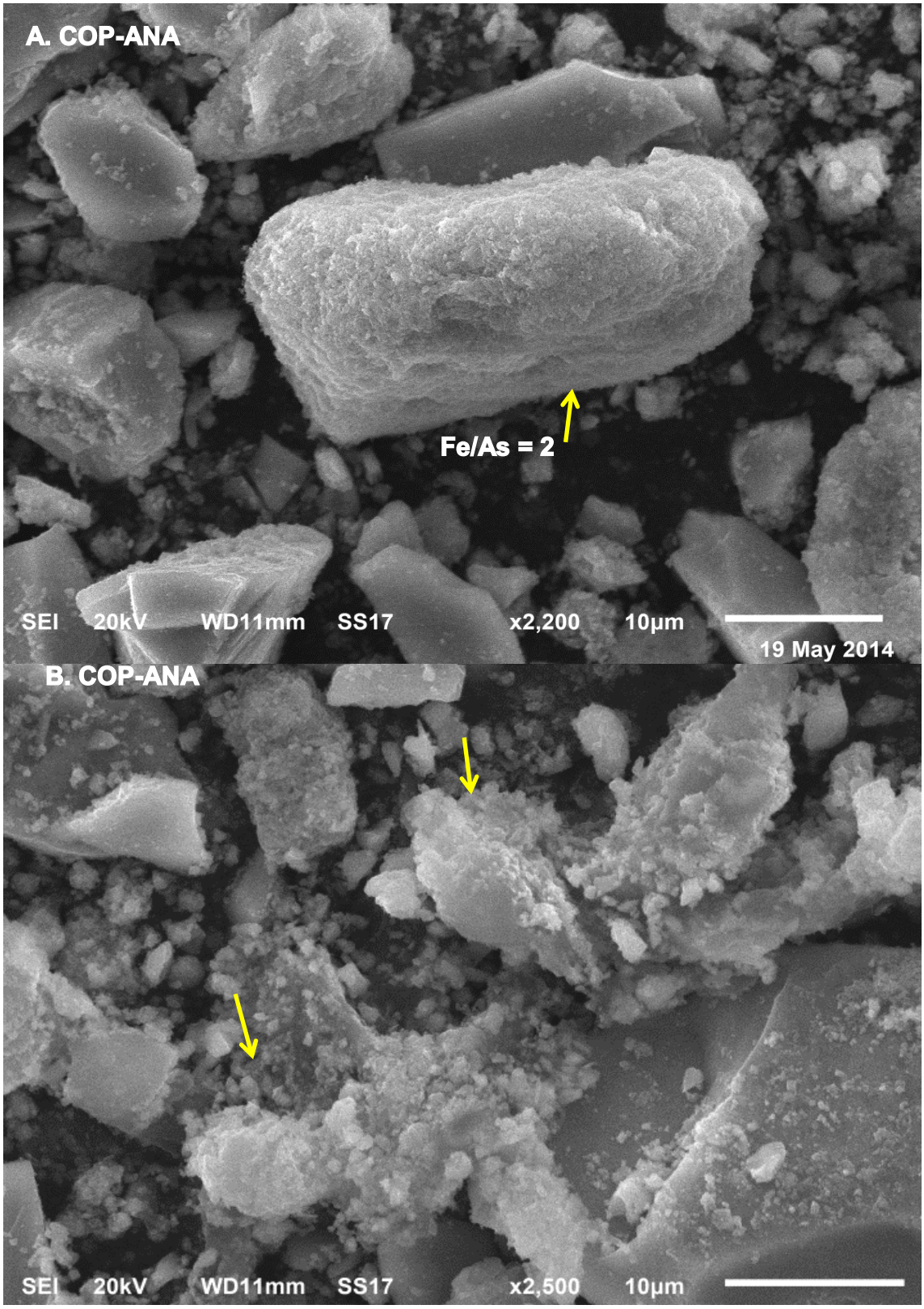

Figure S3.3. SEM images of biotic particles with Fe/As molar ratio of 2 (arrows).

Acknowledgements

This project was partially funded by NSERC Discovery grants to Dr. D. Fortin and Dr. D. Paktunc. E. Revesz thanks D. Smith at CANMET for XRD and Dr. R. Gordon for the XAFS measurements and G. Poirier for the electron microprobe analysis. The XAFS experiments were performed at the Pacific Northwest Consortium—Collaborative Access Team's (PNC/XOR) beamline at the Advanced Photon Source (APS) at the Argonne facility under the user agreement to the senior author. Argonne National Laboratory is supported by the US Department of Energy under Contracts W-31-109-Eng-38 (APS) and DE-FG03-97ER45628 (PNC-CAT).

7. References:

Amstaetter, K., Borch, T., Kappler, A., 2012, Influence of humic acid imposed changes of ferrihydrite aggregation on microbial Fe(III) reduction, Geochim. Cosmochim. Acta 85, 326–341.

Babechuk, M. G.; Weisener, C. G.; Fryer, Brian J.; Paktunc, D., Maunders, C., 2009. Microbial reduction of ferrous arsenate: Biogeochemical implications for arsenic Mobilization. Appl. Geochem. 24, 2332-2341.

Baumgartner, J., Dey, A., Bomans, P.H.H., Le Coadou, C., Fratzl, P., Sommerdijk, N. A. J. M., Faivre, D., 2013, Nucleation and growth of magnetite from solution, Nat. Matter. 12, 312-314.

Baranska, J.A., Sadowski, Z., 2013, Bioleaching of uranium minerals and biosynthesis of UO_2 nanoparticles. Physicochem. Probl. Miner. Process, 49, 71-79.

Boland, D.D., Collins, R.N., Miller, C.J., Glover, C. J., Waite, T. D., 2014. Effect of solution and solid-phase conditions on the Fe(II)- accelerated transformation of ferrihydrite to lepidocrocite and goethite. Environ. Sci. Technol. 48, 5477−5485.

Brookshaw, D.R., Lloyd, J.R., Vaughan, D.J., Pattrick, R.A.D., 2014, Bioreduction of biotite and chlorite by a *Shewanella* species, Am. Mineral. 99, 1746–1754.

Burgina, E.B., Kustova, G. N., Tsybulya, S. V., Kryukova, G. N., Litvak, G. S., Isupova, L. A., Sadyko. V. A., 2000. Structure of the metastable modification of iron(III) oxide J. Struct. Chem. 41, 396-402.

Burnol, A., Garrido, F., Baranger, P., Joulian, C., Dictor, M-C., Bodénan, F., Morin, G., Charlet, L., 2008, Decoupling of arsenic and iron release from ferrihydrite suspension under reducing conditions: a biogeochemical model, Geochem. T. 8, 12.

Cummings, D.E., Caccavo, F., Fendorf, S., Rosenzweig, R.F., 1999, Arsenic mobilization by the dissimilatory Fe(III)-reducing bacterium *Shewanella alga* BrY. Environ. Sci. Technol. 33, 723 -729.

Chatman, S., Zarzycki, P., Rosso, K.M., 2013, Surface potentials of (001), (012), (113) hematite (α-Fe_2O_3) crystal faces in aqueous solution. Phys. Chem. Chem. Phys., 2013, 15, 13911 -13921..

Edwards, K.J., Rutenberg, A.D., 2001. Microbial response to surface microtopography: the role of metabolism in localized mineral dissolution, Chem. Geol. 180, 19–32.

Erbs, J.J, Berquo, T. S., Reinsch, B. C., Lowry G. V., Banerjee, S. K., Penn, R.L., 2010, Reductive Dissolution of Six-Line Ferrihydrite, Geochim. Cosmochim. Acta 74, 3382–3395

Fredrickson, J. K., Zachara, J.M., 2008. Electron transfer at the microbe–mineral interface: a grand challenge in biogeochemistry, Geobiology, 6, 245–253

Gaboriaud, F., Ehrhardt, J-J., 2003. Effects of different crystal faces on the surface charge of colloidal goethite (α-FeOOH) particles: An experimental and modeling study Geochim. Cosmochim. Acta. 67, 967–983.

Glasauer, S., Langley, S., Beveridge, T.J., 2001. Sorption of Fe (hydr)oxides to the surface of *Shewanella putrefaciens*: Cell-bound fine-grained minerals are not always formed de novo. Appl. Environ. Microbiol. 5544–5550.

Glasauer, S., Weidler, P.G., Langley, S., Beveridge, T.J., 2003. Controls on Fe reduction and mineral formation by a subsurface bacterium. Geochim. Cosmochim. Acta. 67, 7, 1277–1288.

Gimenez, J., Martınez, M., de Pablo, J., Rovira, M., Duro, L., 2007. Arsenic sorption onto natural hematite, magnetite, and goethite. J. Hazard. Mater.141, 575–580.

Gomez, M.A., Hendry, M.J., Hossain, A., Das, S., Elouatik, S., 2013. Abiotic reduction of 2-line ferrihydrite: effects on adsorbed arsenate, molybdate, and nickel, RSC Adv., 3, 25812-25822.

Grantham, M.C., Dove, P.M., Dichristina, T.J., 1997. Microbially catalyzed dissolution of iron and aluminum oxyhydroxide mineral surface coatings. Geochim. Cosmochim. Acta 61:467–477.

Handler, R., Beard, B.L., Johnson, C.M., Schrerer, M.M., 2009. Atom Exchange between Aqueous Fe(II) and Goethite: An Fe Isotope Tracer Study, Environ. Sci. Technol. 43, 1102–1107

Hansel, C.M., Benner, S.G., Neiss, J., Dohnalkova, A., Kukkadapu, R.K., Fendorf, S., 2003. Secondary mineralization pathways induced by dissimilatory iron reduction of ferrihydrite under advective flow. Geochim. Cosmochim. Acta 67 (16), 2977–2992.

Hansel, C.M., Benner, S.G., Nico, P., Fendorf, S., 2004. Structural constraints of ferric (hydr)oxides on dissimilatory iron reduction and the fate of Fe (II), Geochim. Cosmochim. Acta 68(15), 3217-3229.

Hansel, C.M., Benner, S.G., Fendorf, S., 2005. Competing Fe(II)-induced mineralization pathways of ferrihydrite. Environ. Sci.Technol. 39. 7147–7153.

Heimann, A.C., Jakobsen, R., 2007. Filtration through nylon membranes negatively affects analysis of arsenic and phosphate by the molybdenum blue method. Talanta 72, 839–841.

Hohmann, C., Morin, G., Ona-Nguema, G., Guigner,J-M., Brown, G.E.Jr., Kappler, A., 2011. Molecular-level modes of As binding to Fe(III) (oxyhydr)oxides precipitated by the anaerobic nitrate-reducing Fe(II)-oxidizing Acidovorax sp. strain BoFeN1, . Geochim. Cosmochim. Acta 75, 4699–4712.

Huang, J-H., Voegelin, A., Pombo, S.A., Lazzaro, A., Zeyer, J., Kretzschmar, R., 2011. Influence of Arsenate Adsorption to Ferrihydrite, Goethite, and Boehmite on the Kinetics of Arsenate Reduction by Shewanella putrefaciens strain CN-32, Environ. Sci. Technol. 45, 7701–7709.

Jambor, J.L., Dutrizac, J.E., 1998. Occurrence and Constitution of Natural and Synthetic Ferrihydrite, a Widespread Iron Oxyhydroxide, Chem. Rev., 98, 2549-2585.

Kerisit, S., Rosso, K.M., Dupuis, M., Valiev, M., 2007. Molecular computational investigation of electron-transfer kinetics across cytochrome-iron oxide interfaces, J. Phys. Chem. C, 111, 11363-11375.

Kocar, B.D., Herbel, M.J., Tufano K.J. and Fendorf, S., 2006. Contrasting effects of dissimilatory iron(III) and arsenic(V) reduction on arsenic retention and transport. Environ. Sci.Technol. 40, .6715–6721.

Kukkadapu, R.K., Zachara. J.M., Fredrickson. J.K., Kennedy, D.W., 2004. Biotransformation of two-line silicaferrihydrite by a dissimilatory Fe(III)-reducing bacterium: Formation of carbonate green rust in the presence of phosphate. Geochim. Cosmochim. Acta 68, 2799–2814.

Langley, S., Gault, A.G., Ibrahim, A., Renaud, R**.,** Fortin, D., Clark, I.D. and Ferris, F.G., 2009. A comparison of the rates of Fe(III) reduction in synthetic and bacteriogenic iron oxides by *Shewanella putrefaciens* CN32. Geomicrobiol. J., 26, 57-70.

Lasaga, A.C., and Lüttge, A., 2001. Variation of crystal dissolution rate based on a dissolution stepwave model. Science 291, 2400–2404.

Lasaga, A.C., and Lüttge, A., 2003. A model for crystal dissolution. Eur. J. Min. 15, 603–615.

Lovley, D.R., 1997. Microbial Fe(III) reduction in subsurface environments. FEMS Microbiol. Rev. 20,305-315.

Lüttge, A., Zhang, L., Nealson, K.H., 2005. Mineral surfaces and their implications for microbial attachment: results for Monte Carlo simulations and direct surface observations. Am. J. Sci. 305, 766-790.

Marcus, R.A., 1956. On the Theory of Oxidation-Reduction Reactions Involving Electron Transfer. I. J. Phys. Chem. 24, 966.

Marcus, R.A.; Sutin, N. 1985. Electron transfers in chemistry and biology. Biochim. Biophys. Acta. 811, 265-322.

Marcus, R.A., 1992. Electron transfer reactions in chemistry: Theory and experiment. Nobel Lecture, December 8.

Murphy, J.N., and C.W., Saltikov. 2007. The *cymA* gene encoding a tetrahemec-type cytochrome is required for arsenate respiration in Shewanella species. J. Bacteriol. 189, 2283–2290.

Ndlovua, S., Monhemius, A.J., 2005. The influence of crystal orientation on the bacterial dissolution of pyrite, Hydrometallurgy 78, 187–197

Neal, A.L., Rosso, K.M., Geesey, G.G., Gorby, Y.A. Little, B.J., 2003. Surface structure effects on direct reduction of iron oxides by *Shewanella onedensis*, Geochim. Cosmochim. Acta 67, 4489-4503.

Neil, C.W., Lee, B., Jun, Y-S., 2014. Different Arsenate and Phosphate Incorporation Effects on the Nucleation and Growth of Iron(III) (Hydr)oxides on Quartz. Environ. Sci. Technol., 48, 11883−11891

Newman, D.K., Beveridge, T.J., Morel, F.M.M., 1997. Precipitation of arsenic trisulfide by Desulfotomaculum auripigmentum, Appl. Environ. Microbiol.. 63, 2022-2028.

Ona-Nguema, G., Morin, G., Wang, Y., Menguy, N., Juillot, F., Olivi, L., Aquilanti, G., Abdelmoula, M., Ruby, C., Bargar, J.R., Guyot, F., Calas, G., Brown Jr. G.E., 2009. Arsenite sequestration at the surface of nano-Fe(OH)2, ferrous-carbonate hydroxide, and green-rust after bioreduction of arsenic-sorbed lepidocrocite by Shewanella putrefaciens. Geochim. Cosmochim. Acta. 73. 1359–1381

Oremland, R.S. and Stolz, J.F. 2005. Arsenic, microbes and contaminated aquifers. TRENDS Microbiol. 13, 45-49.

Pallud. C., Masue-Slowey. Y., Fendorf. S., 2010. Aggregate scale spatial heterogeneity in reductive transformation of ferrihydrite resulting from coupled biogeochemical and physical processes. Geochim. Cosmochim. Acta 74, 2811–2825.

Paktunc, D., Foster, A., Laflamme, G., 2003. Speciation and Characterization of Arsenic in Ketza River Mine Tailings Using X-ray Absorption Spectroscopy, Environ. Sci. Technol. 37, 2067-2074

Paktunc, D., Foster, A., Heald, S., Laflamme, G., 2004. Speciation and characterization of arsenic in gold ores and cyanidation tailings using X-ray absorption spectroscopy. Geochim. Cosmochim. Acta 68, 969–983.

Paktunc, D., Kingston, D., Pratt, A., McMullen, J., 2006. Distribution of gold in pyrite and in products of its transformation resulting from roasting of refractory gold ores. Can. Mineral. 44, 213-227.

Paktunc, D., 2008a. Speciation of Arsenic in Pyrite by Micro-X-Ray Absorption Fine-Structure Spectroscopy (XAFS) Ninth International Congress for Applied Mineralogy Brisbane, QLD, 8 - 10 September.

Paktunc, D., 2008b. Speciation of arsenic in an anaerobic treatment system at a Pb-Zn smelter site, gold roaster products, Cu smelter stack dust and impacted soil. Ninth International Congress for Applied Mineralogy Brisbane, QLD, 8 - 10 September.

Paktunc, D., Dutrizac, J., Gertsman, V., 2008c. Synthesis and phase transformations involving scorodite, ferric arsenate and arsenical ferrihydrite: Implications for arsenic mobility. Geochim. Cosmochim. Acta., 72, 2649–2672.

Paktunc, D., 2009. Arsenic speciation in wastes resulting from pressure oxidation, roasting and smelting. Proceedings of the 24th IAGS, Fredericton.

Paktunc, D., Bruggeman, K., 2010. Solubility of nanocrystalline scorodite and amorphous ferric arsenate: Implications for stabilization of arsenic in mine wastes, Appl. Geochem.25, 674–683

Paktunc, D., 2013. Mobilization of arsenic from mine tailings through reductive dissolution of goethite influenced by organic cover, Appl. Geochem. 36, 49–56.

Papassiopi, N., Vaxevanidou, K., Paspaliaris, I., 2003. Investigating the use of iron reducing bacteria for the removal of arsenic from contaminated soils. Water, Air, & Soil Poll. Focus, 81–90.

Pedersen, H., Postma, D., Jacobsen, R., 2006. Release of arsenic associated with the reduction and transformation of iron oxides. Geochim. Cosmochim. Acta 70, 4116-4129.

Petersen, K.M., Heaney, P.J., Post, J.E., Eng, P.J., 2015. A refined monoclinic structure for a variety of “hydrohematite”. Am. Mineral., in press, DOI:http//dx.doi.org.//10.2138-am-2015-4807.

Peretyazhko, T.S., Zachara, J.M., Kennedy, D.W., Fredrickson, J.K., Arey, B.W., McKinley, J.P., Wang, C.M., Dohnalkova, A.C., Xia, Y., 2010. Ferrous phosphate surface precipitates resulting from the reduction of intragrain 6-line ferrihydrite by Shewanella oneidensis MR 1. Geochim. Cosmochim. Acta 74, 3751–3767.

Qi, P., Pichler, T., 2014. Closer look at As(III) and As(V) adsorption onto ferrihydrite under competitive conditions. Langmuir, 30, 11110-11116.

Ravel, B.; Newville, M.2005. ATHENA, ARTEMIS, HEPHAESTUS:data analysis for X-ray absorption spectroscopy using IFEFFIT. J.Synchrotron. Radiat. 12, 537−541.

Raven, K.P., Jain, A., Loeppert, R.H., 1998. Arsenite and arsenate adsorption on ferrihydrite: kinetics, equilibrium, and adsorption envelopes, Environ. Sci. Technol. 32, 344–349.

Rancourt, D.G., Fortin, D., Pichler, T., Thibault, P.-J., Lamarche, G., Morris, R.V. Mercier, P.H.J. 2001. Mineralogy of a natural As-rich hydrous ferric oxide coprecipitate formed by mixing of hydrothermal fluid and seawater: implications regarding surface complexation and color banding in ferrihydrite deposits. Am. Mineral. 86, 834–851.

Riveros, P.A., Dutrizac, J.E., Spencer, P., 2001. Arsenic disposal practices in the metallurgical industry. Can Metall Q. 40, 395–420.

Roden, E.E., 2003. Fe(III) oxide reactivity toward biological versus chemical reduction. Environ. Sci. Technol. 37, 1319–1324.

Rojas-Chapana, J.A., Tributsch, H., 2004. Interfacial activity and leaching patterns of *Leptospirillum ferrooxidans* on pyrite FEMS Microbiology Ecology 47, 19-29.

Rosso, K.M., Zachara, J.M., Fredrickson, J.K., Gorby, Y.A., Smith, S.C., 2003. Nonlocal bacterial electron transfer to hematite surfaces, Geochim. Cosmochim. Acta 67, 5, 1081–1087.

Saltikov, C.W., Newman, D.K., 2003. Genetic identification of a respiratory arsenate reductase. Proc. Natl. Acad. Sci. USA 100:10983–10988.

Saltikov, C.W., Wildman, R.A. Jr., Newman,D.K., 2005. Expression Dynamics of Arsenic Respiration and Detoxification in Shewanella sp. Strain ANA-3. J. Bacteriol. 7390–7396.

Schwertmann, U., Cornell, R.M., Iron Oxides in the Laboratory Preparation and Characterization, Wiley-VCH, 2000.

Shen, S., Li, X-F., Cullen, W.R., Weinfeld, M., Le, X. C.,2013. Arsenic Binding to Proteins. Chem. Rev. 113, 7769−7792.

Slaughter, D.C., Macur, R.E., Inskeep, W.P., 2012. Inhibition of microbial arsenate reduction by phosphate. Microbiol. Research 167,151–156

Slowey, Y.M., Kocar, B.D., Jofre, S.A.B., Mayer. K.M., Fendorf, S., 2011. Transport implications resulting from internal redistribution of arsenic and iron within constructed soil aggregates, Environ. Sci. Technol. 45, 582–588.

Smith, M.A.D., Rosso, M.K., Dupuis, M., Valiev, M., Straatsma, T.P., 2006. Electronic Coupling between Heme Electron-Transfer Centers and Its Decay with Distance Depends Strongly on Relative Orientation. J. Phys. Chem. B 110, 15582-15588.

Stahl, K., Nielsen, K., Jiang, J., Lebech, B., Hanson, J.C., Norby, P., van Lanschot, J., 2003. On the akaganeite crystal structure, phase transformations and possible role in post-excavational corrosion of iron artifacts, Corros. Sci. 45. 2563–2575.

Stolz, J.F., Oremland, R.S., 1999. Bacterial respiration of arsenic and selenium. FEMS Microbiol. Rev. 23: 615 – 627.

Trainor, T.P., Chaka, A.M., Eng, P.J., Newville, M., Waychunas, G.A., Catalano, J. G., Brown, Jr, G.E., 2004. Structure and reactivity of the hydrated hematite (0001) surface. Surf. Sci. 573, 204–224.

Twidwell, L.G., Robins, R.G., Hohn, J.W., 2005. The removal of arsenic from aqueous solution by coprecipitation with Fe(III), Arsenic Metallurgy: Fundamentals and Applications Edited by R.G. Reddy and V. Ramachandran TMS, The Minerals, Metals & Materials Society. 1-20.

Wander, M.C.F., Rosso, K.M., Schoonen, M. A. A., 2007. Structure and charge hopping dynamics in green rust, J. Phys. Chem. C. 111, 11414-11423.

Waychunas, G.A., Rea, B.A., Fuller, C.C., Davis, J.A., 1993. Surface chemistry of ferrihydrite: Part 1. EXAFS studies of the geometry of coprecipitated and adsorbed arsenate. Geochim. Cosmochim. Acta 57, 2251−2269.

Weisener, C.G., Guthrie, J.W., Smeaton, C.M., Paktunc, D., Fryer, B.J., 2011. The effect of Ca–Fe–As coatings on microbial leaching of metals in arsenic bearing mine waste. J. Geochem. Explor. 110, 23–30.

Williams, A.G.B., Scherer, M.M., 2004. Spectroscopic Evidence for Fe(II)−Fe(III) Electron Transfer at the Iron Oxide−Water Interface, *Environ. Sci. Technol. 38,* 4782–4790.

Wilkie, J.A., Hering, J.G. 1996. Adsorption of arsenic onto hydrous ferric oxide:effects of adsorbate/adsorbent ratios and co-occurring solutes, Colloid Surf. A: Physicochem. Eng. Aspects 107, 97–110.

Yanina, S.V., Rosso, K.M., 2008. Linked reactivity at mineral-water interfaces through bulk crystal conduction. Science, 320, 218-222.

Yang, L., Steefel, C.I., Marcus, M.A., Bargar, J.R., 2010. Kinetics of Fe(II)-Catalyzed Transformation of 6-line Ferrihydrite under Anaerobic Flow Conditions. Environ. Sci. Technol. 44, 5469–5475.

Chapter 4.

Final conclusion and future research

Final conclusion:

Scorodite and adsorbed and coprecipitated arsenical 6-line ferrihydrite can be found in the wastes rocks and tailings of mining environments. These compounds are relatively stable, and can act as arsenic sinks. However, in the presence of bacteria, the solubility and stability of these compounds are significantly altered. In this research scorodite and COP and ADS arsenical 6-line ferrihydrite were subjected to bacterial reductive dissolution to investigate the nature and concentration of post reduction products including dissolved species and solid phases.

The specific objectives of this thesis were:

(1) to determine the changes in the speciation of As and Fe under the influence of bacteria,

(2) to assess the stability of various arsenical compounds in mine wastes and

(3) to assess the long-term environmental stability of common arsenical minerals and compounds for predicting As releases from mining and metallurgical wastes.

The information generated by this study can be used to assess the integrity of various disposal scenarios, such as water covers and soil covers in terms of preventing arsenic releases from mining wastes.

The following conclusions have been made in relationship to the objectives outlined above.

1. The DIRB and DARB *Shewanella* bacteria used in this experiment, at circumneutral pH and under anaerobic conditions, caused the reductive dissolution of scorodite, ($FeAsO_4 \cdot 2H_2O$), and adsorbed and coprecipitated arsenical 6-line ferrihydrite, Fe/As molar ratio 10/1, resulting in the release into solution of Fe(II) and of As(III), a more toxic and more bioavailable form of arsenic than As(V.

2. The concentrations in solution of the products of bacterial reduction of scorodite were about 1.5 mM Fe(II) and about 3 mM As(III), a Fe/As molar ratio of 1/2 compared to the molar ratio of 1/1 in the parent compound.

3. The concentrations of the products of bacterial reduction of the adsorbed and coprecipitated arsenical 6-line ferrihydrites, Fe/As molar ratio 10/1, were about 3.5 mM Fe(II) and about 0.057 mM As(III) for the ADS, and about 4.3 mM Fe(II) and about 0.055 mM As(III) and for the coprecipitated samples. The molar ratio of dissolved Fe/As in the adsorbed arsenical 6-line ferrihydrite samples was 60/1 compared to the Fe/As ratio of 80/1 for the coprecipitated samples. These results indicate that the adsorbed samples released more arsenic than the coprecipitated samples. Both, the adsorbed and the coprecipitated arsenical 6-line ferrihydrites, were more efficient in retaining arsenic than scorodite was in retaining arsenic under anaerobic conditions at circumneutral pH in the presence of bacteria.

4. Based on the findings of this research, of the systems investigated here, the preferred substance for the sequestration of arsenic, resulting from mine wastes and tailings, at circumneutral pH and under anaerobic conditions, is arsenical coprecipitated 6-line ferrihydrite which is somewhat better than the arsenical adsorbed 6-line ferrihydrite.

5. If scorodite is used as a means of sequestering arsenic, the findings of this thesis indicate that the As(III) concentration in solution should be lowest when the concentration of phosphate is the highest.

6. The long term stability of the substances used in this study to sequester arsenic were shown to be compromised by the presence of iron and arsenic reducing bacteria under anaerobic conditions at circumneutral pH.

7. The findings of this thesis are significant and have real world implications for the environmental arsenic problem. The practical measures to be taken to prevent arsenic contamination of ground and drinking water in the mining environment need to be effective and economical.

8. Cover materials, such as biosoil, soil and water covers may not be completely effective in preventing the contamination of ground and drinking water with the highly toxic and bioavailable form of arsenic, As(III) because of the potential for bacterial activity under the anaerobic conditions created by these covers.

9. Based on the available literature on the reduction mechanism of arsenate, the As(V) must be detached from the surface of scorodite or the arsenical ferrihydrite, and released into solution before being taken up by the bacteria.

10. The Fe(II), which was formed by the bacterial reduction of scorodite and arsenical 6-line ferrihydrite, and then re-adsorbed on the surfaces of the remaining solid, underwent a the series of mineral transformations, particularly in the case of 6LFH (Fe/As = 10), to form akaganeite, goethite, hydrohematite and possibly magnetite. It is therefore proposed, based on a mechanism originally developed by Marcus 1956, that the biotically reduced aqueous Fe(II) re-adsorbed on the surfaces of scorodite and also on the ferrihydrite, and the Fe(III) reduction occurred by a self-exchange reaction between Fe(II) and Fe(III) leading to the formation of the secondary minerals.

12. Large imprints formed on the surfaces of secondary minerals obtained from the biotically reduced ADS and COP arsenical ferrihydrite samples appeared to be etched by the bacteria. Some imprints had the shape of the bacterium, other imprints have a circular shape matching the apical diameter of the bacterium. Some small imprints could be caused etching.

13. Based on the log CFU plots, the bacterial counts decreased throughout the time of the experiments, both for the scorodite and arsenical 6LFH, indicating that the bacteria only surviving.

Finally the results from this study show that scorodite ($FeAsO_4 \cdot 2H_2O$) and adsorbed and co-precipitated arsenical 6-line arsenical ferrihydrite were all reduced by the two *Shewanella* strains, resulting in the release of Fe(II) and of As(III) (a more toxic and more bioavailable form than As(V). Ferrihydrite containing sorbed As released more arsenic than the As co-precipitated samples, but both the

adsorbed and the co-precipitated arsenical 6-line ferrihydrites were more efficient in retaining arsenic than scorodite under anaerobic conditions at circumneutral pH in the presence of *Shewanella* sp. ANA-3 and *Shewanella putrefaciens* CN32. Based on these findings, the preferred way of sequestering As present in mine wastes and tailings, at circumneutral pH and under anaerobic conditions favourable to Fe and As reducing bacteria, is arsenical co-precipitated 6-line ferrihydrite which is somewhat better than the arsenical adsorbed 6-line ferrihydrite. Ideally, non-water saturated conditions should prevail in tailings in order to prevent the activity of microorganisms capable of respiring on iron and arsenic, but such a goal remains likely unattainable, especially in temperate climates, where large amounts of precipitations tend to saturate the tailings.

Future research:

In this project, reduction experiments were designed to represent, to a certain extent, the natural conditions prevailing in mine tailings. Phosphate concentrations were for example reduced to levels approaching those found in real settings. However, other conditions were not, including the use of lactate, a simple organic electron donor in the growth medium. The use of pure synthetic mineral phases (scorodite, 6-line ferrihydrite) is a step in the right direction, but natural As-bearing minerals in mine tailings are likely to contain other impurities than As and possess mineral defects. The results also revealed the formation of several secondary minerals at the end of the microbial reduction, and it would be interesting to

determine if the same secondary minerals are present in mine tailings and if they sequester arsenic over a long period of time.

Some suggestions for future research.

1. Obtain information on the rates of bacterial reduction of As(V), and of Fe(III) in solution, in the absence of minerals, using different reducing agents such as lactate and related compounds, at two different temperatures to obtain activation energies for the reduction reactions. This could prove to be a useful comparison with rates of reduction measured for systems in which the iron and arsenic are initially in a solid.

2. Investigate the reduction of scorodite using an exclusively iron reducing bacterium for a period of time until the dissolved Fe(II) concentration reaches a steady state at which point an exclusively arsenate reducing bacterium would be injected after which the rate of reduction of As(V) would be measured. The purpose of this investigation would be to determine whether secondary mineral formation was significantly altered under these conditions from the case where both iron and arsenic were reduced simultaneously.

3. Subject crystalline hematite, magnetite, goethite and other iron oxide compounds to iron reducing bacteria under anaerobic condition in solution to investigate the imprints patterns formed on the solid surfaces as was observed in the current research. The goal of this investigation is to determine if there is a relationship between the locations and size of the imprints and crystal faces.

Appendix.

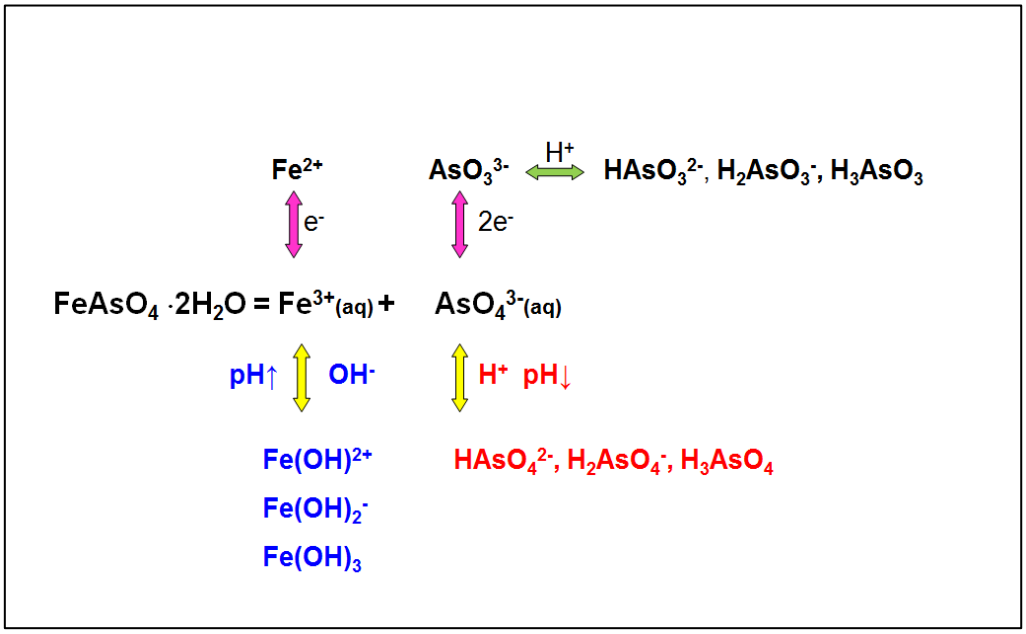

Figure A-1. Simplified schematic diagram illustrates the bacterial dissolution of scorodite.

The species formed are governed by redox reactions and pH of the solution. The distribution diagrams and log concentration diagram, log C, as a function of pH are shown in Section A-1.

Section A-1. Acid-base equilibria of iron and arsenic

Acid-base equilibrium is included in this thesis to show the complexity of the iron and arsenic hydrolysis reactions and the possibility of the formation of many species depending on pH.

Hydrolysis reactions of Fe(III)

Fe^{3+} in aqueous solution at low pH, is octahedrally coordinated to six H_2O molecules, forming the species $Fe(H_2O)_6]^{3+}$. The $Fe(H_2O)_6]^{3+}$ iron-aquo complex is a fairly strong acid, with a pKa of 2.2 due to the ionization of protons from the H_2O ligands. As the solution pH increases, progressively more OH^-'s replace the coordinated H_2O. The hydrolysis reactions are described in Table A-1. It is important to note that for iron hydrolysis, the equations shown are a simplified version of the very complex polymeric oxides formation known as olation or oxolation, which is particularly important in the formation of minerals (Housecroft and Sharpe, 2001).

Table A-1 Hydrolysis reactions of Fe(III).

$Fe^{3+} + H_2O = Fe(OH)^{2+} + H^+$	*$pK_1 = 2.2$	$K_1 = \frac{[Fe(OH)^{2+}][H^+]}{[Fe^{3+}]} = 6.31\,x10^{-3}$
$FeOH^{2+} + H_2O = Fe(OH)_2^+ + H^+$	$pK_2 = 3.04$	$K_2 = \frac{[Fe(OH)_2^+][H^+]}{[Fe(OH)^{2+}]} = 3.98\,x10^{-4}$
$Fe(OH)_2^+ + H_2O = Fe(OH)_3 + H^+$	$pK_3 = 6.80$	$K_3 = \frac{[Fe(OH)_3][H^+]}{[Fe(OH)_2^+]} = 1.58\,x10^{-7}$
$Fe(OH)_3 + H_2O = Fe(OH)_4^- + H^+$	$pK_4 = 9.1$	$K_4 = \frac{[Fe(OH)_3][H^+]}{[Fe(OH)_4^-]} = 7.94\,x10^{-10}$

* Barnum, (1983). Updated values of these hydrolysis and solubility constants of these species and their dependence on ionic strength at 25 °C have been published by Stefánsson, (2007).

The fractions α of the different Fe^{3+} species at a given pH can be determined using the following analysis:

$$\frac{[Fe(OH)^{2+}]}{[Fe^{3+}]} = \frac{K_1}{[H^+]}$$

$$\frac{[Fe(OH)^{2+}][H^+]}{[Fe^{3+}]} x \frac{[Fe(OH)_2{}^+][H^+]}{[Fe(OH)^{2+}]} = K_1K_2$$

$$\frac{[Fe(OH)_2{}^+][H^+]^2}{[Fe^{3+}]} = K_1K_2$$

$$\frac{[Fe(OH)_2{}^+]}{[Fe^{3+}]} = \frac{K_1K}{[H^+]^2}$$

$$\frac{[Fe(OH)_3]}{[Fe^{3+}]} = \frac{K_1K_2K_3}{[H^+]^3}$$

$$\frac{[Fe(OH)_4^-]}{[Fe^{3+}]} = \frac{K_1K_2K_3K_4}{[H^+]^4}$$

$$\frac{[Fe(OH)_2^+][H^+]^2}{[Fe^{3+}]} = K_1K_2$$

$$\frac{[Fe^{3+}]}{[Total\text{Fe(III)}]} = \frac{[Fe^{3+}]}{[Fe^{3+}]+[Fe(OH)^{2+}]+[Fe(OH)_2^+]+[Fe(OH)_3]+[Fe(OH)_4^-]}$$

$$\frac{[Fe^{3+}]}{[Total\text{Fe(III)}]} = \frac{[Fe^{3+}]/[Fe^{3+}]}{\frac{[Fe^{3+}]}{[Fe^{3+}]}+\frac{[Fe(OH)^{2+}]}{[Fe^{3+}]}+\frac{[Fe(OH)_2^+]}{[Fe^{3+}]}+\frac{[Fe(OH)_3]}{[Fe^{3+}]}+\frac{[Fe(OH)_4^-]}{[Fe^{3+}]}}$$

$$[Fe^{3+}] = \frac{[Total\text{Fe(III)}]}{1+\frac{K_1}{[H^+]}+\frac{K_1K_2}{[H^+]^2}+\frac{K_1K_2K_3}{[H^+]^3}+\frac{K_1K_2K_3K_4}{[H^+]^4}}$$

$$[Total\text{Fe(III)}] = [Fe^{3+}]+[Fe(OH)^{2+}]+[Fe(OH)_2^+]+[Fe(OH)_3]+[Fe(OH)_4^-]$$

$$[Total\text{Fe(III)}] = \left[Fe^{3+}\right]\left\{1 + \frac{K_1}{[H^+]}+\frac{K_1K_2}{[H^+]^2}+\frac{K_1K_2K_3}{[H^+]^3}+\frac{K_1K_2K_3K_4}{[H^+]^4} + \right\}$$

Total Fe(III) is the concentration of the Fe^{3+} species, they can be calculated if the pH is known. The calculation is shown below.

$$[Total\ \mathrm{Fe(III)}] = [\mathrm{Fe^{3+}}]+[\mathrm{Fe(OH)^{2+}}]+[\mathrm{Fe(OH)_2^+}]+[\mathrm{Fe(OH)_3^0}]+[\mathrm{Fe(OH)_4^-}]$$

$$\alpha_4 = \frac{\left[\mathrm{Fe^{3+}}\right]}{[Total\ \mathrm{Fe(III)}]} = [1 + \frac{K_1}{[H^+]} + \frac{K_1K_2}{[H^+]^2} + \frac{K_1K_2K_3}{[H^+]^3} + \frac{K_1K_2K_3K_4}{[H^+]^4}]^{-1}$$

$$\alpha_3 = \frac{[\mathrm{Fe\left(OH\right)^{2+}}]}{[Total\ \mathrm{Fe(III)}]} = \alpha_4 \frac{K_1}{[H^+]}$$

$$\alpha_2 = \frac{[\mathrm{Fe(OH)_2^+}]}{[Total\ \mathrm{Fe(III)}]} = \alpha_4 \frac{K_1K_2}{[H^+]^2}$$

$$\alpha_1 = \frac{[\mathrm{Fe\left(OH\right)_3^0}]}{[Total\ \mathrm{Fe(III)}]} = \alpha_4 \frac{K_1K_2K_3}{[H^+]^3}$$

$$\alpha_0 = \frac{[\mathrm{Fe(OH)_4^-}]}{[Total\ \mathrm{Fe(III)}]} = \alpha_4 \frac{K_1K_2K_3K_4}{[H^+]^4}$$

As a result of the above calculations, the Fe^{3+} species distribution diagram as the function of pH is shown in Figure A-2. This diagram was constructed from the mass balance of the hydrolysis products of iron. To simplify the method, concentration was used instead of activity

Table A-2. Calculated constants from pK used for the construction of Figure A-1.

pK	K	
Log K_1 = -2.2	$\mathrm{K_1} = 10^{-2.2} = 0.00631$	
Log K_2 = -3.4	$\mathrm{K_2} = 10^{-3.4} = 3.98 \times 10^{-4}$	K_1K_2 = 2.56 x 10^{-6}
Log K_3 = -6.8	$\mathrm{K_3} = 10^{-6.8} = 1.58 \times 10^{-7}$	$K_1K_2K_3$ = 3.97 x 10^{-13}
Log K_4 = -9.1	$\mathrm{K_4} = 10^{-9.1} = 7.94 \times 10^{-10}$	$K_1K_2K_3K_4$ = 3.15 x 10^{-22}

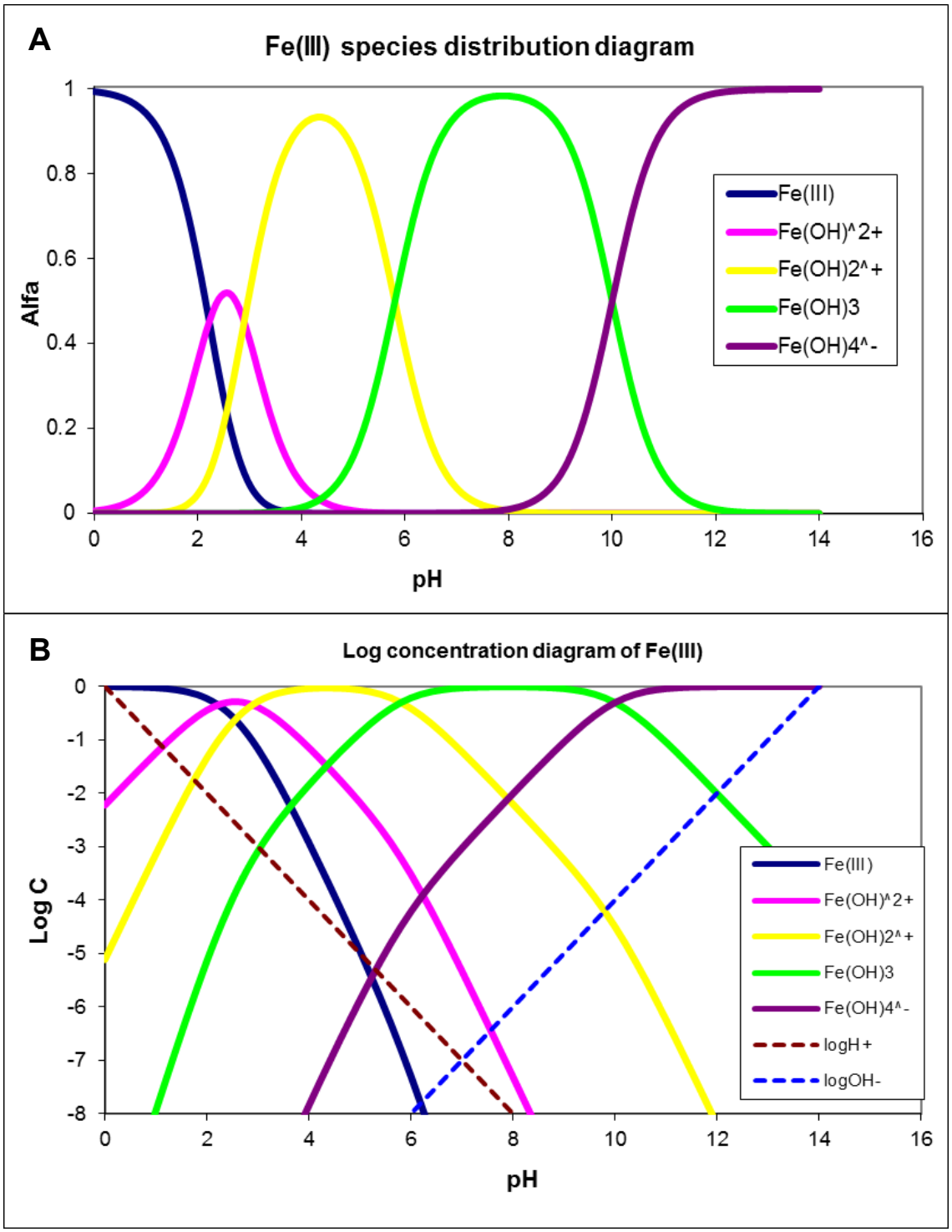

Figure A-2. (A) Fe(III) species distribution and (B) log concentration, Log C, diagram as a function of pH of Fe(III) in aqueous solution (Butler, 1964;Stumm and Morgan,1996).

Mass balance:

$[Fe\,Total] = [Fe^{3+}] + [FeOH^{2+}] + [Fe(OH)_2^{+}] + [Fe(OH)_{3(aq)}] + [Fe(OH)^{4-}]$

$[Fe\,Total] = [Fe^{3+}] + [Fe^{3+}] * K_1/[H^+] + [Fe^{3+}] * \beta^2/[H^+]^2 + [Fe^{3+}] * \beta^3 / [H^+]^3 + [Fe^{3+}] * \beta^4 /[H^+]^4$

$[Fe\,Total] = [Fe^{3+}] \{ 1 + *K_1/[H^+] + *\beta^2/[H^+]^2 + *\beta^3/[H^+]^3 + *\beta^4/[H^+]^4 \}$

$\alpha Fe^{3+} = [Fe^{3+}] / [Fe\,Total]$

The solubility product of ferrihydrite can be written as:

$Fe(OH)_{3(am)} = Fe^{3+} + 3\ OH^-$

$3\ OH^- + 3\ H^+ = 3\ H_2O$

and

$Fe(OH)_{3\ (am)} + 3\ H^+ = Fe^{3+} + 3\ H_2O$

$*K_{SO} = 103.2 = \frac{[Fe^{3+}]}{[H^+]^3}$

Then: $Fe\,Total = (*K_{SO}\ [H^+]^3) \{ 1 + *K_1/[H^+] + *\beta^2/[H^+]^2 + *\beta^3/[H^+]^3 + *\beta^4/[H^+]^4 \}$

Solubility of $Fe(OH)_3(s)$ in terms of the uncharged dissolved species, $Fe(OH)_3$.

Adding the two reactions above:

$Fe(OH)_3(s) + 3H^+ = Fe^{3+} + 3\ H_2O$ pK = - 3.2

$Fe^{3+} + 3H_2O = Fe(OH)_3 + 3H^+$ pK = -12.4

$Fe(OH)_3\ (s) = Fe(OH)_3$ pK = - 9.2

$K = Fe(OH)_3 / Fe(OH)_3(s) \approx Fe(OH)_3$

Dissolved Fe = $Fe(OH)_3 = 10^{-9.2}$ M

Hydrolysis reactions of arsenate

Table A-3. The hydrolysis reactions of arsenate with the corresponding equilibrium constants.

$H_3AsO_4 \Leftrightarrow H_2AsO_4^- + H^+$	*$pK_1 = 2.2$	$K_1 = \frac{[H_2AsO_4^-][H^+]}{[H_3AsO_4]}$
$H_2AsO_4^- \Leftrightarrow HAsO_4^{2-} + H^+$	$pK_2 = 7.0$	$K_2 = \frac{[HAsO_4^{2-}][H^+]}{[H_2AsO_4^-]}$
$HAsO_4^{2-} \Leftrightarrow AsO_4^{3-} + H^+$	$pK_3 = 11.5$	$K_3 = \frac{[AsO_4^{3-}][H^+]}{[HAsO_4^{2-}]}$

* The pKa values of the arsenate species from: (Rivas and Sadowski, 2014)

1. $$K_1K_2 = \frac{[H_2AsO_4^-][H^+]}{[H_3AsO_4]} x \frac{[HAsO_4^{2-}][H^+]}{[H_2AsO_4^-]} = \frac{[HAsO_4^{2-}][H^+]^2}{[H_3AsO_4]}$$

2. $$K_1K_2K_3 = \frac{[H_2AsO_4^-][H^+]}{[H_3AsO_4]} x \frac{[HAsO_4^{2-}][H^+]}{[H_2AsO_4^-]} x \frac{[AsO_4^{3-}][H^+]}{[HAsO_4^{2-}]} = \frac{[AsO_4^{3-}][H^+]^3}{[H_3AsO_4]}$$

$$\frac{[H_2AsO_4^-]}{[AsO_4^{3-}]} = \frac{[H^+]^3}{K_1K_2K_3}$$

$$\frac{[H_3AsO_4]}{As(V)Total} = \frac{[AsO_4^{3-}]}{[AsO_4^{3-}]+[HAsO_4^{2-}]+[H_2AsO_4^-]+[H_3AsO_4]}$$

$$\frac{[H_3AsO_4]}{As(V)Total} = \frac{\frac{[AsO_4^{3-}]}{[AsO_4^{3-}]}}{\frac{[AsO_4^{3-}]}{[AsO_4^{3-}]}+\frac{[HAsO_4^{2-}]}{[AsO_4^{3-}]}+\frac{[H_2AsO_4^-]}{[AsO_4^{3-}]}+\frac{[H_3AsO_4]}{[AsO_4^{3-}]}}$$

$$[H_3AsO_4] = \frac{As(V)Total}{1+\frac{[H^+]}{K_1}+\frac{[H^+]^2}{K_1K_2}+\frac{[H^+]^3}{K_1K_2K_3}}$$

As(V)Total is the concentration *C* of the arsenic acid and its anions, they can be calculated if the pH is known. The calculation is shown below.

$$[H_3AsO_4]+[H_2AsO_4^-]+[HAsO_4^{2-}]+[AsO_4^{3-}] = As(V)Total = C$$

$$\alpha_3 = \frac{[H_3AsO_4]}{C} = \left[1+\frac{K_1}{[H^+]}+\frac{K_1K_2}{[H^+]^2}+\frac{K_1K_2K_3}{[H^+]^3}\right]^{-1}$$

$$\alpha_2 = \frac{[H_2AsO_4^-]}{C} = \alpha_3\frac{K_1}{[H^+]}$$

$$\alpha_1 = \frac{[HAsO_4^{2-}]}{C} = \alpha_3\frac{K_1K_2}{[H^+]^2}$$

$$\alpha_0 = \frac{[AsO_4^{3-}]}{C} = \alpha_3\frac{K_1K_2K_3}{[H^+]^3}$$

The arsenate species distribution and the logarithmic diagram, log C, of arsenate as a function of pH are shown in (Figure A-3 A and B).

H_3AsO_4 range

Log $[H_3AsO_4]$ = log C

Log $[H_2AsO_4^-]$ = log C - pK_1 + pH

Log $[HAsO_4^{2-}]$ = log C - (pK_1 + pK_2) + 2 pH)

Log $[AsO_4^{3-}]$ = log C - (pK_1 + pK_2 + pK_3) + 3 pH)

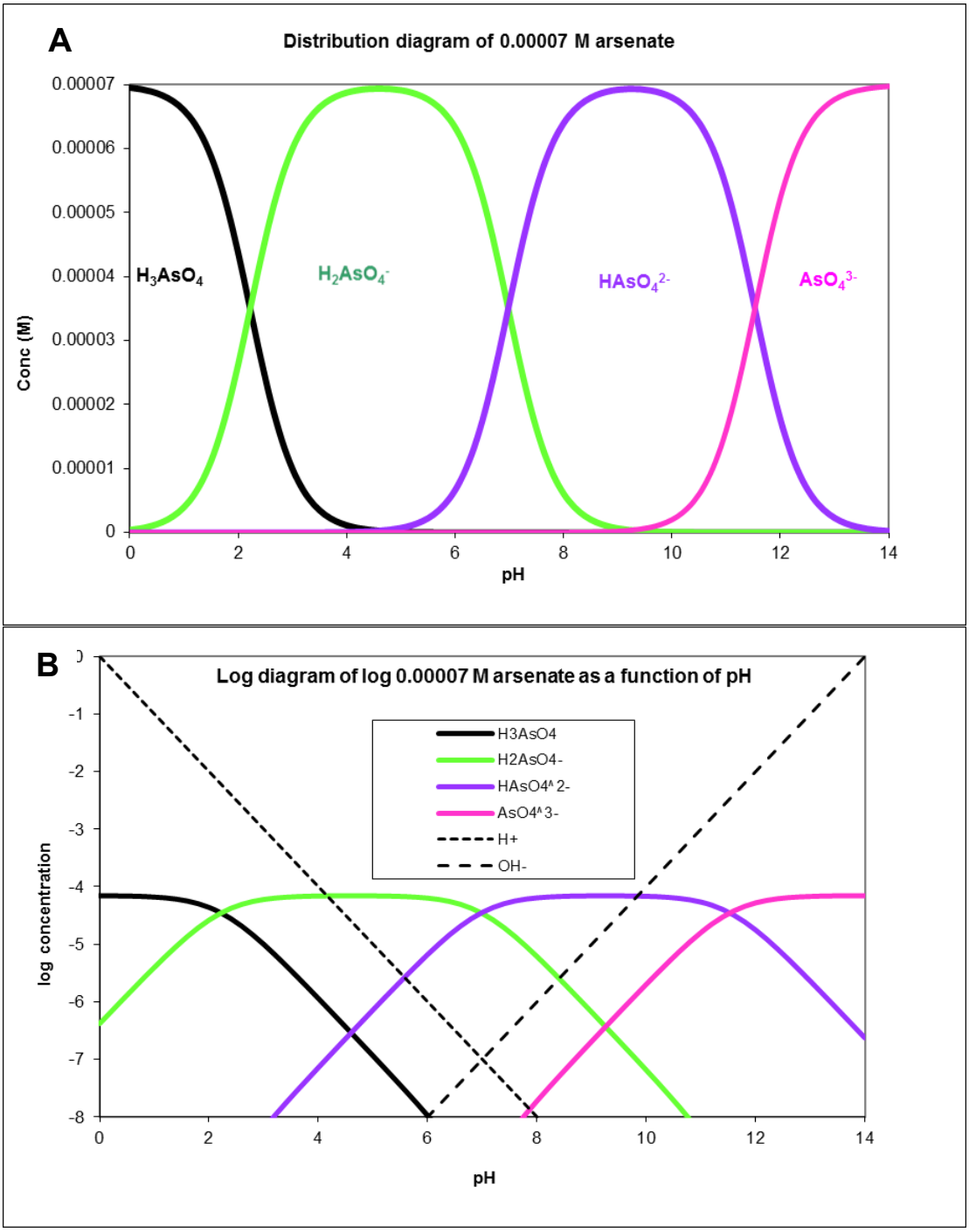

Figure A-3. (A) Arsenate species distribution diagram and (B) logarithmic diagram, log C, as a function of pH of 70 µM As(V) released from the microbial reduction of scorodite.

The concentration of arsenite species in solution are related by the mass balance and can be calculated as shown below

Table A-4. Hydrolysis reactions of arsenite and the corresponding equilibrium constants.

$H_3AsO_3 \Leftrightarrow H_2AsO_3^- + H^+$	*pK_1 = 9.2	$K_1 = \frac{[H_2AsO_3^-][H^+]}{[H_3AsO_3]}$
$H_2AsO_3^- \Leftrightarrow HAsO_3^{2-} + H^+$	pK_2 = 12.1	$K_1 = \frac{[HAsO_3^{2-}][H^+]}{[H_2AsO_3^-]}$
$HAsO_3^{2-} \Leftrightarrow AsO_3^{3-} + H^+$	pK_3 = 13.4	$K_1 = \frac{[AsO_3^{3-}][H^+]}{[HAsO_3^{2-}]}$

* The pKa values of the arsenate species are: (Rivas and Sadowski, 2014)

$$[H_3AsO_3]+[H_2AsO_3^-]+[HAsO_3^{2-}]+[AsO_3^{3-}] = C$$

$$\alpha_3 = \frac{[H_3AsO_3]}{C} = [1 + \frac{K_1}{[H^+]} + \frac{K_1K_2}{[H^+]^2} + \frac{K_1K_2K_3}{[H^+]^3}]^{-1}$$

$$\alpha_2 = \frac{[H_2AsO_3^-]}{C} = \alpha_3 \frac{K_1}{[H^+]}$$

$$\alpha_1 = \frac{[HAsO_3^{2-}]}{C} = \alpha_3 \frac{K_1K_2}{[H^+]^2}$$

$$\alpha_0 = \frac{[AsO_3^{3-}]}{C} = \alpha_3 \frac{K_1K_2K_3}{[H^+]^3}$$

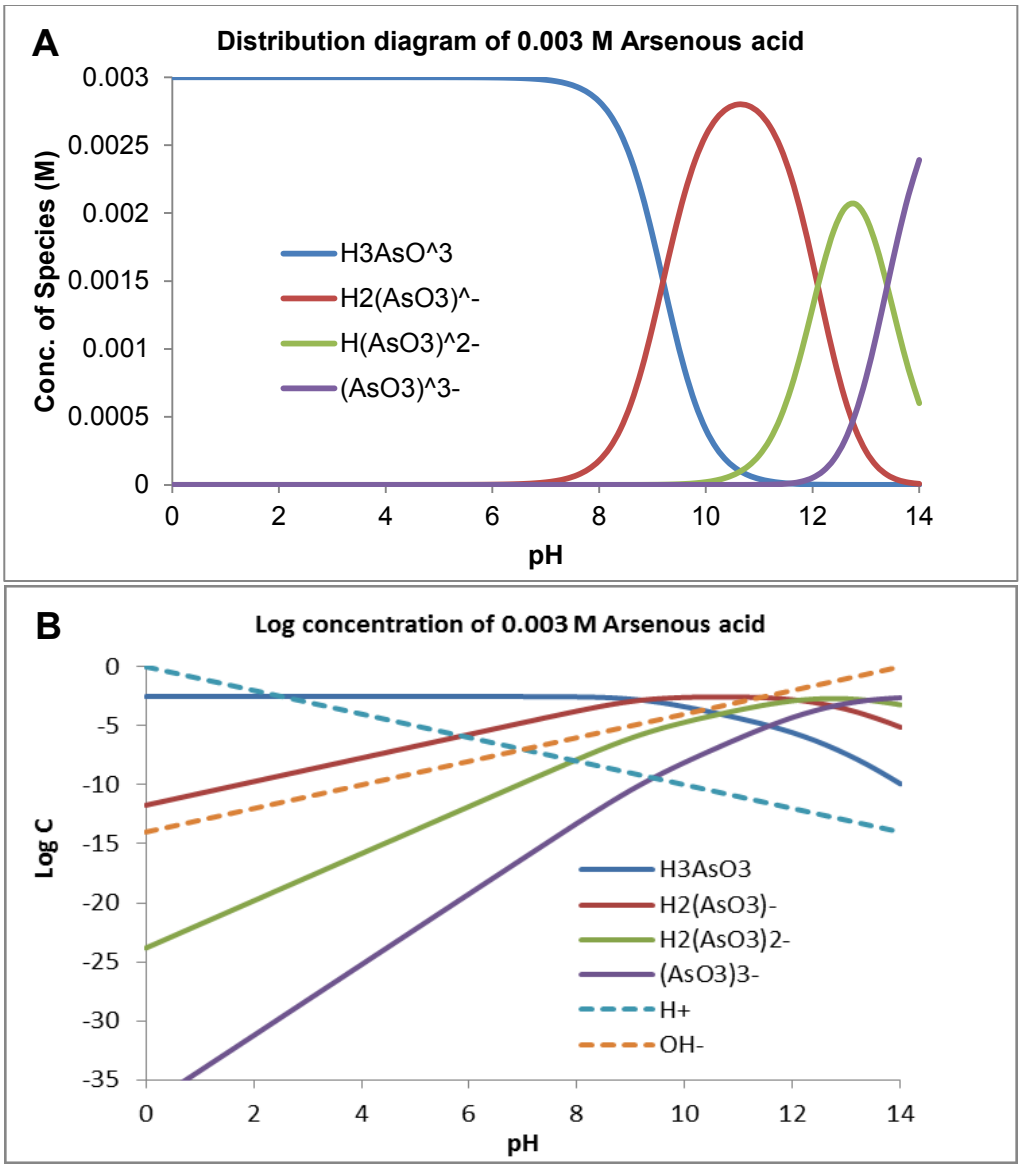

Figure A-4. (A) Arsenite species distribution diagram and (B) log concentration diagram of 3 mM plateau concentration of dissolved As(III) resulting from the biotic reduction of scorodite.

References Section A-1:

Barnum, D.W., Hydrolysis of Cations. 1983. Formation Constants and Standard Free Energies of Formation of Hydroxy Complexes. Inorg. Chem. 22, 2297-

2305.

Butler, J.N., Ionic equilibrium, A mathematical approach. 1964. Addison-Wesley Publishing Company Inc.

Lee, T.S., Gunnar Sillén, L., 1959. Chemical equilibrium in analytical chemistry. Reprinted in full from *Treatise on Analytical Chemistry* edited by I.M. Kolthoff and P.J. Elving. Part I. Volume 1. The Interscience Encyclopedia Inc. page: 277 in Chapter 8. by Lars Gunnar Sillén.

Rivas, B.L., Sadowski, Z., 2014. Bacterial generation of liquid arsenic waste and the application of water-soluble polymers for arsenic ions separation. Rev. Environ. Sci. Biotechnol.13, 277–284.

Stefánsson, A., 2007. Iron(III) Hydrolysis and Solubility at 25 °C, Environ. Sci. Technol. 41, 6117-6123,

Stumm, W., Morgan, J.J., Aquatic Chemistry, Chemical Equilibria and Rates in Natural waters. John Wiley & Sons Inc. 1996. p:267.

Section A-2. ICP-OES instrumental setup for the analysis of the aqueous species.

Figure A-5. Figure A-5. The analyses of the aqueous phase in this research were performed with the Varian Vista Pro ICP-OES instrument.

Table A-5. Sample setup parameters for the Varian Vista Pro ICP-OES.

RF power (W) 1000

Plasma observation height (mm) 10.0*

Plasma gas flow rate (L/min) 15.00

Auxiliary gas flow rate (L/min) 1.5

Nebulizer flow rate (L/min) 0.9

Sample flow rate (mL/min) 2.0

Aerosol carrier gas flow rate (L/min) 0.80

Sample uptake delay (s) 25

Rinse time (s) varied from 120 to 180

* This setting corresponds to approximately 10 mm between the top of the load coil and the centre of the plasma observation window (which is 10 mm in diameter).

General Calibration and Standardization Procedure used with the Varian ICP-OES:

Standards used were a Multielement Standard Solution in diluted nitric acid; (Specpure, Alfa Aesar), Arsenic as Arsenic oxide in 4% nitric acid (PlasmaCal, SCP Science) and Phosphorus as ammonium dihydrogen phosphate in water (SCP Science), all with certified concentrations of 1000 μg/mL. These standards were diluted to provide calibration standards over the detection range of Fe, As and P. The calibration range included 0.5, 1, 5, 10 and 20 μg/mL of the multielements standard and As and P.

Depending on the number of samples to be analysed recalibration of the instrument was performed and generally a blank solution containing 1 % nitric acid and a 5 mg/L control sample was analyzed from very 8 to 12 samples depending on the concentration of the particular analyte. For samples with low concentration a blank solution was analysed after every four samples.

Certified Reference Material: TMDA 70 was used as a high level fortified standard for trace elements prepared in filtered and diluted Lake Ontario water and preserved with 0.2 % nitric acid. The results were in the range for the specific elements.

Preparation of Standards: 0.5, 1, 5, 10, 20 mg/L (ppm) were used. A volume of 100 mL for each standard were prepared for multiple analyses. For example, 2 mL of each of the above standard were added to a 100 mL volumetric flask and diluted to mark with 1 % nitric acid.

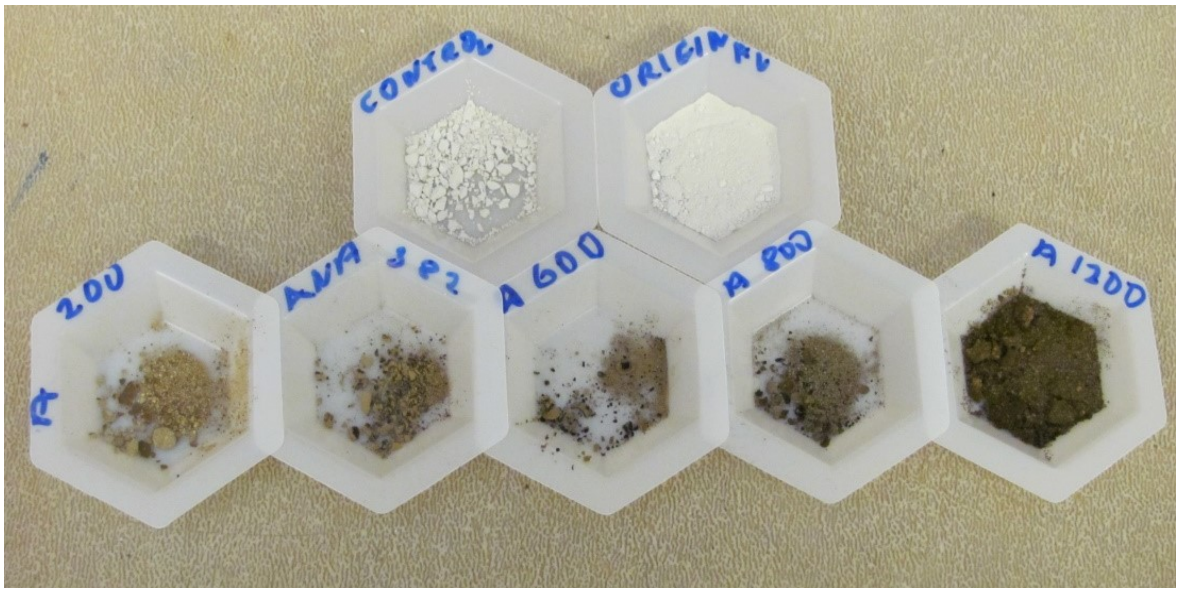

Figure A-6. Change of appearance of the biotic scorodite with time in the presence of *Shewanella* sp. ANA-3 during the 1200 hours bacterial reduction experiment. Times shown are: 200, 382, 600, 800 and 1200 hours. Top plates from left to right are the abiotic control and the original scorodite sample.

Figure A-7. Flow chart of the sampling procedure used for the bacterial

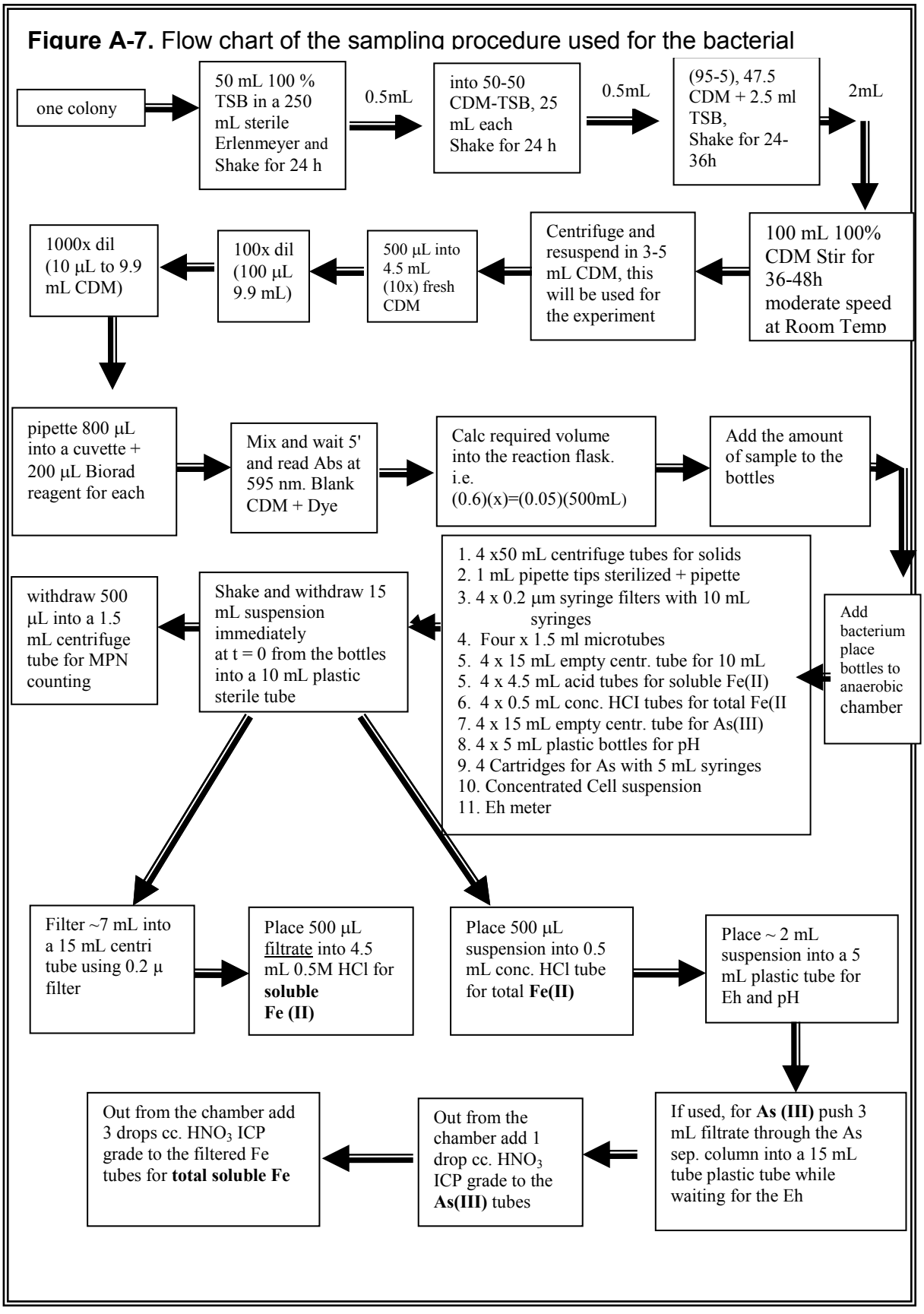

Figure A-8. The experimental microcosm bottles in the anaerobic chamber were protected from light by covering them with Al foil.

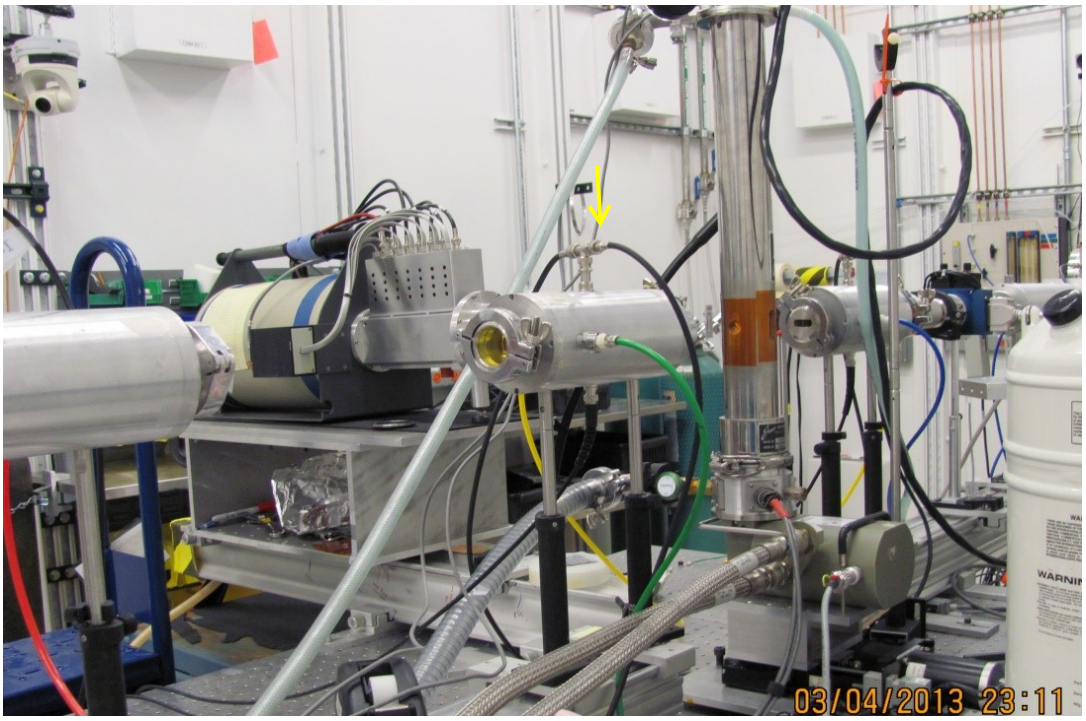

Figure A-9. The XAS measurements were performed at the 20-BM line of the PNC-CAT facility in the Advanced Photon Source at the Argonne National Laboratory in

Chicago. The sample was enclosed in the cryogenic apparatus, the long, standing tube with the brown Kapton taped window labelled by the arrow.

Figure A-10. The XAS control desk during data acquisition. The output parameters, such as the temperature, input-output energy and the XAS signal were monitored as shown on the computer screens from left to right.

Section A-3. XAS sample dilution calculations for post-edge absorption*

*after Kelly, Hesterberg, & Ravel

Sample calculations of absorption length (1/μ) for scorodite:

Density $FeAsO_4 \cdot 2H_2O$ = 3.28 g/cm^3

MW = 230.8 g/mol = 55.9 g/mol (Fe) + 74.9 g/mol (As) + 6 x 16.0 g/mol (O) + 4 x 1 g/mol (H)

f_{Fe} = 55.9/230.8 = 0.242; σ_{Fe} = 393.5 cm^2/g; (photoelectric)

f_{As} = 74.9/230.8 = 0.325; σ_{As} = 173.1 cm^2/g;

f_O = 6 x16/230.8 = 0.416; σ_O = 15.0 cm^2/g;

f_H = 4/230.8 = 0.0174; σ_H = 0.8 cm^2/g;

$$\mu = 3.28\frac{g}{cm^3}(0.242*393.5\frac{cm^2}{g}+0.325*173.1\frac{cm^2}{g}+0.416*15.0\frac{cm^2}{g}+0.074*0.8\frac{cm^2}{g}) =$$

$$= 517.5cm^{-1} = \frac{1}{517.5cm} = 0.00193cm * \frac{10000\mu m}{1cm} = 19.3\mu m$$

∴ The attenuation length for Fe: **19.3 μm.**

Table A-6. Sample dilution calculation of iron in the biotic scorodite with boron nitride to give an edge step of 1.0 across the Fe K-edge of 7112 eV.

The sample holder with a rectangular sample window had a cross-sectional area of 0.60 cm^2 (1.7 × 0.35 × 0.15 cm thick) and a sample capacity estimated to 70 mg of BN, the dominant sample component. In this calculation, the dilution yielding unit edge step would give a total post-edge absorption (1.78) below the desired maximum of 2.5 for a transmission sample.

SCORODITE based on Fe (230.80 g/mol)		**Mass absorption coefficient (μ/ ρ)*** (cm^2/g)			**Element**				
Elem-ent	**Mass frac-tion in Sc#**	**Pre-edge 7111** (eV)	**Post-edge 7113** (eV)	**Δ (μ/ρ)**	**Conc. for unit edge step** (g/cm^2) **	**Amount Fe in sample Holder** (mg) ***	**Mass of scorodite** (mg) 3*	**Conc. of scorodite** (mg/g) ****	**Post-edge Abs.** (/ Fe)5*
Fe	0.241	53.2	407.6	354.4	0.00282	1.69	7.02 x 1.2 = 8.4	104.8	1.15
As	0.325	104.3	104.2						0.39
O	0.415	16.6	16.6						0.08
H	0.0175	0.396	0.396						0
BN									0.16
								Total	**1.78**

* Mass absorption coefficient (μ/ρ) below and above the Fe K-edge at 7112 eV obtained from X-ray absorption tables in Hephaestus for each element, and the change in (μ/ρ) for Fe across the edge.

** Calculated for Fe as 1.0/Δ (μ/ρ) where 1.0 = the target edge step.

3* Iron amount (column 7) in sample (mg) = Fe concentration (g/cm^2) × sample cross-sectional area (0.60 cm^2) × 1000 mg/g; scorodite in mg (column 8) = Fe mg (column 7)/mass fraction of Fe (column 2).

4* Concentration of scorodite (mg/g sample) after diluting in BN = mass of mineral (7.02 mg)/mass sample i.e. [0.067 = 0.00702 g mineral + 0.06 g BN].

5* Total post-edge absorption contribution per element = element mass fraction (column 2) × scorodite in grams (0.001 × column 8) × post-edge mass absorption coefficient (column 4)/sample cross-sectional area (0.60 cm^2). Total absorption = sum of all element contributions including the contribution of BN (0.16).

Scorodite.

Table A-7. Sample calculation for the dilution of As in scorodite ($FeAsO_4 \cdot 2H_2O$) with boron nitride (BN) to give an edge step of 1.0 across the As K-edge of 11867 eV.

SCORODITE As		**Mass absorption coefficient (μ/ ρ) (cm^2/g)**			**Element**				
Element	**Mass fraction in scorodite**	**Pre-edge 11866 (eV)**	**Post-edge 11868 (eV)**	**Δ (μ/ρ)**	**Conc. for unit edge step (g/cm^3)**	**Amount As in sample holder (mg)**	**Scorodite amount (mg)**	**Scorodite conc. (mg/g)**	**Post-edge Absorption/element**
As	0.325	25.8	179.2	153.4	0.00652	3.91	12.04	167.1	1.17
Fe	0.241	107.9	107.9						0.52
O	0.415	3.6	3.6						0.02
H	0.0175	0.382	0.382						0
BN									0.16
								Total	1.87

6-line Ferrihydrite

Table A-8. Sample calculation for the dilution of Fe in arsenical 6-line ferrihydrite with boron nitride (BN) to give an edge step of 1.0 across the Fe K-edge of 7112 eV.

6-line FH based on Fe (150g/mol)		**Mass absorption coefficient (μ/ ρ)*** (cm^2/g)			**Element**				
Elem-ent	**Mass fraction in 6LFH**	**Pre-edge 7111** (eV)	**Post-edge 7113** (eV)	**Δ (μ/ρ)**	**Conc. for unit edge step** (g/cm^2)**	**Amount Fe in sample Holder 3*** (mg)	**Mass of 6-line FH** (mg) 3*	**Conc. of 6-line FH** (mg/g) 4*	**Post-edge Absorption** (per element) 5*
Fe	0.37	53.2	407.6	354.4	0.00282	1.69	4.57	70.8	1.15
As	0.05	104.3	104.2						0.39
O	0.415	16.6	16.6						0.08
H	0.0175	0.396	0.396						0
BN									0.16
								Total	**1.78**

* Mass absorption coefficient (μ/ρ) below and above the Fe K-edge at 7112 eV obtained from X-ray absorption tables in Hephaestus for each element, and the change in (μ/ρ) for Fe across the edge.

** Calculated for Fe as 1.0/Δ (μ/ρ) where 1.0 = the target edge step.

3* Iron (column 7) in sample (mg) = Fe concentration (g/cm^2) × sample cross-sectional area (0.60 cm^2) × 1000 mg/g; scorodite in mg (column 8) = Fe mg (column 7)/mass fraction of Fe (column 2).

4* Concentration of scorodite (mg/g sample) after diluting in BN = mass of mineral (7.02 mg)/mass sample i.e. [0.067 = 0.00702 g mineral + 0.06 g BN].

5* Total post-edge absorption contribution per element = element mass fraction (column 2) × scorodite in grams (0.001 × column 8) × post-edge mass absorption coefficient (column 4)/sample cross-sectional area (0.60 cm^2). Total absorption = sum of all element contributions including the contribution of BN (0.16).

Table A-9. Sample calculation for the dilution of As arsenical 6-line ferrihydrite with boron nitride (BN) to give an edge step of 1.0 across the As K-edge of 11867 eV. As shown in this table, because of the low concentration of arsenic in the sample no BN dilution was done.

6-line FH based on Fe (150 g/mol)		**Mass absorption coefficient (μ/ ρ)*** (cm^2/g)			**Element**				
Elem-ent	**Mass fraction in 6LFH**	**Pre-edge 11866** (eV)	**Post-edge 11868** (eV)	**Δ (μ/ρ)**	**Conc. for unit edge step** (g/cm^2)**	**Amo-unt of Fe in sample holder*** (mg)	**Mass of 6-line FH** (mg) 3*	**Conc. of 6-line FH** (mg/g) 4*	**Post-edge Absorpt.** (per element) 5*
As	0.05	25.8	179.2	153.4	0.00652	3.91	78.2	565.7	0.017
Fe	0.37	104.3	104.2						5.0
O	0.415	16.6	16.6						0.08
H	0.0175	0.396	0.396						0
BN									0.16
								Total	**1.78**

* Mass absorption coefficient (μ/ρ) below and above the As K-edge at 11866 eV obtained from X-ray

absorption tables in Hephaestus for each element, and the change in (μ/ρ) for As across the edge.

** Calculated for As as $1.0/\Delta\ (\mu/\rho)$ where 1.0 = the target edge step.

3* Arsenic (column 7) in sample (mg) = As concentration (g/cm^2) × sample cross-sectional area (0.60 cm^2) × 1000 mg/g; scorodite in mg (column 8) = As mg (column 7)/mass fraction of As (column 2).

4* Concentration of 6-line Fh (mg/g sample) after diluting in BN = mass of mineral (7.02 mg)/mass sample i.e. [0.067 = 0.00702 g mineral + 0.06 g BN].

5* Total post-edge absorption contribution per element = element mass fraction (column 2) × scorodite in grams (0.001 × column 8) × post-edge mass absorption coefficient (column 4)/sample cross-sectional area (0.60 cm^2). Total absorption = sum of all element contributions including the contribution of BN (0.16).

Reference:

Kelly, Hesterberg, & Ravel. Analysis of soils and minerals using X-ray absorption spectroscopy. Chapter 14. in “Methods of Soil Analysis”. Part 5. Mineralogical Methods. SSSA Book Series, no. 5.